UNITED STATES ATOMIC ENERGY COMMISSION

TID-5215

# MAGNETS AND MAGNETIC MEASURING TECHNIQUES

Edited by

R. K. Wakerling
A. Guthrie

June 1949

Radiation Laboratory
University of California
Berkeley, California

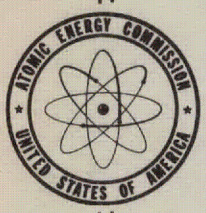


Technical Information Service, Oak Ridge, Tennessee

Classification canceled April 15, 1955

CONTRIBUTING AUTHORS

A. Guthrie
E. Kane
J. De Pangher
W. M. Powell
R. K. Wakerling

Operated by the
University of California
For the U. S. Atomic Energy Commission
Under Contract W-7405-eng-48

Printed in U.S.A., price $1.45. Available from the
Office of Technical Services, Department of
Commerce, Washington 25, D.C.

# Magnets and Magnetic Measuring Techniques

Edited by

R. K. WAKERLING

Radiation Laboratory, Department of Physics
University of California

and

A. GUTHRIE

U. S. Naval Radiological Defense Laboratory;
formerly of Radiation Laboratory, Department of Physics
University of California

University of California Radiation Laboratory
Berkeley, California
June 1949

## PREFACE

The existence of adequate experimental equipment, in particular the two operating cyclotrons of the Radiation Laboratory and the large 184-inch unit under construction, together with a nucleus of trained personnel, made it inevitable that work in connection with the war effort would be prosecuted vigorously at the University of California. Prior to the fall of 1941, studies of the properties of the transuranic elements were carried out and artificial radioactive materials were produced in the cyclotrons for use in various laboratories. This work was done informally and primarily on university funds. The importance of the studies of transuranic elements cannot be overestimated since the results formed a basis for the Plutonium Project.

Although the mass spectrographic method of separating uranium isotopes had been under consideration prior to the fall of 1941, there was no unanimity of opinion among physicists regarding the ultimate success of the method, owing to the space-charge effects. The feeling prevailed in the Radiation Laboratory of the University of California that in spite of this uncertainty the method should be pushed vigorously. The first concrete step in this direction was taken in November 1941, when a group was assigned to convert the 37-inch cyclotron to study this method of separating uranium isotopes. At about the same time two other groups started work on other electromagnetic separation schemes, namely, the ionic centrifuge and the radial magnetic separator. All this work was undertaken with the full support of the Uranium Committee but under no formal contract. The first formal contract designed to further work along these lines was entered into between the university and the Office of Scientific Research and Development in late December 1941, with the Laboratory Director as Project Leader.

The work on the mass spectrographic method, now called the "calutron process," proceeded so satisfactorily that by the early fall of 1942 plans were being formulated for a production plant. Also, owing to the very gratifying results obtained with this method, it was decided to discontinue work on the other methods. From the fall of 1942 to

the end of hostilities in 1945 the Berkeley project was concerned primarily with the design and testing of protoype units for the plant, in addition to the necessary training of personnel. For a good portion of the time Radiation Laboratory personnel was stationed at Oak Ridge to assist directly in putting the plant into operation. It was on May 1, 1943, that the Berkeley project came directly under the jurisdiction of the Manhattan District. This move, however, did not affect the organizational setup of the Radiation Laboratory in any way, and the development work proceeded without any break.

Perhaps the outstanding factor with regard to the entire electromagnetic separation project lies in the general smoothness with which the work proceeded. It was necessary to build a large development laboratory from a relatively small university research laboratory in a matter of months. This involved greatly multiplying the personnel and increasing the physical facilities and necessary experimental equipment appropriately. In spite of the rapid expansion, personnel and organizational difficulties were inconsequential. The entire laboratory organization was characterized by a minimum of formal procedure consistent with the nature of the work. It is indeed remarkable that the scientific and technical personnel of the Radiation Laboratory, many of whom had been accustomed to the academic freedom of educational institutions, could adjust themselves so readily to the necessary security, governmental regulations, and group action of the project. It must also be kept in mind that the work was predominately of a developmental rather than research nature. The form of laboratory organization was such as to allow a maximum of individual expression with regard to the various problems encountered, which undoubtedly contributed considerably to a maximum of cooperation. The fact that the first unit of the Oak Ridge plant was built and put into operation successfully within a matter of two years from the time that the first mass spectrographic unit was built attests to the close cooperation maintained among all people concerned—the Office of Scientific Research and Development, Manhattan District officials, Radiation Laboratory personnel, and the manufacturing and operating companies. It would not be fair to say that the organization used would have been adopted if the project had been built up on a long-range basis. However, in view of the haste with which the project had to be carried through, it worked extremely well.

In preparing the report on the work done at the Radiation Laboratory, the major emphasis has been placed on those subjects of most interest to people working in related fields. The engineering aspects have been minimized in view of the fact that this phase of the work will be covered in other project literature. A number of papers deal-

ing with the chemical problems of the project will similarly be made available in separate reports.

It is impossible to pay proper tribute to the many individuals — scientific, technical, and nontechnical — who participated in the Berkeley project. A cross section of scientific and technical personnel is contained in this report, as authors of the various chapters and in the lists of references at the ends of the chapters. Others are referred to in the text. However, the names of many persons who contributed substantially to the progress of the project do not appear in this report.

The Office of the Director takes pleasure in expressing its deep appreciation to the project personnel for their unfailing loyalty and confidence; to the university as a whole for its support and cooperation; to the Area Engineer's Office for its very effective expediting of all matters pertaining to the rapid development of the Project; to the plant construction contractor, Stone and Webster Engineering Corporation; to the operating company, Tennessee Eastman Corporation; and to the major manufacturing contractors, Allis-Chalmers Company, Westinghouse Electric and Manufacturing Company, and many others, for their close cooperation and effective handling of the engineering and operations problems.

E. O. Lawrence
Professor of Physics
Director, Radiation Laboratory
University of California

June 1949

CONTENTS

Chapter 1

# SOME BASIC CONSIDERATIONS REGARDING MAGNET DESIGN REQUIREMENTS

By Wilson M. Powell and Eneas Kane

## 1. INTRODUCTION

In the design of a magnet for a Dempster-type mass spectrograph, two of the primary considerations are the pole area and the strength of the field desired. The size of the magnet depends on the voltage through which the ions are accelerated. A practical working voltage in connection with the work on the calutron was found to be 35,000 volts. The product of the field strength H, in oersteds, and $\rho$, the radius of the orbit, in centimeters, is given by

$$H\rho = 1.414 \times 10^4 \sqrt{\frac{VM}{e}}$$

where V = accelerating potential in volts
M = mass of uranium 238 ion in grams
e = charge of ion in electromagnetic units

Now

V = 35,000 volts
$M = 238/(6.023 \times 10^{23}) = 3.95 \times 10^{-22}$ g
$e = 1.60 \times 10^{-20}$ e.m.u.

Therefore

$$H\rho = 1.414 \times 10^4 \sqrt{\frac{35{,}000 \times 3.95 \times 10^{-22}}{1.60 \times 10^{-20}}}$$

$= 4.16 \times 10^5$ oersted-cm

Similarly the value of $H\rho$ for uranium 235 is $4.14 \times 10^5$ oersted-cm, so that the fractional difference in the $H\rho$ values for the two isotopes is 0.00481 (i.e., 0.02/4.16). If the radius chosen is very small, the separation between the focuses for the two isotopes will also be small, and the problem of building a satisfactory collector becomes difficult. The most satisfactory size depends on other factors as well, e.g., the length and sharpness of the source of ions, the type of magnetic focusing used, and the magnitude of the recovery problem. In cases in which the recovery problem was not difficult the best radius seemed to be about 4 ft. For this radius the separation between the isotopes is 0.461 in. The best field then becomes $H = \frac{4.16 \times 10^5}{4 \times 12 \times 2.54} = 3410$ oersteds. In those cases in which the recovery problem was difficult, a 2-ft radius and a magnetic field of 6820 oersteds seemed to fulfill the requirements in the most satisfactory manner. There are small corrections which must be applied to these fields because of the effect of magnetic-focusing shims on the radius.

The length of the gap in the direction of the magnetic field was determined by the method used to focus the ion beam. In a Dempster mass spectrograph the focus becomes poorer as the angles $\pm\alpha$ (Fig. 1.1) become greater. The extreme positive- and negative-angle rays focus closer to the source than the zero-angle ray. If the magnetic field were properly strengthened for the zero-angle ray and weakened for the other rays, then all rays could be brought to a single focus at a point near the receiver. Since it was desirable to place several sources and collectors in one magnet, this correction of the field was accomplished by placing an appropriately contoured ridge of iron (Fig. 1.2) on each pole face parallel to the source-receiver line and under the widest part of the beam. These ridges of iron were called "magnetic shims."

The properties of a magnetic field in space make it impractical to obtain a properly shimmed field if the gap length is much greater than one-half the radius $\rho$. For this reason the gap length was taken to be 2 ft in the magnets for the Alpha stage, in which $\rho$ = 4 ft, and 13.5 in. in the Beta-stage magnets, where $\rho$ = 2 ft.

Because the electrical discharge used as a source of ions for the calutron follows the magnetic lines of force, a restriction on the curvature of the lines was necessary. At the outer edge of an air gap this curvature is very marked. If the iron is operated at a low enough flux density so that it can be considered to be a magnetic equipotential surface, then the field at the edge of the gap will fall off at a certain

rate, depending on the shape of the iron and the location of the coils of the magnet. However, if the flux density becomes high locally, because of leakage effects, then the iron is no longer an equipotential surface, and there is an additional increase in the rate at which the field at the edge of a gap decreases. Both of these effects were present in the magnets used, and a great deal of the model work consisted in determining the most economical amount and arrangement of iron at the edges of the gaps.

Measurements of the straightness of the lines of flux near the edges of a gap were simplified by using an indirect method involving only the space rate of change of the field. It can be shown that the curvature of a line at the plane of symmetry between the two poles of a magnet is related to the space rate of change of the field in the following way.

At point O of Fig. 1.3, Hx = 0 and H = Hy. At point P

$$(Hx)_P = \frac{\partial Hx}{\partial y}\, dy + (Hx)_O$$

and

$$(Hy)_P = \frac{\partial Hy}{\partial y}\, dy + (Hy)_O$$

If

$$\frac{\partial Hy}{\partial y}\, dy \ll (Hy)_O$$

then

$$d\theta = \frac{(Hx)_P}{(Hy)_P} \approx \frac{1}{(Hy)_O}\ \frac{\partial Hx}{\partial y}\, dy$$

and consequently

$$\frac{d\theta}{dy} = \frac{\partial Hx}{\partial y}\ \frac{1}{(Hy)_O}$$

Further, it is assumed that curl H = 0, or

$$\frac{\partial Hx}{\partial y} = \frac{\partial Hy}{\partial x}$$

so that

$$\frac{d\theta}{dy} = \frac{\partial Hy}{(Hy)_O} \frac{1}{\partial x}$$

If $d\theta$ is small and the line follows the arc of a circle, then

$$d\theta = 2 \frac{dx}{dy}$$

or

$$dx - \frac{1}{2} d\theta \, dy = \frac{1}{2} \frac{d\theta}{dy} (dy)^2$$

and

$$x = \frac{1}{2} \int_0^h \int_0^\theta d\theta \, dy = \frac{1}{2} \int_0^h \theta \, dy$$

But

$$d\theta = \frac{\partial Hy}{\partial x} \frac{1}{(Hy)_O} dy$$

so that

$$\theta = \int_0^h \frac{\partial Hy}{\partial x} \frac{1}{(Hy)_O} dy$$

$$= \frac{\partial Hy}{\partial x} \frac{1}{(Hy)_O} h$$

If $\partial Hy/\partial x$ is not a function of y, then

$$x = \frac{1}{2} \int_0^h \frac{\partial Hy}{\partial x} \frac{1}{(Hy)_O} h \, dy = \frac{h^2}{2} \frac{\partial Hy}{(Hy)_O} \frac{1}{\partial x}$$

The allowable bowing in the field is 0.5 mm in 250 mm, i.e.,

$h = 125$ mm $= 4.92$ in.

$x = 0.5$ mm $= 0.02$ in.

Hence

$$\frac{\partial Hy}{(Hy)_o}\ \frac{1}{\partial x} = 0.0016 = 0.16 \text{ per cent per inch}$$

is the maximum allowable space rate of change of the magnetic field in a direction toward the edge of a gap.

A further requirement for the magnets was that the field should fall off by less than 0.1 per cent over the region where the ion beam is farthest from the line joining the source and the collector. With these restrictions the problem of designing a magnet becomes chiefly one of obtaining the required magnetic field with the best compromise between convenience, amount of steel, amount of power, and amount of copper.

## 2. NOMENCLATURE

The nomenclature used throughout is as follows (where "consistent units" is given the actual units employed are noted in the text for each formula considered):

H = magnetic field strength in oersteds.
$\phi$ = lines of flux; numerically equal to the product of the field strength H, in lines of flux per square centimeter, and the area, in square centimeters, perpendicular to the magnetic field.
I = electric current in consistent units.
$l$ = linear distance in consistent units.
i = subscript referring to iron portion of magnetic circuit.
g = subscript referring to air-gap portion of magnetic circuit.
V = voltage in consistent units.
E = energy in consistent units.
M = mass in grams.
e = ionic charge in electromagnetic units.
$\rho$ = charged-ion radius in magnetic field in consistent units.
L = leakage coefficient, or subscript referring to leakage.
B = magnetic induction in gauss.
$\mu$ = permeability of magnetic material in gauss per oersted.
F = force in consistent units.
N = number of turns of conductor.
n = "efficiency" of magnet, dimensionless (see Sec. 3).
A = air-gap pole-face area in consistent units.
$A_c$ = cross-sectional area of a single coil conductor in square inches.
mmf = magnetomotive force in consistent units.
$\rho_c$ = resistivity of conductor material in ohm-inches.
$\gamma$ = specific weight of conductor material in pounds per cubic inch.

$W_c$ = weight of coil conductor material in pounds or tons.
$P$ = power in watts or kilowatts.
$W_s$ = weight of steel in coil in pounds or tons.

## 3. DEFINITIONS

1. The work necessary to carry a unit north magnetic pole around a conductor carrying a current of I amperes is $4\pi I/10$ ergs.

2. The force on a unit north magnetic pole is H dynes.

3. If a unit north magnetic pole has a magnetic force of 1 dyne on it, it is said to be in a magnetic field whose intensity H is 1 oersted. It is obvious from definitions 1 and 2 that $\int_0 H\, dl = 4\pi I/10$, where $\int_0 H\, dl$ is taken along a path which circles the wire once and $dl$ is an element of length along that path.

4. The force F in dynes on a conductor $l$ centimeters in length, carrying a current of I amperes in a magnetic field of H oersteds and oriented at right angles to the field, is $F = HIl/10$. The force is at right angles both to the direction of the current and the magnetic field, as shown schematically in Fig. 1.4.

5. A line of flux is defined in the following manner. If the magnetic intensity is H, then the number of lines of flux passing through a square centimeter perpendicular to the magnetic field is equal to the numerical value of H. A field of 10,000 oersteds has 10,000 lines per square centimeter perpendicular to the field.

6. The efficiency n of a magnet is defined as the ratio of the work required to carry a unit north magnetic pole across the air gap to the work required to carry the unit pole around the entire magnetic circuit. Hence

$$n = \frac{\int_0^{l_g} H_g\, dl_g}{\oint H\, dl}$$

If the coils on the magnet have N turns and carry a current of I amperes, then

$$\oint H\, dl = \frac{4\pi NI}{10}$$

Also, if the intensity of the field at the center of the gap is uniform in the direction of the magnetic field, then $\int_0^{l_g} H_g\, dl_g = H_g l_g$, where $l_g$ is the length of the air gap along the field.

For this case the efficiency n becomes

$$\frac{H_g l_g}{4\pi NI/10}$$

7. The leakage coefficient L of a magnet is defined in an arbitrary way, justified only by its convenience. If the air gap in the magnet is bounded by flat parallel surfaces, the magnetic field is quite uniform near the center of the pole face, but near the edge of the gap the field weakens and extends outward beyond the edge for some distance. The quantity $\phi_g$ is called the flux through the gap and by definition is equal to the product of the magnetic field intensity at the center of the gap, $H_g$, and the area A of the pole face. If the total flux passing through the iron at the coils is designated by $\phi_i$, the leakage coefficient L is defined as $\phi_i/\phi_g$.

More briefly, $L = \phi_i/\phi_g = \phi_i/H_g A$ in consistent units. The leakage coefficient, because of this definition, varies from section to section of the iron. The leakage flux is defined by $\phi_L = \phi_i - \phi_g$.

8. The number of lines of flux per square centimeter perpendicular to the flux direction in the iron is called the "magnetic induction." The unit of magnetic induction is called a "gauss" and corresponds to a flux density of one line per square centimeter. The lines of induction in the iron are continuous with the lines of the magnetic field outside the iron. Both are called "lines of flux," and both have the property of producing a voltage in a loop of wire through which the number of lines is changing. This voltage is equal to $(d\phi/dt) \times 10^{-8}$, where $\phi$ is the total instantaneous flux through the loop of wire.

9. The relation between the magnetic intensity $H_i$ and the magnetic induction B inside the iron is expressed by the relation $B = \mu H_i$. The quantity $\mu$, called the "permeability," is different for different types of iron and is determined experimentally. A typical curve of $\mu$ against B for SAE 1010 iron is given in Fig. 1.5.

10. A surface, each element of which is normal to the magnetic flux lines passing through it, may be described as a magnetic equipotential surface. Along such a surface a unit north magnetic pole may be moved without doing work.

## 4. MAGNETIC FORCE CONSIDERATIONS

Consider now a magnet such as is shown in Fig. 1.6. It will be assumed that the total number of turns in the two coils is N and that the current in the coils is I abamperes. Let the pole faces have an area $A = a \times b$ square centimeters and take the gap height to be $l$ centi-

meters. For simplicity the magnetic field H is assumed to be uniform over the whole area A, the leakage flux is assumed to be negligible, and the iron is assumed to have an infinite permeability.

The energy in the magnetic field may be found by calculating the energy which must be put into the coils to energize the magnet. The current may be obtained from the relation

$$Hl = 4\pi NI$$

and the potential opposing the current is $V = N\, d\phi/dt$, where the flux $\phi$ through the magnet and coils is given by $\phi = HA = Hab$.

Therefore, the energy put into the coils is

$$E = \int_0^\infty VI\, dt = \int_0^\infty N \frac{d\phi}{dt} \frac{Hl}{4\pi N}\, dt$$

But

$$\frac{d\phi}{dt} = A \frac{dH}{dt} = ab \frac{dH}{dt}$$

so that

$$E = \int_0^\infty ab \frac{lH}{4\pi} \frac{dH}{dt}\, dt = \int_0^H ab \frac{lH}{4\pi}\, dH = abl \frac{H^2}{8\pi} \text{ ergs}$$

Since $a \times b \times l$ is the volume of the field, the energy per cubic centimeter of the field is $H^2/8\pi$ ergs.

To calculate the force between the poles the gap $l$ will be assumed to increase from zero to $l$. The force will be equal to the energy put into the field plus that put into the coil per unit change in the gap. Now the energy stored in the field is $(H^2/8\pi) \times l \times A$, i.e., the energy change in the field per unit change in the gap is $(H^2/8\pi) \times A$. The energy put into the coil from changing $l$ is

$$E_l = \int_{l=0}^{l=l} VI\, dt = \int_{l=0}^{l=l} IN \frac{d\phi}{dt}\, dt = 0$$

This can easily be shown to be zero by the following consideration. Assume that the flux builds up from 0 to $\phi$ when $l = 0$, after which the gap is increased from 0 to $l$. During the first process the current I is zero because $l$ is zero; thus no work is done. However, during the second process $\phi$ remains constant. Consequently $d\phi/dt = 0$, and hence

$E_l = 0$. This means that the work done in separating the poles is equal to the energy stored in the magnetic field in the gap. Consequently the total is

$$F = \frac{H^2}{8\pi} \frac{lA}{l} = \frac{H^2 A}{8\pi} \text{ dynes}$$

or $H^2/8\pi$ dynes/sq cm. The force is one of attraction.

A second kind of force exists which is often overlooked, namely, one which tends to increase the area of the poles. This force is important wherever a pole face of a magnet is split across the center. The forces tending to separate the halves are surprisingly large and if overlooked can be disastrous. To calculate them, the work done by the coil, when the dimension b is allowed to go from zero to b, is determined.

$\phi = Hab$

Consequently

$$\frac{d\phi}{dt} = Ha \frac{db}{dt}$$

The work done by the coil is $E_b = \int_0^\infty NI \, d\phi/dt \, dt$ and since $I = Hl/4\pi N$

$$E = \int_0^\infty \frac{NHl}{4\pi N} = Ha \frac{db}{dt} dt = \int_0^b \frac{H^2 la}{4\pi} db = \frac{H^2 lab}{4\pi}$$

But the energy in the magnetic field is only $H^2lab/8\pi$; therefore the work done in increasing b must have been done against an external force equal to

$$\frac{H^2 lab}{8\pi b} = \frac{H^2 la}{8\pi} \text{ dynes}$$

It follows from this that if a circular pole piece is split along a diameter, each half will be pushed sideways with a force $\frac{1}{2}(H^2la/8\pi)$, where $l$ is the length of the gap and a is the diameter of the pole.

## 5. MAGNET DESIGN FACTORS

5.1 Magnetic Circuits. The most useful treatment for purposes of design of electromagnets is to define basic quantities so that the equations relating them are analogous to those for electric circuits.

From the preceding discussion we may write

$$\oint H\, dl = \frac{4\pi NI}{10} \tag{1}$$

The line integral is the work done in carrying a unit north magnetic pole once around the path and may be called the "magnetomotive force" (mmf). Thus from Eq. 1

$$\text{mmf} = \frac{4\pi NI}{10} \tag{2}$$

The magnetic flux $\phi$ is equal to $\int \mu H\, dA$, or $\mu HA$, if H is constant over the area A. Then

$$\text{mmf} = \oint H\, dl = \int \frac{\phi\, dl}{A} = \phi \int \frac{dl}{\mu A} \tag{3}$$

since $\phi$ is constant for the circuit. The similarity between this expression and

$$E = iR \tag{4}$$

for an electric circuit will be noted.

When the circuit consists of several parts, for each of which $\mu$ and A can be assumed constant, the magnetic "resistance" of the entire circuit is the sum of the resistances of the separate parts. Therefore

$$\text{mmf} = \phi \left( \frac{l_1}{\mu_1 A_1} + \frac{l_2}{\mu_2 A_2} + \ldots + \frac{l_n}{\mu_n A_n} \right) = \frac{4\pi NI}{10} \tag{5}$$

In most practical cases the exact calculation of the total mmf by adding resistances is laborious or impossible because of the difficulty in specifying the leakage paths and in determining the proper values for $\mu$.

If the subscript g refers to the air gap in a magnetic circuit, Eq. 2 gives for the mmf required in the air gap

$$\frac{4\pi (NI)_g}{10} = (\text{mmf})_g = \phi_g \frac{l_g}{\mu_g A_g} = H_g l_g \tag{6}$$

or since $\mu_g = 1$ for air

$$(NI)_g = 2.02 H_g l_g \tag{7}$$

In this equation $H_g$ is in gauss, $l_g$ is in inches, and $(NI)_g$ is in ampere turns. For the types of magnets and the proportions considered for the calutron, the quantity $(NI)_g$ represents 85 to 95 per cent of the total mmf required (i.e., the efficiency ranges from 85 to 95 per cent), and Eq. 7 can be used to give a useful first approximation to the total ampere turns required.

5.2 Coil and Conductor Sizes. Consider a magnet with a circular pole of diameter D and air-gap length $l$. The field at the center of the gap is to be H. For the moment the allowable change in field with the radius of the pole face will be left unspecified.

In the notation of Sec. 2,

$$P = I^2\rho_c \frac{\pi D_m N}{A_c} = (NI)^2 \rho_c \frac{\pi D_m}{NA_c} \tag{8}$$

However,

$$W_c = NA_c\pi D_m\gamma \tag{9}$$

or

$$NA = \frac{W_c}{\pi D_m\gamma} \tag{10}$$

and therefore

$$P = (NI)^2\rho_c\pi D_m \frac{\pi D_m\gamma}{W_c} \tag{11}$$

or

$$PW_c = \pi^2\rho_c\,\gamma(NI)^2\,D_m^2 \tag{12}$$

Therefore the product of the power and weight of a coil conductor depends on the ampere turns and the mean diameter of the coil. In this equation the quantity NI may be estimated from $(NI)_g$ obtained from Eq. 7. As a first approximation NI is usually taken to be 15 per cent greater than $(NI)_g$.

In estimating the coil dimensions the determining factor is usually the cooling problem. The power dissipated (due to $I^2R$ loss) per unit volume of conductor depends only on the current density. The current density is related to the power and weight of copper as follows:

$$P = (NI)^2 \frac{\rho_c \pi D_m}{NA} = I^2 \frac{\rho_c \pi D_m N^2}{NA_c} = \frac{I^2}{A_c^2} \rho_c \pi D_m N A_c = \frac{I^2}{A_c^2} \rho_c \frac{W_c}{\gamma} \qquad (13)$$

or

$$\frac{I}{A_c} = \sqrt{\frac{\gamma}{\rho_c}} \sqrt{\frac{P}{W_c}} \qquad (14)$$

For continuous operation, 1600 amp/sq in. is about the upper limit used for oil-cooled coils. This compares with 1000 amp/sq in. for open bus bars cooled by free convection, as used in power-plant work. The current density can be increased if necessary by careful design of the cooling system.

From the previous relations, the cross-sectional area of a single conductor can be expressed as follows:

$$A_c = \rho_c \pi \frac{NI\, D_m}{V} \qquad (15)$$

$$= \sqrt{\frac{\rho_c}{\gamma}} \sqrt{\frac{PW_c}{V}} \qquad (16)$$

where V is the voltage drop through N turns. If the coil windings are divided into n parallel circuits consisting of N/n turns each, then $V_n$ should be substituted for V, where V is now the voltage across each section.

These relations are sufficient to determine the power and the weight of copper required by a method of successive approximations. In general, the coil proportions cannot be determined directly since they depend greatly on the methods of construction and cooling, which cause the space factor to vary over a wide range. The space factor is defined as the ratio of the volume of copper to the total inside volume of the coil container. Two of the large magnets and one of the pilot-plant models built on this project had space factors ranging from 0.48 to 0.52 for oil-cooled coils. Two experimental models had values of 0.37 and 0.30, but in both cases it was necessary to use conductor sizes which were available but not specifically designed for the job. An average value of 0.5 is a useful preliminary design figure for oil-cooled coils.

Equations 7, 12, 13, 14, and 16 are summarized in Table 1.1 with the numerical values of the constants for copper and silver conductors inserted.

5.3 Magnet Cost. From Eq. 12 it is seen that

$$PW_c \propto (NI)^2 D_m^2$$

and from Eq. 7

$$NI \propto Hl$$

Consequently

$$PW_c \propto (HlD_m)^2$$

From Eq. 14 it is seen that the current density in the coil conductors depends on the ratio $P/W_c$. The proper ratio, in any actual case, will be determined either by the coil cooling requirements or by an economic balance between initial cost and operating costs. On this project the ratio $P/W_c$ was generally set at about 5, corresponding to a current density of 1050 amp/sq in. for a copper conductor. If the ratio $P/W_c$ is held constant, then for a given type of magnet the above proportionality becomes

$$P \propto HlD_m$$

It has been pointed out that shim requirements fix $l$ approximately proportional to $\rho$, the beam radius. Further, the product $H\rho$ is constant, or $H \propto l/\rho$, so that $P \propto \rho$. As an approximation, the mean coil diameter is proportional to $\rho$, and the gap area varies as $\rho^2$.

The weight is governed by the proportionality $W_s \propto H \times$ gap area $\times$ length of steel path. For magnets of the type adopted for the electromagnetic plant, the length of steel path is approximately independent of the beam radius. For a one- or two-tank unit, such as XAX or XBX, the length of steel path is almost directly proportional to the beam radius.

Summarizing, we may write

$$\left.\begin{aligned} P &\propto \rho \\ W_c &\propto \rho \\ W_s &\propto \rho^n \quad 1 < n < 2 \end{aligned}\right\} \frac{I}{A} = \text{constant}$$

To illustrate, coil data from two actual installations are shown in Table 1.2. The XBX (corrected) figures were obtained from the XBX

figures by adjusting the value of $P/W_c$ to 4.2 for comparison with the XAX figures, as follows:

$$PW_c = 112 \times 21 = 2350$$

$$P = \frac{2350}{W_c}$$

$$P^2 = \frac{P}{W_c} \times 2350 = 4.2 \times 2350$$

therefore

$$P = \sqrt{4.2 \times 2350} = 100 \text{ kw}$$

It will be noted that the power and weight of copper required are approximately twice as great for the 4-ft radius as for the 2-ft radius. It is therefore apparent that both the first cost and the power cost of a magnet increase almost proportionately with an increase in beam radius. However, it was not possible at the time the magnets were designed for the calutron to predict with any accuracy the manner in which the beam output and quality would vary with radius. Thus the selection of a beam radius was based almost entirely on factors other than magnet cost.

## 6. GENERAL DESIGN PROCEDURE

With the size and proportions of the gap selected from the foregoing considerations and the required field strength and uniformity determined, several magnet types could be conceived which might satisfy the requirements. Single-gap magnets use a very large amount of iron in the return path. A cyclotron magnet (see Fig. 1.7) can be improved upon tremendously by using two gaps instead of one (see Fig. 1.8). The return yoke B is increased only by the two C sections, whereas two individual magnets would require two B sections and two C sections.

A third possible design would be that shown in Fig. 1.9, which would employ a smaller amount of iron than the design of Fig. 1.8. The gap is twice as high but is cut in half by the iron plate F. The return yoke B requires only one C and one D section. This magnet would not be satisfactory because the lines of force, L, at the edges of the gap have a tendency to bulge outward and consequently reduce the flux at the edges of the plate F. In Fig. 1.8 the presence of coil 2 prevents this spreading of the lines to some extent. The significance of

this spreading has been discussed in Sec. 1. As a general rule it is desirable to keep the driving coils as close to the air gaps as possible in order to reduce spreading and bowing of the field and to keep the largest possible fraction of the gap area usable.

It will be noted that, as the number of gaps increases, the most satisfactory design is an approximation to an infinite solenoid. The weight of steel per gap decreases with an increasing number of gaps and approaches a constant value, as do also the weight of copper and the power required per gap. The limitation on the maximum size of a single magnet of this type would be dictated by considerations of available magnet power sources, building size, and an evaluation of the risk involved to plant production in the event of a magnet failure for any reason.

After the type of magnet has been selected, it is possible to calculate approximately the weight of copper and steel and the amount of power required and to sketch and dimension the entire magnet.

## 7. SCALE-MODEL TESTS

It is possible to determine with considerable accuracy the shape of the field in a gap, and therefore the leakage factor, by the method of flux-plotting used in potential problems such as fluid flow and heat transfer. For cases where the weight of steel is reduced to the point where saturation occurs, however, the boundary conditions for the field can no longer be specified easily. A number of cases also arise for which a two-dimensional treatment is not sufficient, so that the flux-plotting method becomes complicated and time-consuming. Because of these difficulties and the short time available to develop the plant design, it became standard practice at the laboratory to build a scale model on the basis of a preliminary design. Inspection of Eq. 5 indicates that a linear scale model built from steel with the same magnetic properties as planned for the prototype magnet and operated at the same field strength will give results directly applicable to the prototype. The model can also be used to determine forces on steel members and conductors directly. In general, it proved more economical, and, most important, it was faster and more accurate in measuring the effects of detail-design changes directly on a model.

The techniques used to determine model results are described in Chap. 2 of this volume. The method of reporting model results follows.

7.1 Saturation Curve. $H_g$ is plotted as a function of $NI/l_g$, where NI is the total ampere turns required to give a field strength $H_g$ at the center of the specified gap and $l_g$ is the total air-gap length.

7.2 Efficiency. The efficiency n is defined as $\frac{(NI)_{total}}{2.02\ H_g l_g}$, where $(NI)_{total}$ is the total ampere turns required on the model to produce a field strength $H_g$, and the product $2.02\ H_g l_g$ from Eq. 7 is the total NI required to produce a field $H_g$ if there are no iron losses or leakage. The efficiency is plotted as a function of $NI/l_g$.

7.3 Leakage Coefficient L. The leakage coefficient, defined in Sec. 3 of this chapter, is measured at various points on the model for various values of $H_g$ in the center of a selected gap. The leakage factor thus determined is directly applicable to the full-scale magnets.

7.4 Field Uniformity. From the model tests the field strength at a gap can be determined as a function of position in the gap, and a contour map can be drawn showing lines of constant field strength. These measurements are made over a plane parallel to the gap faces and midway between them. If

J = half the length of the gap face
K = half the width of the gap face
X,Y = coordinates of a point in the gap
H = local field strength at the point (x,y)
$H_G$ = field strength at the center of the gap

then results can be summarized by plotting

$$\frac{H}{H_G} \text{ against } \frac{Y}{K} \times \frac{X}{J}$$

As mentioned in Sec. 1, the space rate of change of the field obtained from such a plot gives a direct measure of the bowing of the field.

7.5 Stray Field. Measurements of field strength outside of the gaps but near the magnet are made and reported in a manner similar to that given in Sec. 7.4. These measurements permit the determination of forces on conductors or magnetic members in the stray fields and are important in determining how close watches, instruments, and magnetic tools can be brought to the magnet.

## 8. DESIGN EXAMPLE

To illustrate the application of the principles and methods discussed, the steps required to fix an actual design will be described.

Assume that a magnet is required for experimental purposes, and it is decided that two process tanks, each to accommodate beams of 2-ft radius, are to be needed.

From the relation used in Sec. 1,

$$H\rho = 4.16 \times 10^5 \text{ oersted-cm}$$

so that

$$H = \frac{4.16 \times 10^5}{2 \times 12 \times 2.54} = 6820 \text{ oersteds}$$

The beam uniformity and straightness restrictions discussed previously are to apply.

As a first design, the required gap area is assumed to be of the shape shown in Fig. 1.10. The corners are cut off to give a minimum length of coil conductor and to save steel. With the gap length set at 14.5 in., a check is made either on the basis of tests on similar models or from a flux plot to see if the required usable gap area will result from the total gap area specified above.

The efficiency of the coil is assumed to be 85 per cent, so that for the total ampere turns required for a field of 6800 oersteds, Eq. 7 gives

$$NI = \frac{2.02 \times 6800 \times 2 \times 14.5}{0.85} = 468{,}000$$

If there were no losses in the iron circuit, this number of ampere turns would be split between one full coil in the middle and two half-coils at the ends. To take care of iron losses, the end coils will be made with two-thirds the number of ampere turns of the middle coil, as a first approximation. Thus the ampere turns for the center coil = 468,000/2⅓ = 200,000.

With a current density of 1140 amp/sq in. corresponding to $P/W_c$ = 6.0, the required copper cross-sectional area for the center coil is

$$\frac{NI}{I/A} = \frac{200{,}000}{1140} = 176 \text{ sq in.}$$

and for the end coils is

$$\frac{2}{3} \times 176 = 117 \text{ sq in.}$$

Assuming a space factor of 0.5, it is found that the areas of the center- and end-coil tanks should be 352 and 234 sq in., respectively. There-

fore the dimensions of the center tank are taken to be 20 by 20 in. and those of the end tank to be 20 by 16 in.

It follows that

$$\text{Mean length of conductor} = \text{core perimeter} + \pi(\text{coil-tank width})$$
$$= [83 + 2(63 - 30) + (83 - 60) + \pi \times 30] + \pi \times 20$$
$$= 266 + 63 = 329 \text{ in.}$$

Consequently

$$PW_c = 0.118\ (10^6 \text{ amp-turns})^2 \text{ (inches of mean turn length)}^2$$
$$= 0.118\ (0.468)^2\ (329)^2 = 2800$$

If the available d-c generator is rated at 150 kw, 250 volts, the conductor cross section is

$$A_c = 2.130\ \frac{\sqrt{PW_c}}{\text{line voltage} \times \text{number of parallel paths}}$$
$$= 2.130\ \frac{\sqrt{2800}}{220 \times 1}$$
$$= 0.512 \text{ sq in.}$$

The actual conductor dimensions selected to give the required cross-sectional area depend on factors such as availability of standard-size strip, minimum required conductor bend radius, and permissible "hot spot" temperatures. For example, if it were decided to fix the maximum temperature difference between center and exposed edge of the conductor at 1°C, then from Table 1.1

$$\Delta t = 1°C = 0.0094 \times 10^{-6} \text{ (width of conductor in inches)}^2 \times \text{(current density in amperes per square inch)}^2$$
$$= 0.0094 \times 10^{-6}\ w^2\ (1140)^2$$

where w designates the width.

Therefore

$$w^2 = \frac{1 \times 10^6}{0.0094 \times (1140)^2} = \frac{1}{0.0122} = 82 \text{ sq in.}$$

or

$$w = 9 \text{ in. maximum width}$$

For this case, assume the width to be 3 in., so that the thickness = 0.512/3 = 0.17 in. Then the required turns for center and end coils are as follows:

$$\text{Center coil, } N = \frac{176}{3 \times 0.17} = 345 \text{ turns}$$

$$\text{End coil, } N = \frac{117}{3 \times 0.17} = 229 \text{ turns}$$

Total number of turns = 345 + 2(229) = 803

This means that

$$I = \frac{468{,}000}{803} = 580 \text{ amp}$$

$$P = 220 \times 580 = 128 \text{ kw}$$

Since this magnet is for experimental purposes, it will be designed to produce its rated field at 220 volts, permitting a $\sqrt{250/220}$ or 7 per cent increase in field strength without exceeding the generator rating.

With these preliminary figures established, it is now possible to make a detailed layout of the coil and to determine the actual mean turn length and coil-tank proportions, revising the preceding calculations as required. The entire magnet can now be drawn schematically, as in Fig. 1.11. Some immediately apparent possibilities for proportioning the yoke to keep the steel required at a minimum are indicated by the dotted lines.

The tank walls are required to be 5 in. thick, a figure set by the permissible deflection of the walls and a requirement that internal supports are not permitted. In order to take advantage of this material and use a minimum conductor length, the core will be reduced in size so that the tank wall overhangs by 1.5 in. around the periphery.

The core must contain enough iron to supply 6800 oersteds in the gap plus the leakage flux. Assuming leakage factors of 1.75 at A – A and 1.2 at B–B, based on estimates from other model tests or from flux graphs, the required steel cross sections at these two sections are computed.

For A–A Total flux = 6800 × area of tank wall × 1.75

= 6800 × 4905 × 6.45 × 1.75

= $376 \times 10^6$ lines

For a maximum B of 14,000 gauss, the required core area is

$$A = \frac{376 \times 10^6}{14{,}000 \times 6.45} = 4170 \text{ sq in.}$$

Allowing the specified 1.5-in. overhang of the tank, the required core area is 4480 sq in. If there were a greater difference between this figure and the area of iron required for B = 14,000 gauss, it might be economical to construct a "cellular" core having only the required iron area (see Chap. 3 for examples of this construction). In this case, the core will be made solid, giving

$$B = 14{,}000 \times \frac{4170}{4480} = 13{,}000 \text{ gauss}$$

Similarly, at B–B the required steel area is

$$A = \frac{6800 \times 4905 \times 6.45 \times 1.2}{2 \times 14{,}000 \times 6.45} = 1440 \text{ sq in.}$$

One dimension must be 60 in. to cover the core, giving 24 in. for the required thickness of iron.

These calculations provide sufficient information for the design and construction of a scale model (see Fig. 1.12). Detail changes can be made readily, and their effects can be studied on the model, giving an accurate basis for the full-scale design. The detail design of the prototype magnet will require consideration of the magnetic forces acting on magnetic parts and conductors. Stray and leakage field measurements made on the model permit application of the formulas for magnetic forces discussed in the foregoing sections.

There are a number of detail-design problems which have been mentioned only briefly or omitted entirely. Problems which must be solved for any proposed installation are, for example, the selection of means for clamping and insulating the coil conductors, evaluation of the pressure drop of the cooling medium for the desired flow velocities, and structural design of the coil tank proper. Detailed discussion of these mechanical questions has been omitted to permit a fuller description of the methods used in specifying magnetic field requirements and in designing large-scale equipment to produce these fields.

Table 1.1 — Magnet Design Data

| | Annealed copper | 99.98% silver |
|---|---|---|
| Modulus of elasticity, lb/sq in. | $17.5 \times 10^6$ | $11.5 \times 10^6$ |
| Specific weight, lb/cu in. | 0.322 | 0.380 |
| Resistivity at 20°C, ohm-in. | $0.679 \times 10^{-6}$ | $0.641 \times 10^{-6}$ |
| Resistivity at 40°C, ohm-in. | $0.732 \times 10^{-6}$ | $0.690 \times 10^{-6}$ |
| Heat conductivity at 20°C, watts/in./°C | 9.76 | 10.52 |
| Specific heat at 20°C, watt-sec/lb/°C | 174.9 | 105.9 |
| Linear coefficient of thermal expansion | $16.8 \times 10^{-6}$ (at 25–100°C) | $18.8 \times 10^{-6}$ (at 20°C) |

Formulas Independent of Material

$$\text{Amp-turns} = 2.02 \times \text{gauss} \times \text{gap (in.)}$$

$$\text{Force on conductor (lb)} = \frac{1}{1750} \times \text{kilogauss} \times \text{amp} \times \text{length (in.)}$$

$$\text{Force between pole faces (lb)} = \frac{1}{1.735} \times (\text{kilogauss})^2 \times \text{area (sq in.)}$$

Formulas for Copper and Silver at 40°C Mean Temperature

$$\text{Kw-tons} = \left.\begin{matrix}0.118\ (\text{Cu}) \\ 0.131\ (\text{Ag})\end{matrix}\right\} \times (10^6\ \text{amp-turns})^2 \times (\text{inches of mean turn length})^2$$

$$\text{Amp/sq in.} = \left.\begin{matrix}469\ (\text{Cu}) \\ 525\ (\text{Ag})\end{matrix}\right\} \times \sqrt{\text{kw/tons}}$$

$$\text{Conductor area (sq in.)} = \left.\begin{matrix}2.130\ (\text{Cu}) \\ 1.903\ (\text{Ag})\end{matrix}\right\} \times \frac{\sqrt{\text{kw} \times \text{tons}}}{\text{volts} \times \text{parallel paths}}$$

$$\text{Conductor area (sq in.)} = \left.\begin{matrix}0.731\ (\text{Cu}) \\ 0.689\ (\text{Ag})\end{matrix}\right\} \times \frac{10^6\ \text{amp-turns} \times \text{inches of mean turn length}}{\text{volts} \times \text{parallel paths}}$$

Formulas for a Rectangular Conductor Losing Heat from Two Edges (40°C Mean Temperature)

$$\text{Heating at center of conductor, °C} = \left.\begin{matrix}0.00940\ (\text{Cu}) \\ 0.00821\ (\text{Ag})\end{matrix}\right\} \times 10^6 \times (\text{inches of width of conductor})^2 \times \left(\frac{\text{amp}}{\text{sq in.}}\right)^2$$

$$\frac{\text{Watts}}{\text{Edge surface (sq in.)}} = \left.\begin{matrix}0.366\ (\text{Cu}) \\ 0.345\ (\text{Ag})\end{matrix}\right\} \times 10^6 \times \text{width of conductor (in.)} \times \left(\frac{\text{amp}}{\text{sq in.}}\right)^2$$

Table 1.2 — Coil Data from Two Magnets

| Magnet | P, kw | $W_c$, lb | $P/W_c$ | $\rho$, ft |
|---|---|---|---|---|
| XAX | 211 | 50 | 4.2 | 4 |
| XBX | 112 | 21 | 5.3 | 2 |
| XBX (corr.) | 100 | 24 | 4.2 | 2 |

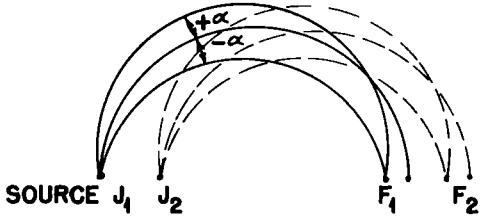


Fig. 1.1 — Ion focuses for uniform magnetic field.

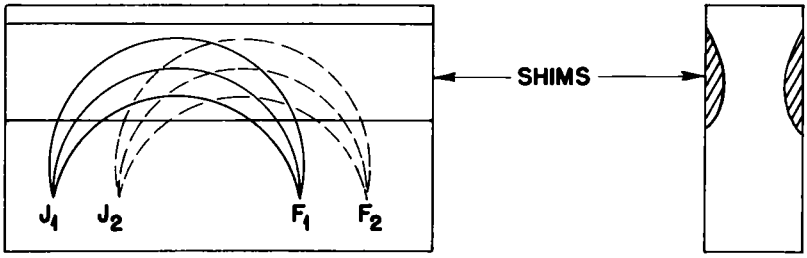


Fig. 1.2 — Effect of linear magnetic shimming field on ion focuses.

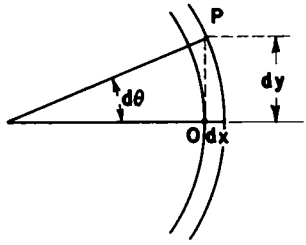


Fig. 1.3 — Sketch used in calculating relation between curvature of a line of force and space rate of change of magnetic field.

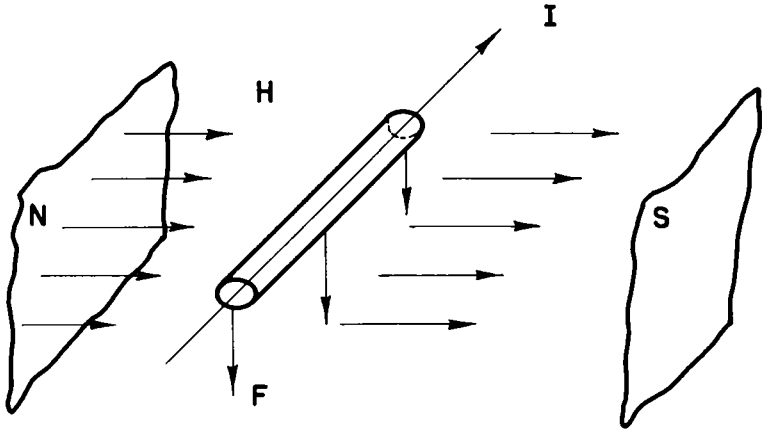


Fig. 1.4—Force on current-carrying conductor in magnetic field.

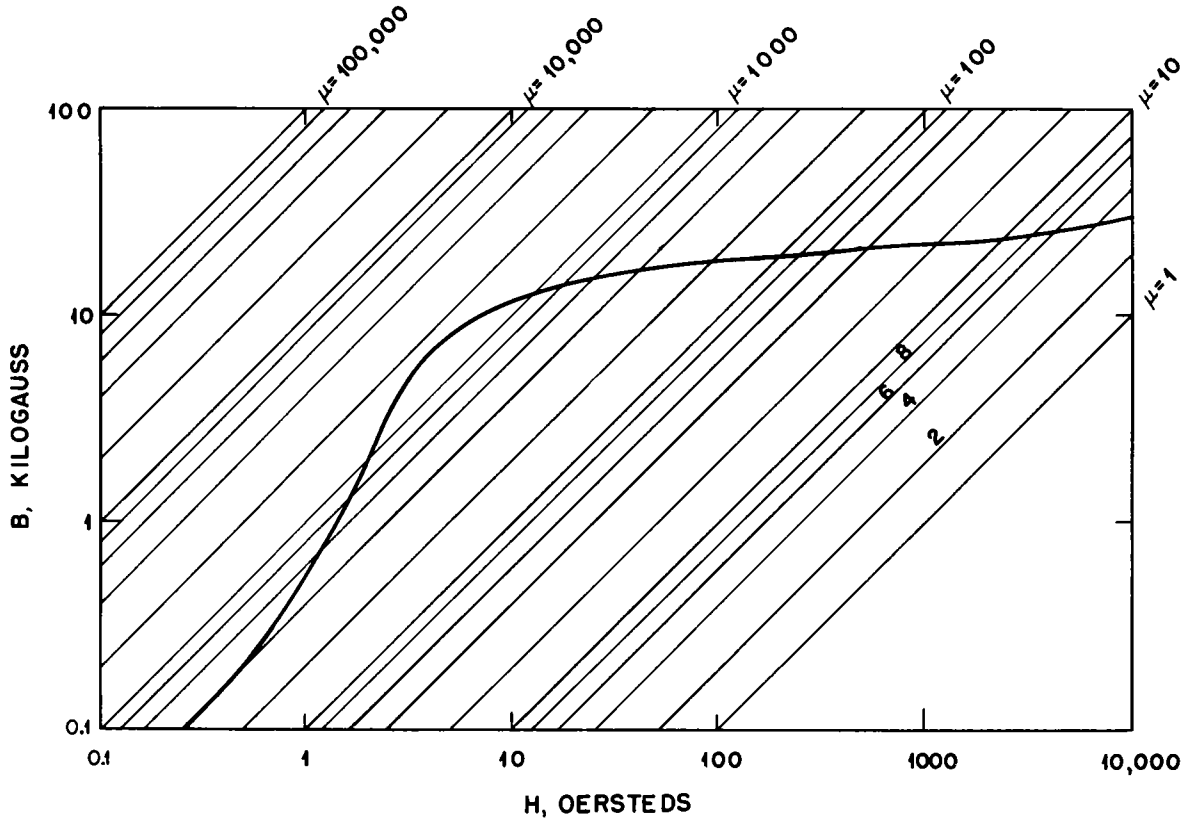


Fig. 1.5—Normal magnetization curve for SAE 1010 iron.

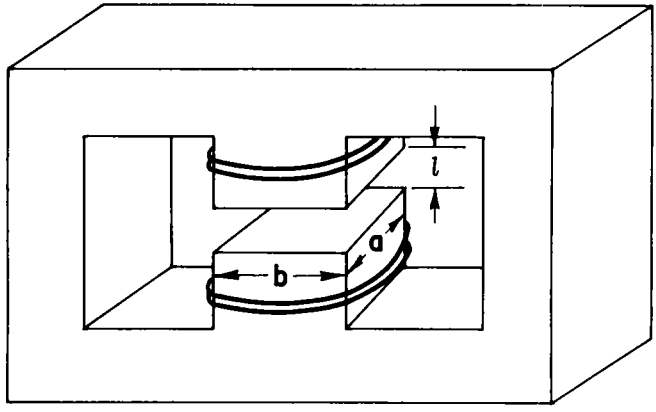


Fig. 1.6—Magnet used in magnetic force considerations.

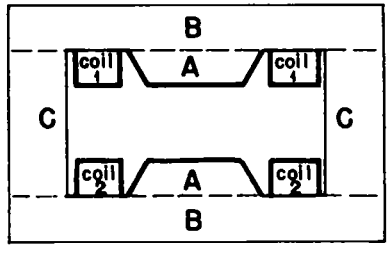


Fig. 1.7—Cyclotron magnet.

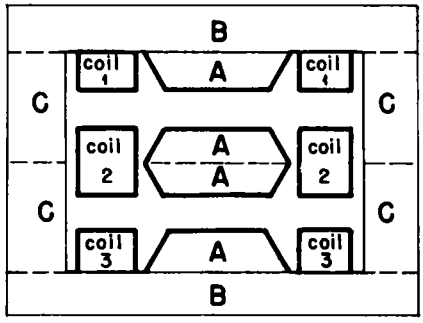


Fig. 1.8 —Improvement in cyclotron magnet by use of two air gaps.

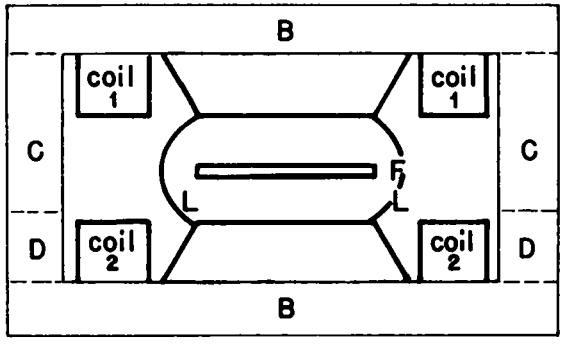


Fig. 1.9 —Alternate design of cyclotron magnet.

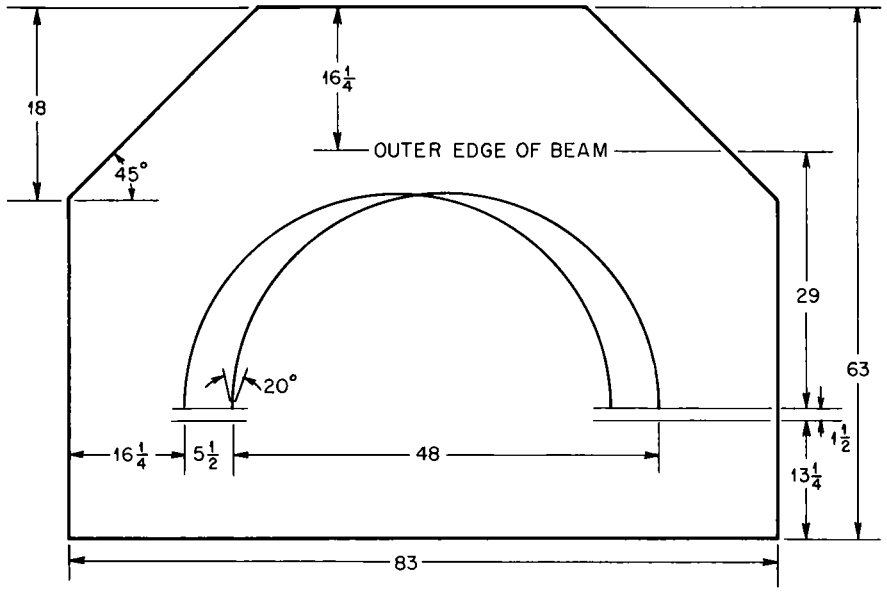


**Fig. 1.10—Shape of gap area taken for first design of cyclotron magnet. All dimensions are given in inches.**

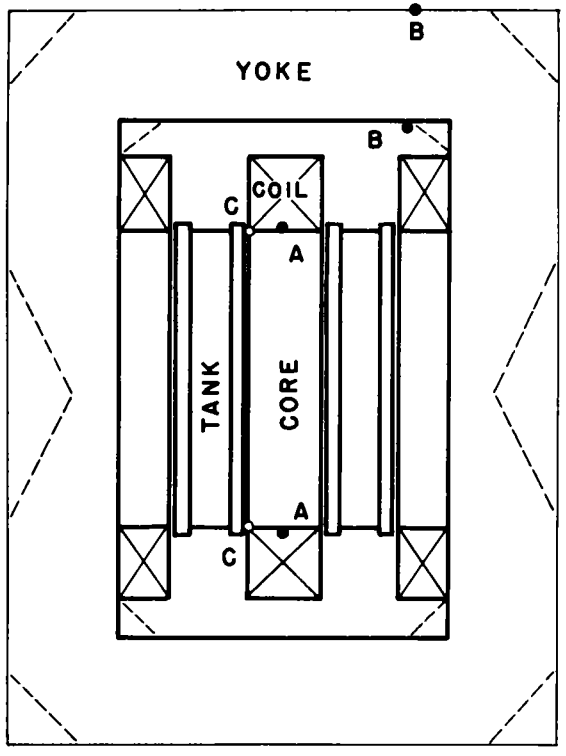


Fig. 1.11—Schematic drawing of entire cyclotron magnet.

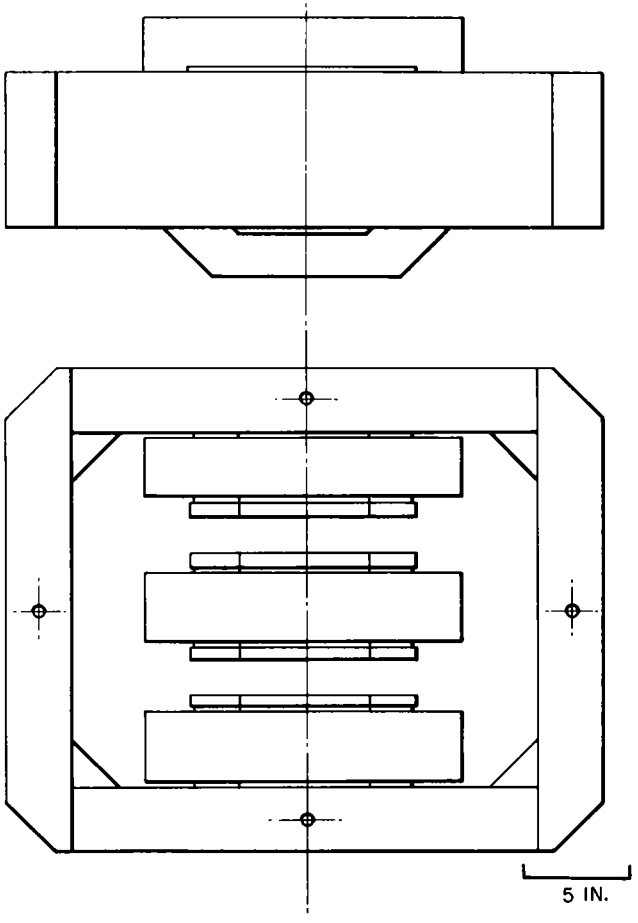


**Fig. 1.12 — Scale model of cyclotron magnet.**

Chapter 2

# MAGNETIC MEASURING INSTRUMENTS AND TECHNIQUES

By John De Pangher, R. K. Wakerling, and A. Guthrie

## 1. BALLISTIC GALVANOMETER

The ballistic galvanometer is used extensively in making magnetic measurements. The theory of its operation and various methods of using it in this field are well known. However, in view of the fact that it has been used extensively in a number of the measuring techniques applied in the University of California Radiation Laboratory, it has been deemed advisable to describe the instrument in some detail for reference purposes.

1.1 Theory. Suppose that a source of flux linkage is in series with the ballistic galvanometer. Let the source of flux linkage be a search coil of effective area A in a magnetic field H. If the flux linkage through the coil is changed suddenly from $\phi_0$ to $\phi_1$, then the voltage V developed in the coil at any time is

$$V = \frac{1}{10^8} \frac{d\phi}{dt} \quad \text{volts} \tag{1}$$

Figure 2.1 is a diagram of the galvanometer circuit. R is the lumped circuit resistance, G is the ballistic galvanometer, F is a flux standard, S is the search coil, and H is the magnetic field strength. Assume that the self-inductance of the circuit is small. The current i flowing at any time is

$$i = \frac{V}{R} \quad \text{amperes} \tag{2}$$

while the time integral of the current is the charge

$$q = \int_0^t i\,dt \qquad \text{coulombs} \tag{3}$$

which is also equal to

$$q = \int_0^t \frac{V}{R}\,dt = \frac{1}{10^8}\frac{1}{R}\int_{\phi_0}^{\phi_1} d\phi$$

or (4)

$$q = \frac{\phi_1 - \phi_0}{10^8 R}$$

The equation of motion of the galvanometer coil is

$$A\frac{d\theta}{dt^2} + B\frac{d\theta}{dt} + C\theta = Di \tag{5}$$

where A, B, C, D = constants of the system
$\theta$ = angular displacement of the coil from equilibrium
i = current flowing

Multiplying the equation by dt and integrating,

$$A\int_0^t \frac{d^2\theta}{dt^2}\,dt + B\int_0^t \frac{d\theta}{dt}\,dt + C\int_0^t \theta\,dt = D\int_0^t i\,dt$$

With the assumption that the current is of short duration so that the coil does not move during passage of the current, then

$$\left(\frac{d\theta}{dt}\right)_0^t = \omega \qquad (d\theta)_0^t = 0 \qquad \int_0^t \theta\,dt = 0 \qquad \int_0^t i\,dt = q$$

and $A\omega = Dq$ or $q = (A/D)\omega$. The quantity $\omega$ is the initial angular velocity imparted to the coil following the surge of current. The equations

$$q = \frac{A}{D}\omega \tag{6}$$

and

$$q = \frac{\phi_1 - \phi_0}{10^8 R}$$

show that the initial angular velocity $\omega$ is proportional to the change of flux $\phi_1 - \phi_0$ or $\Delta\phi$.

The general solution of the equation

$$A \frac{d^2\theta}{dt^2} + B \frac{d\theta}{dt} + C\theta = 0 \tag{7}$$

is now required in order to determine how much the galvanometer will deflect, assuming an initial angular velocity of $\omega$. This equation is a second-order equation with constant coefficients, and the general solution, including arbitrary constants $\alpha$ and $\beta$, is

$$\theta = \alpha \exp p_1 t + \beta \exp p_2 t \tag{8}$$

where

$$p_1 = \frac{-B + \sqrt{B^2 - 4AC}}{2A} \tag{9}$$

and

$$p_2 = \frac{-B - \sqrt{B^2 - 4AC}}{2A} \tag{10}$$

Let

$$a = \frac{B}{2A} \tag{11}$$

and

$$m = \frac{\sqrt{B^2 - 4AC}}{2A}$$

Then

$$\theta = \exp - at (\alpha \exp mt + \beta \exp - mt) \tag{12}$$

To evaluate $\alpha$ and $\beta$, boundary conditions of

$$\theta = 0 \quad \text{at } t = 0 \tag{13}$$

and

$$\frac{d\theta}{dt} = \omega \quad \text{at } t = 0 \tag{14}$$

are assumed.

Combining Eqs. 12 and 13,

$$\theta = \alpha + \beta \tag{15}$$

while Eq. 12 must be differentiated and combined with Eq. 14 to be useful. Differentiating Eq. 12,

$$\frac{d\theta}{dt} = -a \exp -at\,(\alpha \exp mt + \beta \exp -mt) + \exp -at\,(\alpha m \exp mt - \beta m \exp -mt)$$

For $t = 0$

$$\omega = -a(\alpha + \beta) + (\alpha - \beta)m \tag{16}$$

Solving Eqs. 15 and 16 for $\alpha$ and $\beta$,

$$\alpha = \frac{\omega}{2m} \tag{17}$$

and

$$\beta = -\frac{\omega}{2m} \tag{18}$$

The process of substituting these values into Eq. 12 yields

$$\theta = \exp -at \frac{\omega}{m} \left(\frac{\exp mt - \exp -mt}{2}\right) \tag{19}$$

or

$$\theta = \exp -at \frac{\omega}{m} \sinh mt \tag{20}$$

The condition for maximum value of $\theta$ may be determined by differentiating the right-hand side of Eq. 20 and setting it equal to zero.

$$\frac{d}{dt}\left(\exp -at\,\frac{\omega}{m}\sinh mt\right) = \exp -at\,\frac{\omega}{m}\,m\cosh mt - a\exp -at\,\frac{\omega}{m}\sinh mt = 0$$

Therefore

$$\cosh mt = \frac{a}{m}\sinh mt$$

or

$$\tanh mt = \frac{m}{a} \tag{21}$$

The result of combining Eqs. 20 and 21 is

$$\theta_{max} = \frac{\omega}{\sqrt{a^2 - m^2}}\exp -\frac{a}{m}\tanh^{-1}\frac{m}{a} \tag{22}$$

making use of the relation

$$\operatorname{csch}^2 mt = \coth^2 mt - 1$$

But

$$\omega = \frac{D}{A}\,\frac{\phi_1 - \phi_0}{10^8 R}$$

from Eqs. 4 and 6, so

$$\theta_{max} = \frac{\phi}{\sqrt{a^2 - m^2}}\,\frac{D}{A10^8 R}\exp\frac{a}{m}\tanh^{-1}\frac{m}{a} \tag{23}$$

Thus the deflection is proportional to the change of flux.

1.2 Operation. Suppose a magnetic field strength H is to be measured. Let the flux linkage $\phi$ in the search coil of effective area A be changed by one of the following methods:

1. The coil is suddenly jerked completely out of the field.
2. The current producing the field is rapidly reduced to zero.

3. The coil is flipped through 180 deg in the field, thus cutting the lines of force twice.

4. The coil is moved in jerks from point to point in the field to yield uniformity data.

The basic circuit for this setup is shown in Fig. 2.1. The section on ballistic galvanometer theory has shown that the instrument is linear, provided the differential equation describes the motion of the coil accurately and the assumption about a short current pulse is fulfilled. Now the galvanometer may be calibrated.

The flux standard (to be described in detail in Sec. 5.2) produces a galvanometer deflection $d_s$ for a change of line turns $\phi_s$. Evaluation of the field H that links an effective area A and produces a galvanometer deflection d is accomplished by making use of the following relation:

$$\frac{\phi}{\phi_s} = \frac{AH}{\phi_s} = \frac{d}{d_s} \tag{24}$$

Equation 24 is a statement of linearity. In another form it may be written as

$$H = \frac{\phi_s}{d_s}\frac{d}{A} \tag{25}$$

If the coil were flipped, a factor of 2 would enter into the denominator of the right member of Eq. 25.

The linearity relation holds true to about 1 per cent accuracy for a moderately bad case in which the standard deflection is approximately half the deflection to be calibrated. This slight deviation from linearity occurs because the damping term B in Eq. 5 changes with the galvanometer deflection. The galvanometer magnetic field in which the suspension rotates is not quite uniform. The recording scale should be circular and should be located at a distance equal to its radius of curvature from the galvanometer. Field measurements may be made to 0.5 per cent accuracy by bracketing the deflections to be interpreted with deflections from the flux standard and then interpolating.

The circuit resistance R must be kept constant during measurement and calibration. The manner in which the sensitivity varies with circuit resistance is described by Eq. 23. The quantities a and m are, of course, functions of R.

1.3 Relative Merits. The most desirable characteristic of the ballistic galvanometer is that, although thermal and contact emf's displace the zero of the instrument a constant amount during the

course of a test not more than half an hour in duration, ballistic readings are not in error by this amount since the zero of each reading is taken at the point of equilibrium of all torques acting on the galvanometer coil. For convenience in calculation, the zero of the instrument may be corrected periodically by applying a compensating emf in series with the galvanometer. Undesirable characteristics are:

1. The cycle of pulse, deflection, and return to zero is time-consuming.
2. The galvanometer coil suspended by a single wire is extremely susceptible to vibration. During transport the coil may be damaged easily unless certain precautions are taken.
3. The pulse must be of short duration compared to the period of the instrument.

## 2. ELECTRONIC FLUXMETER[1]

The electronic fluxmeter was developed for measuring small changes in a uniform magnetic field in the shortest time possible. This was necessary because of the excessive heating of small models of very large magnets. The search coil S in Fig. 2.2 was pulled rapidly through the magnetic field being measured. The flux measurements appeared as a vertical deflection on a 9-in. oscilloscope and were photographed. The sweep of the oscilloscope gave an indication of the location of the coil in the field.

2.1 Theory. When the search coil S in Fig. 2.2 is drawn through the magnetic field, a voltage is developed across it. This voltage is amplified by the amplifier and is then fed into the condenser C through the resistance R. The voltage from the amplifier is

$$E(t) = \frac{G}{10^8}\frac{d\phi}{dt} \quad \text{volts} \tag{26}$$

where G = amplification factor of the amplifier
$d\phi/dt$ = rate of change of flux through the search coil

The RC circuit is used as an integrating network, the operation of which will be discussed here.

The equation for the RC circuit is

$$iR + \frac{q}{C} = E(t) \tag{27}$$

where i = charging current of the condenser
q = charge accumulated by the condenser

Upon making the substitution $i = dq/dt$ and dividing the entire equation by R, Eq. 27 may be rewritten as

$$\frac{dq}{dt} + \frac{q}{RC} = \frac{E(t)}{R} \tag{28}$$

The solution of Eq. 28 is

$$q = \exp\left(-\int \frac{dt}{RC}\right) \int \frac{E(t)}{R} \exp\left(\int \frac{dt}{RC}\right) dt + C \exp\left(-\int \frac{dt}{RC}\right)$$

or

$$q = \exp\left(-\frac{t}{RC}\right) \left[\frac{G}{10^8 R} \int \frac{d\phi}{dt} \exp\left(\frac{t}{RC}\right) dt + C\right] \tag{29}$$

after substituting the value of E(t) from Eq. 26. The function $d\phi/dt$ must be known in order to perform the integration. The following assumptions are made to permit solution of the problem: (1) The flux change $\phi$ occurs in a very short time; (2) the time constant RC is large.

The quantity t/RC is now assumed to be so small that exp (t/RC) and exp (−t/RC) may be expanded in an infinite series neglecting all but the first two terms. Thus

$$\exp \frac{t}{RC} = 1 + \frac{t}{RC} \tag{30}$$

and

$$\exp -\frac{t}{RC} = 1 - \frac{t}{RC} \tag{31}$$

Equation 29 upon substitution of these quantities becomes

$$q = \left(1 - \frac{t}{RC}\right) \left(\frac{G}{10^8 R} \int_t \frac{d\phi}{dt} + \frac{G}{10^8 R^2 C} \int_t t \frac{d\phi}{dt} dt + C\right) \tag{32}$$

The boundary condition q = 0, $\phi = \phi_0$, at t = 0 will permit determination of the arbitrary constant C. Equation 32 becomes

$$q = \left(1 - \frac{t}{RC}\right) \left[\frac{G}{10^8 R} (\phi - \phi_0) + \frac{G}{10^8 R^2 C} \int_0^t t \frac{d\phi}{dt} dt\right] \tag{33}$$

The output voltage e(t) = q/C is

$$e(t) = \left(1 - \frac{t}{RC}\right) \left[\frac{G}{10^8 RC} (\phi - \phi_0) + \frac{G}{10^8 R^2 C^2} \int_0^t t \frac{d\phi}{dt} dt\right] \tag{34}$$

Good integration occurs when RC is large and t is small. For the ideal case

$$e(t) = \frac{G(\phi - \phi_0)}{10^8 RC} \tag{35}$$

where the output voltage is linearly dependent on the change of flux in the search coil. Poorer integration with a shorter time constant and longer period of integration demands that e(t) be represented by

$$e(t) = \frac{G}{10^8 RC} (\phi - \phi_0) + \frac{G}{10^8 R^2 C^2} \int_0^t t \frac{d\phi}{dt} dt \ldots \tag{36}$$

in which the form of the function $d\phi/dt$ must be determined.

The fractional error in integration (s) is

$$s = \frac{\frac{G}{10^8 R^2 C^2} \int_0^t t \frac{d\phi}{dt} dt}{(G/10^8 RC)(\phi - \phi_0)} = \frac{1}{RC} \frac{\int_0^t t \frac{d\phi}{dt} dt}{\phi - \phi_0} \ldots \tag{37}$$

If RC is large then the fractional error becomes small, but at the same time the output voltage e(t) in Eq. 35 becomes small, thereby reducing the sensitivity of the instrument.

The electronic fluxmeter is used to measure the drop-off in field at the edge of a gap. It is moved from inside the gap out over the edge. The function $\phi(t) = \phi_0(1 - bt^2)$ comes sufficiently close to representing the actual experimental curve to warrant a discussion. The purpose

of the discussion is to find out how large the fractional error s becomes.

Now

$$\frac{d\phi}{dt} = 2\phi_0 bt$$

and

$$s = \frac{1}{RC} \frac{\int_0^t 2bt^2\, dt}{bt^2} = \frac{2}{3}\frac{t}{RC}$$

It is possible to move the coil out of the gap in about 0.2 sec to a point where the field has dropped by 10 per cent. This means that

$$s = \frac{2}{3}\frac{0.2}{RC}$$

and if an error in measurement of not more than 2 per cent is wanted, then

$$RC = \frac{2}{3}\, 0.2\, \frac{1}{0.02} = 6.67 \quad \text{sec}$$

A reasonable and satisfactory value for RC then is approximately 7 sec.

2.2 Operation. The voltage output e(t) varies too rapidly with time to be recorded accurately by a moving-coil type of instrument. It may be recorded by photographing the screen of a cathode-ray oscilloscope as the signal is applied to the vertical plates.

A block diagram of the circuit used is shown in Fig. 2.3. The complete circuit drawings will not be shown here nor will the circuits be discussed in detail, since such a discussion is considered beyond the scope of this volume. Several points are of interest, however, and are noted here.

High gain in the d-c amplifier is necessary to translate a small change of flux into a satisfactory electron-beam deflection in the cathode-ray tube. Some drift of the output voltage of the d-c amplifier occurs as a result of (1) plate voltage variations, (2) variation in filament emission, and (3) thermal emf's in the search-coil circuit, in spite of all efforts to reduce these quantities to a minimum. The over-all maximum gain achieved in the last electronic fluxmeter built was several million.

Deflections resulting from changes of flux linkage in the search coil are calibrated by comparing them with deflections produced by the flux standard F (see Fig. 2.3) in series with it.

The search coil is connected mechanically with the moving contact of a potentiometer. The voltage across the potentiometer is amplified and fed to the horizontal plates of the oscilloscope so that the photograph of the oscilloscope gives the flux linkages as a function of position.

An electronic fluxmeter with a 9-in.-diameter cathode-ray tube is shown in Fig. 2.4. Beside the instrument is the camera holder that contains a Sept camera during operation. Figure 2.5 shows the fluxmeter with the camera holder in operating position. Figure 2.6 shows the electronic equipment contained within the chassis of the fluxmeter. Part of the equipment shown here is used in transforming an input signal from the sliding contact of a potentiometer to a horizontal-plate-deflection voltage in the cathode-ray tube.

2.3 Relative Merits. Desirable features of the electronic fluxmeter are:

1. A continuous record of flux change is achievable.
2. The electronic fluxmeter has no mechanical inertia to limit the recording of rapidly varying flux.
3. Any quantity associated with the change of flux may be plotted as a function of it on the cathode-ray screen.
4. The instrument is practically unaffected by vibration.

Undesirable features of the electronic fluxmeter are:

1. Accuracy is limited by (a) nonlinearity of the cathode-ray tube, (b) errors in photography of a curved screen, (c) nonlinearity of d-c amplifier, and (d) error in integration where the time constant is low for high sensitivity.
2. Considerable patience must be exercised and time consumed in correcting for and checking the drift of the instrument. Sometimes drift may occur during the time in which the flux change occurs, thus making necessary repeat measurements for checking purposes.

## 3. THE GENERAL ELECTRIC FLUXMETER[2]

Details regarding this instrument are available in the trade literature prepared by the General Electric Company. However, since the instrument has been used extensively in various magnetic measuring techniques applied in the Radiation Laboratory, it will be discussed in some detail here.

3.1 Theory. Consider a D'Arsonval galvanometer connected in series with a search coil. Let R be the resistance of the search coil,

galvanometer suspension, and armature, and suppose that the search coil has n turns of average effective area A. If the magnetic field H through the coil changes at a rate dH/dt, then the voltage developed by the coil is

$$\frac{nA}{10^8}\frac{dH}{dt} = \frac{\dot{\phi}}{10^8}$$

As the armature turns through an angle $\theta$ at the rate $\dot{\theta} = d\theta/dt$, the n turns of the armature cut through the magnetic lines of the field H of the galvanometer magnet. The number of cuts G made for an angle of 1 radian is $2Hnal$, where a is the average radius of the armature and $l$ is its length. Hence $G = 2Hnal = ng$, where $g = 2Hal = H$ times the area of a turn of the armature. The voltage developed in the circuit due to the turning of the coil is $(G/10^8)\dot{\theta}$.

If a current of I amperes flows in the armature the torque in dyne centimeters produced on the suspension is $2HnalI/10 = GI/10$. This follows from the fundamental law that the force in dynes on a conductor of length $l$, in a field H, carrying a current I, is $HIl/10$, where H is in oersteds, I is in amperes, and $l$ is in centimeters.

If L is the inductance in the circuit, then the voltage around the circuit must satisfy the equation

$$IR + L\dot{I} + \frac{G\dot{\theta}}{10^8} = \frac{\dot{\phi}}{10^8} \tag{38}$$

If J is the moment of inertia of the armature, N is the air damping and suspension friction of the armature, and $\psi$ is the torsion constant of the suspension, then the equation of motion of the armature is

$$J\ddot{\theta} + N\ddot{\theta} + \psi\dot{\theta} = \frac{GI}{10} \tag{39}$$

From Eq. 38

$$I = \frac{\dot{\phi}}{10^8R} - \frac{L}{R}\dot{I} - \frac{G\dot{\theta}}{10^8R}$$

Substituting for I in Eq. 39, it becomes

$$J\ddot{\theta} + \left(N + \frac{G^2}{10^9R}\right)\dot{\theta} + \psi\theta = \frac{\dot{\phi}G}{10^9R} - \frac{GL\dot{I}}{10R} \tag{40}$$

Now, if there is a steady torque T on the armature and a thermal or contact emf E, then Eq. 40 becomes

$$J\ddot{\theta} + \left(N + \frac{G^2}{10^9R}\right)\dot{\theta} + \psi\theta = T + \frac{\dot{\phi}G}{10^9R} - \frac{GLI}{10R} + \frac{EG}{10R} \tag{41}$$

Attached to the armature of the G. E. fluxmeter is a small permanent magnet oriented in opposition to the stray magnetic field of the fluxmeter magnet. The strength of the stray field can be altered by adjusting the position of two iron pads. When set properly, the effect of this addition is to cancel out the restoring torque of the suspension almost completely, so that $\psi = 0$. The constants of the armature are such that N is negligible with respect to $G^2/10^9R$. Equation 41 simplifies to the form

$$J\ddot{\theta} + \frac{G^2\dot{\theta}}{10^9R} = T + \frac{\dot{\phi}G}{10^9R} - \frac{GL\dot{I}}{10R} + \frac{EG}{10R} \tag{42}$$

If the boundary conditions are chosen so that $\theta$, $\dot{\theta}$, $\ddot{\theta}$, and $\phi$ are all zero when t = 0, then Eq. 42 when integrated becomes

$$J\dot{\theta} + \frac{G^2\theta}{10^9R} = \int_0^t T\,dt + \frac{\phi G}{10^9R} - \frac{GL}{10R}(I_t - I_0) + \frac{G}{10R}\int_0^t E\,dt \tag{43}$$

where $I_t$ = current at time t
$I_0$ = current at t = 0

If both T and E are constants, then Eq. 43 becomes

$$J\dot{\theta} + \frac{G^2\theta}{10^9R} = Tt + \frac{G}{10R}Et + \frac{\phi G}{10^9R} - \frac{GL(I_t - I_0)}{10R} \tag{44}$$

To see how this equation behaves in practice, the usual procedure for measuring a magnetic field will be set up.

The search coil is moved into a field and held there until the fluxmeter armature stops moving. Then the deflection is recorded. Before and after this process $\dot{\theta} = 0$. This is impossible if the two terms Tt and (G/R)Et are not zero. In order to make them zero a small voltage is introduced into the circuit of such a magnitude as to produce a current canceling out both of these terms. When this is done $I_t = I_0$, and the equation becomes

$$J\dot{\theta} + \frac{G^2\theta}{10^9R} = \frac{\phi G}{10^9R} \tag{45}$$

In operation the armature comes to rest before the reading is taken. This means that $\dot{\theta}$ is zero and that the sensitivity of the fluxmeter is $\theta/\phi = 1/G$.

Since the magnetic compensation is not perfect, T (the torque on the armature) changes with $\theta$. This is particularly troublesome because in practice it means that the instrument may show no drift at the beginning of an observation and then show considerable drift after the armature has rotated. Then it becomes difficult to decide when the motion due to the change in flux ceases and only a drift remains. From Eq. 42 it is apparent that the rate of drift due to T alone is

$$\dot{\theta} = \frac{10^9RT}{G^2} \tag{45a}$$

This comes from the second and third terms in Eq. 42 by setting all other terms equal to zero. For this drift to be small it is an advantage to have R small but more particularly to have G large.

If readings are to be made rapidly, then the armature must come to rest quickly after a deflection. The dynamic characteristics of the armature determine this behavior.

Assume that the armature has a rate of rotation of $\dot{\theta}$, that the self-inductance L is negligible, that there is no drift, and that N and $\psi$ are negligible. Then the equation of motion is

$$J\ddot{\theta} + \frac{G^2\dot{\theta}}{10^9R} = \frac{\dot{\phi}G}{10^9R}$$

Let the flux through the coil stop changing. Then $\dot{\phi} = 0$, and the equation becomes

$$J\ddot{\theta} + \frac{G^2\dot{\theta}}{10^9R} = 0$$

Let $\dot{\theta} = \dot{\theta}_0 \exp -Kt$. Then $\ddot{\theta} = -K\dot{\theta}$, and the equation becomes

$$-JK\dot{\theta} + \frac{G^2\dot{\theta}}{10^9R} = 0$$

or

$$K = \frac{G^2}{10^9 RJ} \tag{45b}$$

This satisfies the boundary condition that $\dot{\theta}_0$ is the rate of rotation of the armature at t = 0. It also means that if $\theta = 0$ at zero time, then

$$\theta = \int_0^t \dot{\theta}\, dt = -\frac{1}{K}\,\dot{\theta}_0 \exp(-Kt - 1) = \frac{10^9 RJ\,\dot{\theta}_0}{G^2}\left(1 - \exp\frac{-G^2 t}{10^9 RJ}\right) \tag{45c}$$

The time it takes for $1 - (\theta_t/\theta_\infty)$ to become a small quantity such as 0.001 may be determined from

$$\exp\frac{-G^2 t}{10^9 RJ} = 0.001$$

or

$$\exp\frac{G^2 t}{10^9 RJ} = 1000$$

or

$$\frac{G^2 t}{10^9 RJ} = 6.9$$

For a typical instrument, $G^2 = n^2 g^2$, g = 6450, n = 1170, J = 0.420, and R = 3600. Thus

$$\frac{G^2}{10^9 RJ} = 37.7$$

$$t = \frac{6.9}{37.7} = 0.186$$

and

$$\theta_\infty - \theta_t = \frac{\dot{\theta}_0}{37.7} \times 0.001 = 2.7 \times 10^{-5}\,\dot{\theta}_0$$

If $\dot{\theta}$ is the angular velocity of the armature resulting from a change of flux producing a 10-cm deflection in 0.1 sec, then 0.2 sec later the angular velocity of the armature will be $0.001 \times \frac{10}{100 \times 0.1} = 0.001$

radian per second, or 0.1 cm/sec. The subsequent deflection $\theta_\infty - \theta_t$ becomes $2.7 \times 10^{-3}$ cm, which is completely negligible.

The question of what advantages a more sensitive fluxmeter has over a less sensitive one arises. This involves the design of the search coil if the magnitude of the signal resulting from a particular magnetic field is of concern.

Two armatures with the following properties are compared: $g_1 = g_2$; $n_1 > n_2$; and $J_1 = J_2$. Armature 1 is wound with many turns of fine wire, and armature 2 is wound with a few turns of heavy wire. Let $S_i$ be the space occupied by the insulation, $S_c$ the space occupied by the copper, $W_i$ the weight of the insulation, and $W_c$ the weight of the copper. In order to simplify the argument, the assumption will be made that

$$\frac{W_{i_1}}{W_{i_2}} = \frac{W_{c_1}}{W_{c_2}} \qquad \frac{S_{i_1}}{S_{i_2}} = \frac{S_{c_1}}{S_{c_2}} \tag{46}$$

Let $\theta/\phi$ be defined as the maxwell-turn sensitivity. Then the maxwell-turn sensitivity is equal to

$$\frac{\theta}{\phi} = \frac{1}{ng} \tag{47}$$

This equation follows from Eq. 45 if $J\dot{\theta}$ is small compared to $(G^2\theta/10^9R)$.

Two search coils are designed to fit in a certain fixed volume. If it is assumed that Eq. 46 holds for the search coils and if the search coil for armature 1 is wound with $n_{S_1}$ turns and the search coil for armature 2 with $n_{S_2}$ turns, the maxwell turns delivered for the coils when they are inserted in a magnetic field of strength H will be $n_S A_S H$, where $A_S$ is the average area of the turns. Let

$$\frac{n_{S_1}}{n_{S_2}} = \frac{n_{A_1}}{n_{A_2}} \tag{48}$$

Then from Eqs. 47 and 48 the deflections produced in the two armatures will be

$$\theta_1 = \frac{n_{S_1} A_S H}{n_{A_1} g} = \frac{n_{S_2} A_S H}{n_{A_2} g} = \theta_2 \tag{49}$$

Let $R_A$ be the resistance of the armatures and $R_S$ be the resistance of the search coils. If $\rho$ is the resistivity of the copper, then the resistance of one turn becomes $r_S = l_S\rho/a_S$, where $l_S$ is the length of a turn and $a_S$ is the cross-sectional area of the copper. The resistance of the whole coil will be

$$R_S = \sum_{n=1}^{n=n_S} \frac{l_S\rho}{a_S} = \frac{\rho}{a_S} \sum_{n=1}^{n=n_S} l_S \tag{50}$$

but because of the assumptions of Eq. 46

$$\frac{a_{S_1}}{a_{S_2}} = \frac{n_{S_2}}{n_{S_1}} \tag{51}$$

If $\bar{l}_S$ is the average length of a turn, then $R_S = \frac{\rho}{a_S} n_S \bar{l}_S$. Therefore

$$R_{S_1} = \frac{\rho}{a_{S_1}} n_{S_1} \bar{l}_S \qquad R_{S_2} = \frac{\rho}{a_{S_2}} n_{S_2} \bar{l}_S \qquad \frac{R_{S_1}}{R_{S_2}} = \frac{a_{S_2}}{a_{S_1}} \frac{n_{S_1}}{n_{S_2}}$$

or

$$\frac{R_{S_1}}{R_{S_2}} = \frac{n_{S_1}^2}{n_{S_2}^2} \tag{52}$$

A similar argument holds for the ratio of the resistances of the armature windings. It follows from Eqs. 48 and 52 that

$$\frac{R_{A_1}}{R_{A_2}} = \frac{n_{A_1}^2}{n_{A_2}^2} = \frac{n_{S_1}^2}{n_{S_2}^2} = \frac{R_{S_1}}{R_{S_2}} \tag{53}$$

and

$$\frac{R_{A_1} + R_{S_1}}{R_{A_2} + R_{S_2}} = \frac{R_1}{R_2} = \frac{n_{A_1}^2}{n_{A_2}^2} = \frac{n_{S_1}^2}{n_{S_2}^2} \tag{54}$$

Now from Eq. 49, both instruments with their search coils have the same sensitivity. Drift and speed of deflection will be examined to determine which instrument gives the best performance.

From Eq. 45a the rate of drift due to a constant torque is $\dot{\theta} = 10^9 RT/G^2$.

Therefore

$$\frac{\dot{\theta}_1}{\dot{\theta}_2} = \frac{10^9 R_1}{10^9 R_2} \frac{G_2^2}{G_1^2} = \frac{n_{A_1}^2}{n_{A_2}^2} \frac{n_{A_2}^2}{n_{A_1}^2} \frac{g^2}{g^2} = 1 \tag{55}$$

The drift is independent of the choice of windings.

The speed of deflection depends only on the value of K in Eq. 45b. Therefore

$$\frac{K_1}{K_2} = \frac{G_1^2}{10^9 R_1 J} \frac{10^9 R_2 J}{G_2^2} = \frac{G_1^2}{G_2^2} \frac{R_2}{R_1} = 1 \tag{56}$$

Hence the speed of deflection is independent of the choice of windings.

The drift due to a constant electromotive force in the instrument is, from Eq. 42, $\dot{\theta} = 10^8 E/G$. Therefore

$$\frac{\dot{\theta}_1}{\dot{\theta}_2} = \frac{G_2}{G_1} = \frac{n_{A_2}}{n_{A_1}} \tag{57}$$

Hence the rate of drift due to a constant electromotive force is directly proportional to the sensitivity or inversely proportional to the number of turns on the armature.

3.2 Practical Considerations. If a search coil of many turns is used with a less sensitive instrument, then there are advantages which make it more desirable than a coil of few turns with a more sensitive instrument. These advantages are:

1. The resistance of the leads to the search coil and of standardizing mutual inductances in the search-coil circuits can be large.
2. Poorer contacts in the search-coil circuits can be tolerated.
3. The effective area of the search coil is large in comparison with the areas of loops in the leads. Not so much care is necessary in handling the leads.
4. The drift due to a constant thermal or contact emf is less for the many-turn armature.

All these advantages outweigh the disadvantages arising from the necessity of constructing a search coil of many turns of fine wire. Two disadvantages arise from using very fine wire: (1) the difficulty of winding the wire without breakage and (2) the larger proportion of the available area occupied by the insulation on the fine wire. This

alters the assumptions made in Eq. 46. One factor tends to cancel this effect. The resistance of the suspension itself is about 12 ohms. This 12 ohms is added to the resistance of the armature. For very sensitive instruments with few turns this becomes an appreciable proportion of the total resistance in the circuit and makes the instrument more sluggish.

For speed of operation a low value of J is important. As long as J is approximately 0.420 g-sq cm and $G^2/10^9RJ \approx 40$, readings can be made with an accuracy of 0.1 per cent in 0.3 sec. Motion pictures of the deflections of the fluxmeter prove that this is a reasonable speed at which to take readings.

Since drift is the most troublesome feature of a fluxmeter, the advantages of the low-sensitivity fluxmeter far outweigh those of the high-sensitivy fluxmeters for accurate, reliable measurements.

3.3 Operation. The fluxmeter circuit contains a search coil S, a compensating low-impedance emf unit E, a flux standard F, a shunting resistance A, a series resistance B, and an external lumped resistance K, as shown in Fig. 2.7. The unit E is also capable of providing a positive or negative voltage for zeroizing the fluxmeter. The shunting resistance A is used to change the sensitivity of the fluxmeter.

The fluxmeter responds only to the voltage between the points C and D across shunt A. The difference of potential is

$$E_{CD} = \frac{1}{10^8}\frac{d\phi}{dt} - IK \tag{58}$$

where I = current in amperes flowing through K ohms

The current I is

$$I = \frac{\frac{1}{10^8}\frac{d\phi}{dt}}{K + \frac{AB}{A+B}} \tag{59}$$

Thus

$$E_{CD} = \frac{1}{10^8}\frac{d\phi}{dt}\left[1 - \frac{K}{K + \frac{AB}{A+B}}\right] \tag{60}$$

The current i through the fluxmeter is

$$i = \frac{E_{CD}}{B} = \frac{1}{10^8 B} \frac{d\phi}{dt} \left[ 1 - \frac{K}{K + \frac{AB}{A + B}} \right] \tag{61}$$

The torque U on the suspension due to this current is

$$U = \frac{Gi}{10} = \frac{G}{10^9 B} \frac{d\phi}{dt} \left[ 1 - \frac{K}{K + \frac{AB}{A + B}} \right] \tag{62}$$

G has already been defined as torque per unit current.

The damping term (see Eq. 42) is $\frac{G^2}{10^9 R} \frac{d\theta}{dt}$, where R is the resistance of the fluxmeter circuit.

$$R = B + \frac{AK}{A + K} \tag{63}$$

The operation of equating damping and torque terms gives

$$\frac{G^2}{10^9 \left( B + \frac{AK}{A + K} \right)} \frac{d\theta}{dt} = \frac{G}{10^9 B} \frac{d\phi}{dt} \left( 1 - \frac{K}{K + \frac{AB}{A + B}} \right)$$

which yields

$$\frac{d\theta}{d\phi} = \frac{1}{G} \frac{A}{A + K} \tag{64}$$

The sensitivity of the fluxmeter is independent of the resistance B but can be altered by changing A. In practice it is important to keep K large when A is small. When this is done, contact resistances in the external circuit remain small in comparison to K, and changes in contact resistance have a negligible effect on the sensitivity of the fluxmeter.

The drift of the fluxmeter must be kept to a minimum. For deflections over 10 cm in length (see Sec. 3.4) there may be drift occurring while the reading is being made, even though initially the emf compensator E (see Fig. 2.7) may be adjusted perfectly. This phenomenon occurs since magnetic compensation is not perfect for all values of $\theta$, the angular deflection of the fluxmeter. The torque T (see Eq. 41) is a function of $\theta$.

3.4 Mounting. The light from an automobile headlight bulb L passes through a short-focal-length lens $C_1$ (Fig. 2.8). A narrow index line is drawn vertically across the front of lens $C_1$. The light is focused on the mirror M through the objective lens O, which is adjusted to focus the index line on the scale S. The scale is placed 50 cm from the mirror M and is drawn with black lines 1 mm apart on transparent lucite. The condenser lens $C_2$ covers 6 cm of the scale and focuses an image of mirror M on the objective lens of camera K. Readings can be made by visual observation of the scale, in which case lens $C_2$ is removed and the scale is 25 cm long, or the readings can be photographed by camera K. Positive film of low sensitivity, high contrast, and fine grain is used so that the room can be illuminated without affecting the film. A typical picture is shown in Fig. 2.9.

The camera is a Sept motion-picture camera using 35-mm film. By depressing the release a single frame is exposed, and the film is readied for the next picture. The release is depressed by a solenoid puller so that an exposure may be made by remote control. Views of the various parts of the fluxmeter are shown in Figs. 2.10, 2.11, and 2.12.

3.5 Relative Merits. The chief advantages of this instrument are:

1. The cycle of signal, deflection, and reading does not include resetting to zero unless the readings are so large as to go off scale.

2. The difference between the reading of the fluxmeter with the search coil at point A and the reading of the fluxmeter with the search coil at point B is dependent only on the change of flux linkage of the search coil between point A and point B under the achievable conditions of (a) the search coil being held at point B long enough (0.2 sec is sufficient) for the fluxmeter coil to come to rest and (b) the drift being held to a minimum. Condition a is easily achievable, but the fulfillment of condition b is more difficult. Slight amounts of drift due to changing thermal emf and imperfect magnetic compensation are always present. However, if a set of readings is taken quickly under favorable conditions (say 10 readings in 10 sec), the drift error can be made negligible.

3. The fluxmeter is reasonably insensitive to vibration (as compared with the ballistic galvanometer) because of the marine-type suspension. Adequate protection of the fluxmeter coil during transport is achieved by merely shorting it. Two operational disadvantages of the instrument are: (a) Magnetic compensation requires considerable patience and time although it is performed infrequently. (b) Drift must continually be checked and compensated for during a set of readings.

## 4. MAGNETIC BALANCE FOR MEASURING LOW PERMEABILITIES[3]

In order to measure the magnetic permeability of large sheets of stainless steel (a permeability that ranges from 1.003 to values in excess of 1.05), a magnetic balance was constructed. Figure 2.13 illustrates the principles involved. At one end of an equal-arm balance is a small horseshoe magnet of cobalt steel; at the other end is a coil which has a total area (i.e., the product of the number of turns and the average area of the turns) of approximately 5000 sq cm. This coil is in series with a 12-volt battery supply, a variable resistor, a milliammeter, and a single-pole single-throw switch and is placed 1 or 2 cm above a second permanent magnet.

In order to calibrate the balance, a solenoid was used to determine the permeability of several cylindrical samples of stainless steel, each sample being roughly 2 in. long and 0.5 in. in diameter. Symmetrically placed inside the large solenoid were two short coils 0.75 in. long; coil 1 had a total area of 15,614 sq cm and 4578 turns, and coil 2 had approximately the same area and 4506 turns. A bakelite cylinder 6-in. in length was machined to hold these coils securely in place, one coil fitting snugly into one end of the cylinder, the other coil into the other end. These two coils were connected in series with each other and with a ballistic galvanometer. The polarities of the two coils were such that the induced emf in one opposed that in the other, thus giving only a slight deflection of the galvanometer when the field of the solenoid was varied. Included in the galvanometer circuit was a flux standard for the purpose of calibrating the galvanometer. By comparing the galvanometer deflection for a given change in the magnetic field of the solenoid when the two bucking coils had no magnetic cores with the galvanometer deflection for the same change in the solenoid field when coil 2 had a core of stainless steel, the magnetic permeability of the stainless-steel core was obtained.

Figure 2.14 illustrates the two types of solenoid measurements that are involved.

In the derivation of the formula for the magnetic permeability the following terminology is employed:

$\phi_c$ = the line turns produced by the Cenco variable inductor.
$\phi_1$ = total flux turns for coil 1 (i.e., the product of the number of turns of coil 1 and the flux produced by the solenoid S).
$\phi_2$ = total flux turns for coil 2 with an air core.
$\phi_3$ = total flux turns for coil 2 with metallic core.
$A_1$, $A_2$ = the total areas of coils 1 and 2 respectively.
$A$ = the cross-sectional area of the stainless-steel sample.

$H$ = the magnetic field intensity at the center of the solenoid.
$N_2$ = the number of turns of coil 2.
$\mu$ = the magnetic permeability of the stainless-steel sample.
$\Delta A$ = the difference in the total areas of coils 1 and 2.
$d_c$ = the galvanometer deflection in centimeters produced by the flux standard.
$d_0$ = the galvanometer deflection for case I, when the solenoid field is reduced from H to 0.
$d_x$ = the galvanometer deflection for case II, when the solenoid field is reduced from H to 0.

For case I

$$\phi_1 = HA_1$$

$$\phi_2 = HA_2$$

$$\phi_2 - \phi_1 = H(A_2 - A_1) = H\,\Delta A = \frac{d_0}{d_c}\,\phi_c$$

For case II

$$\phi_3 = H(A_2 - AN_2 + A\mu N_2)$$

$$\phi_3 - \phi_1 = H\,\Delta A + AN_2H(\mu - 1) = \frac{d_x}{d_c}\,\phi_c$$

Therefore

$$H(\mu - 1)AN_2 = \frac{\phi_c}{d_c}\,(d_x - d_0)$$

And

$$\mu - 1 = \frac{\phi_c(d_x - d_0)}{AN_2Hd_c}$$

When, as was the case in this work, the field H of the solenoid is reversed rather than reduced to zero, a factor of 2 appears in the denominator of the final expression, giving

$$\mu - 1 = \frac{\phi_c(d_x - d_0)}{2AN_2Hd_c}$$

The error involved in disregarding the demagnetizing field produced by poles at the ends of the cylindrical samples was estimated and

found to be negligible for low-permeability cylinders having a length of 2 in. and a diameter of 0.5 in.

When the flux standard was set for 87,000 line turns, the galvanometer deflection was 5.30 cm. Thus $\phi_c = 87{,}000$; $d_c = 5.30$. Also $N_2 = 4506$ turns; and $H = 2.6$ oersteds.

The results of the measurements on three cylindrical samples are as follows:

Sample Permeability Measurements

| Sample | A, sq cm | $\lvert d_x - d_0 \rvert$, cm | $\mu - 1$ |
|---|---|---|---|
| 1 | 1.06 | 0.335 | 0.00267 |
| 2 | 1.11 | 0.555 | 0.00422 |
| 3 | 1.23 | 1.205 | 0.00803 |

The magnetic balance was adjusted to be slightly heavy at the end carrying the permanent magnet. The current $I_0$ is the least current through the balancing coil which will raise the magnet when no magnetic material is placed beneath the magnet. The currents $I_1, I_2, \ldots$, are then measured, these being the least currents that will raise the magnet when samples 1, 2, ... are placed beneath the magnet. The calibration curve consists of a graph of $I_1 - I_0, I_2 - I_0, \ldots$, against the values of the magnetic permeability of samples 1, 2, .... This curve is a straight line within the region considered (see Fig. 2.15). Some difficulty was encountered in obtaining a sample whose permeability was (1) greater than that of sample 3, (2) less than the upper limit measurable with the balance, and (3) uniform throughout the sample; but there is reason to believe that the calibration curve of the balance remains a straight line to values of the magnetic permeability at least as high as 1.05.

## 5. MAGNETIC STANDARDS

In the course of designing magnets and testing their performance, it is necessary to resort to the use of standards, the expected behavior of which can be calculated from geometrical considerations. In this section the various factors guiding the design of search-coil and flux standards will be discussed. Some standards found to be suitable for the type of work done in the Radiation Laboratory will be described briefly.

5.1 Search Coils.[4] The measurement of a magnetic field H by the inductive method generally involves the determination of the two fundamental quantities expressed in the formula

$$H = \frac{\phi}{A} \tag{65}$$

where A = effective area of the search coil employed in the measurement

$\phi$ = number of lines of flux through the coil

In all cases the physical size of the coil is assumed to be small enough that the average field strength in the volume occupied by it is the field strength at the center of it, within the experimental error associated with the measuring instruments. The search coil is usually wound on a small spool of bakelite, ivory, or lucite with many turns of fine wire. Effective areas of randomly wound coils may be calculated only approximately from geometrical considerations; consequently other methods are needed to calibrate coils to greater precision.

In one method, comparison of an unknown area with a known area is achieved quite easily through the use of standard coils, a very uniform magnetic field, and a rotatable coil mount. The standard coil of effective area S is rotated to balance inductively the search coil of effective area X, provided, of course, that S is greater than X. Let $\theta$ be the angle between the null position of the standard coil alone in the magnetic field and the null position of the standard coil in the series bucking combination. Then the effective area of the search coil is

$$X = S \sin \theta \tag{66}$$

If S is less than X, the standard coil is oriented normal to the magnetic field while the search coil is rotated to balance it inductively. In the latter case the effective area of the search coil is

$$X = S \csc \theta \tag{67}$$

Fine enameled copper wire wound on an accurately machined cylindrical form of bakelite or lucite in a single uniform layer represents the essential element of a search coil, the effective area of which can be determined to great precision from geometric considerations and simple calculations. Such a coil that is checked and cross-checked against similar coils by inductive means is suitable for use as a primary standard of area in a magnetic testing laboratory.

The effective area of a winding of N turns in a single cylindrical layer of mean diameter D is

$$A = \frac{\pi D^2 N}{4} \tag{68}$$

Here the mean diameter is measured along a line perpendicular to the axis of the cylinder through the center of the cylinder from center of wire to center of wire. As verified by practice, Eq. 68 holds true to at least 0.1 per cent accuracy when the diameter of the wire is small compared to the diameter of the cylinder.

Leads attached to the solenoidal winding of a standard coil are twisted as carefully as possible so as to be noninductive. Since the start and terminus of the winding are separated by the length of the solenoid, one loop is unavoidable. For all practical purposes, however, the plane of the loop can be aligned parallel to the magnetic field for normal operation.

Figure 2.16 shows a drawing of a circular solenoidal winding representative of the winding of a standard search coil. Figures 2.17a, 2.17b, 2.17c, and 2.17d show drawings of the component parts and of the assembly of a standard search-coil form. Holes to accommodate start and terminus leads are shown in Fig. 2.17a. After the coil is wound and the leads are attached and twisted, the winding protector of Fig. 2.17b is slipped over the spool. The end disk protector of Fig. 2.17c serves the twofold purpose of holding the winding protector in place and providing a protection for the twisted pair of leads coming out of the exit hole of the spool. The twisted pair is wrapped around the winding protector in the grooves provided and is held in place by an elastic band until it is needed.

Figure 2.18 shows two types of standard coils, one wound and calibrated, the other disassembled to show bakelite spool, lucite winding protector, and end disk protector. The winding and end disk protectors of the disassembled coil form are of a different type from that shown in Fig. 2.17, in that the end disk protector has a groove provided in it for the twisted pair of leads while there are no grooves cut in the winding protector.

In a second method, comparison of an unknown area with a known area is achieved quite easily through the use of a long solenoid with a centrally tapped, externally located secondary winding. The search coil to be calibrated is placed inside the solenoid under the centrally located secondary. It is connected in series bucking with the secondary, and the number of secondary turns is adjusted to give best inductive balance, i.e., a null reading when current is passed through the long

solenoid. The effective area of the search coil is then the product of the number of the secondary turns and the primary area. In this method the solenoid primary winding is the standard coil.

The mutual inductance[5] of the long solenoid and secondary shown in Fig. 2.19 is

$$M_0 = 4\pi^2 a^2 n_1 n_2 (\rho_2 - \rho_1) + \ldots \tag{69}$$

where

$$\rho_1 = \left[\left(\frac{x - l}{2}\right)^2 + A^2\right]^{1/2} \tag{70}$$

$$\rho_2 = \left[\left(\frac{x + l}{2}\right)^2 + A^2\right]^{1/2} \tag{71}$$

$$n_1 = \frac{N_1}{x} \tag{72}$$

$$n_2 = \frac{N_2}{l} \tag{73}$$

Only the first term of an infinite series is shown in Eq. 69. This equation may be written in another form,

$$M_0 = \frac{4\pi^2 a^2 N_1 N_2}{\rho_1 + \rho_2} + \ldots \tag{74}$$

with the aid of Eqs. 72 and 73 and the following mathematical reasoning:

$$\frac{\rho_2 - \rho_1}{x l} = \frac{\rho_2^2 - \rho_1^2}{x l(\rho_2 + \rho_1)} = \frac{\left(\frac{x + l}{2}\right)^2 - \left(\frac{x - l}{2}\right)^2}{x l(\rho_2 + \rho_1)}$$

$$= \frac{\frac{x^2}{4} + \frac{x l}{2} + \frac{l^2}{4} - \frac{x^2}{4} + \frac{x l}{2} - \frac{l^2}{4}}{x l(\rho_2 + \rho_1)} = \frac{1}{\rho_2 + \rho_1}$$

If A = a and $l$ = 0 then Eq. 74 becomes

$$M_0 = \frac{2\pi^2 a^2 N_1 N_2}{\left(\frac{x^2}{4} + a^2\right)^{1/2}} + \ldots \tag{75}$$

The mutual inductance of the long solenoid and inner search coil shown in Fig. 2.20 is

$$M_I = 4\pi^2 B^2 n_1 n_3 (\rho_4 - \rho_3) + \ldots \tag{76}$$

where

$$\rho_3 = \left[\left(\frac{x + m}{2}\right)^2 + a^2\right]^{1/2} \tag{77}$$

$$\rho_4 = \left[\left(\frac{x - m}{2}\right)^2 + a^2\right]^{1/2} \tag{78}$$

$$n_1 = \frac{N_1}{x} \tag{79}$$

$$n_3 = \frac{N_3}{m} \tag{80}$$

Equation 76 may be written in the form

$$M_I = \frac{4\pi^2 B^2 N_1 N_3}{\rho_3 + \rho_4} + \ldots \tag{81}$$

If m = 0, then Eq. 81 becomes

$$M_I = \frac{2\pi^2 B^2 N_1 N_3}{\left(\frac{x^2}{4} + a^2\right)^{1/2}} + \ldots \tag{82}$$

If $M_I = M_0$ then $\pi^2 B^2 N_3 = \pi^2 a^2 N_2$ or $\pi B^2 N_3 = \pi a^2 N_2$. The quantity $\pi a^2 N_2$ is the product of the area of the primary and the number of turns in the outside secondary.

The main design problem here is to determine how large the quantities A and $l$ can be and yet produce no appreciable error in the determination of the mutual inductance from Eq. 74. Constants of the primary which was constructed are:

X = length of primary = 95.95 cm
$N_1$ = number of turns in primary = 680 turns
a = mean radius of primary = 2.9566 cm
$n_1$ = turns per centimeter of primary = 7.0866 turns per centimeter

The primary was wound with 680 turns of No. 16 enameled copper wire on a threaded canvas bakelite tube. Constants of the secondary are:

$l$ = length of secondary = 6.00 cm
A = outside radius of secondary = 3.64 cm
$N_2$ = maximum number of turns = 4110 turns

Calculated quantities associated with the primary are:

H = magnetic field at center of solenoid = 8.902I oersteds
I = primary current in amperes
$P_A$ = primary area = 27.462 sq cm

Calculated quantities associated with the secondary are:

M = mutual inductance per turn = 0.024447 millihenry
$M_{max}$ = maximum M possible = 4110M = 100.48 millihenrys

With secondary constants of A = 3.64 cm and $l$ = 6.00 cm, the error in using Eq. 74 in the determination of the mutual inductance is less than 0.05 per cent.

The apparatus is shown in Fig. 2.21. The turns of the secondary winding B about the long solenoid A are adjusted by means of the four dials on the control box D. The search coil is placed inside the primary A, just under the secondary winding B, by means of the coil holder C.

Figure 2.22 shows the coil holder C in greater detail. The leads of the search coil are inserted into the jaws of the gold-plated clamps F and are held in place as the clamps are tightened by the screws E. The search coil and secondary winding are placed in series bucking with a Leeds & Northrup type R galvanometer as indicated in Fig. 2.23, while the turns of the secondary winding are adjusted to give the smallest galvanometer deflection possible as the current is turned on or off in the primary of the long solenoid.

The effective area of the search coil in turn-square centimeters for perfect balance is 27.462 times the number of turns indicated at the control box.

5.2 Flux Standards.[6] The quantity $\phi$ in Eq. 65 is usually determined by comparing the deflection it produces in an instrument with the deflection a flux standard produces in the instrument. Let the flux linkage $\phi$ of a search coil with effective area A in a magnetic field H be reduced to zero, yielding an instrument deflection d. The instrument is calibrated by means of a flux-linkage standard. A deflection $d_s$ is produced by a flux-linkage change $\phi_s$. If the quantity $\phi_s/d_s$ is constant throughout the range of the instrument then

$$\frac{\phi}{\phi_s} = \frac{d}{d_s} = \frac{AH}{\phi_s} \tag{83}$$

In general, however, the instrument will depart from linearity. Then Eq. 83 cannot be assumed. In such cases the situation is improved by bracketing the deflections d with flux-standard deflections $d_s$ and making linear interpolations or plotting a calibration curve for the instrument.

One type of flux standard illustrated in Figs. 2.24 and 2.25 (type I) consists of a tapped coil that is movable from positions of maximum to nearly zero flux linkage with a 5-in.-long cylindrical Alnico bar magnet. Coil A, with 10 resistance-compensated taps, is dropped from position 1 to position 2 under the action of gravity as the release mechanism is operated. The range of flux values covered by this type of instrument is indicated by a few characteristic values:

Flux standard OS
- Tap 1 16,500 line turns
- Tap 10 164,100 line turns

Flux standard JB
- Tap 1 248,000 line turns
- Tap 10 2,527,000 line turns

A second type of flux standard (type II) consists of a rotatable coil in the gap of a fairly large Alnico permanent magnet. Stops are provided so that each successive angular throw of the coil changes its flux linkage with the magnetic field in approximately equal increments. Three different views of this type of flux standard are shown in Figs. 2.26a, 2.26b, and 2.26c. The arm A is connected by the shaft F through the circular board G and the yoke of the magnet to the coil B. The shaft rotates the coil in the gap formed by the two Alnico pole pieces C. Stops D determine the angular throw of the coil. The range of flux covered by this second type of flux standard is 189,000 to 3,290,000 line turns.

Both of these standards are calibrated by comparing their deflections in an instrument with deflections produced by a standard mutual inductance in the same instrument. Figure 2.27 shows the standardizing circuit. Deflections produced by flux changes in the standard are matched by deflections produced by the mutual inductance for current changes in the primary after trial-and-error adjustment of the current. The current is measured with a Leeds & Northrup type K1 potentiometer across a standard shunt. When deflections are matched, the value of the secondary standard line turns is given by

$$\phi = 10^5 Mi \qquad (84)$$

where **M** = mutual inductance of the standard in millihenrys
i = current change in amperes

The probable error in calibrating the secondary standards may be predicted from the error formula

$$X = \pm\sqrt{X_1^2 + X_2^2} \tag{85}$$

where $X_1$ = error in calibration of the standard mutual inductance (±0.25 per cent)
$X_2$ = error in matching deflections (±0.25 per cent)

The value of X is 0.35 per cent, which is verified in practice.

## 6. PROCEDURES FOR OBTAINING MAGNETIZATION CURVES

The problem here is to measure the absolute magnetic field intensity in the gap of a magnet as a function of the current flowing in the exciting coils. The method is to record the change of the flux linkage of a search coil in the magnetic field with a ballistic galvanometer or fluxmeter. Four ways of doing this are:

1. While a current is flowing in the exciting coils of the magnet the search coil is pulled out of the gap. The current is then turned off.
2. The search coil is held stationary in the gap while the exciting current is reduced to zero.
3. The search coil is held stationary in the gap while the magnet current is increased from zero to the selected value.
4. While the current is held constant, the search coil is rotated through 180 deg.

Of the procedures listed, the most satisfactory choice is dependent on the magnet characteristics and the type of instrument employed in the measurement.

Suppose that a large d-c generator supplies the exciting current I for the magnet. The current is turned on and off by the breaker shown in Fig. 2.28. The size of the current is varied by means of the rheostat and switch in the field-coil circuit of the generator. The current to the magnet is reduced by lowering the generator field and is finally turned off by opening the breaker. The time of rise of I is, of course, dependent on the values of resistance and inductance in the circuit. Figure 2.28 shows a schematic drawing of the control circuit.

6.1 Ballistic Galvanometer Method. In Fig. 2.29 search coil S is placed in series with a ballistic galvanometer G, variable resistance R, flux standard F, and switch SW. The ballistic galvanometer frequently employed in obtaining magnetization data is a Leeds & Northrup type P reflecting galvanometer with a sensitivity of approximately 100,000 maxwell turns per centimeter of deflection and a 30-sec

period. The external circuit resistance R is adjusted to give the most satisfactory galvanometer damping characteristics. The function of the damping switch D is to provide a means of either shorting out an unwanted signal from the search coil or of overdamping the movement of the galvanometer coil. The switch SW opens the galvanometer circuit. Under the condition of open circuit the galvanometer coil rotates more rapidly than it does under the condition of a low resistance load, a feature which is utilized in resetting to zero.

6.2 General Electric Fluxmeter Method. In Fig. 2.30 search coil S is placed in series with a G. E. fluxmeter G, a thermal electric compensator E, a flux standard F, and a resistance K. The fluxmeter usually employed in obtaining magnetization data is a G. E. type 92 fluxmeter with a sensitivity of 67,000 maxwell turns per centimeter of deflection. In cases where the shunt A is not necessary for reduction of sensitivity, K (the lumped external resistance) is kept as low as possible to hold drift to a minimum.

## 7. MAGNETIZATION CURVES ON MODEL MAGNETS

The current densities in the exciting coils of model magnets are extremely high, sometimes reaching 20,000 amp/sq in. The insulation begins to burn after the current has been on for 20 sec, so the usual time is limited to about 10 sec.

Of the four procedures listed above, only the first one is suitable for use with the ballistic galvanometer. The signal to the ballistic galvanometer is short, and the magnet current is flowing just long enough for the operator to adjust it, read it, and reduce it to zero. Personnel needed are a galvanometer operator, a current operator, and a person to pull the search coil out of the gap of the model magnet.

While all four procedures are possible with the G. E. fluxmeter, the second one is considered most satisfactory. The residual field, though not taken into consideration by this procedure, is usually negligible. Personnel needed are a fluxmeter operator and a current operator. Because this method is now most frequently employed, the cycle of operation will be described in detail with the aid of Fig. 2.30. Either photographic or visual readings are possible.

First the breaker is closed; then the generator field current i is turned on and adjusted with the rheostat so that the desired value of I is obtained. The fluxmeter operator records his reading upon receipt of a signal from the current operator, or the current operator can take a picture of the fluxmeter reading by depressing the camera release. The fluxmeter operator must keep a close check on the drift of the instrument. To reduce I to zero, the current operator opens

the switch in the generator field circuit, waits until I drops to about one-tenth its peak value, and then opens the breaker. The final reading is recorded either visually or photographically by the fluxmeter operator. This has to be done by the fluxmeter operator because of a small drift which always appears after the current is turned off. Recording of the reading is done after all drift has ceased.

## 8. MAGNETIZATION CURVES ON FULL-SCALE MAGNETS

Flip coils are used for full-scale magnet measurements, other methods in general not being practical. Two kinds of flip-coil mounts are shown in Fig. 2.31 (type I) and Fig. 2.32 (type II). Referring to Fig. 2.31, level indicators and adjusting screws are denoted by A and B respectively. Variation in sensitivity is accomplished through selection of search coils of suitable areas or by varying the angle of throw. [In accurate determinations of the absolute magnetic field intensity, only angular throws of 180 deg are considered satisfactory. Of course, angular throws less than 180 deg permit fairly accurate magnetic field intensity determinations, but the protractor scale was really provided for cases in which the search coil is employed as a bucking coil in uniformity measurements.] The protractor can be read to 0.1 deg.

A type II mount is shown in Fig. 2.32. The square rod A that holds the flip-coil support B is oriented perpendicularly to the magnet pole pieces by means of the leveling screws C. The whole unit is wedged in place by partially unscrewing the square rod from the base and locking it. A set of square rods is provided for gaps of various widths. The setscrew F clamps A to B at the proper location.

## 9. UNIFORMITY MEASUREMENTS ON MODEL MAGNETS

The magnetic field in the calutron must be uniform over a certain well-defined region, as indicated in the discussion in Chap. 1. The measuring apparatus must be capable of detecting changes in the magnetic field of 0.1 per cent. Usually the largest changes amounted to about 5 per cent of the field. Hence the maximum deflection of the instrument should amount to 5 per cent of the field.

The general procedure used is as follows: The magnet is excited by the circuit shown in Fig. 2.28. During a run the operator holds the exciting current as constant as possible. Variations of 1 per cent in the current during a run are not uncommon and make it necessary to use a technique which reduces to a minimum the effect of variations in the exciting current. In order to accomplish this, two coils S and T are used, connected in series bucking (Fig. 2.33). Coil T is usually

slightly larger in effective area than the moving coil S. At the beginning of a run, coil S is placed in the center of the gap as shown in Fig. 2.33, and the bucking coil T is fixed at some convenient point in the gap. Then the exciting current is turned on and off. If the fluxmeter deflects, the bucking coil is tilted or a shunt is placed across it and adjusted until no deflection occurs. Once this adjustment is made a run can be started. The moving coil is drawn out of the magnetic field, and the corresponding deflections of the fluxmeter are recorded as a function of the position of the moving coil. The deflections of the fluxmeter correspond to the difference between the magnetic field at the starting point and the magnetic field at the other points covered by the motion of the coil. A 1 per cent change in the exciting current produces an error of only 1 per cent in the changes in the magnetic field.

9.1 Search Coils.[4] The search coil S must be very small so as to measure the magnetic field at a point rather than to average it over an area. It was desirable to know the magnetic field accurately to within 0.5 in. on the full-scale magnet. This corresponded to $\frac{1}{32}$ in. on the models. The smallest search coils measured 0.15 in. in height and 0.20 in. in diameter, contained about 2000 turns of No. 46 wire, and had an effective area of about 350 sq cm. A careful check of typical runs showed that the measurements were accurate to $\frac{1}{32}$ in. in spite of the size of the coil. Errors in placing the coil in the gaps of the model magnet were kept to less than $\frac{1}{64}$ in.

9.2 Electronic-fluxmeter Method.[1] The electronic fluxmeter is especially suitable for uniformity runs because of its extremely short operational cycle and its ability to deliver a continuous record of flux change with distance. Figure 2.33 shows a schematic drawing of the electrical circuit employed in this method.

As the search coil moves from position A to position X along the straight line AX, the contact C slides along the potentiometer. The varying voltage from the potentiometer is amplified and applied to the horizontal plates of the cathode-ray tube. The electron beam is deflected an amount proportional to this voltage or to the distance AX.

Figure 2.34 shows two uniformity runs (the unmarked uniformity run is a repeat run) complete with horizontal fiducial lines and horizontal- and vertical-sweep calibrations. The picture, taken by a Sept camera on 35-mm film, was enlarged to give the photograph shown as Fig. 2.34.

Figure 2.35 shows the apparatus employed in moving the search coil along any prescribed straight-line path in the gap of a model magnet. Search coil A attached to the pantograph B follows the path of the stylus C in the stylus guide or potentiometer D. The frame of reference represented by the fixed scales E may be adjusted parallel to

any chosen frame of reference in the gap of the model magnet by means of adjusting screws F. Pantograph holder G and the board enclosing the frame of reference E are rigidly attached to the base plate H, and adjustment in the direction of the magnetic field is possible by loosening the clamp screws I and moving the base plate H with respect to the fixed base plate K. Movable scale L or M, to which is attached the stylus guide, is fastened either horizontally or vertically to the frame of reference E. (M is longer than L since the scales E form a rectangle.) A pair of movable scales L and L′ or M and M′ (not shown) is necessary for diagonal runs.

Figure 2.36 is a close-up view of the stylus guide or potentiometer holder shown in Fig. 2.35. Stops O and P (Fig. 2.36) determine the starting point and the length of uniformity run being made. The operator moves the search coil quite rapidly through a distance determined by the stops by means of the arm R. Horizontal-sweep stop screws N with retrieving springs are located 0.5 in. apart in the brass bar Q. For convenience, usually the stylus guide is adjusted with respect to the movable scale L, and the stops are adjusted with respect to the operating arm R, so that the start of a run corresponds with a stop position determined by one of the screw heads.

The oscilloscope deflection is not linear, and the voltage from the sliding potentiometer is not linear. Therefore it is necessary to calibrate each photograph. The stops N in Fig. 2.36 are used to calibrate the photographs. The steps followed are as follows: The camera shutter is opened, and the coil is then placed at its starting point. The spot on the oscilloscope is swept vertically across the scope making the first vertical line 0.0 (Fig. 2.34). The first stop N is depressed, and the arm R is moved up to the stop. The coil has then moved 0.5 in. The spot on the oscilloscope is swept vertically across the scope as before, making the second vertical line 0.5. This is repeated until the set of vertical lines is complete.

Horizontal fiducial lines are made by shorting the input to the fluxmeter and moving the arm R rapidly through its excursion back to the starting point. This is done while the magnet is excited. As soon as the coil reaches its starting point, the input is unshorted and the coil is swept back through its run.

Vertical-sweep calibrations (Fig. 2.34) are performed by photographing the deflection produced by the flux standard. This amounts to 2.43 in. for 82,800 maxwell turns. This is done twice on each record. The cycle of operation employed in obtaining the record shown in Fig. 2.34 will be described by the listing of the following steps:

1. The magnet current is turned on and held steady.
2. The camera shutter is opened.

3. The horizontal fiducial line is made by moving the search coil rapidly from position 3.0 to position 0.0 with vertical input to the fluxmeter shorted.

4. A run is made by moving the search coil from position 0.0 to position 3.0 very rapidly. The pause at 0.0 in steps 3 and 4 is just long enough to permit the vertical input to be unshorted.

5. The magnet current is turned off.

6. The horizontal-sweep calibration is performed by sweeping the electron beam across the fluorescent screen for each coil position 0.0, 0.5, . . . , 3.0.

7. Vertical-sweep calibration is performed by photographing the flux-standard deflections at positions 0.75 and 2.25. Overexposure is avoided through use of an auxiliary external shutter, the operation of which does not advance the film to a new frame.

8. Steps 1, 3, 4, and 5 repeated in order yield a repeat run.

9. The camera shutter is closed.

The 0.5, 1, 2, 3, 4, and 5 per cent field-variation points are determined from the formula

$$\frac{\Delta H \times 100}{H_0} = \frac{\phi_s}{d_s}\frac{d_s}{AH_0} \times 100 \qquad (86)$$

where $\Delta H$ = change of field strength in coil in oersteds
$H_0$ = field strength at start of run = 6300 oersteds
$\phi_s$ = flux standard value = 82,800 maxwell turns
A = effective area of coil = 351.4 turn-sq cm
$d_s$ = fluxmeter deflection recorded = 2.43 in.
d = fluxmeter deflection that corresponds to A $\Delta H$

On the diagram in Fig. 3.34, the sensitivity of the fluxmeter is $\frac{82{,}800 \text{ maxwell turns}}{2.43 \text{ in.}}$ = 34,100 maxwell turns per inch or 13,420 maxwell turns per centimeter. Since the thickness of the trace (heavy part) is about 0.06 in. the data are resolvable to at least

$$\frac{34{,}100 \times 0.06 \times 100}{351.4 \times 6300} = 0.09 \text{ per cent}$$

change of magnetic field.

Figure 2.37 shows a search coil with effective area of 351.4 turn-sq cm mounted in its holder.

9.3 General Electric Fluxmeter Method.[2] The G. E. fluxmeter is especially suitable for uniformity measurements on model magnets

when the search coil is moved in steps from one point to another in the magnetic field. At the end of each deflection the torques on the moving element are in equilibrium, a property not characteristic of either the electronic fluxmeter or the ballistic galvanometer.

Figure 2.38 shows the circuit employed in this method. The circuit is identical with the circuit shown in Fig. 2.30 except for the bucking coil B and the shunting resistor R across it.

Figure 2.39 shows the small search coil A mounted on one end of the pantograph B. The other end is attached to a rack C, which is moved by a one-tooth pinion E, shown in Fig. 2.40. This pinion moves the pantograph arm during 180 deg of revolution, and for the remaining 180 deg the arm and the coil remain stationary. The pinion is rotated by means of a flexible cable D and a small crank F (Fig. 2.41). A cam integral with the crank closes a microswitch G while the coil is stationary. The microswitch excites the solenoid puller for the Sept camera, and the fluxmeter is photographed (Fig. 2.42).

A clamp placed on the rack limits the travel to the required number of steps. The check readings are made by manually pushing the rack back and forth between the end stops and photographing the readings by the manually operated switch C′.

Typical constants are as follows:

| | |
|---|---|
| Effective area of search coil | 200 turn-sq cm |
| Diameter of search coil | 0.20 in. |
| Height of search coil | 0.15 in. |
| Sensitivity of fluxmeter | 67,000 maxwell turns per centimeter |
| Cyclotron field strength | 15,000 oersteds |
| Deflection for 0.1 per cent or 15 oersteds | 0.45 mm |

Since the readings are photographed they can be read with an accuracy of 0.1 mm. This corresponds to a change in the main field of 0.025 per cent. Errors due to drift amount to about 0.1 mm. The resistance of the search coil is about 500 ohms, and a fluxmeter of twice this sensitivity could be used with no loss in the speed with which readings can be made. However, as pointed out in the discussion of the theory of the fluxmeter, drift due to spurious electromotive forces would be increased, and the added care necessary makes the present arrangement probably the most satisfactory. Flux-standard readings are made on the same film, and each run is performed twice as a check.

## 10. UNIFORMITY MEASUREMENTS ON FULL-SCALE MAGNETS

Two handicaps encountered in performing uniformity measurements associated with small geometry and unsteady current conditions in model work are not present in full-scale work. First, it is easier in full-scale magnets to satisfy the criterion that the average magnetic field in the space occupied by the search coil is the magnetic field at the center of it, within the experimental error associated with the instruments. This fact makes possible construction of physically larger search coils with low resistances and large effective areas and employment of less sensitive flux-recording instruments. Secondly, magnet-current regulation, being possible to at least 0.1 per cent because of oil cooling of the magnet coils, permits long and extensive measurements under the conditions of time-invariant magnetic fields.

In general, apparatus designed to move the search coil along a prescribed path in full-scale work is bulky and hence time-consuming in setup. Sometimes it must be designed for use in vacuum in order to disclose information that may be influenced by movement of magnetic components under atmospheric pressure. Occasionally an accurate description of the shape of the lines of force in a localized region is required. In order to meet the general demands of full-scale uniformity measurements, three types of apparatus were developed.

10.1 Contour-mapping Device. Figure 2.43 shows the search coil, flip coil, and bucking coil in a conventional G. E. fluxmeter circuit like the circuits shown in Figs. 2.30 and 2.38. During the time the measurements are being carried out, the flip coil (see Fig. 2.32) is held stationary in the field after it has been used to establish the operating field $H = H_0$.

Suppose the search coil starts from a point A where $H = H_0$ and moves to a point P where $H = 0.99H_0$. Then the fluxmeter deflects an amount d which corresponds to a 1 per cent change of field strength. The locus of P where $H = 0.99H_0$ is the 1 per cent contour line. As the search coil moves along this contour line no fluxmeter deflection occurs.

In Fig. 2.44 an image of the collimating slit A appears on the scale B as light originating from bulb C passes through the collimating slit and the focusing lens D and is reflected from the fluxmeter mirror E. A photocell F located at the center of the scale receives light and generates a signal as long as the fluxmeter is reading mid-scale to within the width of the image of the collimating slit.

Figure 2.45 shows the search coil in the magnetic field to be explored. It is mounted on a lucite base which is separated from a metal

sheet by tracing paper. Figure 2.46 shows the output of the induction coil connected across the metal sheet and a wire tip just beneath the center of the search coil. Legs with rounded tips are provided in order that the lucite mount might be moved easily and smoothly about on the tracing paper. Whenever the image of the collimating slit falls on the photocell, sparking occurs through the tracing paper from the wire to the metal plate.

If the fluxmeter zero, for the search coil located in a field of strength $H = H_0$, is set at a deflection distance d that corresponds to a 1 per cent change of field, when the coil is moved to the 1 per cent contour a spark will jump from the wire through the paper to the metal sheet, leaving a hole burned in the paper. Other points on the 1 per cent contour can be obtained by trial and error until enough are obtained to show a smooth continuous curve. The 2 per cent contour line is obtained in a similar fashion except that the coil starts from the 1 per cent contour instead of from the uniform field.

A simple method will now be described for obtaining fluxmeter deflections that correspond to the 0.5, 1.0, 2.0, 3.0, 4.0, etc., per cent changes of field. The field strength in the gap of a magnet as measured with a flip coil is

$$H_0 = \frac{\phi_s}{d_s} \frac{d_f}{2A_f} \tag{87}$$

where $\phi_s/d_s$ = line-turn sensitivity of the fluxmeter
$d_f$ = deflection of the fluxmeter for a 180-deg flip
$A_f$ = effective area of the flip coil

The difference in the field strengths between two points in the nonuniform field as measured with the search coil is

$$\Delta H = \frac{\phi_s}{d_s} \frac{d}{A} \tag{88}$$

where d = deflection of the fluxmeter that follows as a result of translating the search coil from one point to the other
A = effective area of the search coil

The per cent change in field strength between the two points under consideration is

$$\frac{\Delta H \times 100}{H_0} = \frac{d}{d_f} \frac{200A_f}{A} \tag{89}$$

Suppose the condition is imposed that $d = d_f$ for a 1 per cent change of field. Then $A = 200A_f$. This condition can be realized quite easily by adjusting the turns of the search coil.

Operation of the contour-mapping device is described by the listing of the following steps:

1. After the search coil is located in the uniform field, the fluxmeter zero is adjusted to mid-scale. Sparking occurs.
2. A deflection corresponding to 0.5 per cent change of field occurs as the flip coil is turned through 90 deg.
3. The search coil is moved to the 0.5 per cent contour. Sparking occurs if the polarity of the search coil is correct.
4. The operator who moves the search coil hunts for additional points on the 0.5 per cent contour.
5. The 0.5 per cent contour is checked frequently against the deflection produced by the 90-deg throw of the flip coil.
6. As soon as enough holes are burned in the paper to distinguish the contour line, the operator returns the search coil to the uniform field.
7. A deflection corresponding to 1 per cent change of field follows as the flip coil is turned through 180 deg.

The process continues until all the contours desired are plotted. Frequent check of drift is made as well as check of calibration.

Typical constants are listed as follows:

$A = 20{,}000$ turn-sq cm
$A_f = 100$ turn-sq cm
$\frac{\phi_s}{d_s} = 67{,}000$ line turns per centimeter of deflection
$H_0 = 3000$ oersteds

From Eq. 87

$$d_f = \frac{2 \times 100 \times 3000}{67{,}000} = 8.96 \text{ cm}$$

Thus the deflection d for 1 per cent is $d = d_f = 8.96$ cm. The resolving power of the photocell is about 0.30 cm or $(0.30/8.96) \times 1 = 0.03$ per cent change of field.

10.2 Boxcar Technique. The circuit employed is the conventional circuit containing search coil, bucking coil, flip coil, G. E. fluxmeter, thermal emf compensator, and flux standard. Point-by-point determination of the uniformity of the magnetic field along straight lines is accomplished by moving a car supporting the coil in steps along a

track. Readings are photographed by closing a microswitch just before moving the coil each time.

Figure 2.47 shows a knurled knob A on the end of a long shaft on which are mounted many stops. Car C is moved along the track away from the operator by pulling line D, or it is moved along the track toward the operator by pulling line E. In the photograph a small clockwise motion of the knurled knob would cause a stop to be rotated into position. At that point a tooth-and-gear arrangement prevents further motion of the knob A. Now line D is pulled, and the car moves the distance between stops of 1 in. To obtain further motion of the car, the operator of the device must push down on the machine screw H that depresses the microswitch I to permit further rotation of the knurled knob. Depressing the microswitch sends a surge of current through the solenoid puller that operates the camera release. After the knurled knob is rotated to the next position set by the tooth-and-gear arrangement, the car may be moved another inch and so on. It is possible to turn the knurled knob to a position where the car can be moved along the entire length of the track without stopping for resetting purposes.

10.3 Mercury-arc Tube. Figure 2.48 shows a sketch of a mercury-arc tube that can be used to determine the shape of the lines of magnetic force in a localized region. Electrons emitted from the filament A are accelerated by the anode B to form a diffuse glow in the evacuated glass tube C. The glow occurs as the electrons, bombarding atoms of mercury vapor arising from the mercury drop D, excite them into radiation.

When the tube axis is located along a magnetic field the diffuse glow sharpens into a tight beam, the cross section of which has the shape of the hole in the anode, with very sharp boundaries. This phenomenon occurs since the electrons initially directed along the axis of the tube cannot travel perpendicular to the lines of force. Deviation of the lines of force from a straight line perpendicular to the pole pieces from which the magnetic field emanates can be plotted from readings taken on a cathetometer.

## 11. STRAY-FIELD MEASUREMENTS

Fairly extensive measurements of stray fields of model magnets are necessary to determine forces on ferromagnetic materials located near the full-scale prototype. For example, the question of how much the reading of an ammeter is affected a given distance away from the magnet may arise. In some cases only the direction of the stray field is required. A satisfactory answer to the problem lies in the deter-

mination of both magnitude and direction of the magnetic field at each point in question.

Fine iron filings located on a horizontal sheet in the stray field around a model magnet will arrange themselves along the lines of force if the sheet is gently tapped and will produce a satisfactory pattern in a range limited by the rate of change of the magnetic field. In a region of sharp corners in the iron filings, a gap in the pattern occurs because the iron particles are pulled to the iron and accumulate there. However, stainless-steel filings (being slightly magnetic) sprinkled in this area will arrange themselves along the lines of force without accumulation. Stray-field patterns, altered by changes in magnet current, must be obtained for each operating condition.

A white sheet of paper mounted on a horizontal board that fits the contours of the model magnet provides an excellent background for the filings in photography. However, since the usual photographic process includes formation of an image on film, development of the negative, and enlargement, the record is not immediately available. An alternative method has been developed for obtaining a permanent record of an iron-filing pattern.

A large sheet of sensitized paper (Bruning B and W direct-printing black-line paper) is placed on the horizontal board in subdued light. After the magnet current is adjusted and held steady, the sheet is gently tapped so that a pattern of stainless-steel and iron filings is formed. Flood lamps are turned on for approximately 10 sec and then turned off, leaving the sensitized paper in subdued light again. The magnet current is turned off, and the iron-filing pattern rearranges itself to a pattern characteristic of a low field. As soon as the sensitized paper is cleared of filings, it is rolled up, taken to a blueprinting machine, developed, and dried in a few minutes. It is then available as an aid in obtaining stray-field intensity measurements.

Normal procedure called for making field-strength measurements with a search coil and G. E. fluxmeter while the permanent filing pattern record is in place. Normally a stray-field run is made along a straight line. In all cases the search coil is oriented at the time of reading with the plane of its effective area normal to the lines of force. While the magnet current is held steady, the search coil is flipped at a number of positions in succession along the straight line until the run is completed. All pertinent data are written on the record, including the calculated magnetic field intensities.

## 12. MAGNETIC TESTS IN PROCESS TANKS

Before the first race track in the Alpha plant was put into operation, tests of the magnetic field were made to determine whether the theo-

retically specified fields were obtained (see Division I, Volume 4, of the National Nuclear Energy Series). Two regions of the tank were investigated, namely, the regions between the linear shims and the region of the source. Two magnetic measuring devices[7] were designed especially to afford rapid magnetic surveys of these regions of the tanks. These devices will be referred to as the "shim-region device" and the "source-region device." The equipment was designed and built at the Radiation Laboratory and shipped to Oak Ridge in the summer of 1943 for the tests. The tests were carried out by Radiation Laboratory personnel with the assistance of the personnel from Tennessee Eastman Corporation and Stone & Webster Engineering Corporation. No attempt will be made to go into detail regarding the mechanical construction of these devices. However, the component parts of each piece of equipment and the function of each part will be considered briefly. In the discussion a rectangular coordinate system will be used, with the X axis in the direction of the source-receiver line, the Z axis in the direction of the homogeneous magnetic field, and the Y axis directed into the tank.

12.1 Shim-region Device. This device consisted essentially of three component parts, arcs of coils, a flip coil, and a roving coil. All these parts were attached rigidly to a faceplate in order to allow their use with the tank under vacuum. In practice the tank needed only to be pumped down to a fraction of a pound per square inch in order to carry out the measurements. At this pressure the shims are essentially in the position they assume under operating conditions.

Actually there were three arcs of coils located in the median and the Z = ±8 in. planes, respectively, of the tank (Z = 0 is taken in the median plane). Each arc of coils consisted of 30 coils that were arranged at equal intervals in X along the arc of a circle of radius 48.15 in. (see Fig. 2.49). The supporting mechanism was so arranged that these arcs of coils could be moved as a unit in the Y direction. In the initial position the circles of coils passed through the source and the receiver locations since the diameter of the circles was equal to the distance between these positions. Each coil had its axis parallel to the Z axis, and all the coils in any one arc were connected in series with a galvanometer, so that when the coils cut the magnetic flux a measurement of this change was given by the galvanometer reading.[6] The range of positions of the arcs of coils in a tank is indicated in Fig. 2.49. The entire unit could be moved in the Y direction by means of an external motor control in jumps of 0.8 in. Each arc of coils was moved from its zero position into the tank, a total of 31 or 32 jumps, and the galvanometer reading corresponding to each jump was recorded photographically. Normally three runs were made in each tank

with the galvanometer connected successively to each of the three arcs of coils. The nature of the equipment can be visualized by referring to Figs. 2.50 and 2.51.

The object in placing the coils along an arc of a circle that approximated the path of an ion going from the source to the receiver was to give an approximate measure of the quantity $\int h_z \, dx$ around the orbit. This integral is proportional to the X displacement at the receiver.[8] In this way a comparison could be made with the values of the displacement expected from the theory.

The flip coil consisted of a single coil which could be rotated through 180 deg, located at a given point in the median plane of the tank. One purpose of this coil was to standardize the galvanometer deflections from tank to tank. A fixed galvanometer deflection was taken as standard, and the deflection of the flip coil was adjusted to this standard for each tank by altering the resistance of the galvanometer circuit.

The roving coils[9] were single coils with their axis in the Z direction, one in each of the planes of the arcs of coils. They could be moved along a circle of radius 49.4 in., in jumps of approximately 3 in. (see Fig. 2.52). The coils were connected in series with their respective arcs of coils, the flip coil, and the galvanometer. The galvanometer deflections for the 3-in. jumps were recorded photographically. The movement of the coils along the circular arcs was controlled from outside the tank by an electric motor through a screw arrangement. A counter attached to the device read 8 revolutions per 3-in. (3°28.77′) jump of the coil.

It was the function of the roving coil to aid in properly positioning the curve obtained from the reading of the arcs of coils with respect to the theoretical comparison curves. This was thought to be necessary at first because the zero or initial position of the arcs of coils was such that some of the coils were in the inhomogeneous field. This meant that the flux cut by the arcs of coils in traveling from the homogeneous field to the zero position was not taken into consideration in the arcs-of-coils reading.

In carrying out the measurements in the region of the shims, the first step consisted in testing the separation of the shims and of the tank pads with a measuring rod. This being done, the arcs-of-coils unit was placed in the tank, and the tank was evacuated. After a satisfactory vacuum had been obtained, flip-coil readings were made, and the resistance of the galvanometer circuits was adjusted to obtain the standard deflection on the photographic film or visual scale. These particular deflections depended upon the area of the particular flip coil in use. Tables and graphs were available for the determina-

tion of the necessary change in resistance for any particular deflection. The final readings of the flip-coil deflections were recorded photographically, as were also readings taken with a Hibbert magnetic standard made for the purpose of determining the absolute values of the magnetic field in the tank. Further flip-coil readings were also taken after making the runs with the arcs of coils. Following this, runs with the arcs of coils were made in the left, center, and right planes (median and ±8-in. planes).

The data obtained from the arcs-of-coils measurements were in the form of data sheets and photographs of galvanometer deflections produced by the coils. An example of an arcs-of-coils measurement is given in Fig. 2.53. The heavy black dots on the sides are used to indicate when the readings are to be taken with a positive or negative sign. If the readings lie between the heavy dots and the zero readings they are taken to be positive, otherwise negative. The top part of each photograph is devoted to the Hibbert-standard readings.

The first step in the interpretation of the data was the reading of the galvanometer deflections from the photographs. The readings were made to the nearest 0.1 mm and were totaled successively. Once the sum of the galvanometer deflections had been obtained, it was possible to plot the curve of the $\int h_z\, dx$ for each plane. This curve was plotted on tracing graph paper with the same scale used for the theoretical comparison curves. A reproduction of such a curve is shown in Fig. 2.54. Standard comparison curves were available for the ±8-in., ±7.75-in., and ±8.25-in. planes. The magnetic field was then checked by observing the fit of the experimental curves to the theoretical curves by the use of an illuminated screen. The principal difficulty in carrying out the comparison of theoretical and experimental curves arose from the fact that there was no unique way of comparing the curves; i.e., there was no unique way of placing the experimental curves on the theoretical curve for comparison. It had been decided before making the measurements at the plant that the roving coils would not determine the value of the $\int h_z\, dx$ for the initial position of the arcs of coils with sufficient accuracy. In tests made on the XA unit at the Radiation Laboratory it was found that the errors in the measurements with the roving coil were large and unsystematic and that the device was of little use in helping to decide whether the field was satisfactory. Consequently, the roving-coils arrangement was not used in the measurements at the plant.

It had been determined upon theoretical grounds that in order to have the focal pattern of the beam limited to a one-half mass-unit spread from its theoretical width, it was necessary for the values of the quantity $\int h_z\, dx$, experimental and theoretical, to differ by less

than 3 cm, in terms of galvanometer deflection. This implied that the curves must be compared in some definite manner. In view of the uncertainty regarding the actual placement of the zero on the vertical scale of the experimental curves, the method of fitting may appear to be somewhat arbitrary. However, on the basis of tests made in the XA units at the Radiation Laboratory, the method was believed to be satisfactory in deciding whether a given tank passed the theoretical criteria.

The method used is essentially the following: Keeping the first few points of the curves together, the curves were adjusted vertically with respect to one another in such a manner as to distribute the discrepancies between them. The first few points refer to the sums of the galvanometer deflections when the arcs of coils are nearest the mouth of the tank. Once the curves have been fitted together with the best possible distribution of the differences and with the initial points coinciding, the remaining portions of the curves were checked to see if they deviated from one another by more than 3 cm. Various distinguishing features of the experimental curves such as flaring in certain regions, bulging of the peaks, etc., were also noted.

12.2 Source-region Device.[7] The second large piece of equipment used in making magnetic surveys of tanks was a device designed to test the quality of the magnetic field in the region of the source. This unit was made up essentially of three parts: the source-exploring coil, or swinging-gate unit, the flip coil, and the center-line device. The unit was also provided with a mercury arc. The entire unit was mounted on a faceplate so that any part of it could be used with the tank under vacuum. The source search-coil unit was comprised of a single search coil which could be moved in a number of directions in order to investigate the character of the magnetic field in the vicinity of the source. This search coil could be moved in the Z direction at any point in the XY plane from +61° 41′ to −6°, measured with respect to the Y axis with the origin located at the point M of Fig. 2.55. Radial motions were possible along any radius through the Z axis as well as motions along arcs of circles with centers on the axis. The network of positions which could be covered is shown in Figs. 2.55 and 2.56. The motions were controlled by an electric motor through a screw arrangement from outside the tank. Figures 2.57 and 2.58 show the general appearance of the equipment.

The radial runs were made for the purpose of measuring the quantity $dh_z/dr$, where r represents the distance along a radius. In this way the field $h_z$ at one point can be related to the field at some other point in the same plane. The arc runs gave the values of $dh_z/d\xi$ where $\xi$ represents the distance measured along an arc. Finally, the runs in

the Z direction were made for the purpose of measuring the quantities $dh_z/dz$. The manner in which these quantities enter into the theoretical consideration is discussed in Chap. 3, Division I, Volume 4, of the National Nuclear Energy Series.

The flip-coil unit consisted of a coil at the end of a supporting rod which could be rotated about the point F in Fig. 2.55. The rotation was from −5° 11′ to 45°, as measured with respect to the Y direction. The coil could be rotated through 180 deg about the axis of the supporting rod so as to measure the magnetic field strength at the point where it was located. The flip-coil measurements were usually made at the point designated Z in the figure, the same point at which the flip-coil readings were made with the shim-region exploring device. This provided a means of linking together the measurements made by these two exploring devices. Included with the flip-coil device was a search coil attached to the rod supporting the flip coil. This search coil could be moved along the rod to measure changes in the Z component of the magnetic field.

The center-line device consisted of a search coil which could be moved in 2-in. jumps along the center line of the tank in any one of nine planes (see Fig. 2.55). The tank center line in the median plane was parallel to and 5.225 in. from the middle plane or axis of symmetry of the arc-of-coils device.

The mercury-arc unit was similar to that described in Sec. 10.3. The device enabled the observer to see if the magnetic field was tilted. The tube was located near the receiver so that when the faceplate was turned end for end the tube assumed a position with its axis along the Z direction and at the location of the actual source. It was intended to use this device only when the measurements with the source device indicated the need of a closer study of the magnetic field in the source region.

In the use of the source-testing device the procedure consisted first in taking measurements with the flip coil, as in the case of the arc of coils, except that the flip-coil reading was adjusted to a different standard deflection. Following this the excursions of the search coils were made, starting at the point designated as $M_0$ in Fig. 2.56. It was first moved to point A and then from A to point Z in 21 jumps, the deflection for each jump being recorded photographically. The coil was next returned to A, moved to B, and the second radial run from B to C was made also in 21 jumps. Following this, the coil was moved back to $V_0$, thence to $P_0$, and the first arc run from $P_0$ to $W_0$ in three jumps was carried out. The coil was then returned to $P_0$, moved to $O_0$, and the arc run from $O_0$ to $X_0$ was made in three jumps. The same procedure was carried out for the third arc run $N_0$ to $Y_0$.

Altogether two radial runs and three arc runs were made in the median plane, giving a total of 51 readings. Next, three arc runs were made in the planes 8 in. on either side of the median plane. Finally four runs in the Z direction were made at points $V_0$, $U_0$, $T_0$, $M_0$, each run consisting of eight 2-in. jumps between the +8-in. and −8-in. planes.

In the interpretation[7,10] of the runs with the source search coil, it was not necessary to plot curves for comparison purposes. All the information for each tank could be entered on a data sheet and the criteria for satisfactory tank performance then applied. The data sheets were so designed that the theoretical criteria concerning the performance could be applied by the use of a template that could be laid over the data sheets. Numbers on the template gave the maximum differences allowed between the numbers on the data sheets left uncovered by the template. These maximum values were obtained from the theory.

On the assumption that the focal pattern must not disagree by more than 0.5 mass unit with the theoretical pattern, it was decided that the variation of the Z component of the field between two points in the neighborhood of the arc 1 in. apart in the direction of an arc run with the search coil must be less than 0.2 per cent of the homogeneous field. The variation in the Z component of the field between any two points in the neighborhood of the source and 1 in. apart in the Z direction was to be less than 0.1 per cent of the homogeneous field. These criteria, when translated into terms of the maximum allowable galvanometer-deflection differences, were the ones entered upon the templates. From the magnitude of the magnetic field at the flip coil and the network of search-coil measurements made in the source region, it was possible to determine the actual value of the magnetic field for enough points to give an adequate picture of the character of the field in this region.

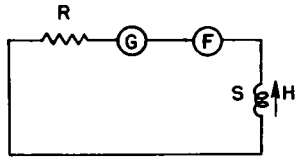


Fig. 2.1—Ballistic galvanometer circuit.

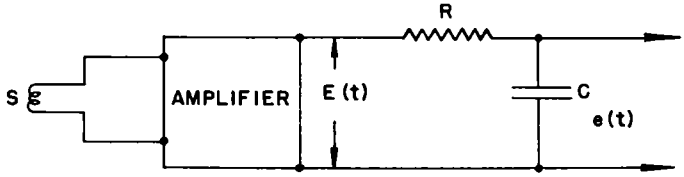


Fig. 2.2—Basic circuit for electronic fluxmeter.

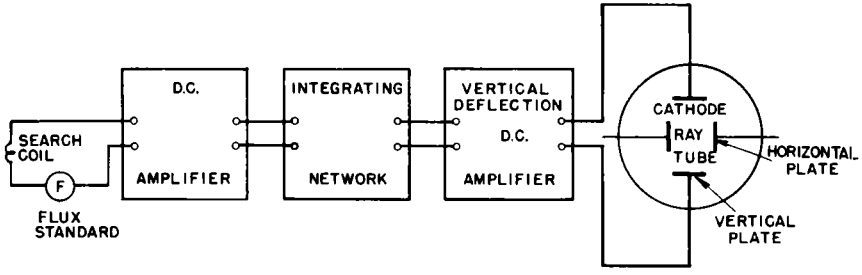


Fig. 2.3—Circuit for electronic fluxmeter with oscilloscope.

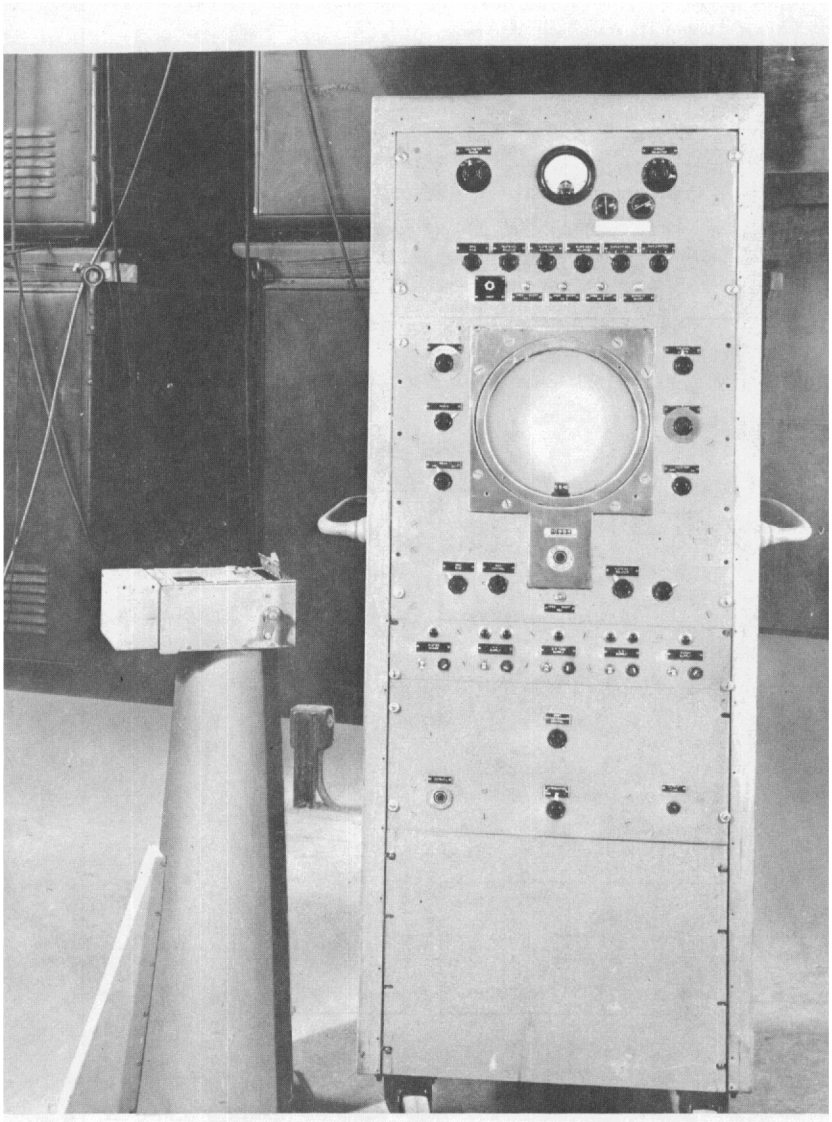

Fig. 2.4 — Electronic fluxmeter with 9-in. cathode-ray tube (magnet 336).

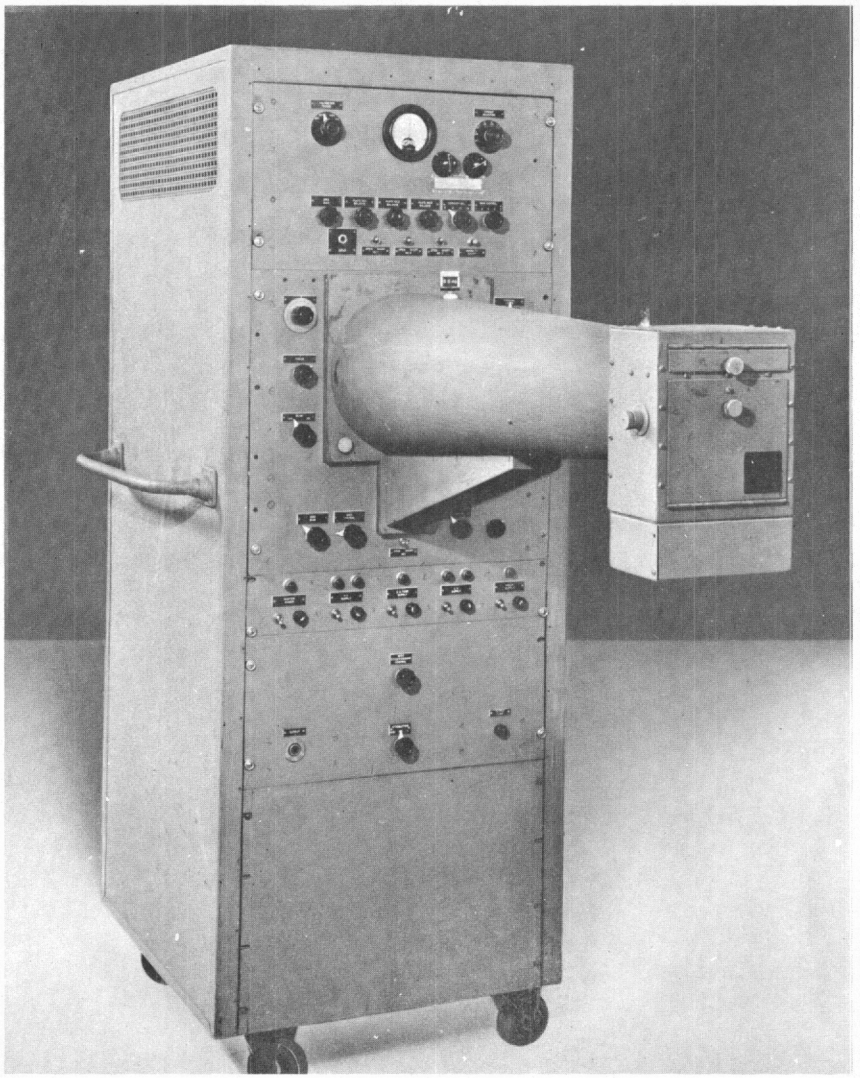

Fig. 2.5—Electronic fluxmeter with camera holder in operating position (magnet 334).

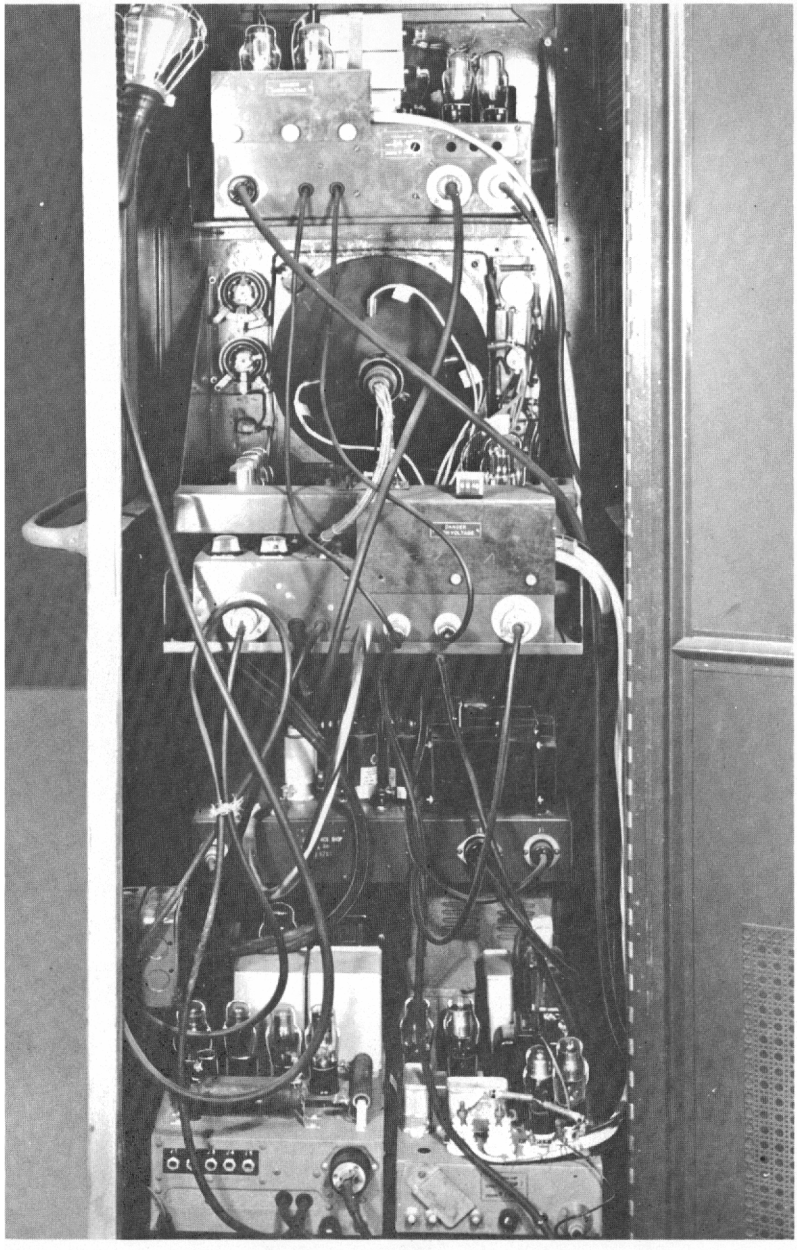

Fig. 2.6—Electronic equipment in chassis of electronic fluxmeter (magnet 335).

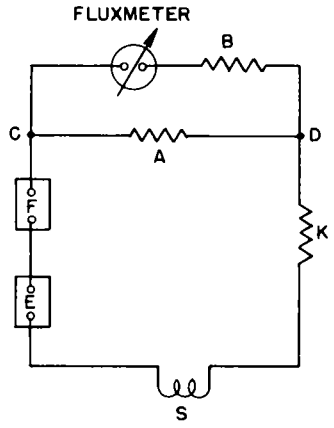


Fig. 2.7—Fluxmeter circuit.

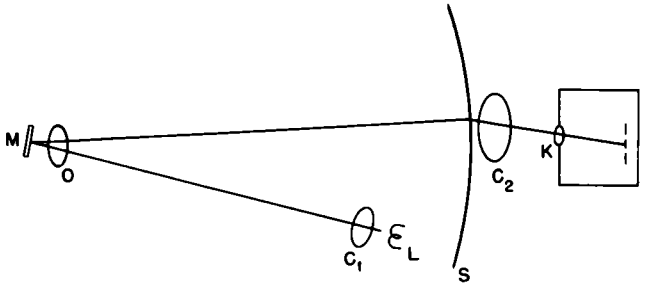


Fig. 2.8—Optical system for fluxmeter.

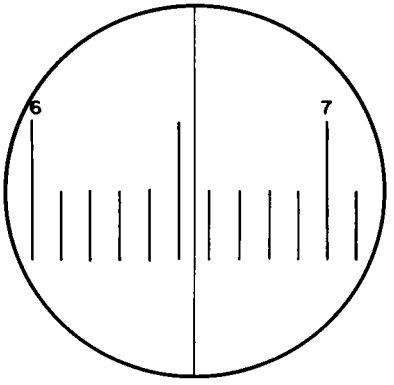


Fig. 2.9—Typical appearance of scale when photographed.

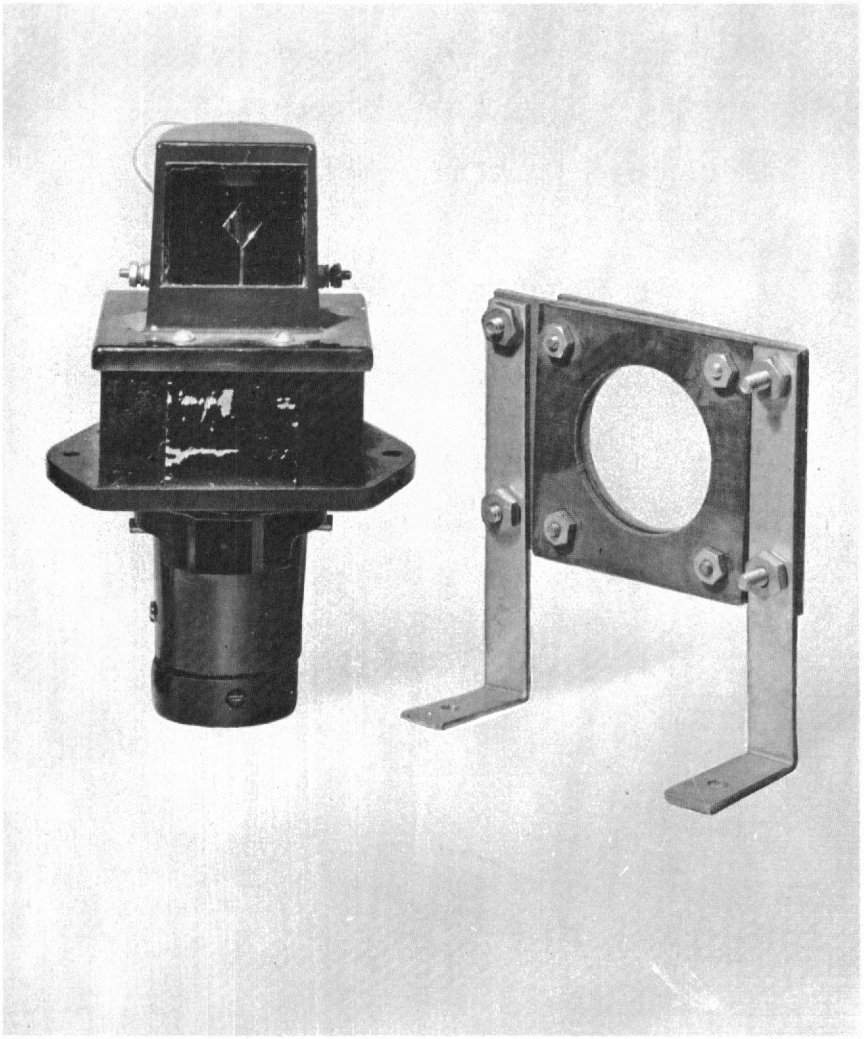

**Fig. 2.10 — Fluxmeter and objective lens mount (magnet 321).**

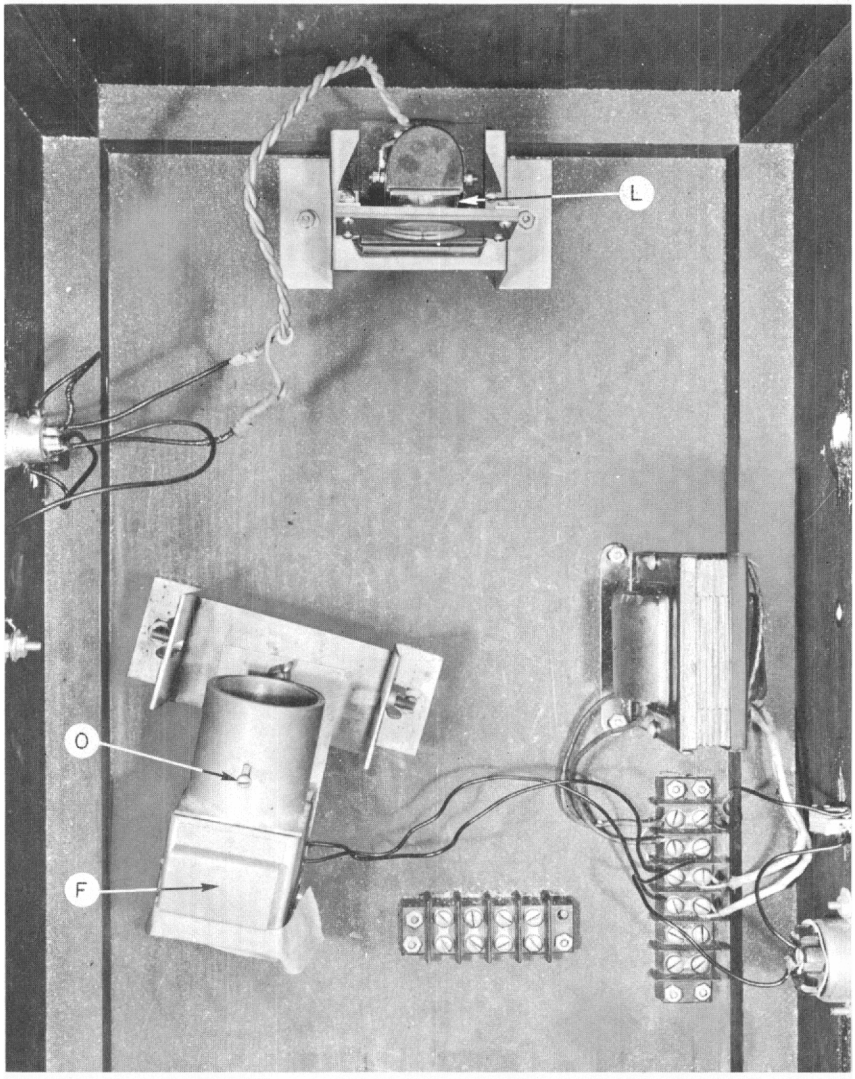


Fig. 2.11—View of light source, fluxmeter, and objective lens (magnet 322). L, light source. F, fluxmeter. O, objective lens.

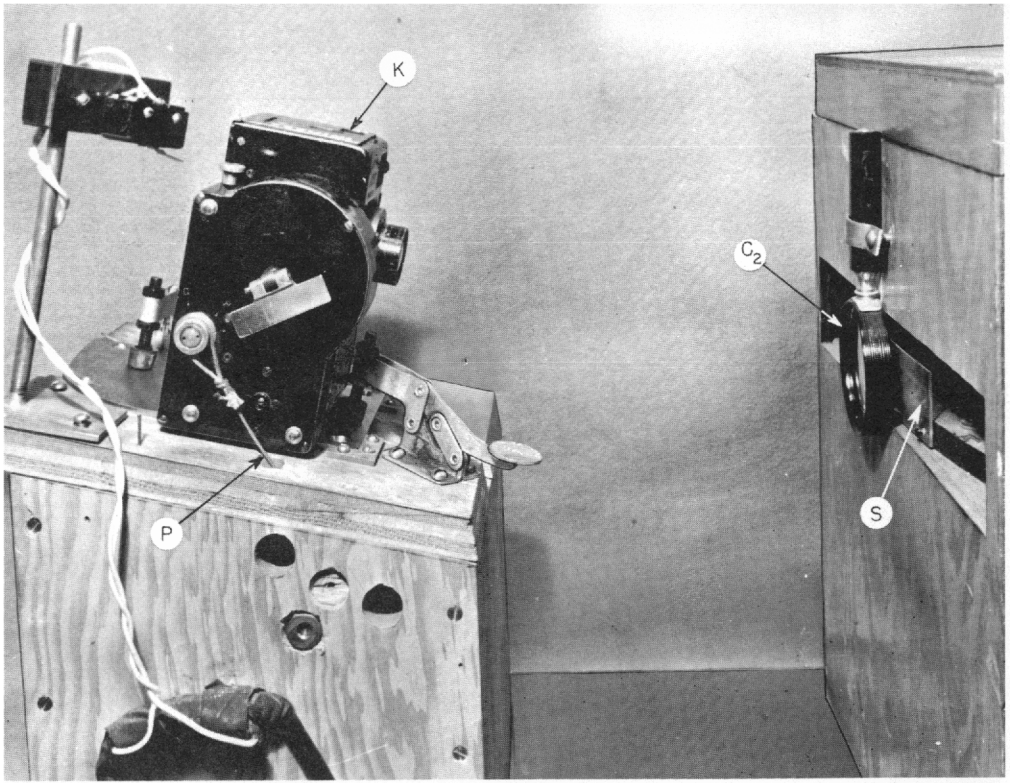


Fig. 2.12—View of camera, condenser lens, and scale (magnet 324). S, scale. $C_2$, condenser lens. K, Sept camera. P, string going to solenoid puller.

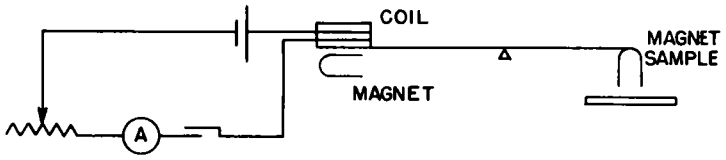


Fig. 2.13—Principle of operation of balance.

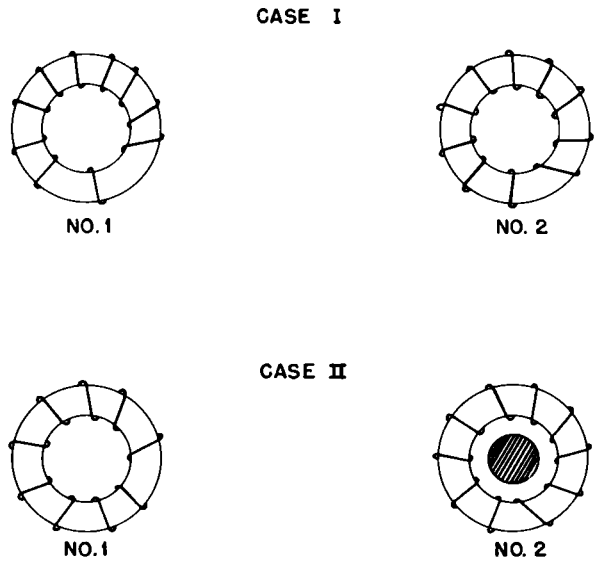


Fig. 2.14—The two types of solenoid measurements involved. Case I, air cores in both coils. Case II, air core in coil 1, stainless-steel core in coil 2.

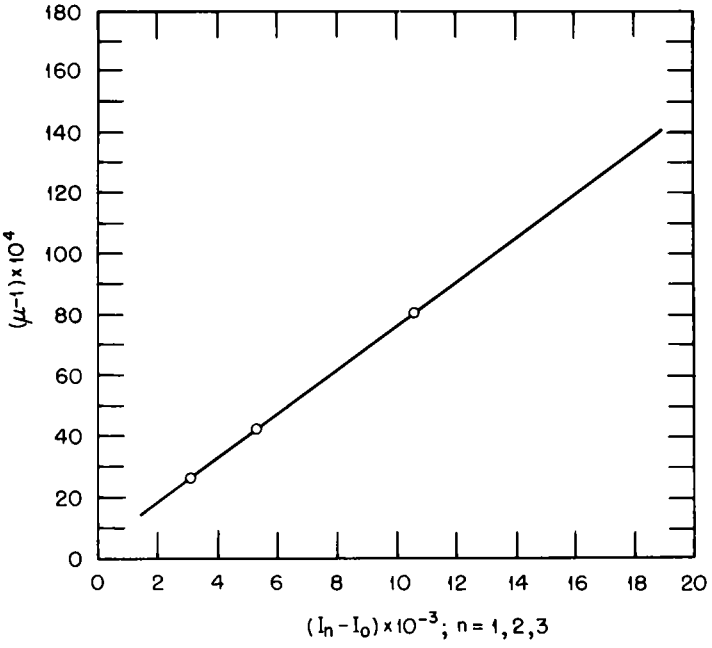


Fig. 2.15—Calibration curve for magnetic balance.

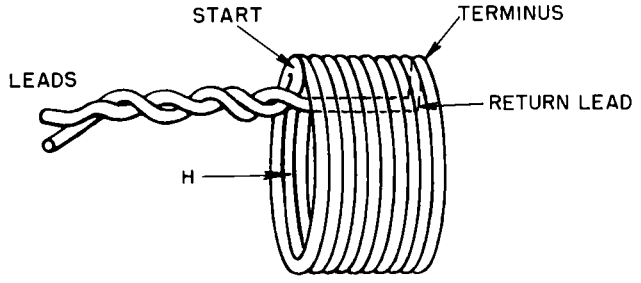


Fig. 2.16—Circular solenoid winding as used in standard search coil.

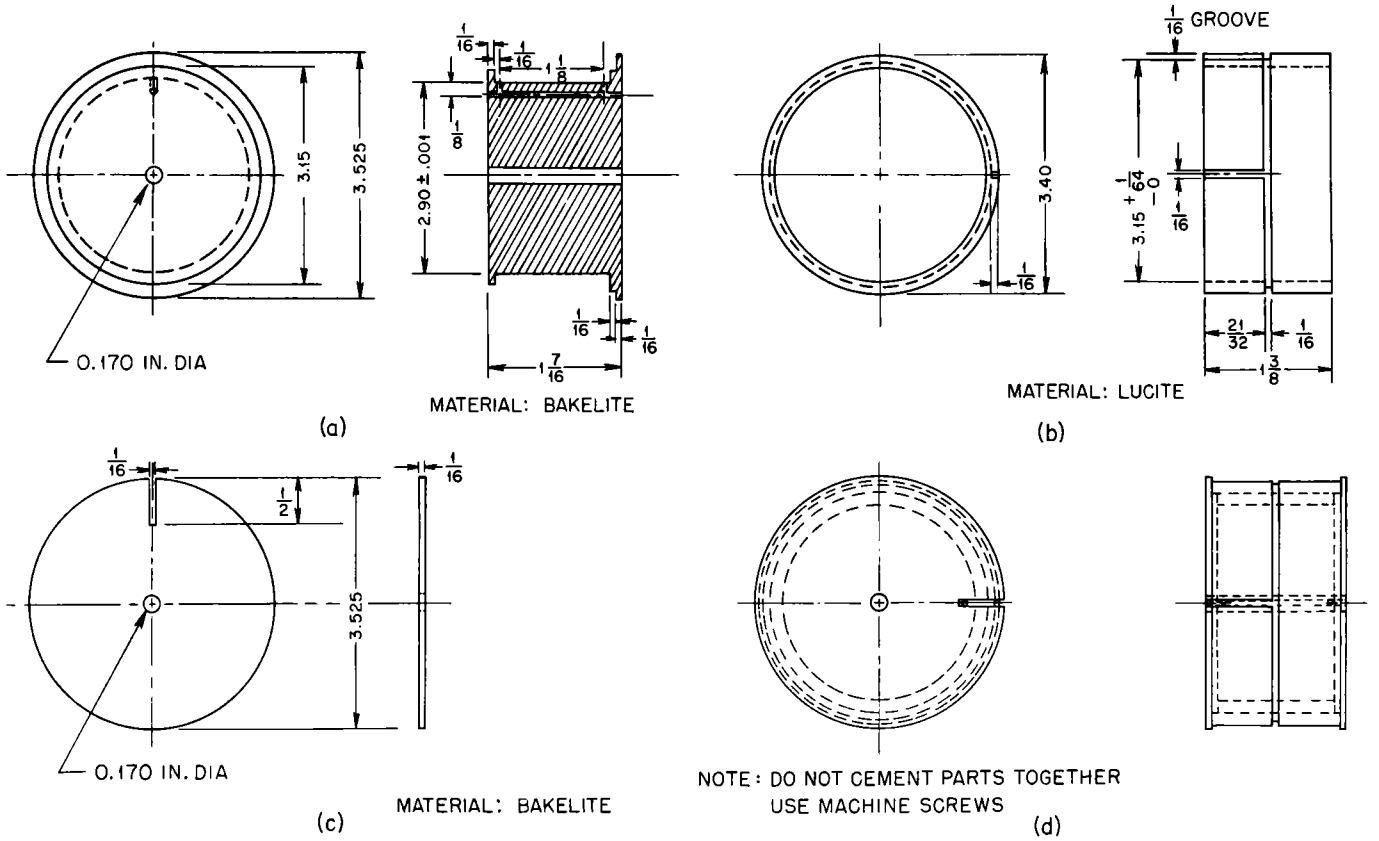


Fig. 2.17 — Parts and assembly of standard search-coil form.

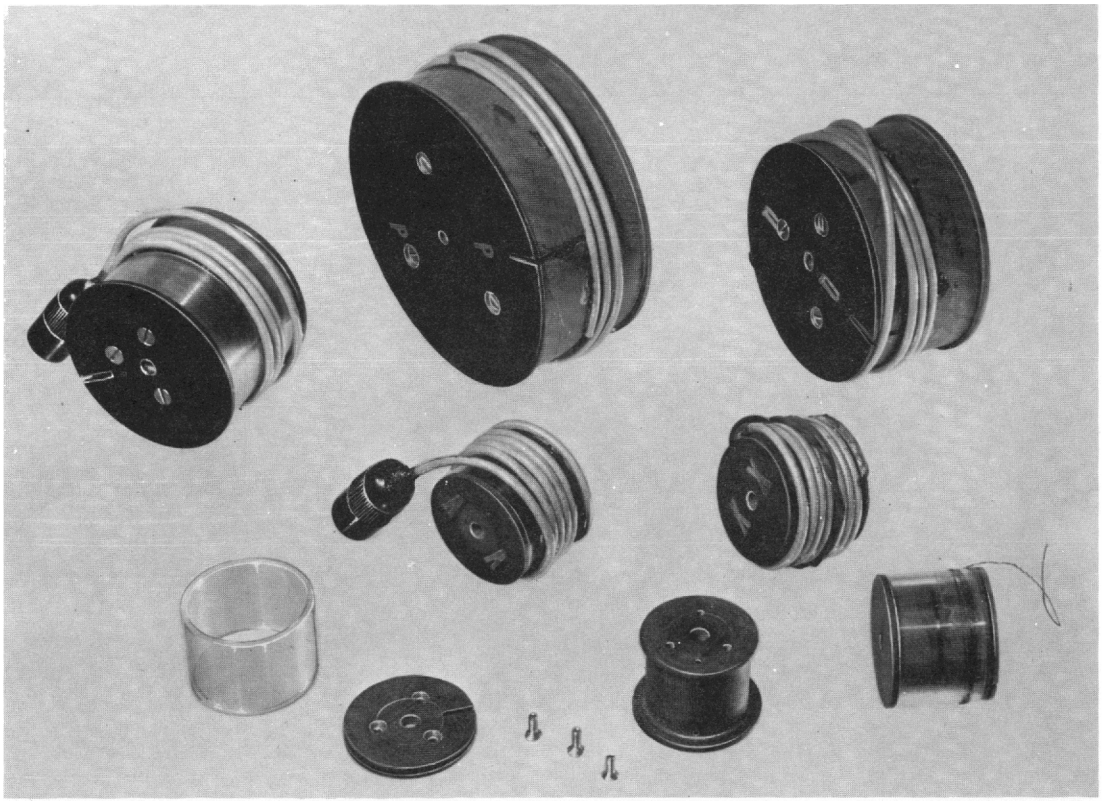

Fig. 2.18—Standard coils, with one disassembled to show components (magnet 276).

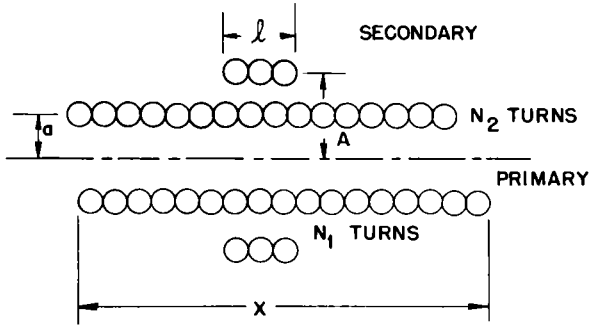


Fig. 2.19 — Long solenoid with short secondary outside.

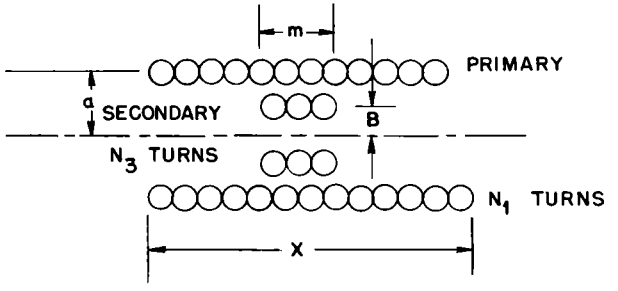


Fig. 2.20 — Long solenoid with short secondary inside.

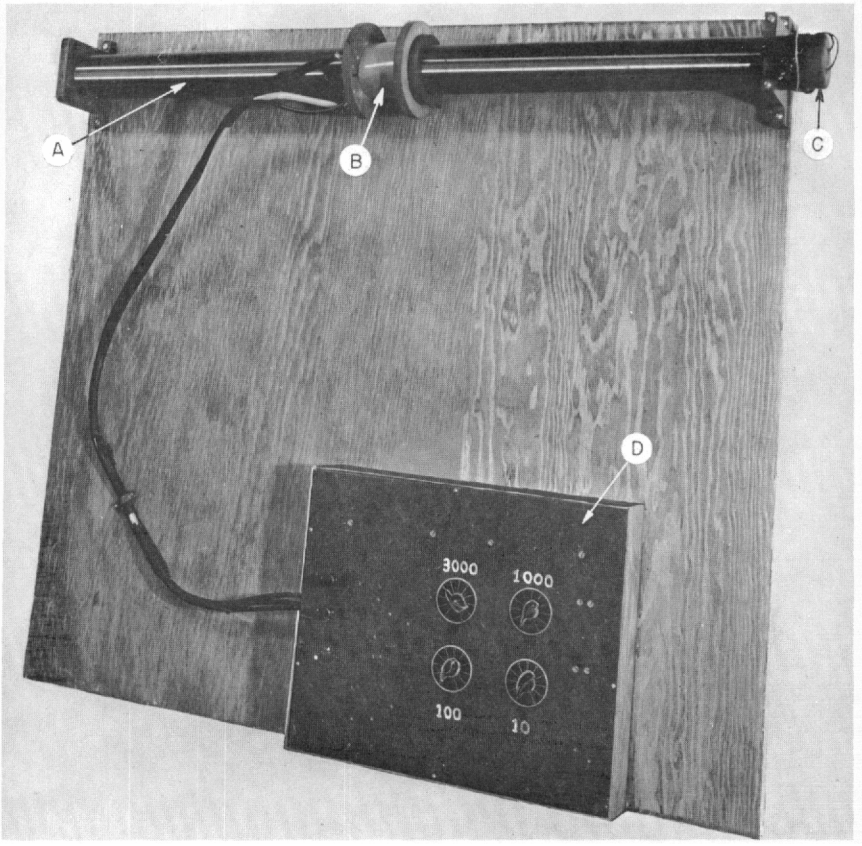


**Fig. 2.21 — General view of apparatus involving use of long solenoid to calibrate search coils (magnet 196).**

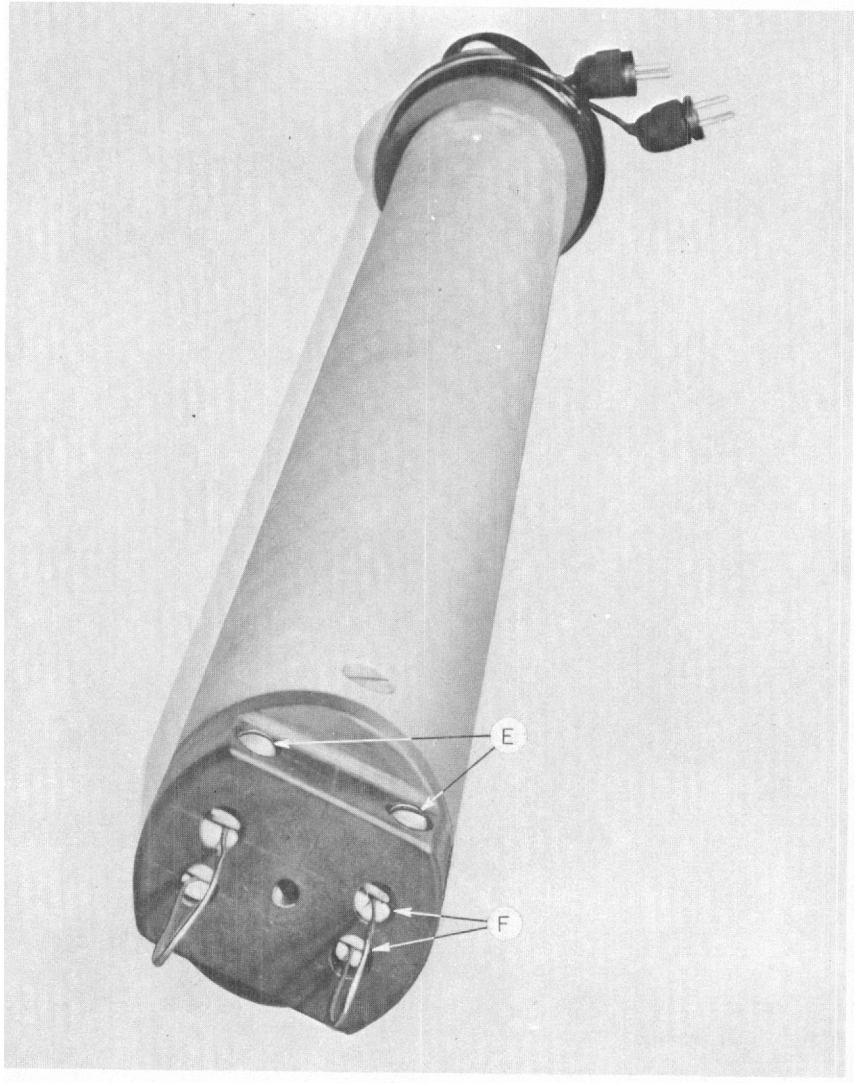


Fig. 2.22—Coil holder (magnet 197).

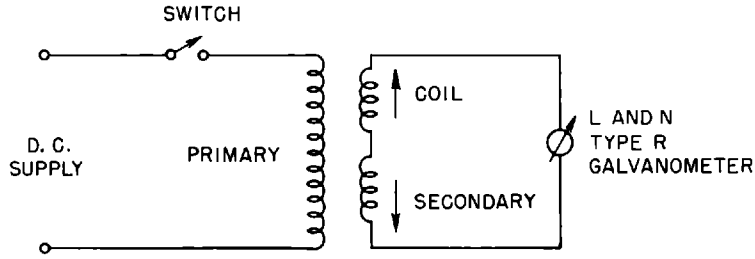


Fig. 2.23 — Electrical connections for solenoid method of calibrating search coils.

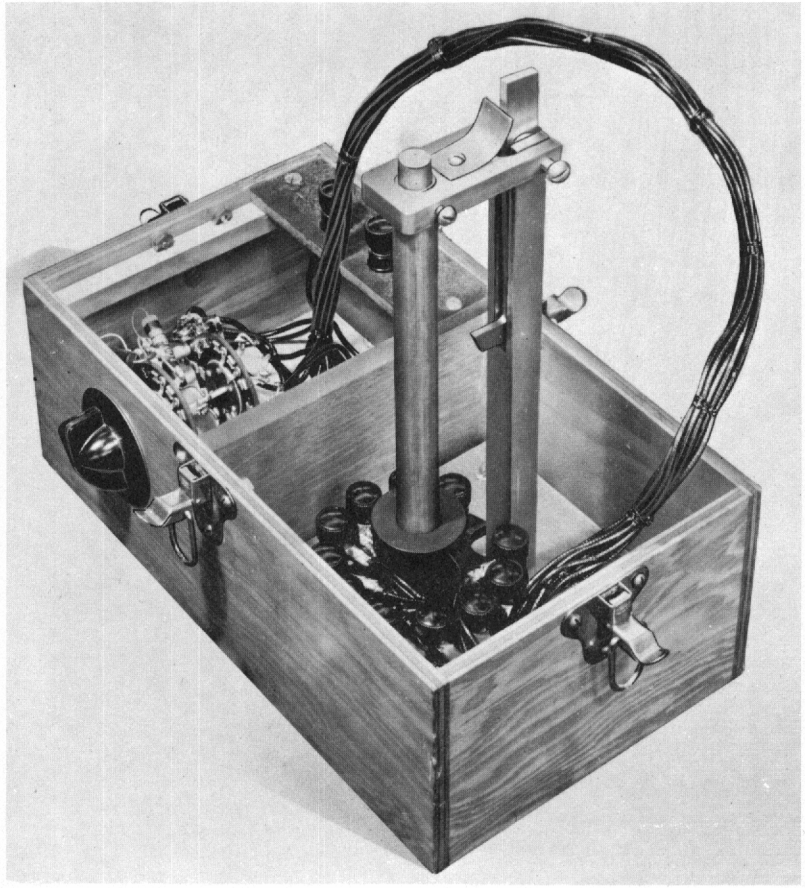

Fig. 2.24 — General view of flux standard, type I (magnet 258).

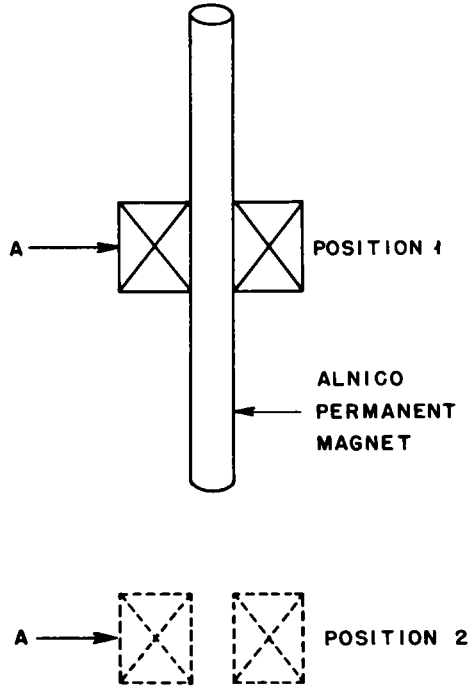


Fig. 2.25—Method of operation of flux standard.

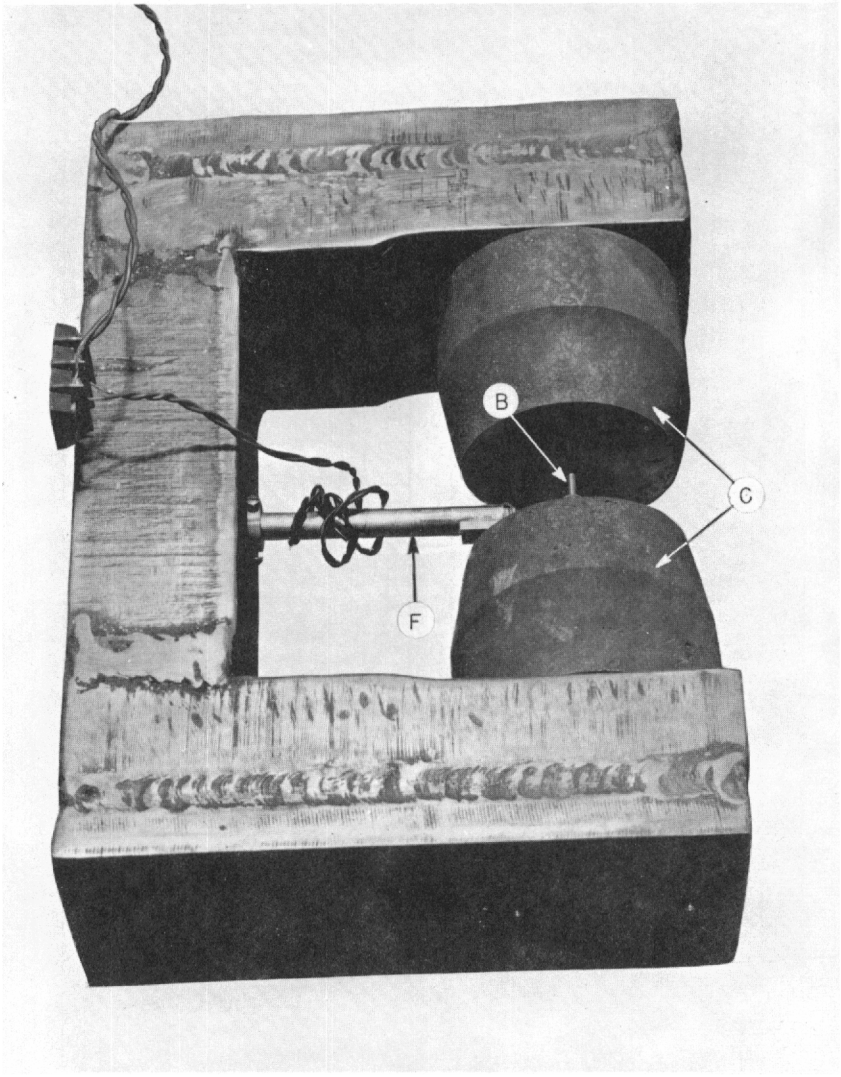


Fig. 2.26a — View of flux standard, type II. Magnet 326.

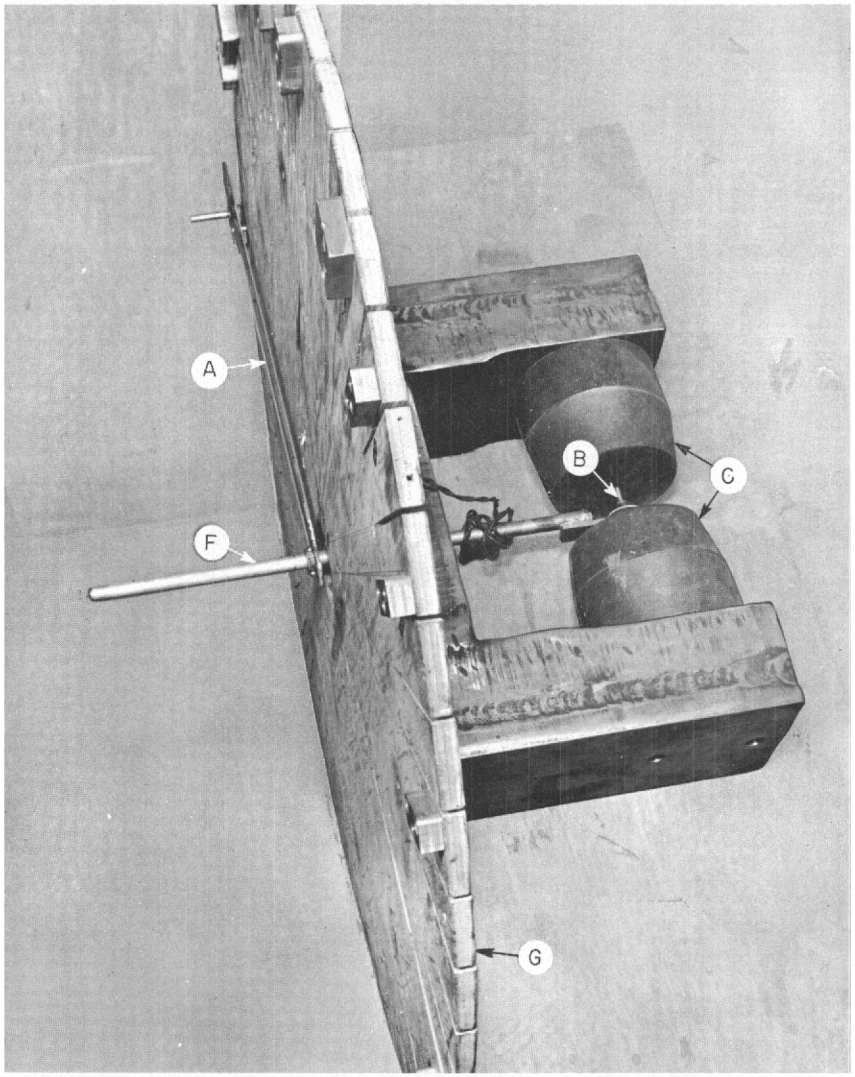


**Fig. 2.26b—View of flux standard, type II. Magnet 327.**

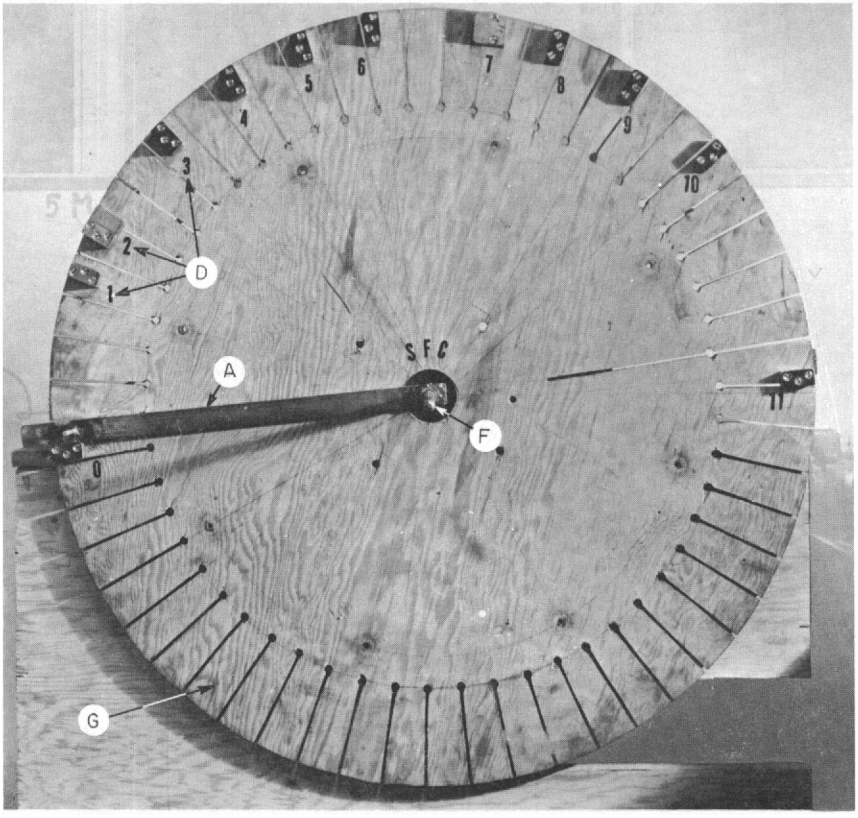


**Fig. 2.26c —View of flux standard, type II. Magnet 325.**

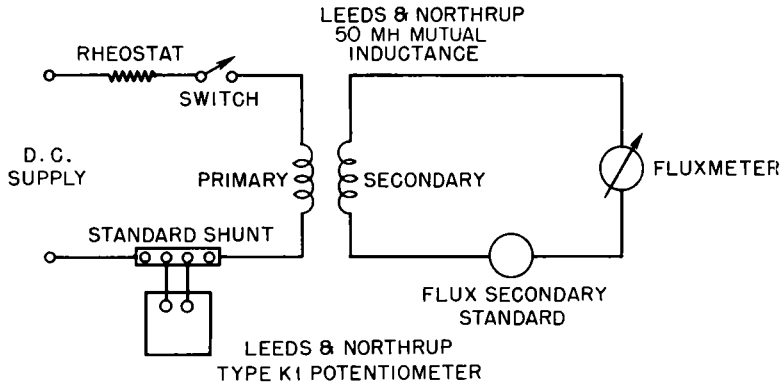


Fig. 2.27—Standardizing circuit for flux standards.

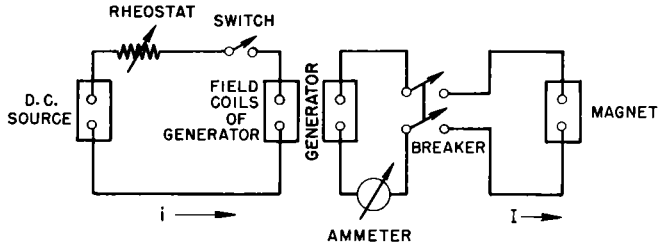


Fig. 2.28—Control circuit used in obtaining magnetization curves.

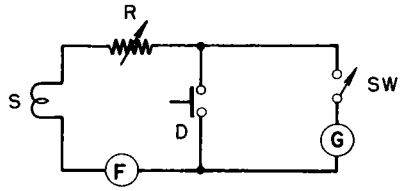


Fig. 2.29—Electrical circuit for ballistic galvanometer method of obtaining magnetization curves.

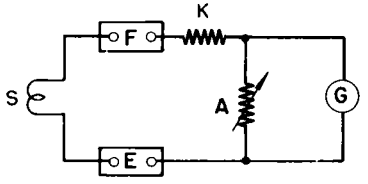


Fig. 2.30—Electrical circuit for using G.E. fluxmeter in obtaining magnetization curves.

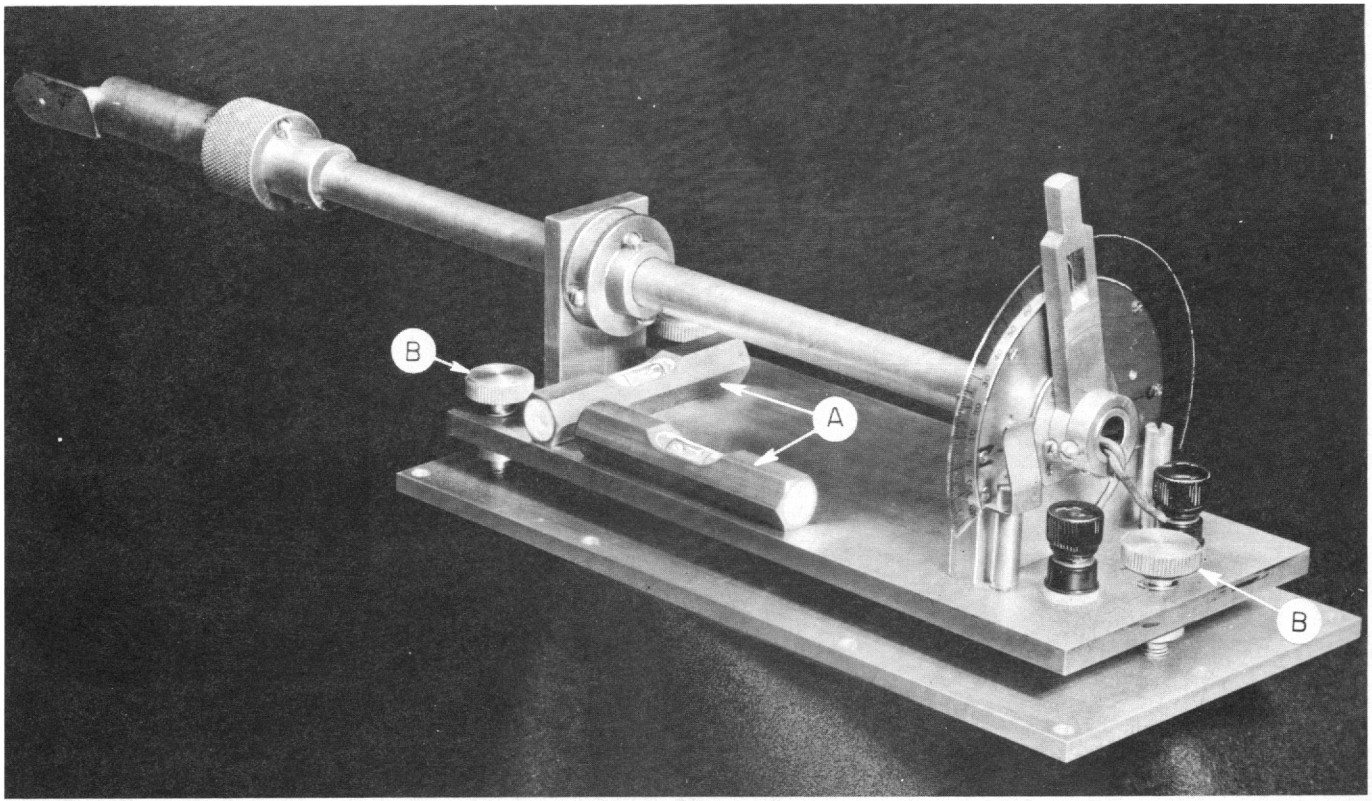


Fig. 2.31 — Flip-coil mount, type I (magnet 203).

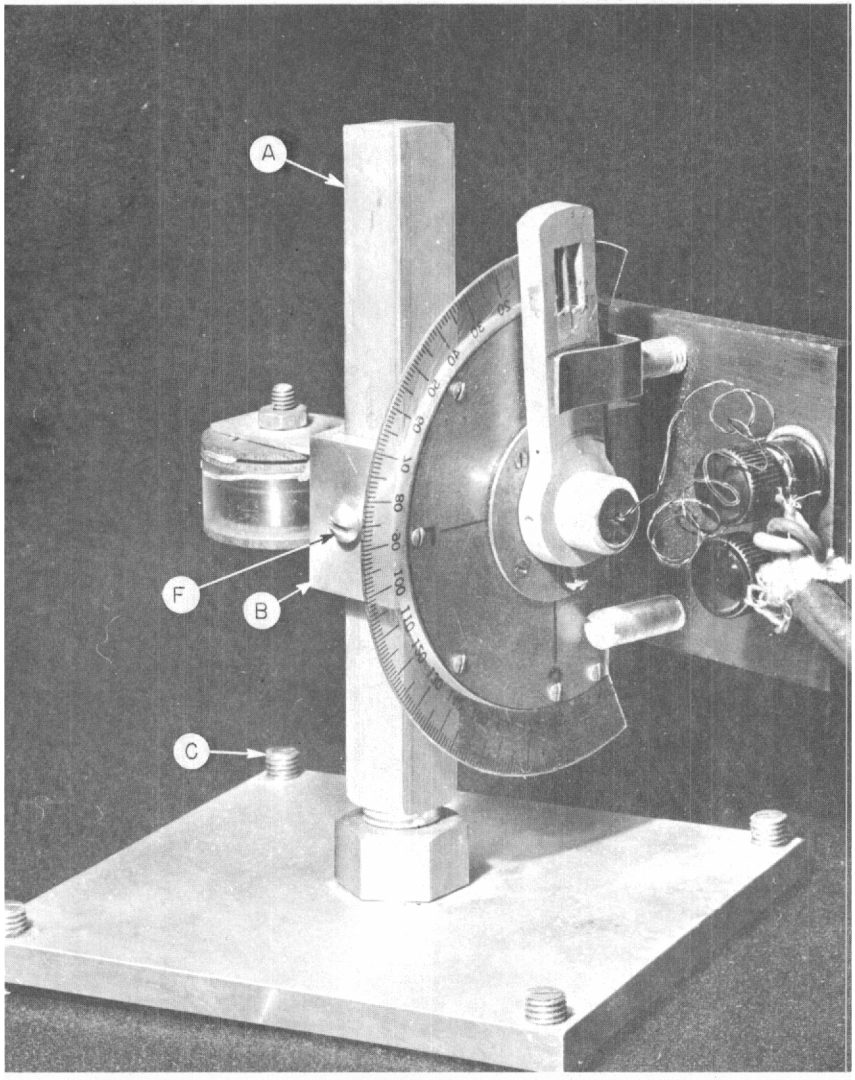


**Fig. 2.32 — Flip-coil mount, type II (magnet 323).**

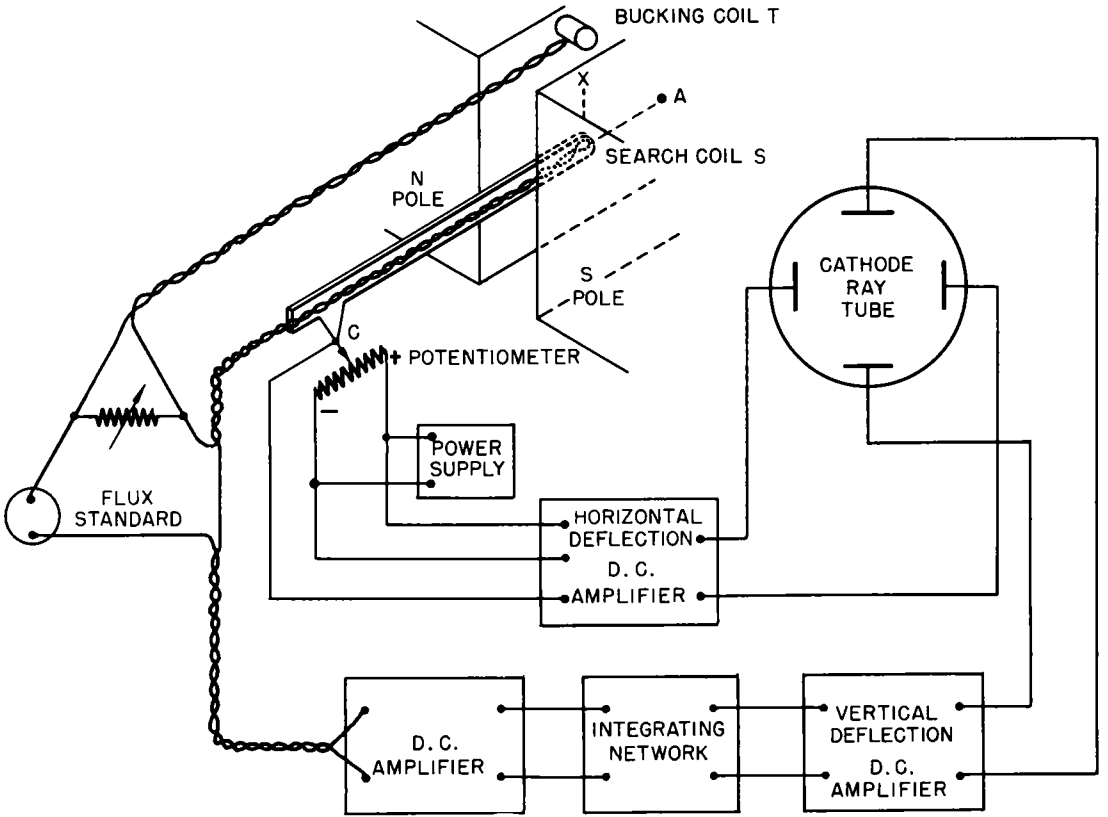


Fig. 2.33—Electrical circuit for electronic-fluxmeter method of making uniformity measurements.

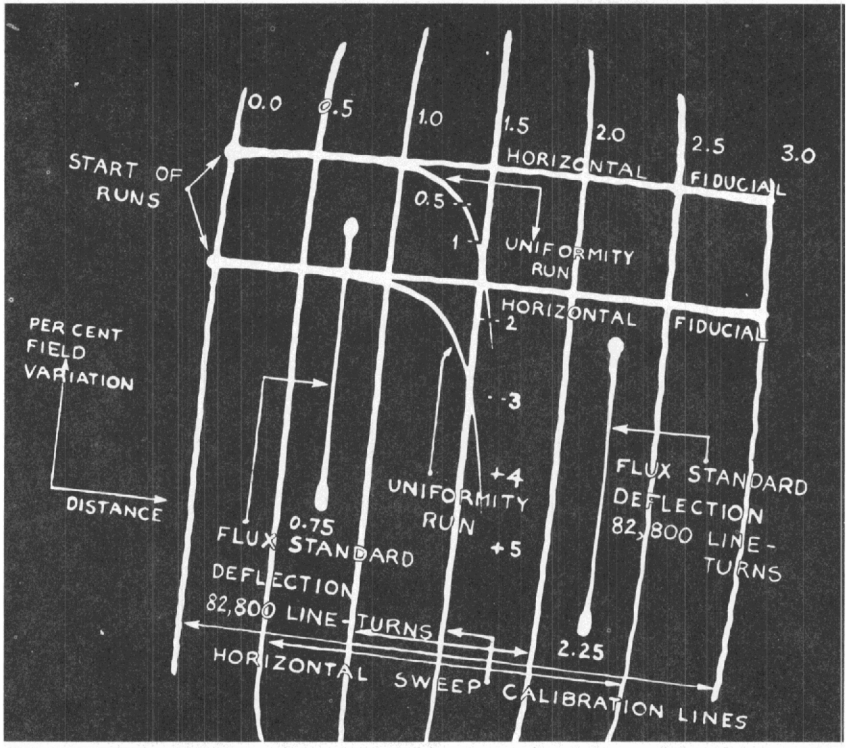


Fig. 2.34 — Two uniformity runs with electronic fluxmeter (magnet 349).

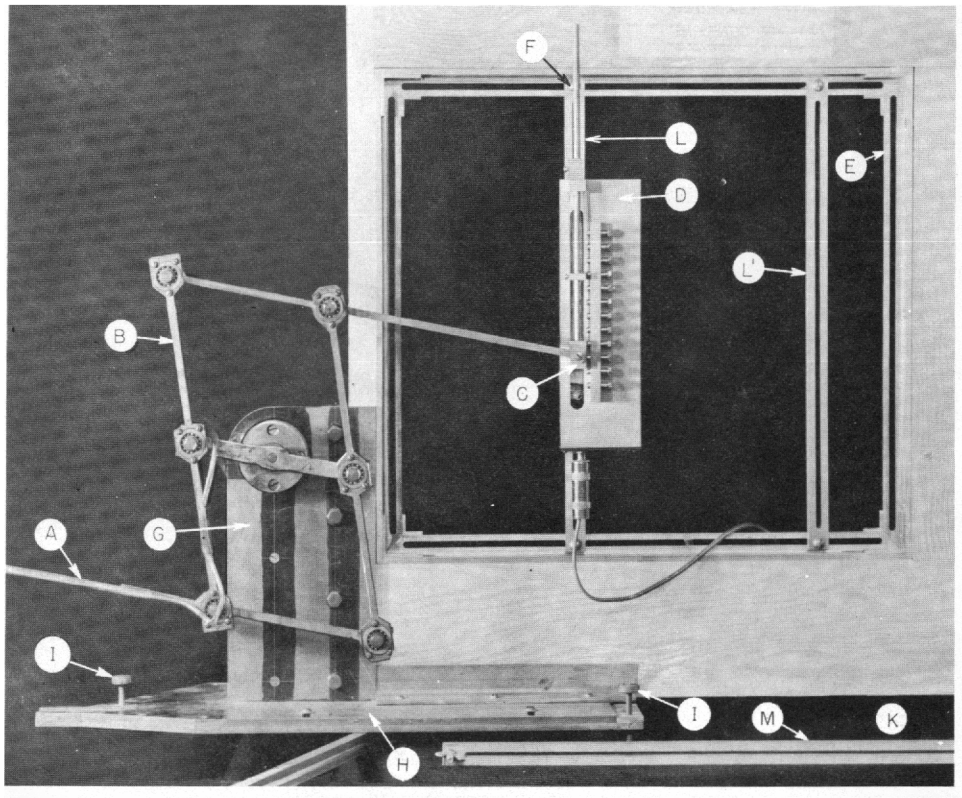


Fig. 2.35 — Apparatus for moving search coil along any prescribed straight-line path in gap of magnet (magnet 201).

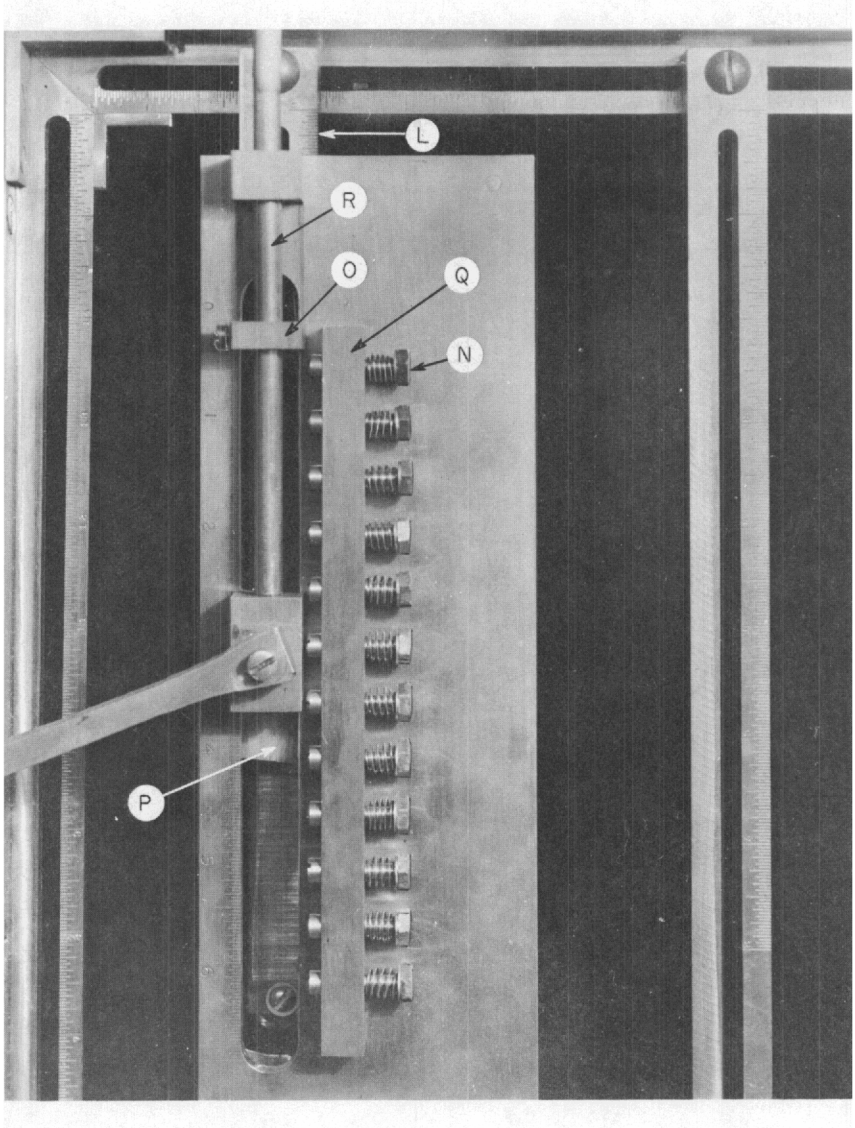


Fig. 2.36—Close-up of stylus guide (magnet 202).

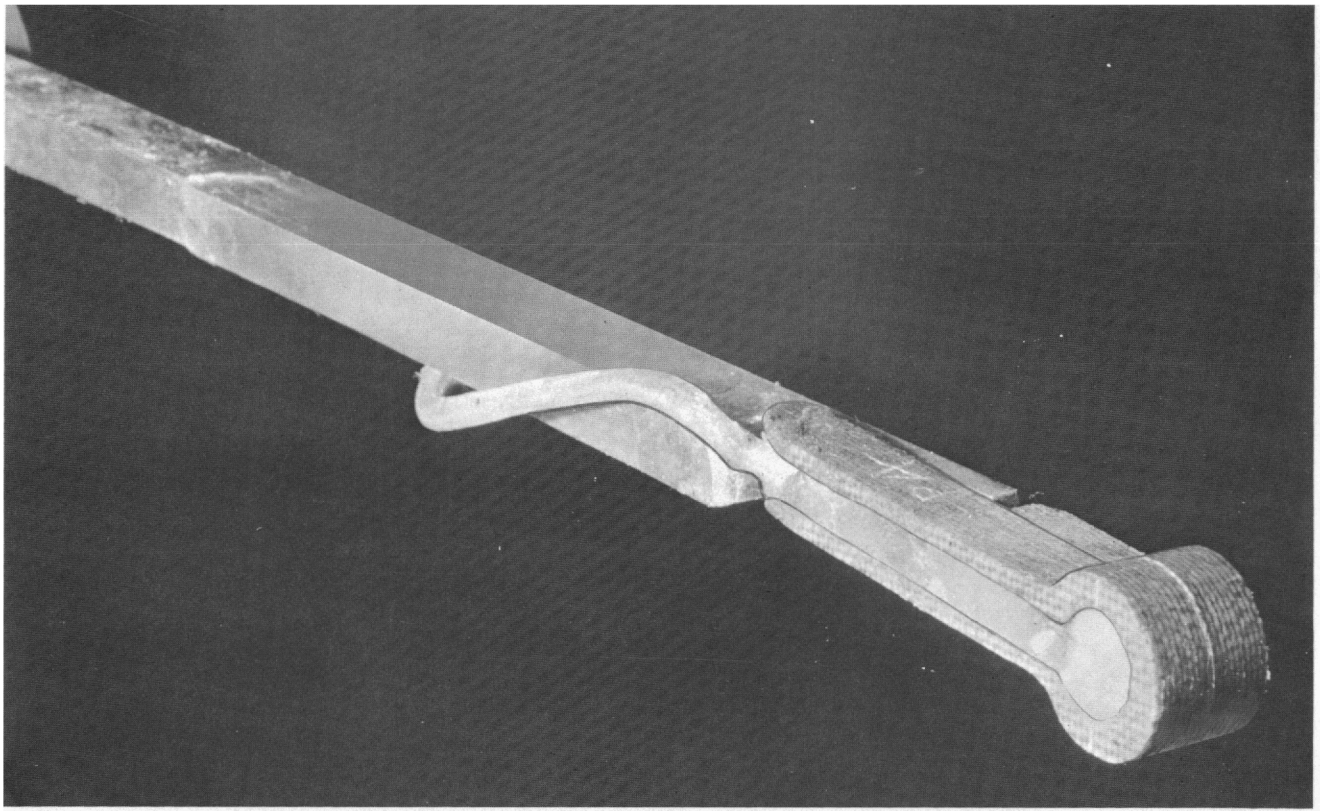

Fig. 2.37—View of 351.4 turn-sq cm search coil mounted on its holder (magnet 316).

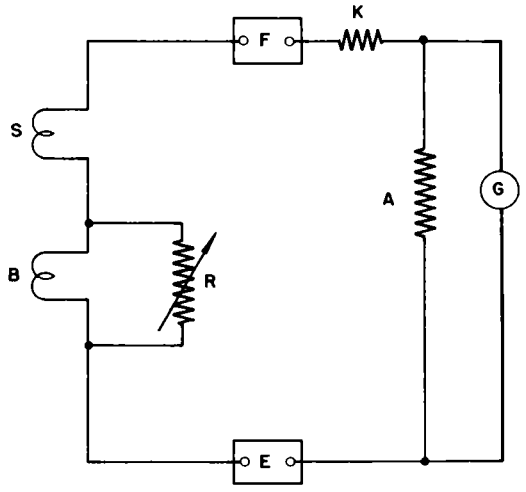


Fig. 2.38 — Electrical circuit used with G.E. fluxmeter for uniformity measurements.

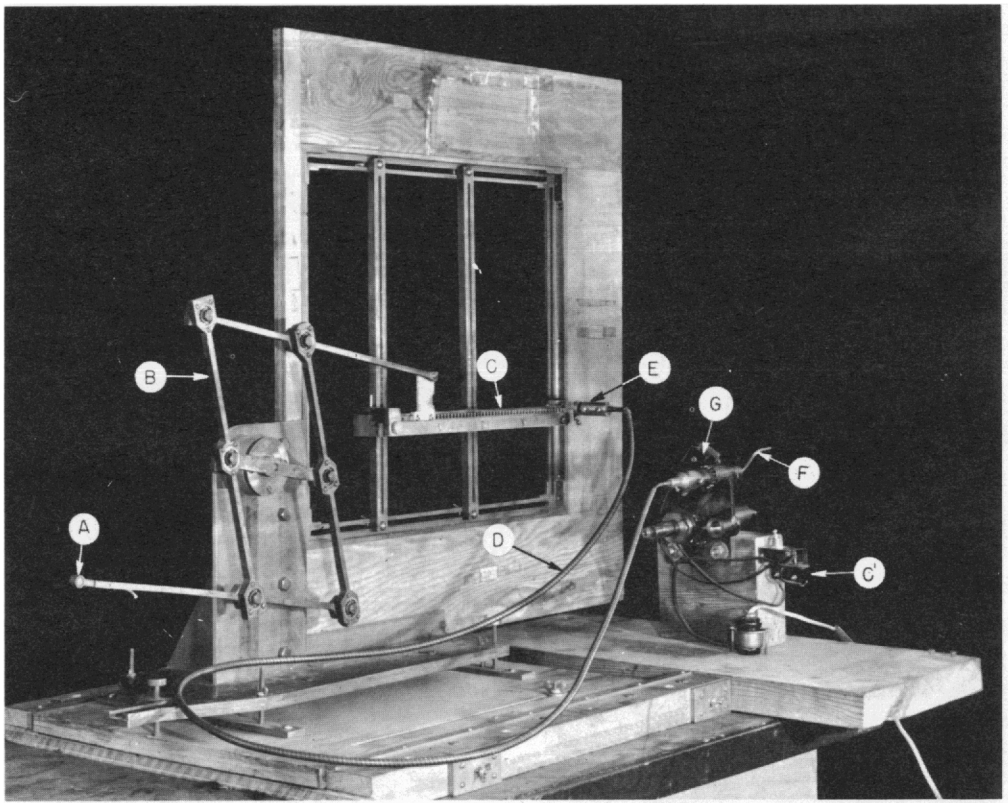


Fig. 2.39 — Search coil A and pantograph B in G.E. fluxmeter method (magnet 312).

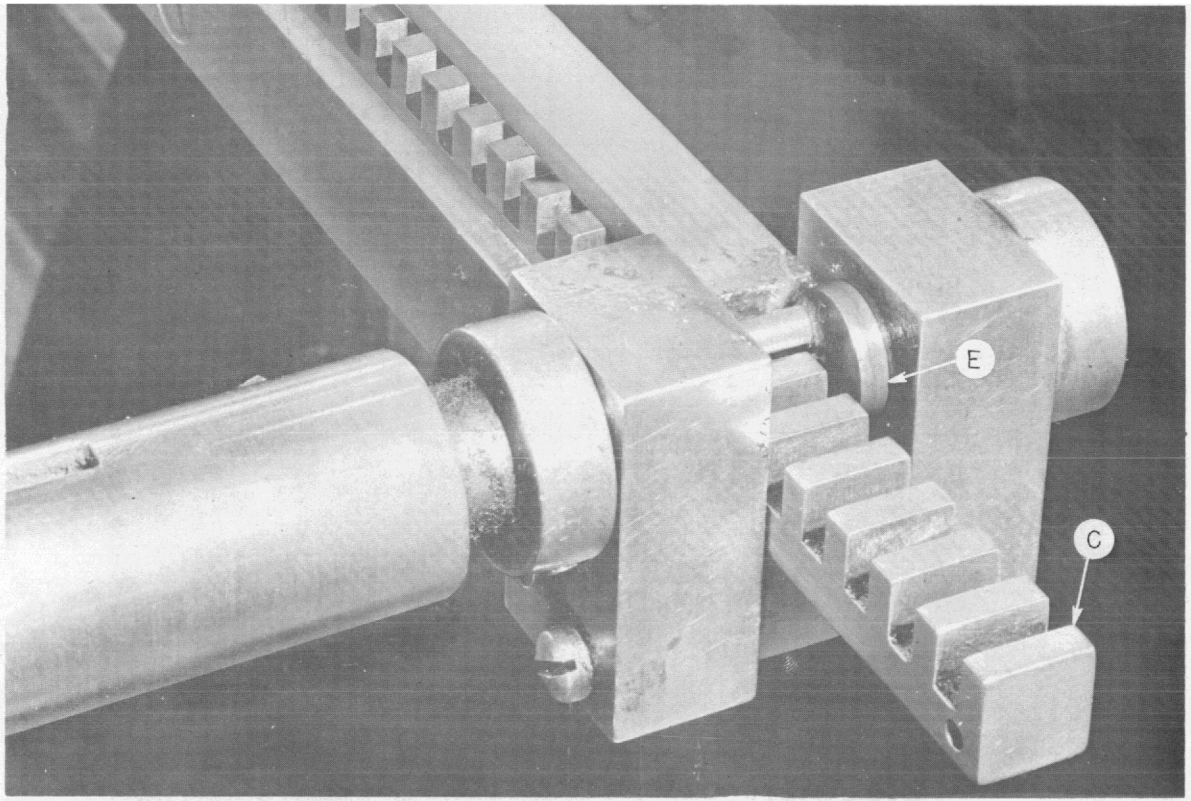


Fig. 2.40—Details of rack and pinion in G.E. fluxmeter method (magnet 318).

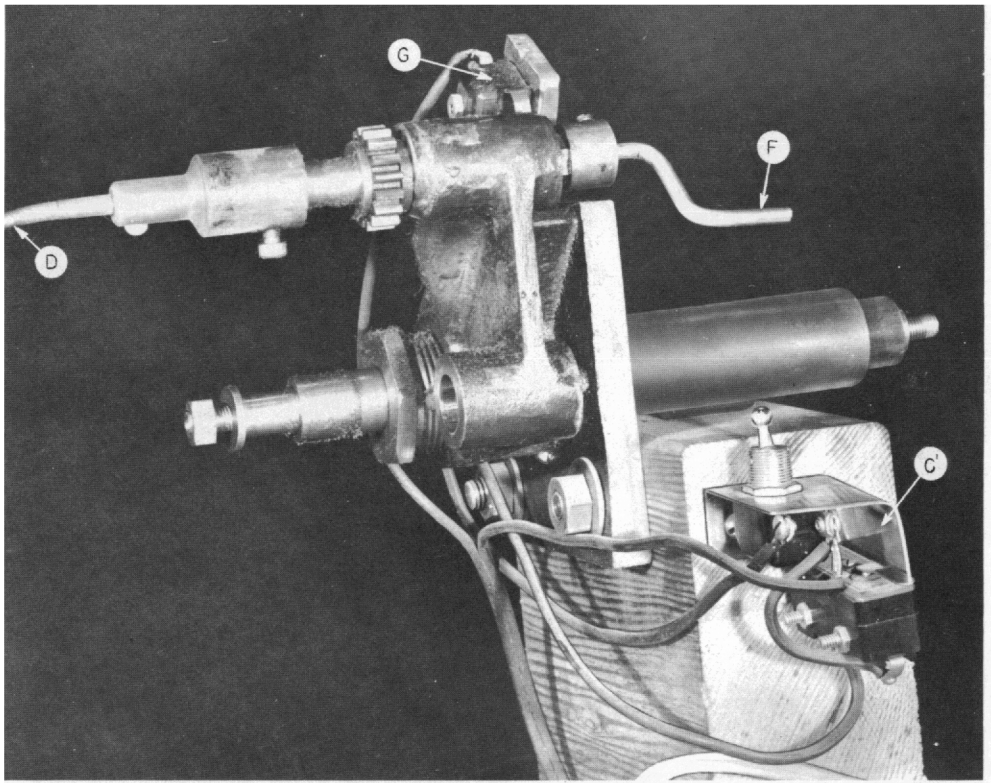


Fig. 2.41 —Details of crank F and flexible cable D for rotating pinion in G.E. fluxmeter method (magnet 319).

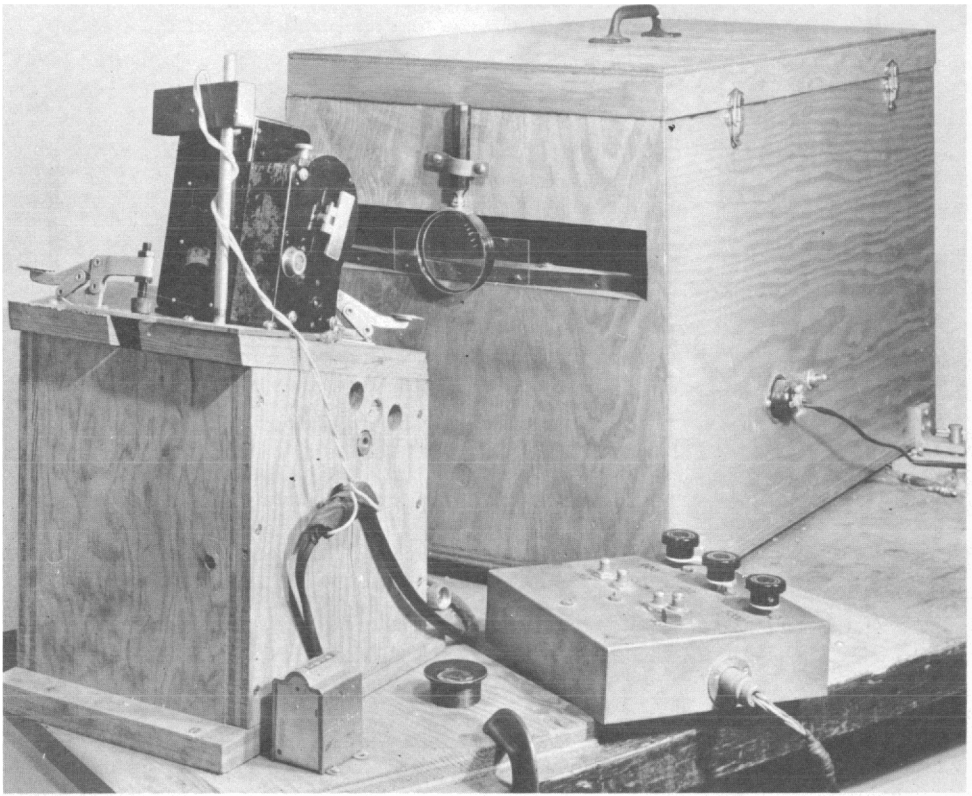

Fig. 2.42 — Sept camera and fluxmeter in G.E. fluxmeter method (magnet 333).

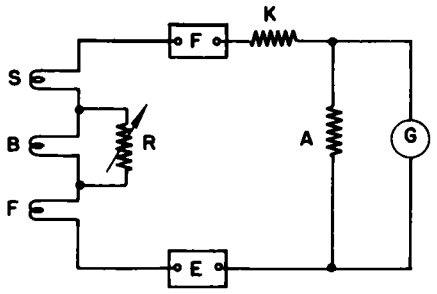


Fig. 2.43—Electrical circuit used in connection with contour-mapping device.

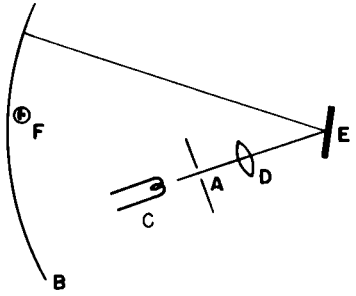


Fig. 2.44—Optical system for contour-mapping device.

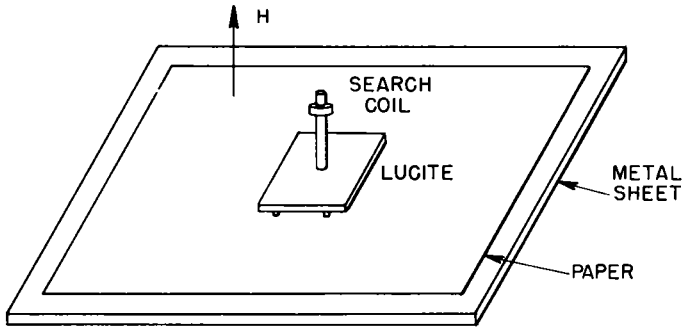


Fig. 2.45—View of search coil in field to be explored in contour-mapping device [Fig. 5A of Daily Log (Z Group), Aug. 7, 1944].

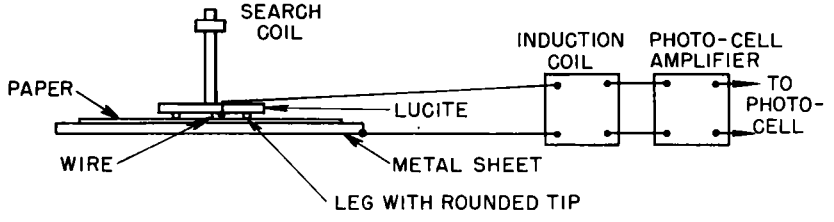


Fig. 2.46—Apparatus for recording points on a contour for contour-mapping device [Fig. 5B of Daily Log (Z Group), Aug. 7, 1944].

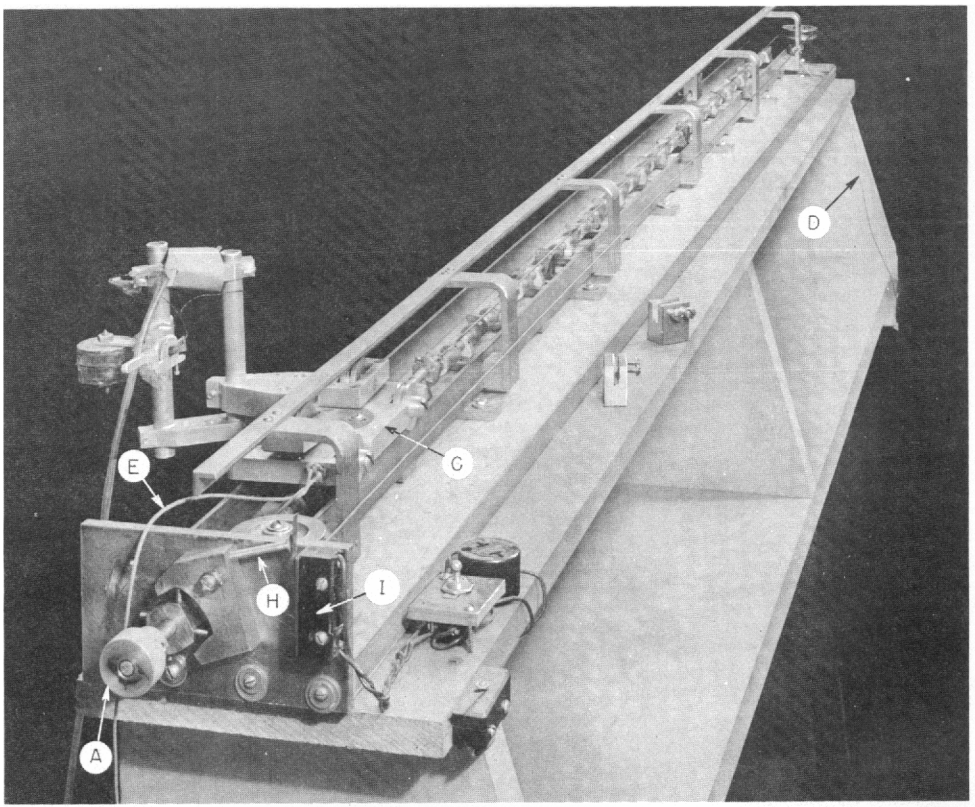


Fig. 2.47—View of boxcar used in making uniformity measurements (magnet 328).

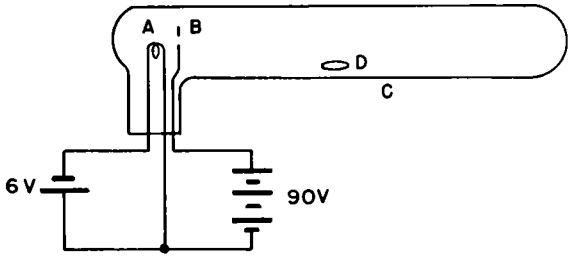


Fig. 2.48 — Mercury-arc tube.

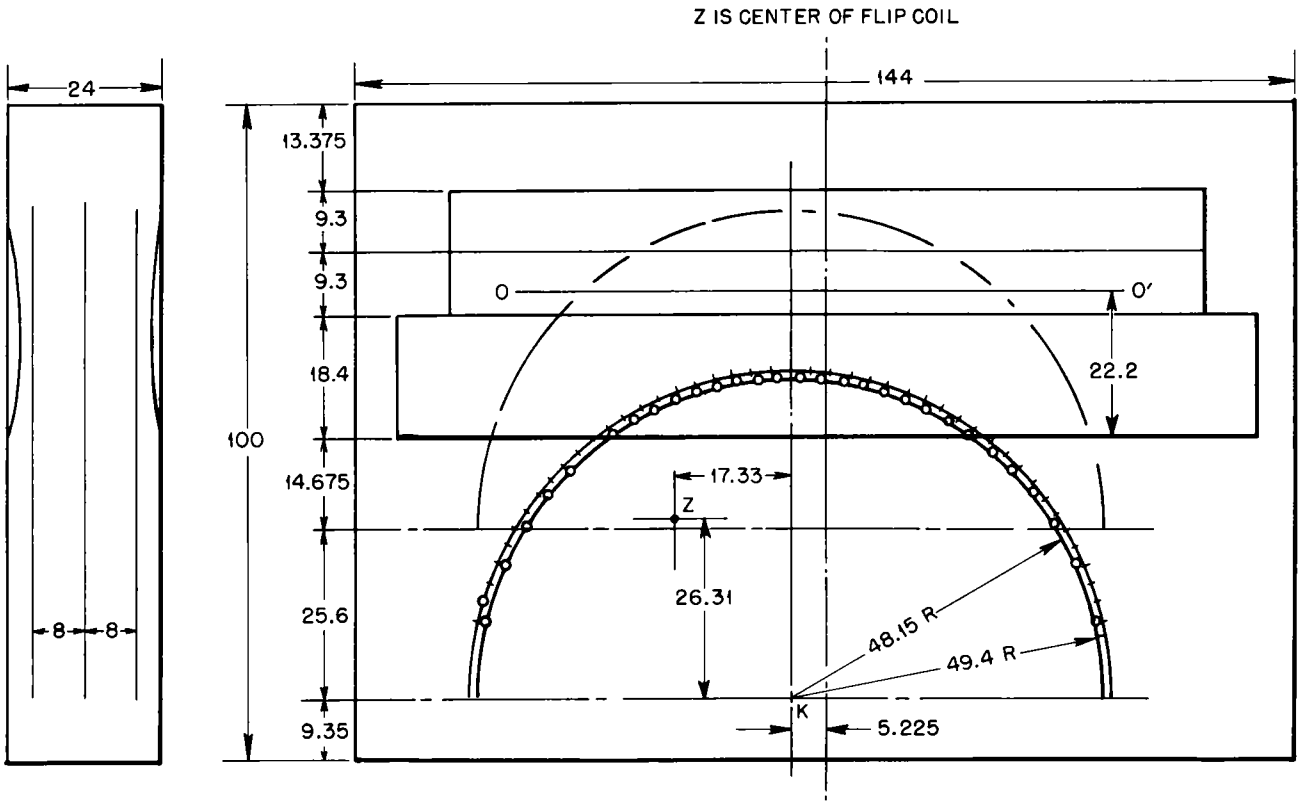


Fig. 2.49—Location of shim-device measurements in Alpha I tanks.

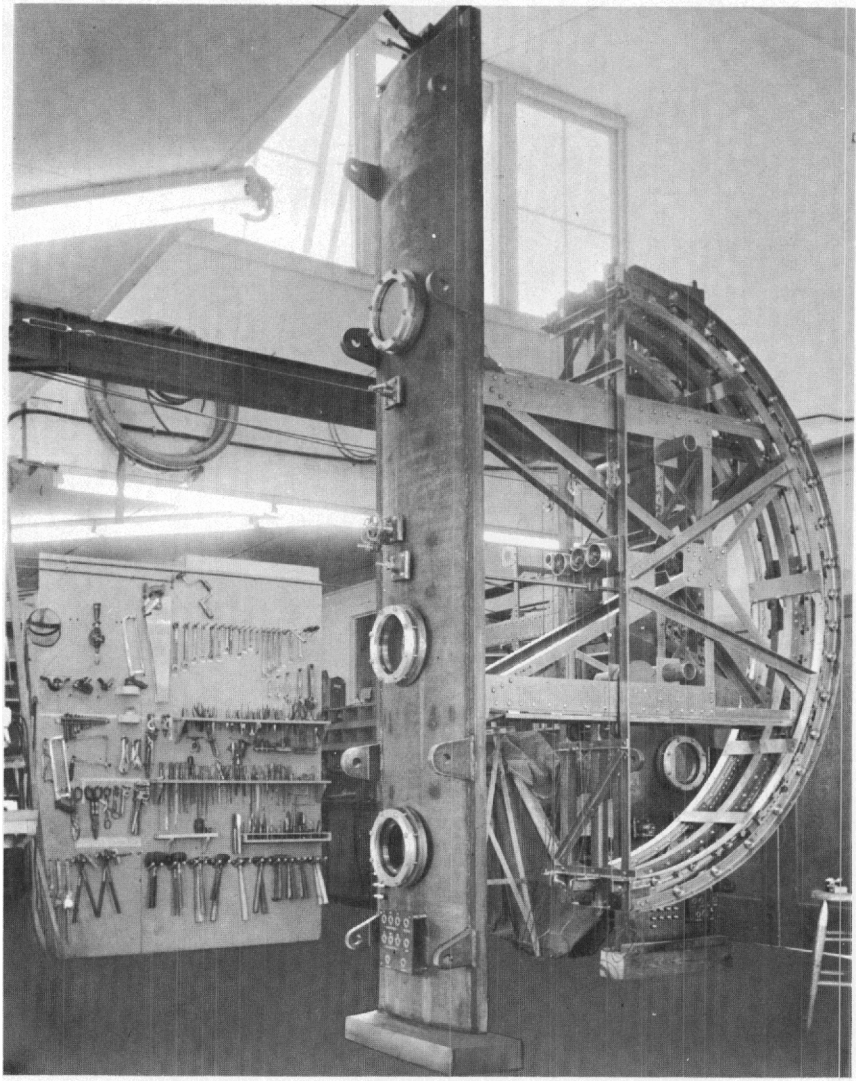

Fig. 2.50 — View of shim-region device I (magnet 121).

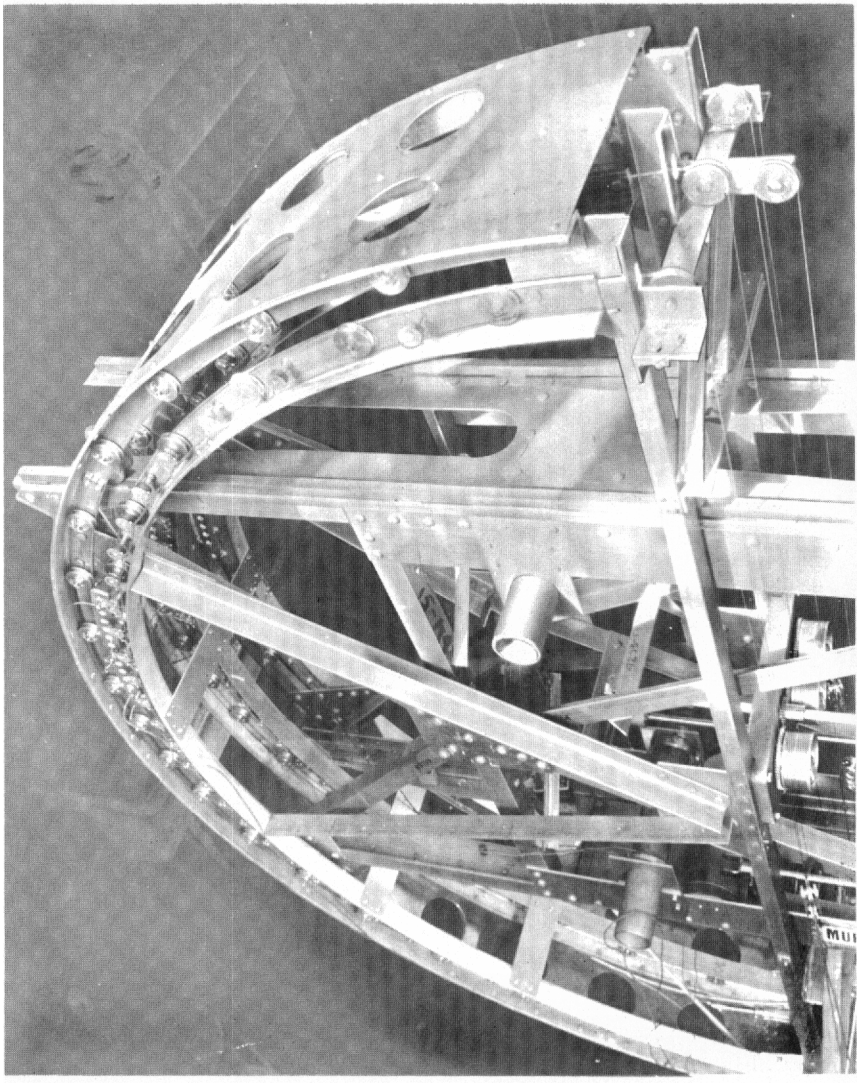

**Fig. 2.51 — View of shim device II (magnet 108).**

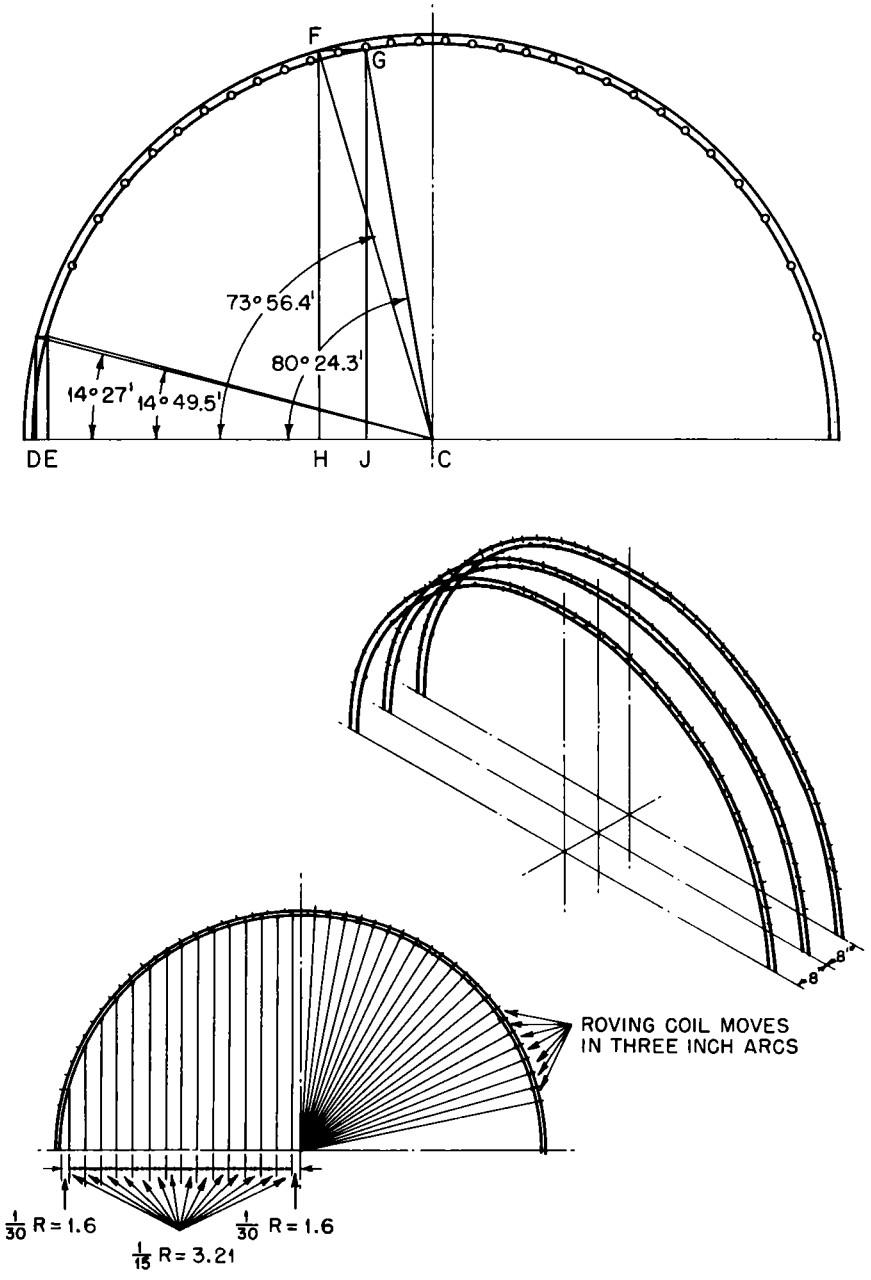


Fig. 2.52—Location of roving-coil measurements.

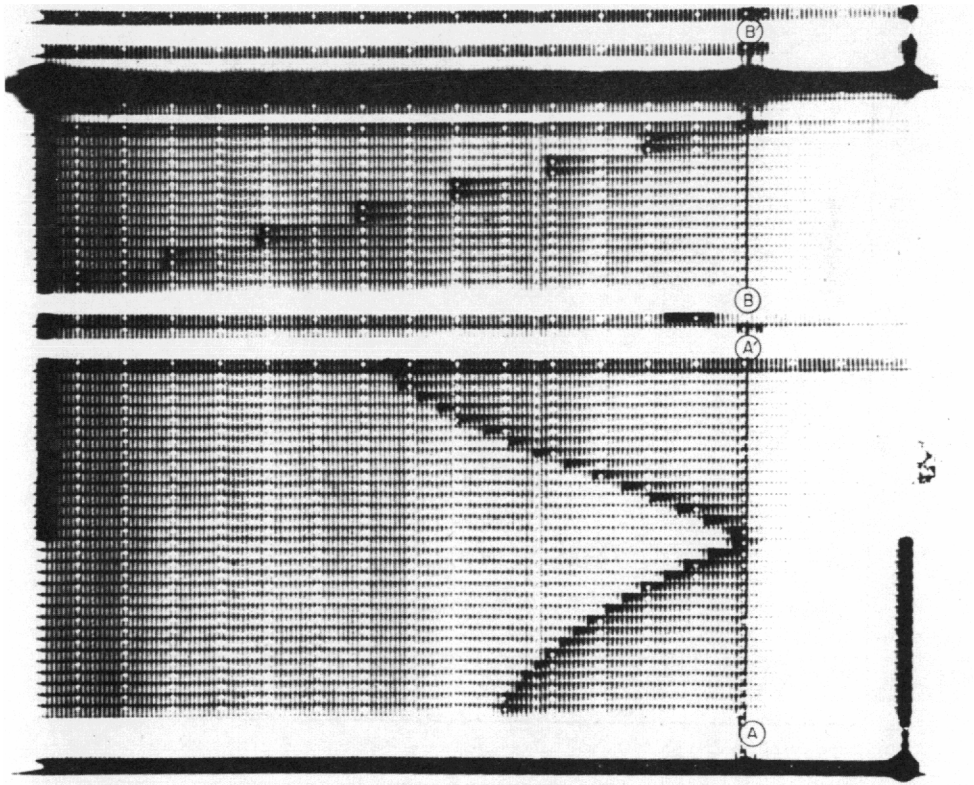


Fig. 2.53—Arc-of-coils photographed data (magnet 350).

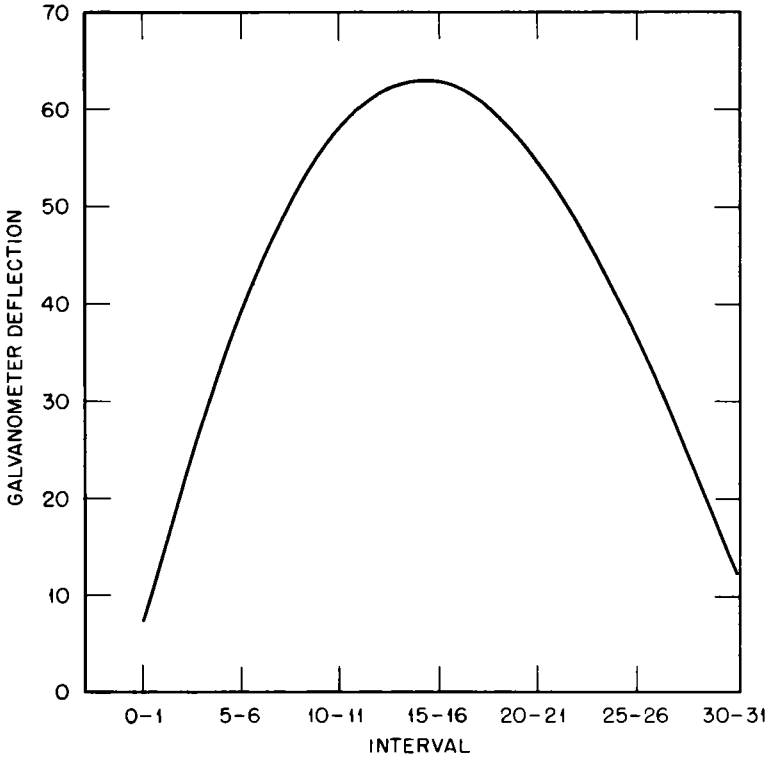


Fig. 2.54 — Example of experimental $\int h_z\, dx$ curve.

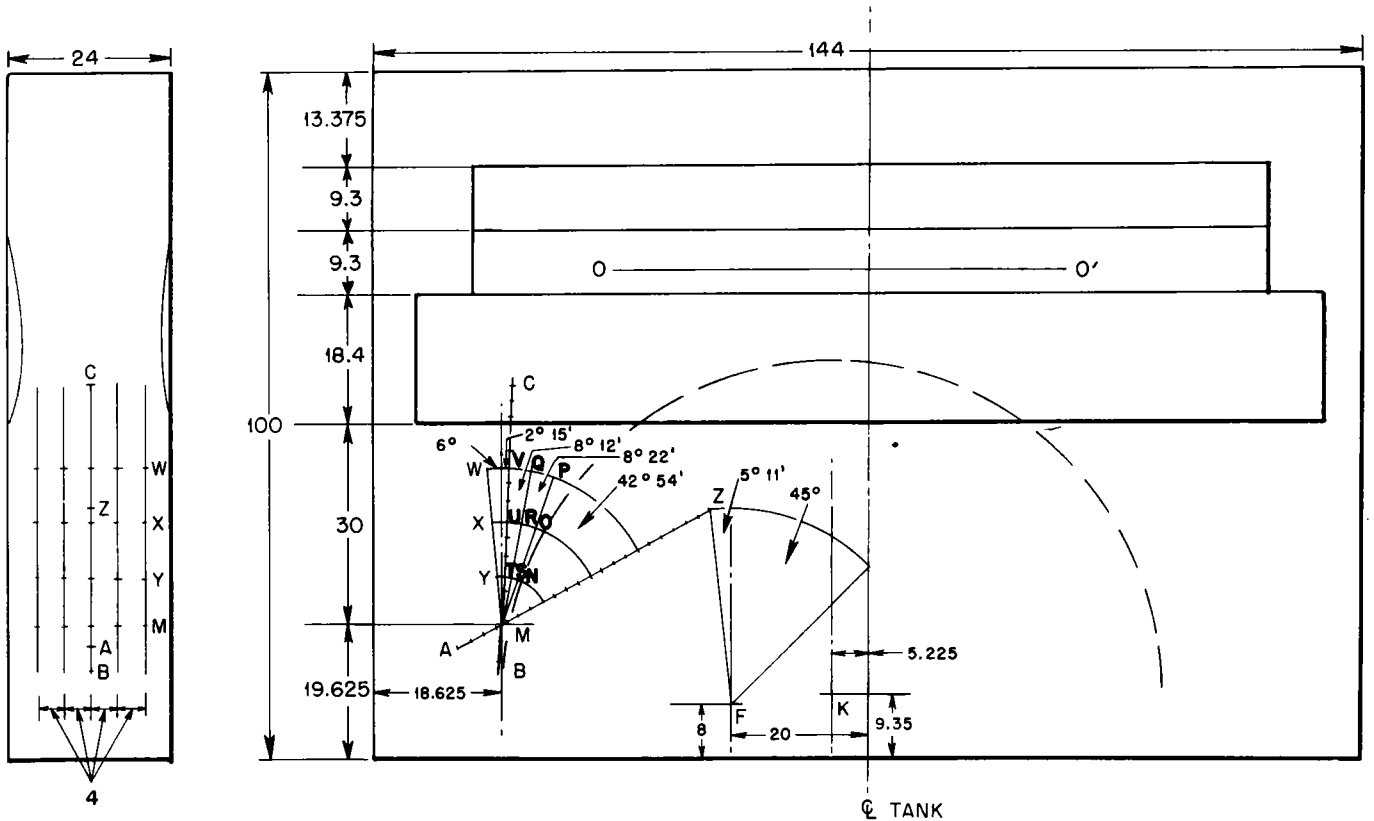


Fig. 2.55—Location of source-region-device measurements in Alpha I.

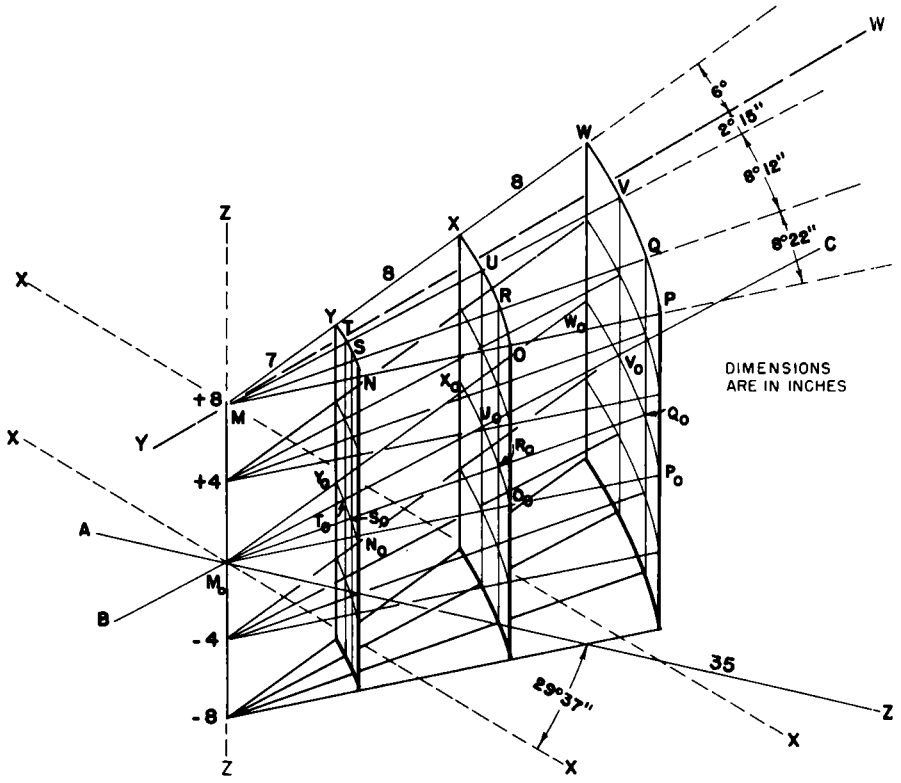


Fig. 2.56—Details of source-region device, showing location of measurements.

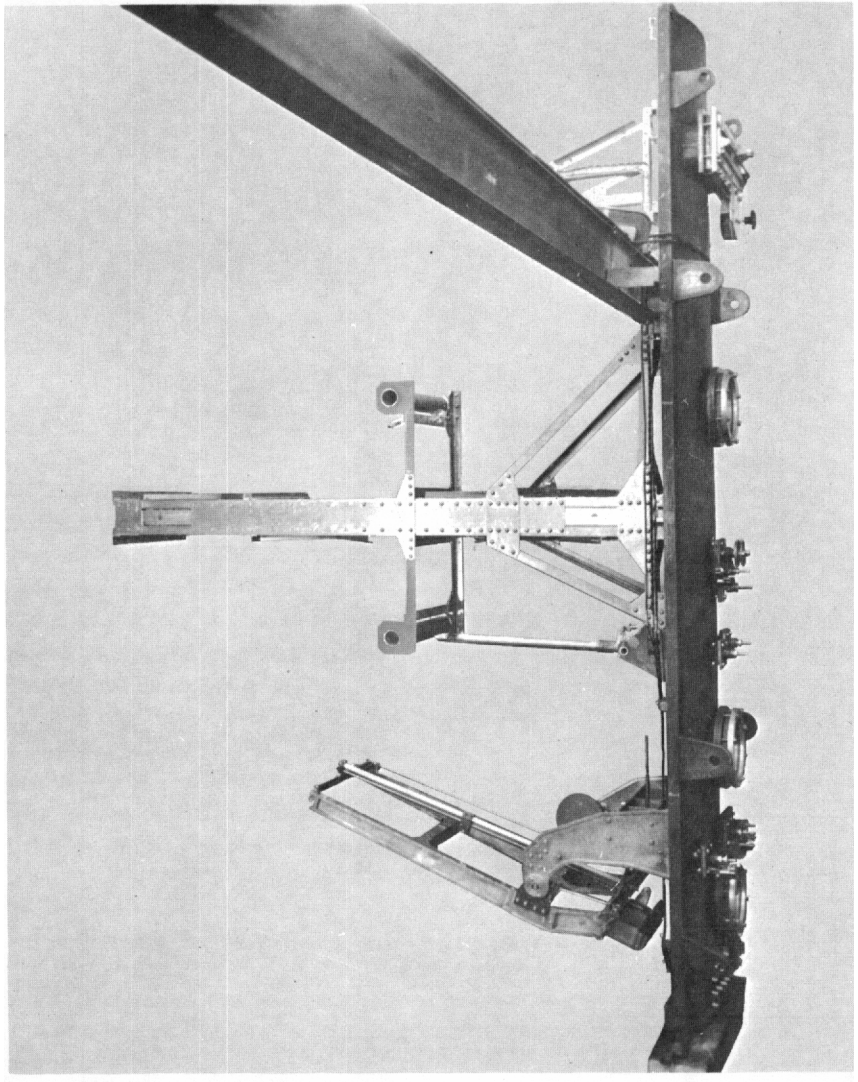

Fig. 2.57—General view of source-region device (magnet 118).

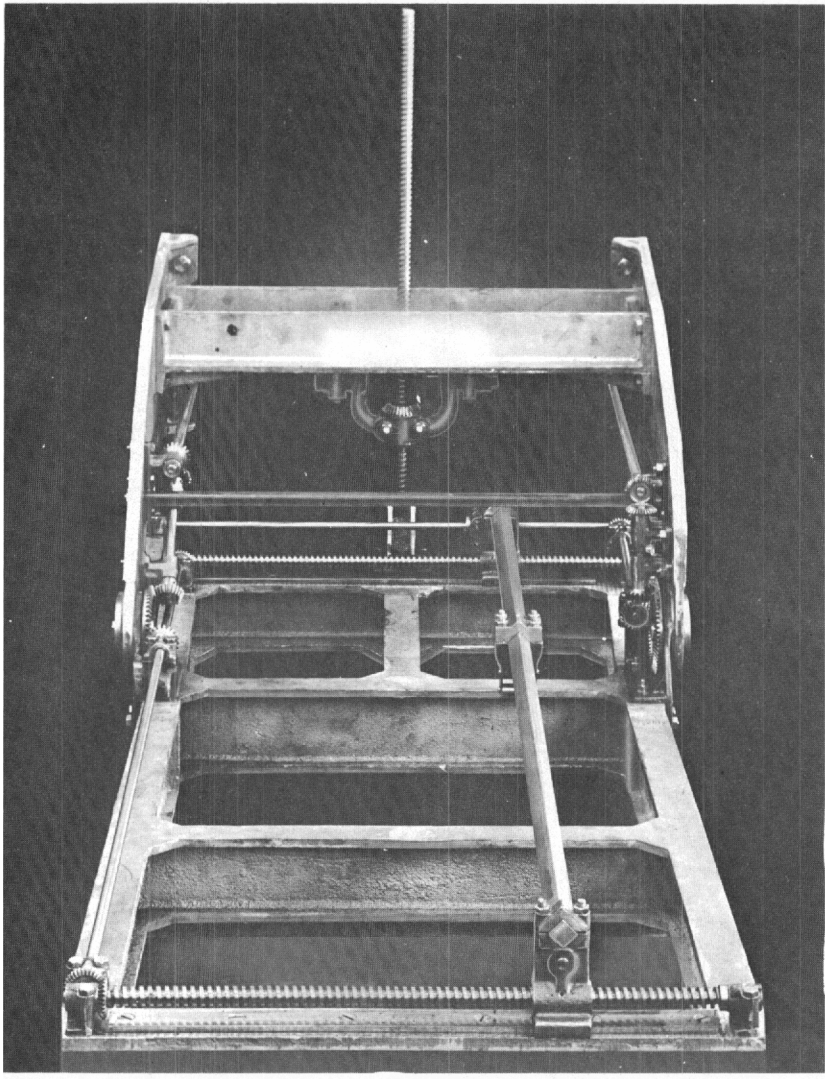

Fig. 2.58—Close-up of portion of source-region device (magnet 76).

## REFERENCES


1. E. Plesset, Electronic Fluxmeter, Report RL 16.6.14, Apr. 23, 1943.
2. Wilson M. Powell, The General Electric Fluxmeter, Report BP-28, May 22, 1946.
3. G. Brown, J. DePangher, and W. M. Powell, Magnetic Balance for Measuring Low Permeabilities, Report RL 27.6.17, Aug. 28, 1943.
4. J. DePangher, M. Hammond, and M. Seegmiller, Areas of Search Coils, Report RL 27.6.11, June 19, 1943.
5. Rosa and Grover, Tables for Computation of Self and Mutual Inductances, Natl. Bur. Standards, U. S., 8: 57 (January 1912).
6. E. Stearns, Calibration of the Hibbert Magnetic Standard Using a Standard Mutual Inductance, Report RL 27.6.10, June 26, 1943.
7. A. Guthrie, Use of Muriel and Cedric in Checking Magnetic Fields, Report RL 27.19, Sept. 23, 1943.
8. A. Guthrie, Design of Magnetic Shims, Report RL 16.6.17, July 5, 1943.
9. A. L. Latter, The Roving Coil on Muriel, Report RL 27.6.18, Sept. 25, 1943.
10. A. L. Latter, Acceptance Criteria for the Measurements with Cedric-J, Report RL 27.6.16, Aug. 9, 1943.

Chapter 3

# MODEL MAGNETS AND THEIR PERFORMANCE

By R. K. Wakerling

## 1. INTRODUCTION

Scale models of all of the types of magnets used in the calutron process were built and their performance characteristics measured. Estimates of the performance of the field-scale units could then be made with some assurance. By the use of models, the effects of changes in design could be explored quickly and with a sufficient degree of accuracy. Later tests made on the full-scale magnets showed the model tests to be dependable and accurate.

The models of the magnets used in the production design were constructed on a scale of 1/16. The usual measurements made included a magnetization curve, a comparison of gap performance at different points in the magnet, uniformity contour maps, determination of magnetic forces, the density of flux through various parts of the magnet, and the determination of the stray field.

As an illustration of the work done on models, the performance tests on the revised Alpha II model will be discussed in some detail in Sec. 2 of this chapter. The results of the tests of other models will be given in brief form in Sec. 3.

## 2. TESTS ON THE MAGNET MODEL ALPHA II (REVISED)[1]

2.1 Procedure. The 1/16-scale model was assembled as shown in Fig. 3.1. The full-scale magnet contains 96 tanks and was designed to operate normally at fields up to 4600 oersteds. It is symmetrical about the mid-yoke, with 48 tanks in each half of the track. It is designed so that half of the track may be shut down for repairs, etc., while the other half continues to operate. The power for the model was supplied by a 1000-amp 250-volt d-c generator. Because of power

limitations, it was necessary to limit the model to 42 active tanks. Forty-two inactive tanks from the original Alpha II model were placed on the other side of the mid-yoke to aid in dispersing the flux and to give a performance more nearly equal to that of the full-scale half-track. The performance of the model should approximate closely the performance of the full-scale magnet when half the track is excited.

An estimate of the difference in performance between the half-track and full-track operation was made on the basis of results from tests of the original Alpha II model. Because of the power operating field in the original, it was possible therefore to test a nearly full model of that track and make comparisons between half-track and full-track operation. A similar proportional difference between full- and half-track operation was assumed for the revised Alpha II. Many of the characteristics for each magnet remain essentially the same whether the half-track or the full track is excited.

Tanks 1 to 21 were especially chosen for the accuracy of their construction and most of the measurements were carried out in them. The field strength vs. magnet current relation was determined for tank 13, and a magnetization curve was drawn for it. The relative field strengths with end coils having only half the standard number of turns next to the yokes were determined for the tanks near the yokes. The field was found to be low in these tanks. Extra turns were placed on the end half-coils next to the yokes to increase the field strength in the adjacent low tanks. Two extra turns on each half-coil, representing 57.7 per cent end coils, were tried and the relative field strengths determined for tanks 1 to 21. These were found in two cases, when there were fields of 4600 and 3400 oersteds in the middle of the standard tank 13. The fields in the tanks near the yokes were still found to be slightly low. By extrapolation, however, it was possible to calculate the optimum number of turns for the coils next to the yokes to bring their fields up to average. The uniformity of field strength inside tank 5 was determined both with 4600 and 3400 oersteds in the middle of the tank, and contour maps of the field strengths were made. The flux through various parts of the magnet was measured, and the magnetic forces in the magnet and on the coils were determined. An investigation of the shape and intensity of the stray magnetic field in various regions near the magnet was made as well as measurements of the permeability of the iron in the model and in the full-scale magnet.

The efficiency of the magnet, defined here to be the percentage of the magnetomotive force which is effective in producing a field in the gaps, was determined from the average of the results of the field-

strength measurements. The results are given in Secs. 2.3 to 2.6 inclusive.

2.2 Discussion of the Model. The cores were constructed as shown in Fig. 3.2. The iron plates were cut from 1/16-in. auto-body steel with the magnetic characteristics shown in Fig. 3.3. The iron at the edge of the core consisted of six 1/16-in. plates. It was made thick to take care of the flux which must be supplied to the walls of the coil cooling tanks, the field in the overhanging edge of the process tank, and the steel side walls of the process tank.

The first step in assembling the core edge was to spot-weld the three outermost plates together. Four sets of these triple plates were then formed into a rectangle and electrically welded at the corners to hold them together. This made a core edge which was three plates thick. Three additional plates were then placed inside each edge of the welded frame, making the core edge six plates thick. The core inserts were then placed in position with 5/32-in. maple spacers between, as shown in Fig. 3.2. The 3-3-2 plate arrangement was used so that, except at the edges, the iron occupied half the space.

The coils were constructed as shown in Fig. 3.4. Each coil consisted of 13 turns of 1/2- by 1/16-in. annealed copper strip. The successive turns were insulated from one another by a double strip of paper. The coil then was covered with cloth tape. Fish paper was placed on the inside of the coil to insulate it from the core. The leads were taped and insulated with fish paper at the point where they came through the covers. In addition, the pieces of fish paper between the core faceplate and the process tanks, used to simulate a tolerance gap, served further to insulate the individual core units from one another. This reduced the maximum possible potential difference between any part of the coil and its corresponding core to 10 volts. The coils were used in pairs, making a total of 26 turns for a full double coil.

To obtain the proper voltage drop for the available generator, alternate coils were connected in series, forming two complete sets. These sets were then connected in parallel. By arranging the circuit in this manner, any differences in current through one of the branches was distributed uniformly throughout the entire magnet. A current of 577.5 amp through the coils gave a field of 4600 oersteds in gap 13, taken as a standard. A current of 428.5 amp gave a field of 3400 oersteds in the same gap.

The coil cooling tanks, shown in Fig. 3.5, were made of two layers of 1/32-in. steel with a slot cut through the top pieces to permit the leads to come out. The covers were double everywhere except in the corners and where the leads were brought out. They were held in

place by the friction of their sides against the fish-paper insulation and against one another.

The process tanks were made as shown in Fig. 3.6. The tanks overhung the cores by $\frac{5}{16}$ in. on every side, corresponding to a 5-in. overhang on the full-scale unit. This is twice the overhang used on Alpha I. Owing to construction difficulties, some of the process tanks were made less accurately than others. A selection was made and the tests were conducted mostly in the better tanks. Owing to symmetry in the design, it was necessary to conduct most of the tests in only half the model, or what represents one-fourth the full-scale unit. The performance of the rest of the magnet was assumed to be the same because of symmetry.

The yokes were constructed as shown in Figs. 3.7a and 3.7b. The butting contact surfaces were machined to ±0.002 in., and a V weld was used to pull them together. On the full-scale unit, pieces are overlapped, so that good magnetic contact is obtained without the accurate machining of the parts necessary when a butt contact is used.

2.3 Field in the Tanks. A magnetization curve was obtained for the model using gap 13 as the standard, and the magnet currents necessary to obtain 4600 and 3400 oersteds, respectively, in gap 13 were determined. This curve is given in Fig. 3.8.

If there were no reluctance in the yokes at the ends and the middle of the magnet, then the coils next to the yokes should have half the number of turns of the coils elsewhere. These small coils are designated by the percentage of turns of a full coil, hence they are called "50 per cent coils." The relative field strengths of gaps 1 to 3, 19 to 21, 22 to 24, and 40 to 42 with respect to gap 13 were determined with 50 per cent end coils next to the yokes, with the results shown in Fig. 3.9. From these data it was seen that the field in the tanks adjacent to the yokes was low. This was due to the reluctance of the yokes. Extra turns equivalent to 7.7 per cent were placed on the end half-coils next to the yokes to overcome this drop, and the results were used to determine the correct number of turns by extrapolation. It was found that when the number of turns on the end coils was 50 per cent of a full coil, the field in tanks adjacent to the yokes was 4.0 per cent low. When the number of turns on the end coils was 57.7 per cent of a full coil, the field in those tanks was 0.73 per cent low. By extrapolating, the optimum number of turns for the end coils was determined to be 59 per cent of the turns on a full coil.

2.4 Efficiency. The efficiency of the magnet is defined as the ratio of magnetomotive force in an average air gap to the magnetomotive force developed by one of the coils adjacent to the air gap. This value is unique if we do not consider the gaps next to the yoke,

where it is necessary to have a few extra turns to compensate for the reluctance of the yokes. From the field-strength measurements the average field in the gaps was determined and the efficiency calculated by the formula

$$\text{Efficiency} = \frac{\text{mmf in gaps}}{\text{total mmf}}$$

$$= \frac{2.02 \times \text{average oersteds} \times \text{total inches of gap}}{\text{amperes through coils} \times \text{turns}}$$

The number of turns used assumes one full coil for each gap. Extra turns beyond that are neglected in the calculations. With a field of 4600 oersteds in the gaps, approximately 95.6 ± 2.0 per cent of the magnetomotive force is effective in producing fields in the gaps. With 3400 oersteds in the gaps the efficiency obtained was 95.4 ± 2.0 per cent. Within experimental error they were the same at both field strengths. This indicates that the magnet design is rather conservative.

Contour maps of the field strength in tank 5 are shown in Figs. 3.10 and 3.11. These were taken with 3400 and 4600 oersteds at the middle of the tank. The results showed that the uniformity of the field in the revised Alpha II model tank at both 4600 and 3400 oersteds compared favorably with that in the Alpha I model at 3400 oersteds. The Alpha II process tanks overhang the edge of the core by 5 in., while Alpha I had only a 2½-in. overhang. Preliminary measurements on Alpha I had indicated that a 5-in. overhang would be satisfactory, but until the full-scale magnet was built and tested it was not considered wise to go to the limit of 5 in. The reason for the comparable uniformity even at the higher field in Alpha II is probably due to the fact that the Alpha II core has much more iron in it. The edge of the Alpha II model core was solid for ⅜ in., whereas in the Alpha I model it was only 5/16 in. thick. The rest of the Alpha II core was half air and half iron, whereas the Alpha I core was three-fourths air and one-fourth iron. The thicker core rim is less saturated and is more capable of carrying flux to the outer regions of the tank. The field at the edges of the tanks then has less tendency to drop off. In the full-scale Alpha II magnet the core rim is 7 in. thick instead of 6 in. This should make the performance of the full-scale unit better still than that of the model.

2.5 Flux-density Measurements. The flux was measured through various parts of the magnet by means of loops of wire wound around the cores and yoke. The lines of induction collapsing through a loop create an electric pulse which can be measured by a galvanometer.

The results are shown in Figs. 3.12 and 3.13. By measuring the area of the loops and dividing this figure into the total flux through the loop, the average flux density was determined through various sections of the magnet. It should be noted that this is the average flux density through the entire loop and does not account for local variations inside the loop.

Exclusive of the core rim, the core was 50 per cent steel. The steel in the cores carries by far the greater part of the flux through the core. A loop was placed inside the core rim so that it looped all the flux going through the middle of the core, exclusive of the core rim. The quantity of the flux was measured and this value divided by the cross-sectional area of the steel in the core. When there was a field of 4600 oersteds in the tanks, the flux density through the steel in the core was 12,000 gauss.

Since the flux density in the steel is twice as great as the average flux density being emitted by the core proper, it would take twice as much magnetomotive force to drive it across the tolerance gap to the process tank, if nothing were done to spread out the flux uniformly over the core face area. The force tending to pull the tank walls outward would also be twice as great. To counteract this in the model, a $\frac{1}{16}$-in. steel faceplate was placed over the face of the core, as shown in Fig. 3.14, to spread out the flux evenly before it crossed the gap. The flux density between the core and process tank then became uniform. In the full-scale unit the core inserts are comprised of H beams. When stacked on one another they form a rather continuous plane over the core ends next to the process tanks and thus spread the flux out uniformly before it spans the tolerance gap to the process tank.

A similar loop was placed around the outside of the core and the quantity of flux through it was measured. By taking the difference between the flux through this outside loop and that through the loop encircling the inside of the core rim it was possible to determine the amount of flux threading the middle of the core rim. By dividing this flux through the rim by the cross-sectional area of iron in the rim, the flux density through the rim was obtained. When there was a field of 4600 oersteds in the tanks, the average flux density in the iron rim was found to be 17,460 gauss. This value is rather high for best operation, but since the rim on the model corresponds to a 6-in. rim on the full-scale unit and that of the full-scale magnet will be 7 in. thick, the flux density in the rim of the full-scale magnet will be slightly more than $\frac{6}{7}$ that in the model. This should make the flux density in the rim of the full-scale unit approximately 15,000 gauss, which is very satisfactory, since the steel is carrying a good load of flux and yet is not

pushed to the point where the permeability has dropped considerably. The permeability of the iron in the core shell at 15,000 gauss is approximately 550.

A loop was wound around the outside of the process tank in its median plane. The total flux threading the loop was found to be $1.886 \times 10^6$ maxwells when there was a field of 4600 oersteds in the tanks. Assuming that the flux density through the tank walls parallel to the smallest dimension of the tank was 30,000 gauss, as determined in the original Alpha II model, the total number of maxwells passing through the narrow side walls was $1.36 \times 10^5$. By subtracting this flux from the total flux through the tank loops, the number of maxwells passing through the inside of the process tank was found to be $1.75 \times 10^6$. The ratio of the total flux passing through the middle of the core to the flux passing through the inside is seen to be 1.45. This means that the fraction of the total flux through the middle of the core which went through the inside of the process tank was 0.69.

The flux density in the coil cooling tanks can be estimated by assuming that the flux which goes through the core and does not emanate from the face of the core goes through the coil cooling tanks. On this basis it was calculated to have the value $4.99 \times 10^5$ maxwells. The cross-sectional area of the model coil cooling tanks was 11.85 sq cm, so that the flux density through the coil cooling tanks was 42,000 gauss. In obtaining this value it was assumed that all the flux which went through the middle of the core and did not emanate from the face of the core was restricted to the iron in the cooling tanks. Actually, since the iron in the cooling tanks is well saturated, much of the flux will not be restricted to the iron. A fair guess as to the flux density in the iron walls of the cooling tanks would be approximately 30,000 gauss.

The flux densities through various parts of the yokes were determined. Figure 3.12 shows the results and the locations of the measurements. When there was a field of 4600 oersteds in the process tanks, in no place was the flux density through the yokes greater than 14,500 gauss. The flux densities found for the various sections of the yokes indicated that the design of the yokes was very satisfactory. In the neighborhood of 10,000 to 15,000 gauss the flux density is good, yet the yokes are not overloaded to the extent that the permeability of the steel drops excessively.

Loops were wound around the inside and outside of the magnet coils in the various locations shown in Figs. 3.15 and 3.16, and the flux threading these various loops was measured. By observing the magnitude and direction of the flux through the various loops, we can trace the magnetic circuit of the lines through the coil cooling tanks. As

shown on Fig. 3.16, there were $2.08 \times 10^5$ lines flowing up from the core shell between loops 2 and 3. Of these, $1.44 \times 10^5$ lines passed between loops 3 and 6 and $0.62 \times 10^5$ between loops 5 and 6. The remaining $0.02 \times 10^5$ lines passed back between loops 2 and 5. The subtraction of the flux threading one loop from that through another gives rise to several combinations of differences of flux. By dividing the flux difference between any two loops by the area enclosed in the difference of the two loops, the average leakage flux density in that area can be calculated. Through the proper selection of pairs, either the vertical component of the leakage flux or the horizontal component may be found.

For the horizontal component of the leakage flux we take the difference between the values of the flux through loops 1 and 4 of Figs. 3.15 and 3.16. The difference for loops 3 and 6 should give approximately the same value, because of symmetry. At a field of 4600 oersteds the flux through the loops had the values

$\phi_1 = 2.526 \times 10^6$ maxwells $\qquad \phi_3 = 2.487 \times 10^6$ maxwells

$\phi_4 = 2.650 \times 10^6$ maxwells $\qquad \phi_6 = 2.631 \times 10^6$ maxwells

so that $\phi_4 - \phi_1 = 1.24 \times 10^5$ maxwells and $\phi_6 - \phi_3 = 1.44 \times 10^5$ maxwells. By averaging these last two values, we get $1.34 \times 10^5$ lines. The area between the pairs of loops was 214.14 sq cm, whence dividing the flux by the area we get 626 gauss for the flux density. Since the permeability of the air and copper inside the coil cooling tanks is 1, we get 626 oersteds for the horizontal component of the field inside the coil cooling tanks. It is to be noted that the flux difference between loop 2 and loop 5 is nearly zero. This shows that the leakage flux through the coils finds its way to the iron in the cooling tank and the iron in the core by the time it reaches the middle of the coils. This indicates that the average horizontal leakage flux inside the coil cooling tanks must be lower than the indicated value of 626 oersteds.

The difference in flux through loop 1 and loop 3 is seen to be practically zero except in those cooling tanks next to the yokes, for near the yokes the symmetry is disturbed. On the straightaway the flux would cancel out because of symmetry. However, by taking the difference of flux through loop 1 and loop 2, the vertical component of flux through half the coil cooling tank is found. Averaging the two parts we get a crude approximation to the vertical component of the leakage flux through the coil cooling tanks. The following table gives the flux through the six loops:

| Loop | Flux in maxwells |
|---|---|
| 1 | $2.526 \times 10^6$ |
| 2 | $2.695 \times 10^6$ |
| 3 | $2.487 \times 10^6$ |
| 4 | $2.650 \times 10^6$ |
| 5 | $2.693 \times 10^6$ |
| 6 | $2.631 \times 10^6$ |

From these data it is found that the average flux difference is $1.33 \times 10^5$ maxwells. The average area difference is 118 sq cm, so that the average vertical flux density is 1100 gauss. Since $\mu = 1$, the average vertical component of leakage flux field through the coil tanks is 1100 oersteds.

2.6 Magnetic Forces. In making magnetic-force calculations, if there is a smaller flux density in some regions and a greater density in other regions, the forces calculated on the basis of the average over the entire region will be lower than the true force. This results from the fact that the force over any area is proportional to the square of the field times the area. The average field in the space between the core and the process tank was found to be 6682 oersteds. On this basis the forces on the main tank walls were calculated, assuming that the field was uniform. The magnetic forces were then combined with the force of the atmospheric pressure to give the total force.

$$\text{Magnetic force in tons} = \frac{(\text{kilogauss})^2\,(\text{area in square inches})}{(1.735)(2000)}$$

Force of atmospheric pressure tending to push tank walls inward:

$$\frac{(14.7 \text{ lb/sq in.})\,(105 \text{ in.})\,(150 \text{ in.})}{(2000 \text{ lb/ton})} = 116 \text{ tons}$$

Magnetic force tending to pull tank walls outward:

$$\frac{(6.682)^2(95)(140)}{(1.735)(2000)} = 171 \text{ tons}$$

Magnetic force tending to pull tank walls inward:

$$\frac{(4.6)^2(105)(150)}{(1.735)(2000)} = 96 \text{ tons}$$

Net magnetic force tending to pull tank walls outward: 75 tons
Net resultant force on tank walls: 41 tons

Thus in the full-scale magnet there is a force of 41 tons pushing inward on the tank walls.

Knowing the lengths of the conductors in the full-scale magnet and the current which they will be carrying, we can now calculate the forces on the current-carrying conductors due to their reaction on the leakage flux. The forces on the conductors are given by the formula

$$\text{Tons of force on conductors} = \frac{\text{kilogauss} \times \text{amp} \times \text{length in inches}}{1750 \times 2000}$$

From the horizontal component of flux density through the coil cooling tanks we get the following inward component of force tending to squeeze the coils down on the cores for the full-scale magnet:

Average field = 626 oersteds
I = (46/34)1470 = 1990 amp
Average length of sides = 160 in. for 132 conductors
Average length of top and bottom = 115 in. for 132 conductors

Tons of force on sides pushing conductors into core (approximate):

$$\frac{(0.626)(1990)(160)(132)}{(1750)(2000)} = 7.5 \text{ or } 8 \text{ tons}$$

Tons of force on top and bottom pushing conductors into core (approximate):

$$\frac{(0.626)(1990)(115)(132)}{(1750)(2000)} = 5.4 \text{ or } 5 \text{ tons}$$

It was concluded that a safe estimate of the maximum force between a core and the tanks would be 200 tons and that the unbalanced forces on cores or tanks would amount to about 30 tons. The average tension in the race track tending to pull it together was estimated to be 175 tons on each side, while the total force on the end yokes was put at 350 tons. The process tanks are in a position of unstable equilibrium, with a possible magnetic force of 20 tons tending to push them out of the gaps. Figure 3.17 presents these data graphically.

From the component of the flux density through the coil cooling tanks toward the core we get the following horizontal forces tending to push each half of the coils together toward that center plane of the core which is parallel to the face of the core:

Mean perimeter of coil = 526 in.
132/2 or 66 turns per half-coil
Vertical component of field = 1100 oersteds

Tons of force on each half-coil tending to push them together toward middle of core:

$$\frac{(1100)(1990)(526)(66)}{(1750)(2000)} = 21.712 \text{ tons}$$

The forces on the coils next to the yokes will differ from these because of the influence of the yokes.

2.7 Stray Field. Permeability of Material. Gap Tolerance. The results of stray-field measurements are shown in Fig. 3.18. Measurements were made on the inside of the track as well as on the outside and also in the region of the yokes. The stray-field measurements were made when half of the magnet was excited, so that the results for the immediate region of the mid-yoke will be somewhat altered when the full magnet is excited. The direction of the flux was determined by photographing iron-filing patterns, one of which is shown in Fig. 3.19. The intensity of the flux was measured with a coil and a ballistic galvanometer. In summary it may be said that the stray field falls to about 10 oersteds at 10 ft from the magnet in any direction when the field in the tanks is 4600 oersteds.

Figure 3.3 shows the permeability of the core material of the model and the full-scale unit. The permeability of the material of the full-scale unit is higher than that of the model. This indicates that a slightly better performance could be expected from the full-scale unit than from the model.

If the space between the core and the process tanks is not kept within certain tolerances, the field inside the tanks will not be suitable. Calculations have been made by E. Nelson, S. Frankel, and J. Richardson to determine the condition that must be satisfied. They found that the space between the tank and the cores must be great enough so that the maximum separation is never more than twice the minimum separation.

## 3. TESTS OF OTHER MODEL MAGNETS[2]

3.1 Magnet Model A.[3] Model A was built to test the design of the magnet for the Alpha I plant. A plan view of the model, which was built to a $\frac{1}{16}$ scale, is shown in Fig. 3.20. The power source was the 2000-amp 210-volt d-c generator set used for the 184-in. magnet. A section of the magnet, of the size indicated in Fig. 3.21, was more

convenient to use for many of the tests. It was supplied by the 500-amp 125-volt generator of the 37-in. magnet. The cores were of such a construction that one-fourth of the area supplied by the core was filled with iron. There were two tanks in each gap, but for simplicity they were made as one unit. The coils were of the same construction as those described in Sec. 2.

Approximately 95 per cent of the magnetomotive force was effective in producing the field in the gap of the full model. The cooling tanks caused a reduction of the efficiency from 98 per cent to the above value. Variations in the field strength from tank to tank were small. The tanks on the curved portion of the magnet had, on the average, fields which were 1.75 per cent lower than those on the straight portion. Without the cooling tanks the field in the process tanks opening toward the inner space enclosed by the magnet averaged 1.5 per cent higher than those in the tanks opening outward. The cooling tanks caused the field in the inner tanks to drop by 3.2 per cent but left that in the outer tanks practically unchanged. The average field in an inside tank was 3222 oersteds and in an outside tank was 3343 oersteds.

It was calculated that in the full-scale magnet the force between one tank and a core would be 61.7 tons, so the total force on a core due to two tanks would be 123.4 tons. A safe estimate of 150 tons was made on the basis of these computations. The forces on the coils on the straight part of the magnet were in a direction to compress the windings and to force them toward the core. On the curved parts of the magnet there was a force which was estimated for the full-scale unit to be not greater than 10 tons, tending to move the coils back from the edges of the gap. This force might be as low as 2 tons. The average tension in the magnet was estimated to be about 125 tons.

From the model test it was thought that uniformity of the magnetic field would be improved by inserting more iron in the cores near the sources, in the amount of about 1076 tons. The stray field was found to fall to about 9 oersteds at 8 ft from the magnet in any direction. Since the permeability of the iron in the model was less than that for the full-scale magnet, the performance of the full-scale unit would be expected to be better.

3.2 Magnet Model X Beta.[4] The X Beta model (Fig. 3.22) was built on a ⅛ scale. The cores, which were solid, were assembled from 1/16-in. milled-steel plates. The return path of the magnet was made of the same material, with the plates overlapping at the corners. The tank walls were simulated by ⅝-in. steel plates held apart by brass spacers. The coils were made of 25 turns of ½- by 1/16-in. copper strip with paper insulation. A piece of iron ⅛ in. thick was placed under each coil tank to produce the effect of the heavy 1-in.-thick iron plate

upon which each coil tank of the full-scale unit was to rest. The center core had four coils on it, held in the center of the coil tank by wooden wedges. Only three coils were put on each of the side cores. Wooden spacers held these in the center of the coil tanks. The use of a smaller number of coils on the end core was based on experience with models using the same type of return path but with more than two gaps. This effect had been observed in the XA magnet, the field of which was corrected by reducing the number of turns in the outside coil. This change produced a considerable improvement in the behavior of the beam.

It was found that the efficiency of the model was 87.5 per cent at a field of 6300 oersteds. Contour maps of the field in the gaps showed it to be adequately uniform in every way necessary to produce an excellent focus. It was considered that the field was exceptionally good at all parts of the beam and could be used at values as high as 7000 oersteds. If it is assumed that 85 per cent of the magnetomotive force is effective in producing a field of 6800 oersteds in the gap, then with a total air path of 29 in. the number of ampere turns in the full-scale unit should be 468,000. This means that the total power necessary would be 130 kw.

Measurements of the flux density at various places in the model showed that for the full-scale magnet a force of 140.2 tons would exist between the core and the tanks. This force is considerably greater than the magnetic force tending to pull the tank walls together. Even under vacuum there would be a force of 54.5 tons tending to pull the tank walls apart. This force was so large that an investigation of the distribution of flux over the surface of the tank was made in an effort to discover if there was a crowding of the lines of force at the edge of the core. No such effect was discovered. None of the flux densities which were measured were found to be in any way excessive, a fact further evidenced by the high efficiency of the magnet and the linear appearance of the magnetization curves even at fields as high as 7000 oersteds.

The measurement showed that the flux density through the core nearest to the return path was somewhat smaller than the average, resulting in an unbalanced force on the tank of 31 tons tending to pull the tank toward the core nearest the return paths of the magnet. It appeared that the field might be slightly higher at the sides of the tank toward the return paths. It was therefore recommended that taps be provided on the outside coils which would permit the number of turns to be lowered. The unbalanced force on the tank depends directly on this lack of balance in the field and should be reduced by this proposed change in the ratio of the number of turns in the coils. The field in

the tanks would also be improved by this process. However, it was so uniform that no more than a small change was expected from this cause.

3.3 Magnet Model Beta.[5] Model Beta was a 1/16-scale magnet built to test the design of the magnets for the Beta plant. A plan view of the model is shown in Fig. 3.23. The cores were made of mild steel and were solid, like those in the magnet model X Beta. The return path was made of the same material. The walls of the tanks were simulated by 5/16-in. steel plates, and no gaps were provided between these and the cores. Brass spacers held the tank walls apart, simulating a gap of 14 in. on the full-scale magnet. The coils were made with 13 turns of 1/2- by 1/16-in. copper strips, paper-insulated, with two coils mounted on each core. Wooden spacers held the coils in the center of the coil tanks, which were made of two layers of 1/32-in. mild steel.

At first all of the coils were connected in series and magnetization curves were obtained for gaps 1 to 10. The results indicated that gaps 1 and 10 were approximately 15 per cent higher than the average of all the gaps. In order to correct this effect, one of the coils was removed from the circuit at either end of the line of gaps. With this new arrangement gaps 1 and 10 gave fields about 1.8 per cent low. On the basis of these two measurements it was recommended that the end coils be supplied with 55 per cent of the number of turns on the other coils. When the end coils were removed, 96.7 per cent of the magnetomotive force was effective in producing fields in the gaps at an average of 6300 oersteds. Contour maps were not made for this model, since it seemed to be perfectly reasonable to assume that the contour maps for the X Beta model would be identical with those from this model, and since the X Beta model was built to 1/8 scale it seemed true that the results would be more accurate than those which could be obtained on a 1/16-scale model.

Flux-density measurements were made and from them the forces between the cores and the tanks were calculated at various positions in the model. In tanks away from the return paths of the magnet the force had an average value of 128 tons. The force between the tanks adjacent to the end yoke and the yoke was 149 tons, but since the core butts up against the return path, no special provision need be made for this additional force. The force on the end yoke due to the two sides of the magnet was computed to be not more than 300 tons.

Measurements of the stray field were made, and its distribution was plotted by means of iron-filing patterns. Along the center line of the magnet the stray field was found to drop to a value of 7.9 oersteds at a distance of 7 ft from the magnet.

3.4 Magnet Model Alpha II (As Originally Proposed).[6] This model, shown in Fig. 3.24, is essentially the same as that discussed in Sec. 2 of this chapter. The tests outlined there were carried out in the same detail upon this model. The principal difference between the two models was that the revised model was designed to operate at fields as high as 4600 oersteds, whereas the model under consideration here was designed to operate at 3400 oersteds. Experience gained from weakness observed in this original model was utilized in designing the revised one.

The full-scale magnet was to contain 96 tanks; however, because of power limitations it was necessary to construct the model with only 84 tanks. The cores were constructed from $\frac{1}{16}$-in. auto-body steel with the iron occupying only one-fourth the space except at the edges of the core, which consisted of four $\frac{1}{16}$-in. plates. Maple spacers were used to hold the steel sheets in place. The coils were of the same design as those used in the revised model, and they were connected in the same way, i.e., every third coil was connected in series to form three complete sets that were then connected in parallel. With the full magnet excited, a current of 445 amp through the coils gave a field of 3400 oersteds in gap 11, which was taken as a standard. It required 448 amp to produce the same field when half the magnet was excited.

The field strength was determined in the middle of each of the tanks. Tanks 1 and 21 were selected for their better qualities, and the field strength was determined in them both when half and when the entire magnet was excited. There was a general decrease of the field from one end of the model to the other, owing to the selection of good tanks placed at one end with the poor ones at the other. This drop should not exist in the full-scale magnet. From the data on field strength the field was found to be low in tanks adjacent to the yokes. Extra turns were placed on the end half-coils next to the yoke to overcome this drop and to make the field strength essentially the same in all the tanks. It was found that the optimum result was obtained when the number of turns on the end coils was 61.5 per cent of a full coil. From the measurements the average field in the gaps was determined and the efficiency calculated. It was found that when the full magnet was excited the efficiency was approximately 92.2 per cent, this figure dropping to 91.3 per cent when only half the magnet was excited.

Contour maps of the fields in several of the tanks were made with a field of 3400 oersteds in the middle of the tank. The results showed that the uniformity of field strength in this model compared favorably with that in the model Alpha I. It was concluded that, since the Alpha I field uniformity had proved satisfactory in the full-scale unit, the Alpha II field should prove equally satisfactory at 3400 oersteds, this

being true despite the fact that the Alpha II process tank overhangs the edge of the core by 5 in. instead of by 2.5 in. as in the case for Alpha I. The difference should be made up by the thicker core shelf or rim in the Alpha II magnet.

The flux was measured through various parts of the magnet and the flux density determined. From these data the forces on the tank walls were calculated. It was found that in the full-scale unit there would be a force of 68 tons pushing in on the tank walls, while a safe estimate of the maximum force between a core and a tank was taken to be 125 tons. Unbalanced forces on cores or tanks could amount to 15 tons. Provision must be made to anchor the tanks in place since there is a possible force of 10 tons tending to push the tanks out of the gaps. The average tension in the track tending to pull it together was calculated to be about 100 tons on each side, with a total force of 200 tons on the end yokes. It was further found that the flux density in the steel of the cores was 17,200 gauss. At this value of the flux density, the permeability of the steel had dropped to approximately 150. In the material of a full-scale unit, the corresponding permeability would drop to 118, which is dangerously low. In certain localized regions it might even be lower. The flux density through the tank walls was found to be 30,000 gauss, showing that they were well saturated. The flux density through the coil cooling tanks was measured to be 28,000 gauss, while that through the yokes ran between 14,000 and 15,000 gauss. In this range the permeability of the steel is still good, so that the yokes would prove satisfactory as designed.

Stray-field measurements were made on the inside of the track as well as the outside; the direction of the flux was determined by photographing iron-filing patterns. The stray field of the magnet falls to about 10 oersteds at 7 ft from the magnet in any direction, with the possible exception of the corners of the end yokes.

It was concluded from the measurements on this model that the high flux density in the cores indicated the necessity for more iron. It was estimated that an increase of 24 per cent in the amount of iron would reduce the flux density to approximately 14,000 gauss and would result in more efficient and better operation of the magnet. The fact that the permeability of the iron in the model is greater than that of the iron which would be used in the full-scale magnet should contribute toward making the full-scale magnet perform slightly more poorly than the model. On the other hand, the iron at the edges of the cores was proportionately 1 in. thinner, and that in the coil tanks 0.5 in. thicker, on the model than that proposed for the full-scale unit. Both of these factors should tend to make the performance of the model poorer than that of the full-scale magnet.

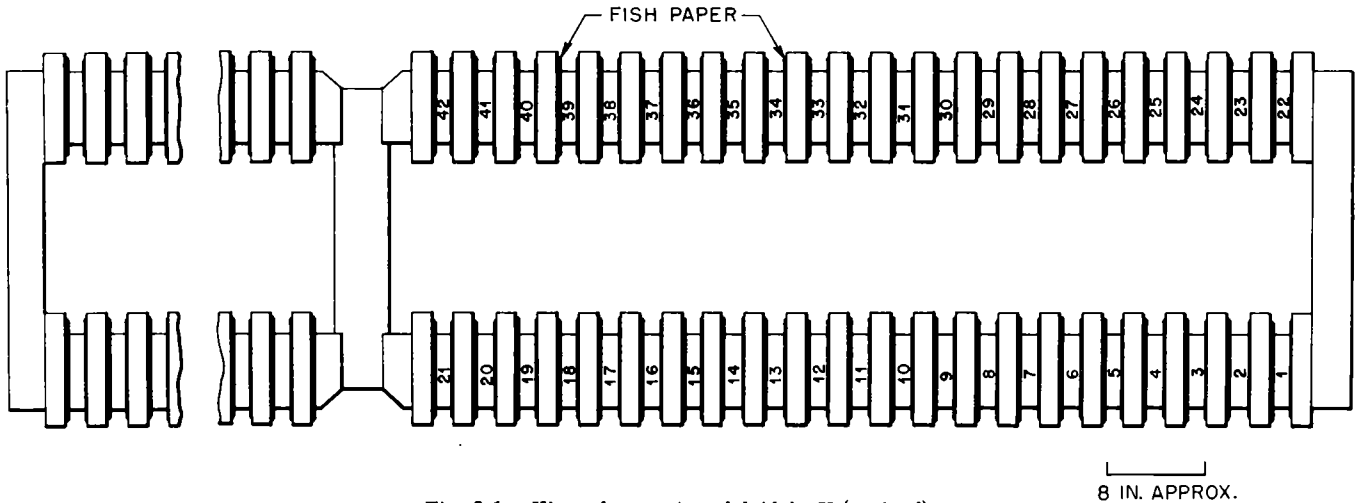


Fig. 3.1—View of magnet model Alpha II (revised).

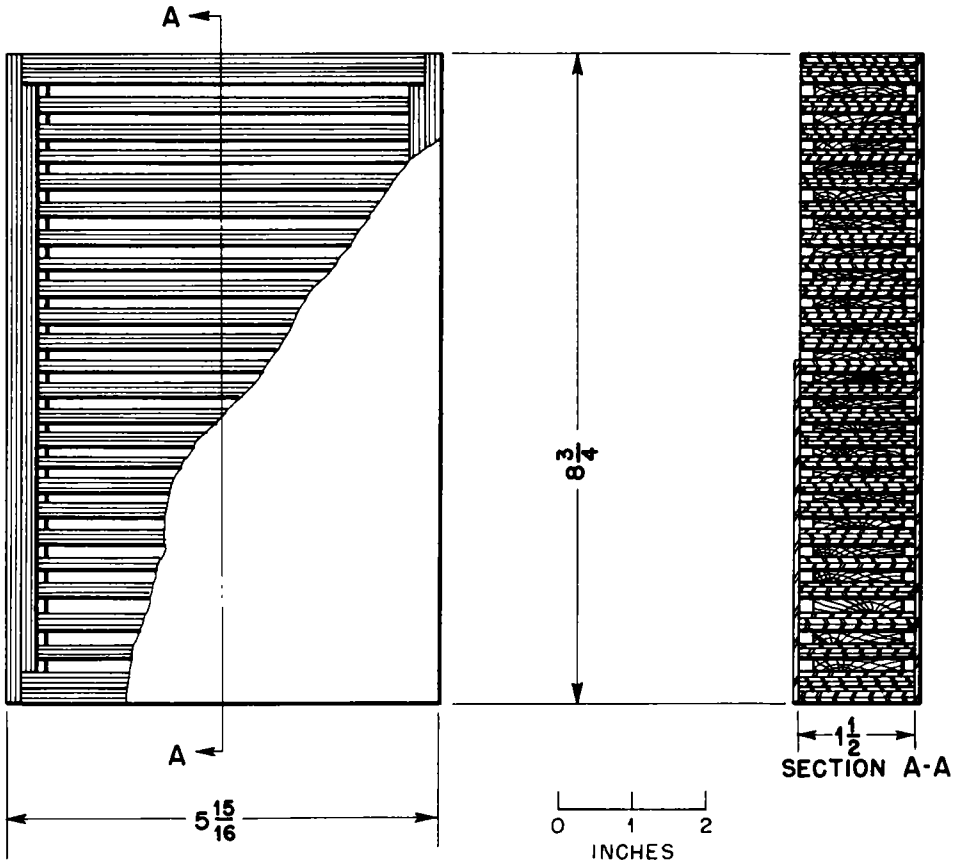


Fig. 3.2—Construction of cores for magnet model Alpha II (revised).

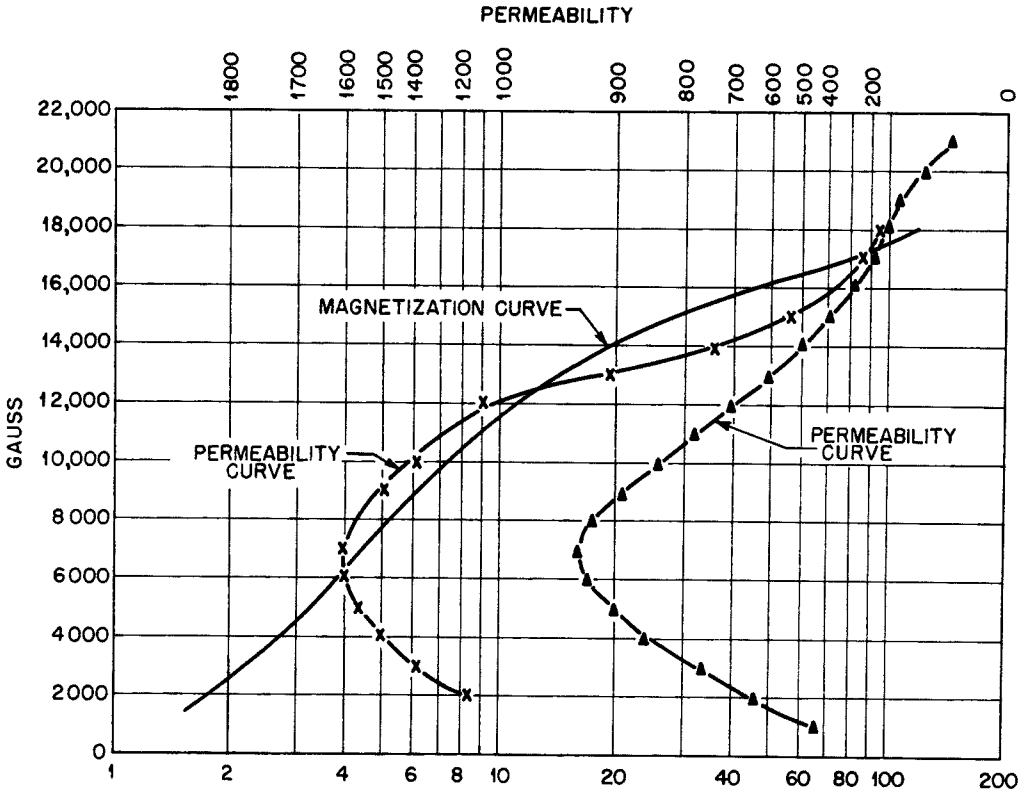


**Fig. 3.3—Permeability and magnetization curves. ×, full-scale magnet core material. ▲, model magnet core material.**

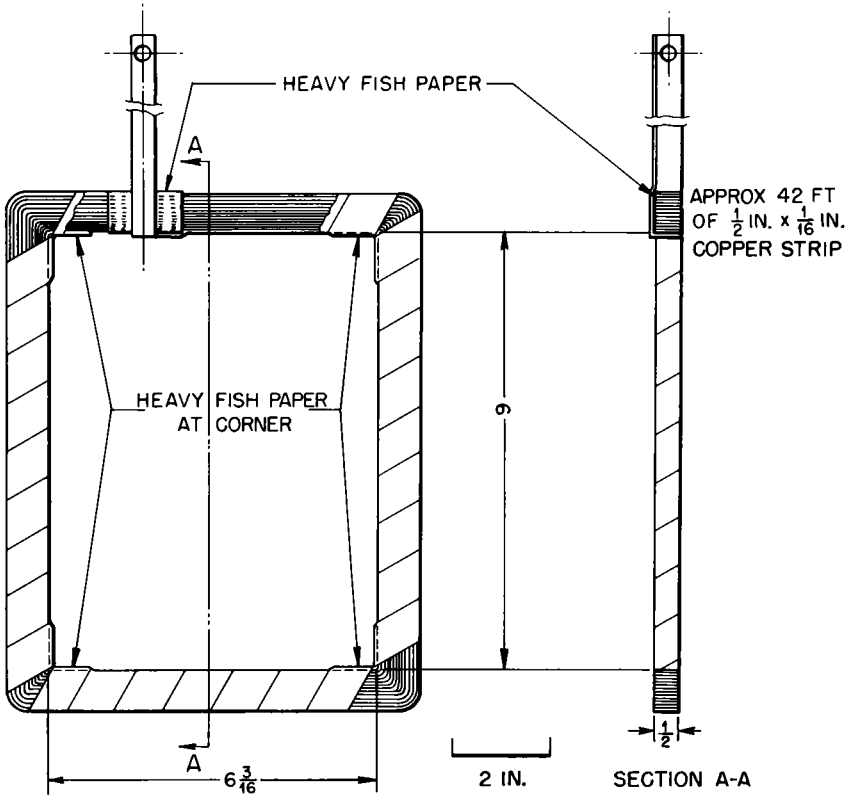


**Fig. 3.4—Coil construction in magnet model Alpha II (revised).**

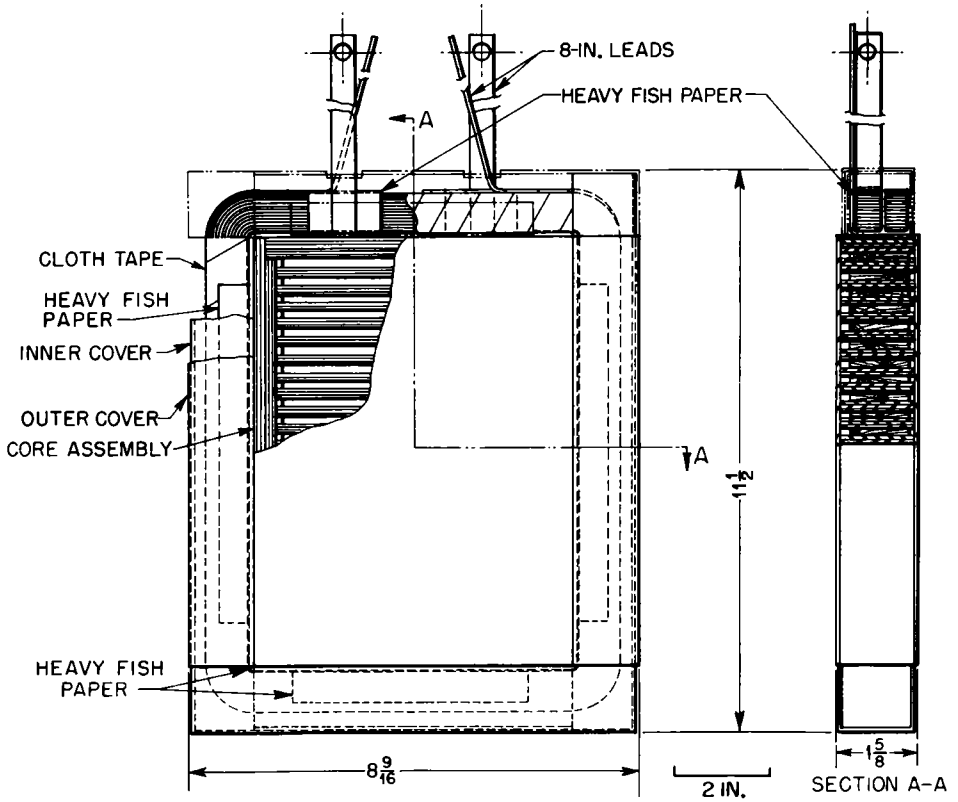


**Fig. 3.5—Coil cooling tanks for magnet model Alpha II (revised).**

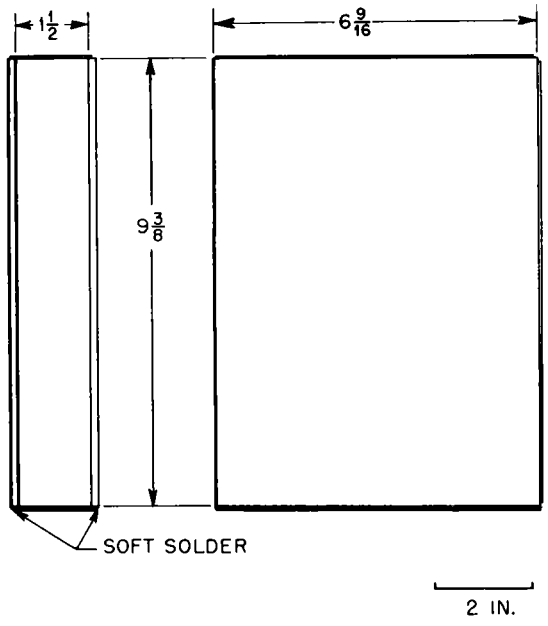


**Fig. 3.6—Process tanks for magnet model Alpha II (revised).**

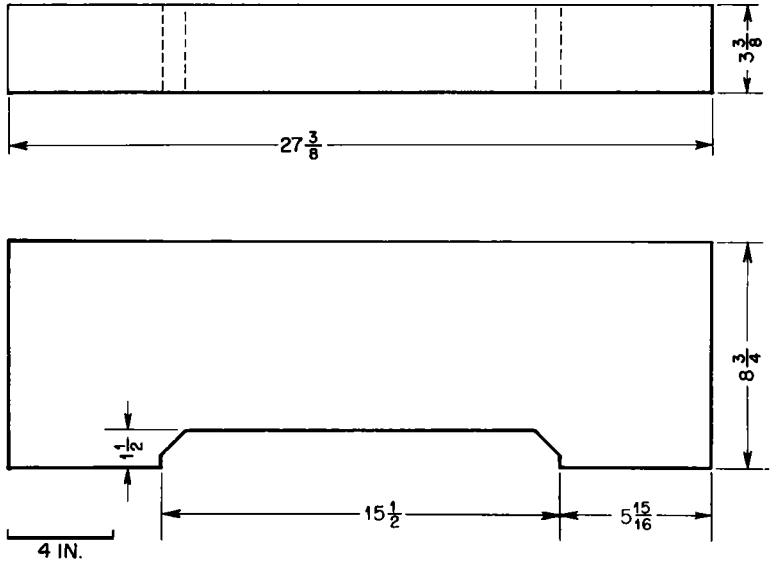


Fig. 3.7a—Construction of yokes for magnet model Alpha II (revised).

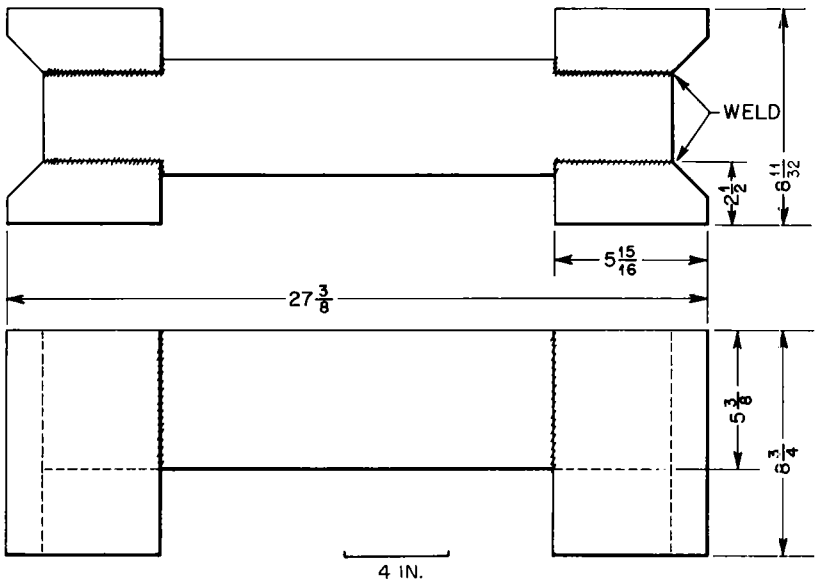


Fig. 3.7b—Construction of yokes for magnet model Alpha II (revised).

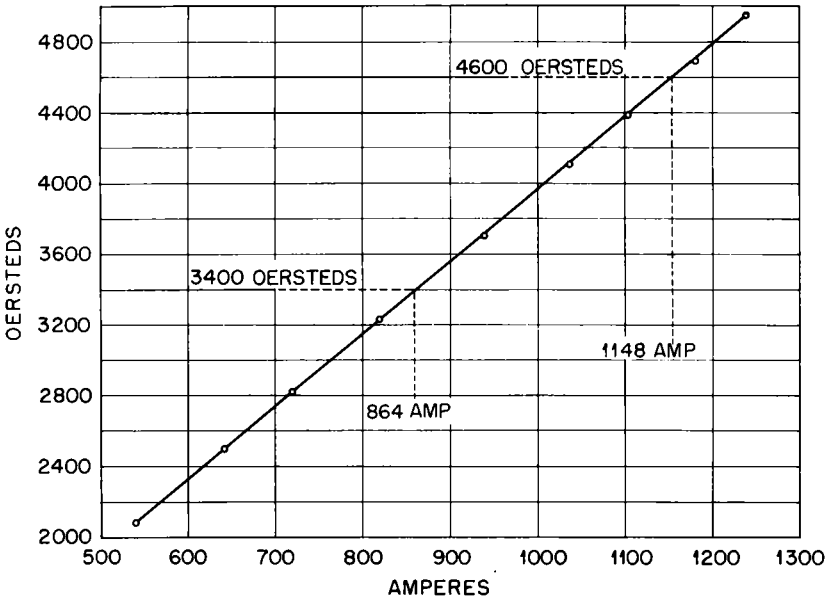


**Fig. 3.8—Magnetization curve for gap 13 of magnet model Alpha II (revised).**

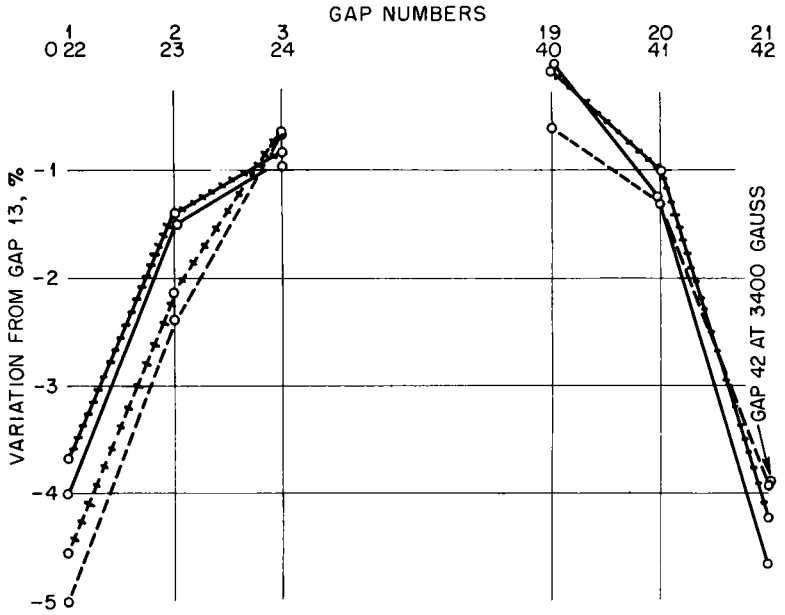


**Fig. 3.9—Relative field strengths for Alpha II model (revised) with 50 per cent end coils only.**

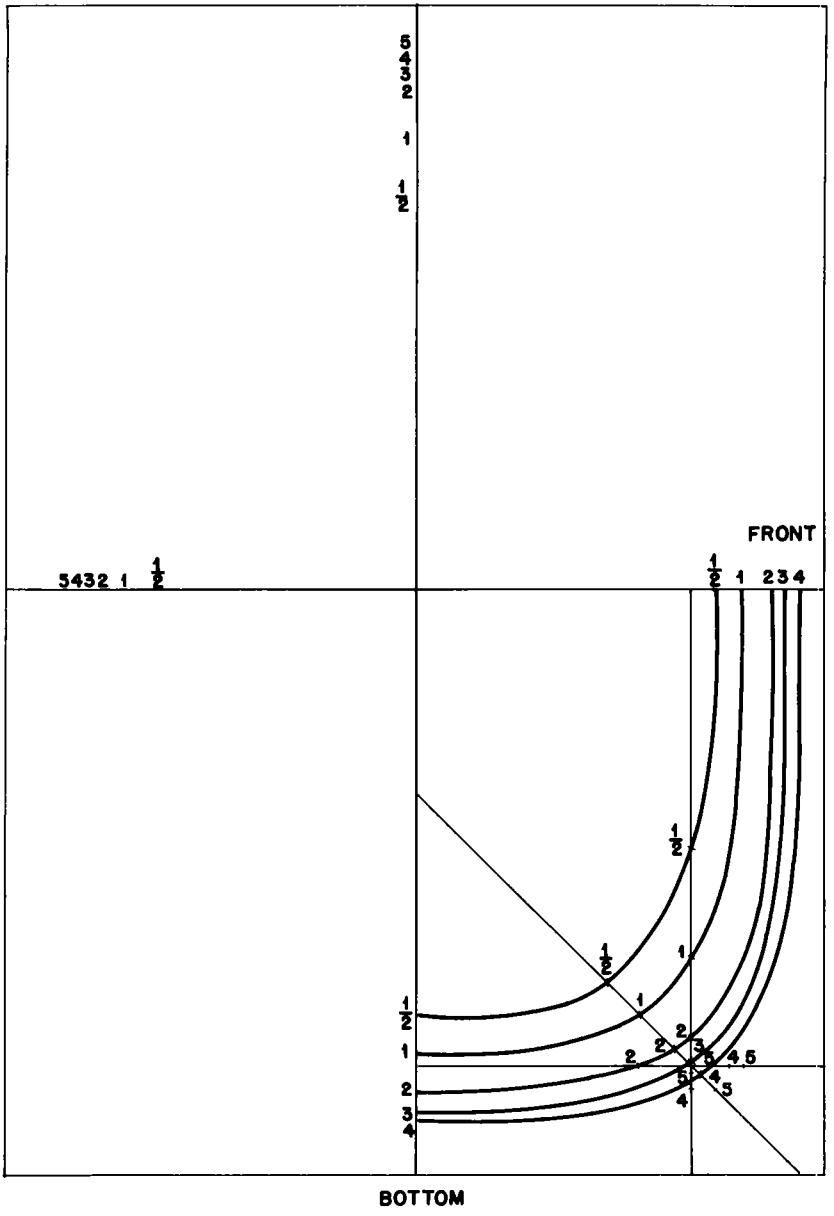


Fig. 3.10 — Contour map of field in tank 5, Alpha II model (revised). Magnetic field = 3400 oersteds.

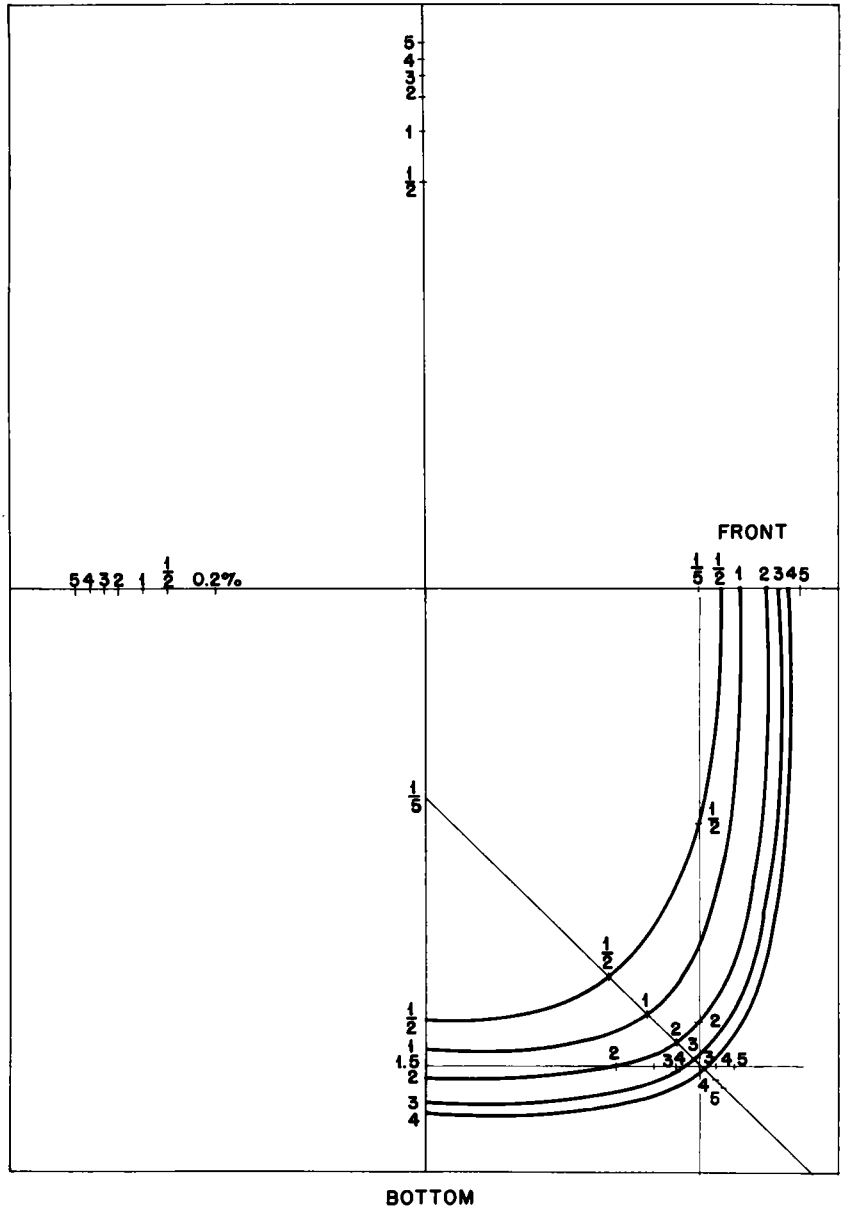


Fig. 3.11—Contour map of field in tank 5, Alpha II model (revised). Magnetic field = 4600 oersteds.

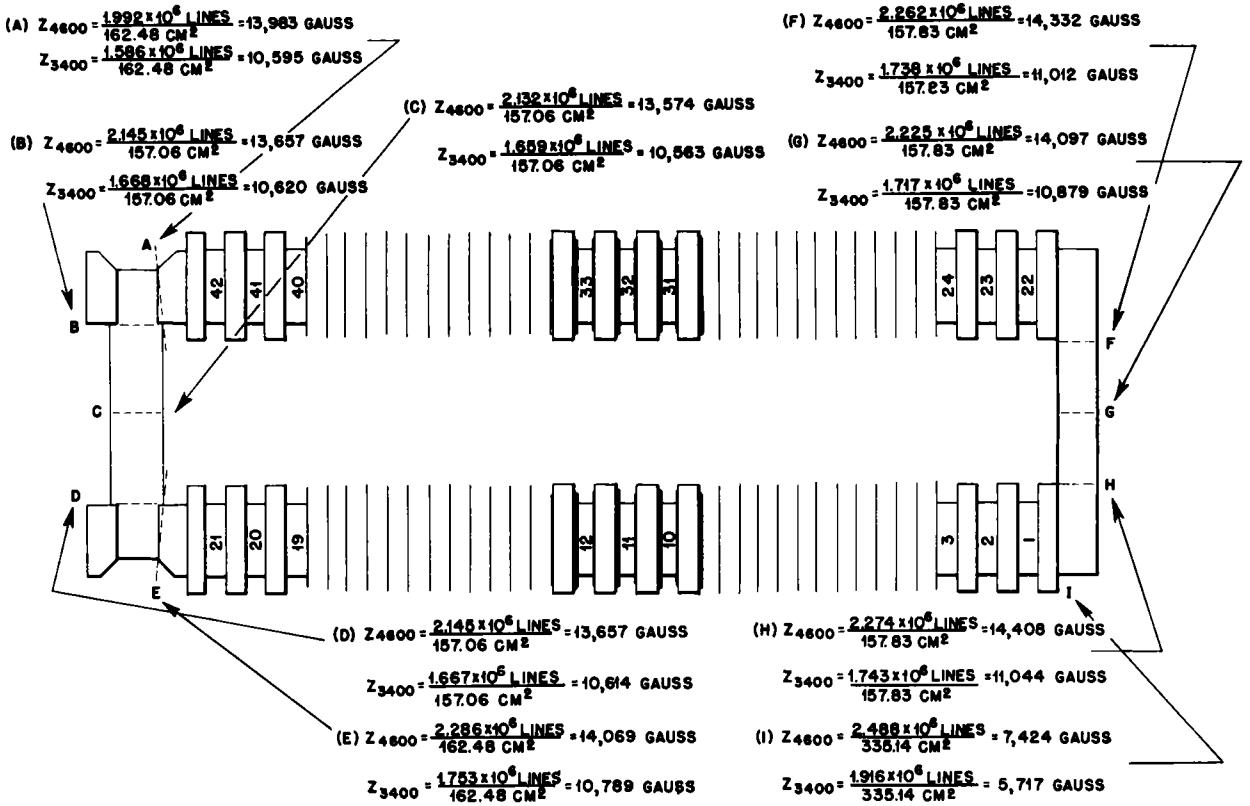


Fig. 3.12—Flux measurements in magnet model Alpha II (revised), case 1.

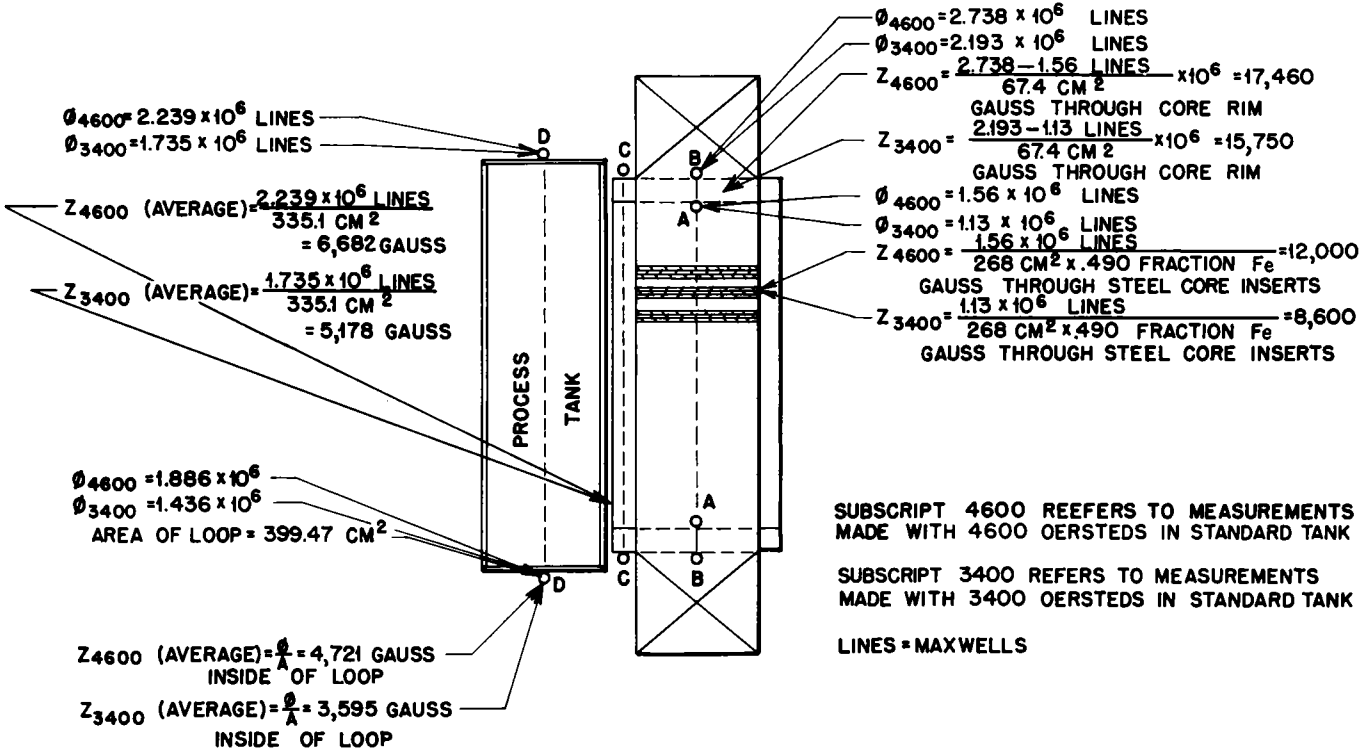


Fig. 3.13—Flux measurements in magnet model Alpha II (revised), case II.

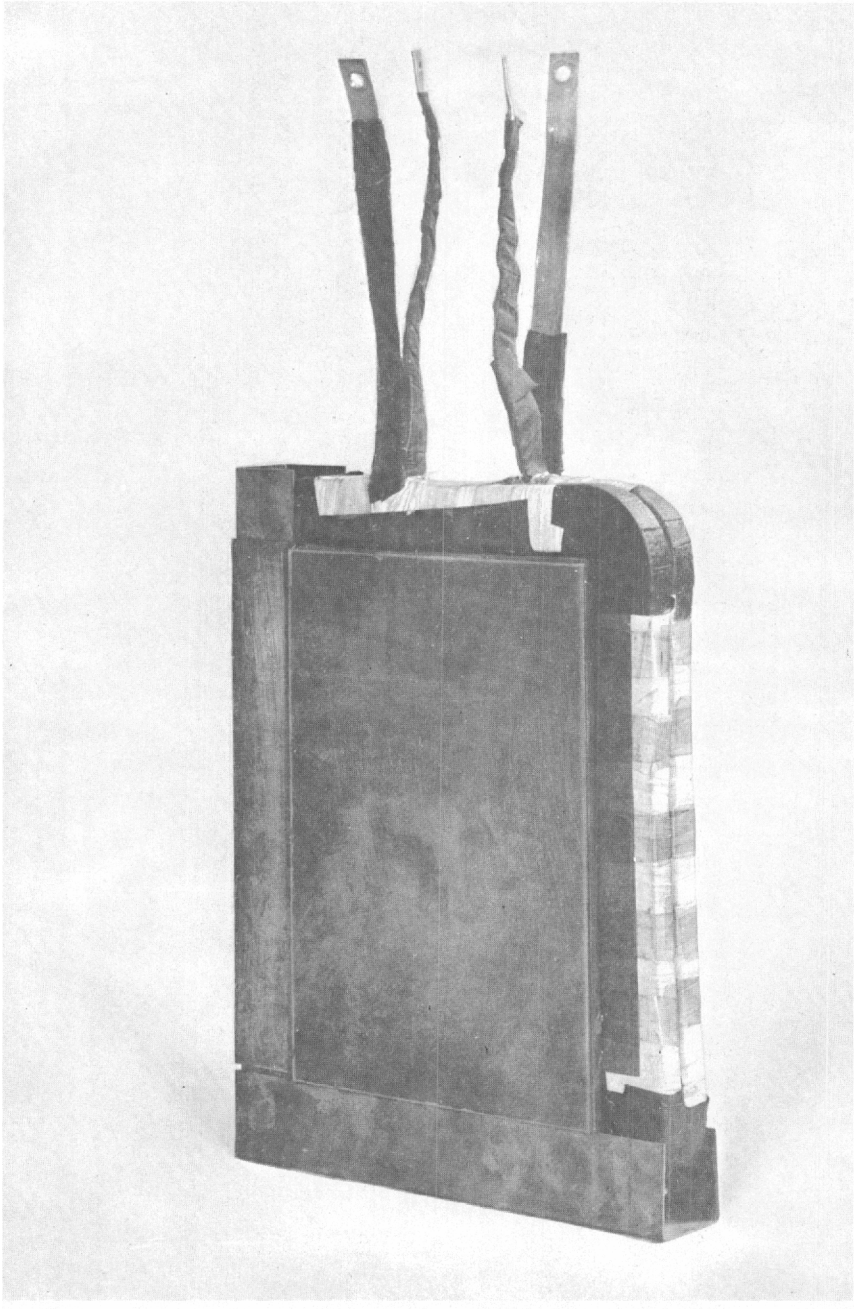

Fig. 3.14 — Photograph of coil, core, and 1/16-in. steel cover plate, Alpha II model (revised).

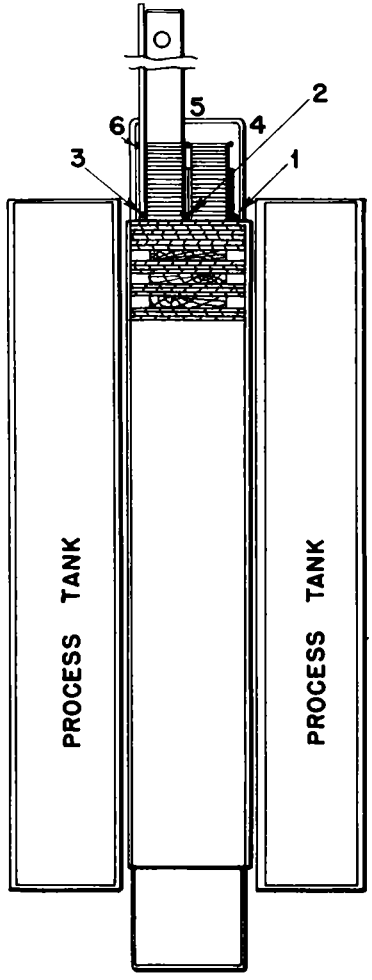


Fig. 3.15—Location of loops for measuring flux in coil case, Alpha II model (revised). Areas of loops: 1, 2, 3 = 335.08 sq cm; 4, 5, 6 = 549.22 sq cm.

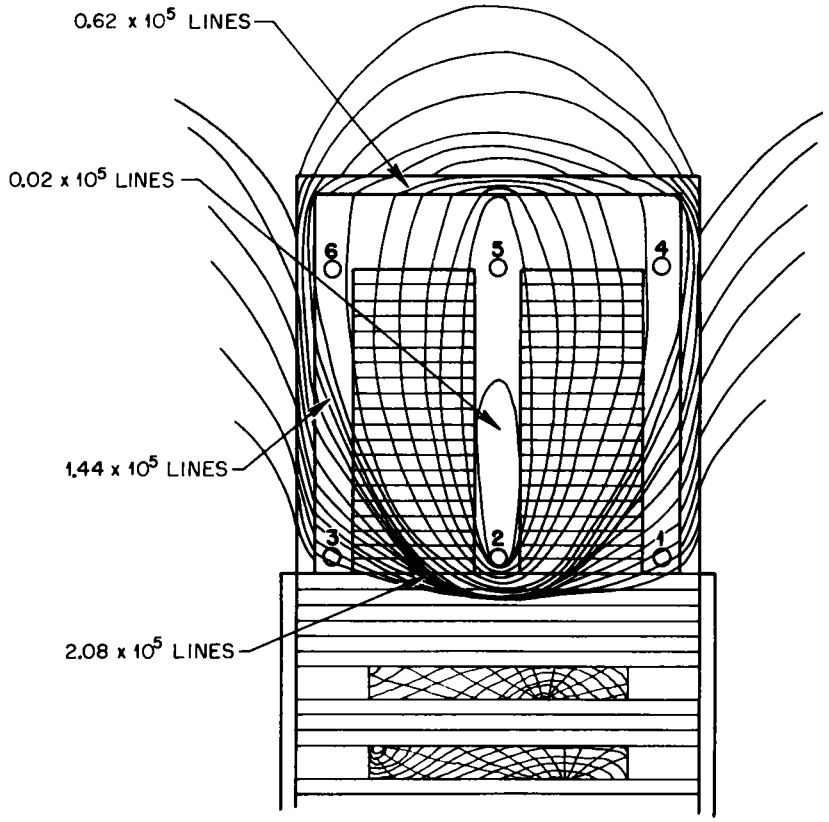


**Fig. 3.16—Distribution of flux through coil cooling tanks, Alpha II model (revised). Numbers refer to loops.**

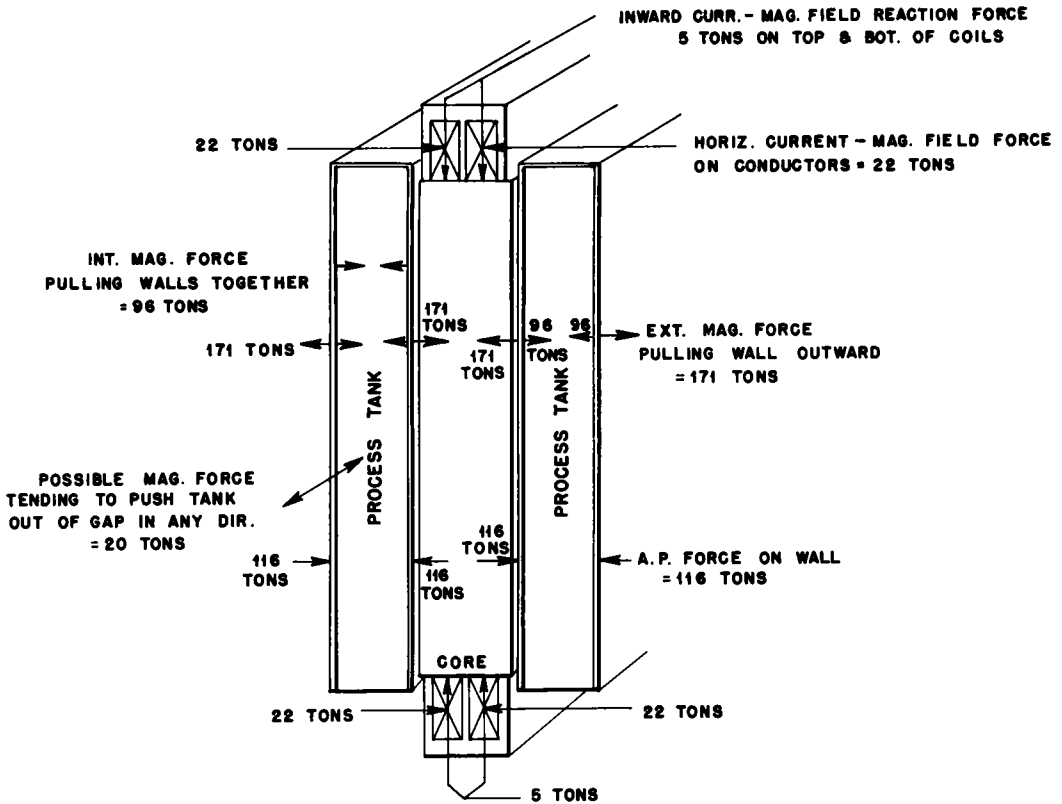


Fig. 3.17—Forces on magnet, magnet model Alpha II (revised).

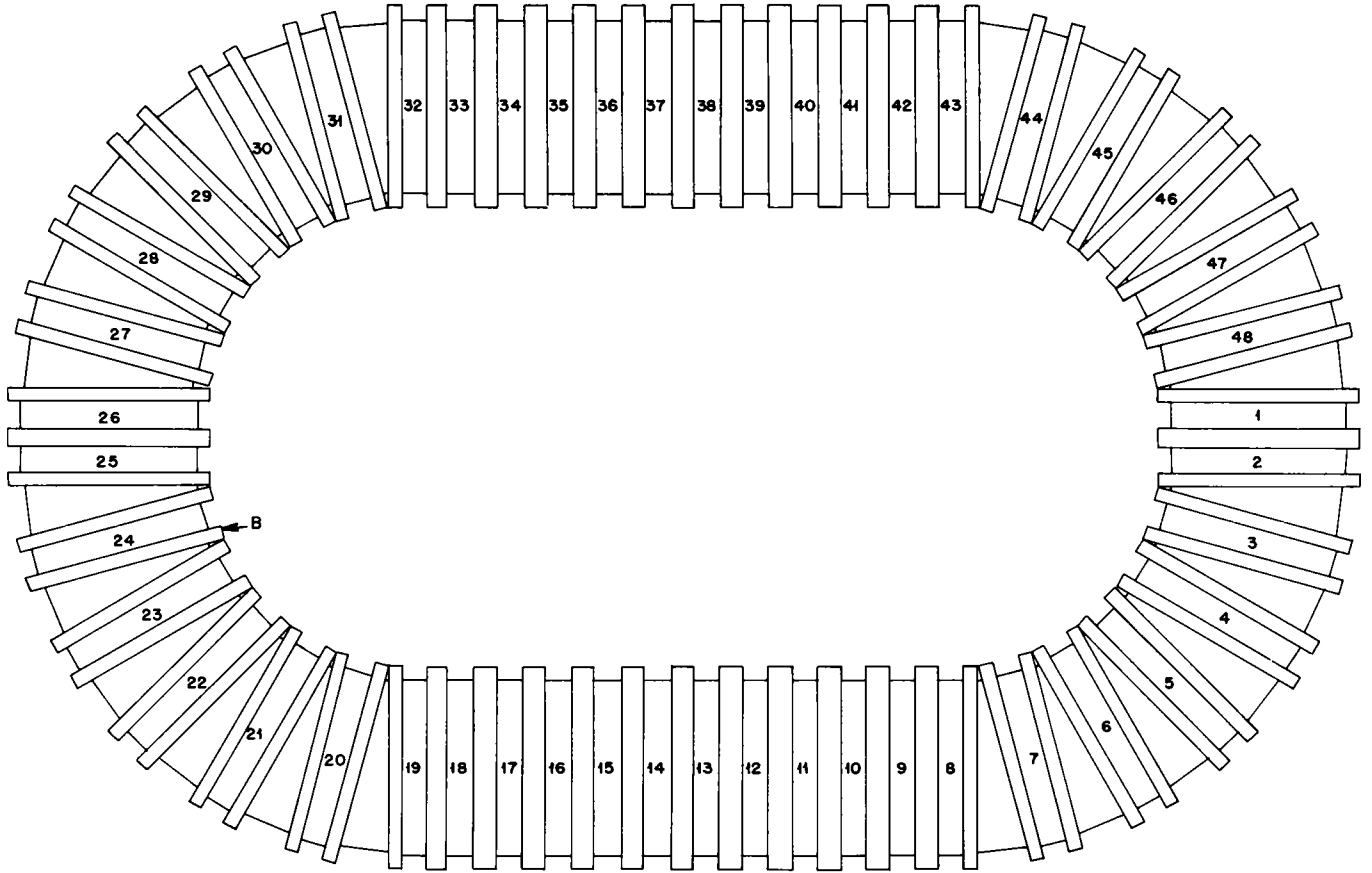


Fig. 3.20—Plan view of magnet model A.

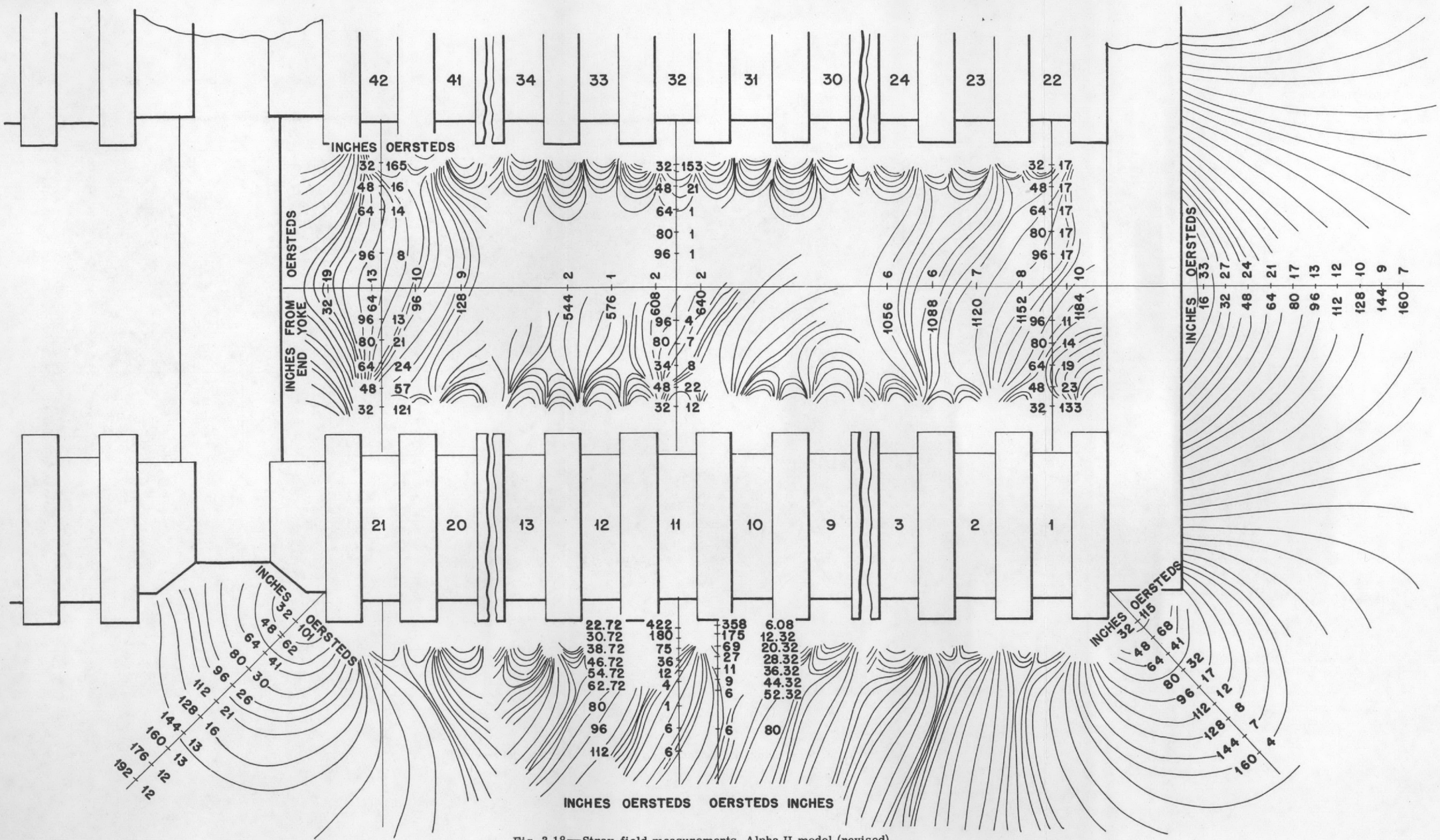


Fig. 3.18—Stray-field measurements, Alpha II model (revised).

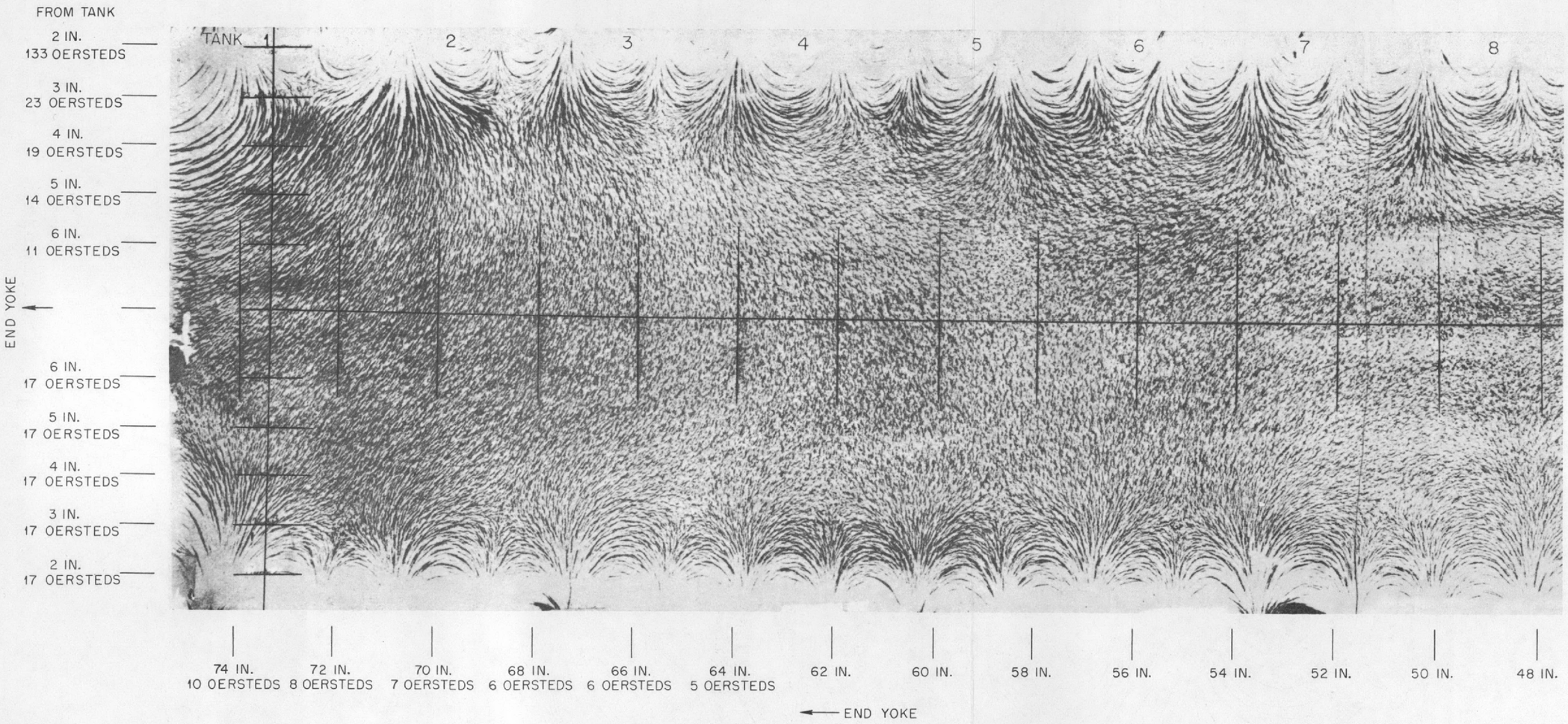


Fig. 3.19—Photograph of iron-filing pattern, Alpha II model (revised).

Fig. 3.20—See page 176.

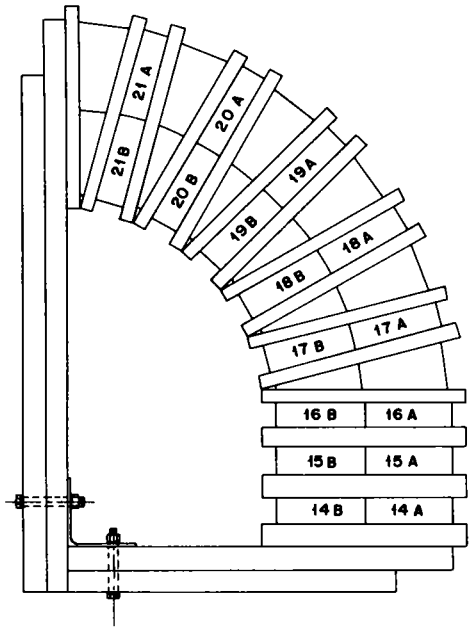


Fig. 3.21—Section of magnet model A.

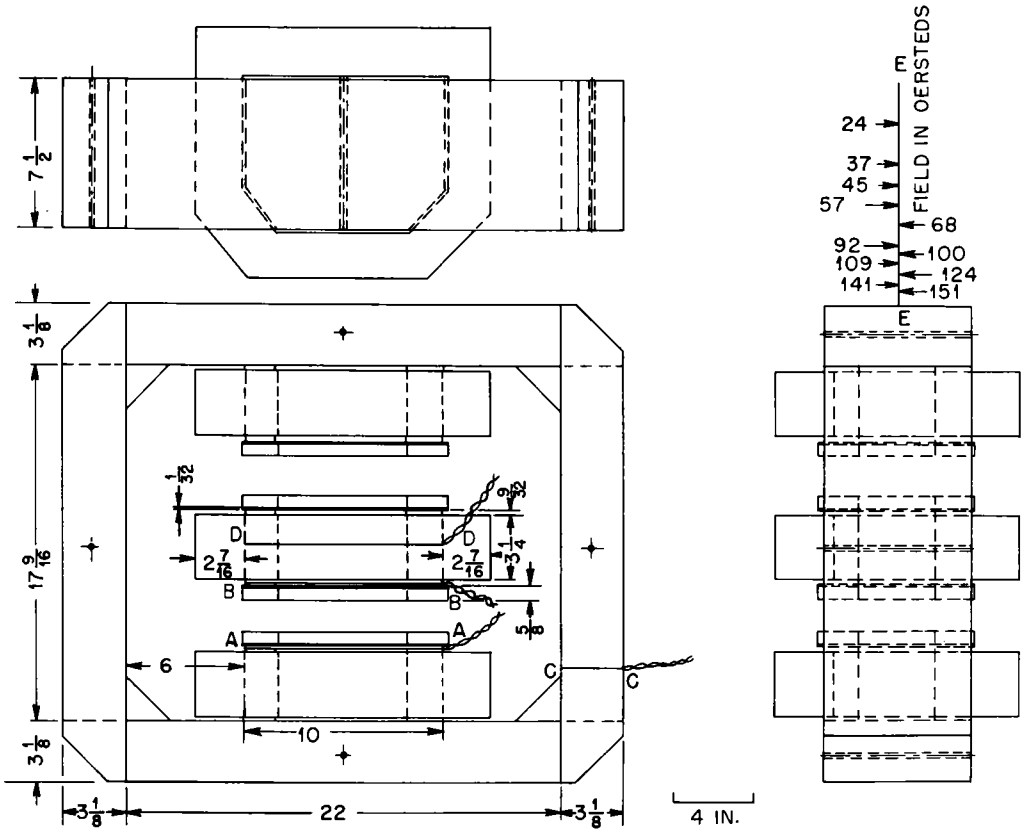


Fig. 3.22—View of magnet model X Beta.

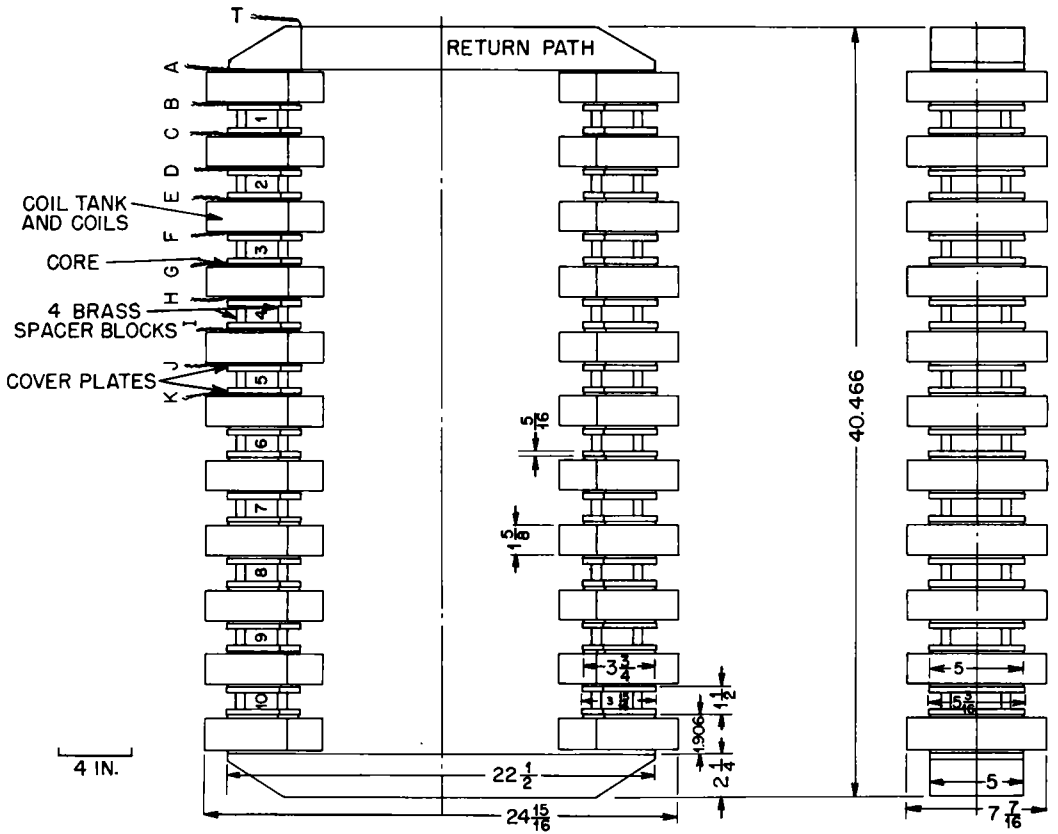


Fig. 3.23—Plan view of magnet model Beta.

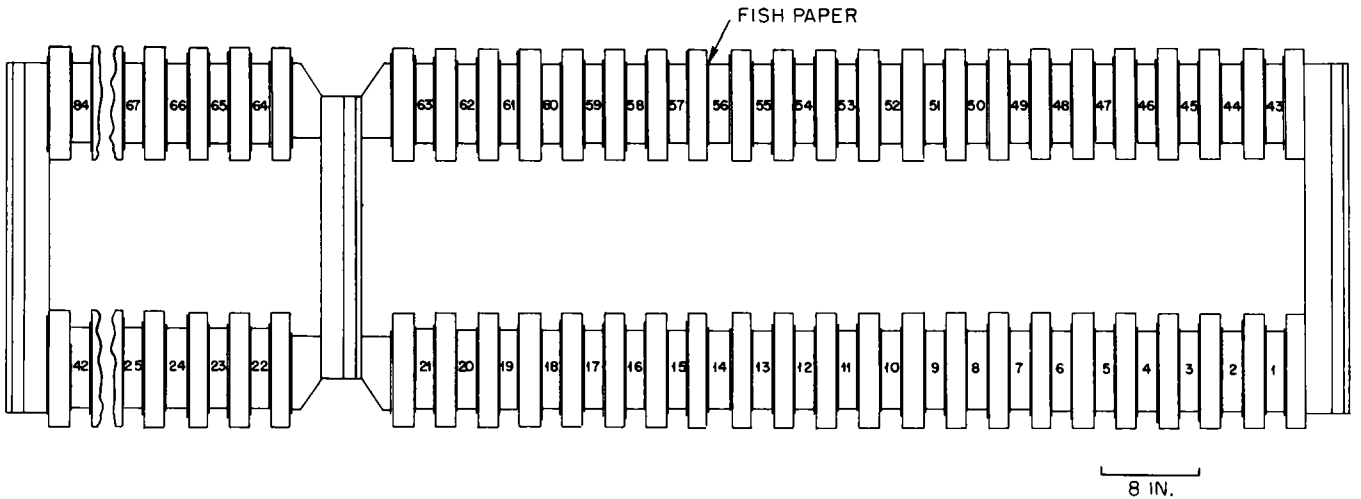


Fig. 3.24—View of magnet model Alpha II (as originally proposed).

## REFERENCES

1. W. M. Powell, W. P. Ball, J. R. Akers, A. J. Hulse, J. DePangher, H. Hauck, and M. Viehman, Performance Tests on Magnet Model Alpha-2 (Revised), University of California Radiation Laboratory Report RL 27.6.46, Oct. 7, 1944.
2. W. M. Powell, R. W. Penn, J. DePangher, and E. D. Kane, Performance Tests on Magnet Model V, University of California Radiation Laboratory Report RL 27.6.1, Oct. 29, 1942.
3. W. M. Powell and Group, Performance Tests on Magnet Model A, University of California Radiation Laboratory Report RL 27.6.2, Apr. 10, 1943.
4. W. M. Powell, Performance Tests on Model X Beta, University of California Radiation Laboratory Report RL 27.6.5, May 5, 1943.
5. W. M Powell, A. B. C. Anderson, R. W. Penn, J. DePangher, A. Schmidt, E. Stearns, and G. Brown, Performance Tests on Magnet Model Beta, University of California Radiation Laboratory Report RL 27.6.43, Aug. 15, 1944.
6. W. M. Powell, W. P. Ball, A. J. Hulse, J. R. Akers, and H. Hauck, Performance Tests on Model Alpha-2 (original plan), University of California Radiation Laboratory Report RL 27.6.40, Apr. 20, 1944.

Chapter 4

# MAGNETIC TESTS ON FULL-SCALE MAGNETS

By R. K. Wakerling and A. Guthrie

## 1. INTRODUCTION

In this chapter some of the tests which have been made on full-scale magnets will be discussed briefly. Section 2 deals with tests made on magnets at Berkeley, and Sec. 3 with tests on some of the magnets at the plant.

The tests at Berkeley were quite incomplete. As long as the experimental tests being conducted on the separation of the uranium isotopes were giving satisfactory results, it was not felt advisable to interrupt operations to investigate the magnetic field characteristics too closely. The most detailed magnetic studies were carried out in preparation for the plant tests and for various contemplated programs in the Radiation Laboratory. Most of the studies were made on the XA magnet, which was constructed as a pilot unit for the Alpha plant. Consequently more attention is given in this chapter to the XA unit than to any of the other Berkeley magnets. The large magnets used at Berkeley were the XA magnet, the 184-in. cyclotron magnet, the 37-in. cyclotron magnet, the 60-in. cyclotron magnet, and the XC magnet. Some magnetic tests are described for all of these magnets except the last one.

The criteria adopted for the plant tests, together with the equipment and techniques used, are described in Chap. 2 of this volume. The most complete tests were carried out on the Alpha I plant, on race track 1. Tests on race track 6, on XBX, and on XAX are also described briefly.

## 2. MAGNETIC TESTS IN THE BERKELEY MAGNETS

2.1 XA Magnetic Tests. In view of the fact that the XA magnet was constructed to test the operating characteristics of the Alpha

units, the magnetic field was studied more carefully than was the case for the other magnets. A view of the magnet is shown in Fig. 4.1. In this section, the method used to obtain a magnetization curve will be described briefly. Succeeding sections will treat a number of other magnetic tests.

A magnetization curve was obtained in tank 1 (XA-1) in the region of the receiver,[1] at a point 25.5 in. inside the tank measured from the face and 37 in. up from the bottom of the tank, in the median plane halfway between the tank walls. The curve, as well as the magnet coil connections, is shown in Fig. 4.2. The two coils nearest the tank in the return yoke sections were left unexcited. The measurements were made with a ballistic galvanometer and a 582 turn-sq cm flip coil, which was flipped through 180 deg. Figure 4.2 shows that there is no effect of iron saturation in any part of the magnet up to the maximum field strength measured (3190 gauss).

2.2 External Field about XA.[2] Knowledge of the magnitude of the stray field about the XA magnet was of some importance in order that measures might be taken to avoid bringing magnetic material too close to the magnet; this information was also useful in evaluating the performance of the magnet. The procedure adopted to obtain information regarding the stray field was that involving the use of drawing board and compass, in which the positions of the poles of the compass were marked on the board as the compass was moved progressively along the board. The position assumed by the compass indicates, of course, the field direction. In view of the fact that the compass used was 0.5 in. in length, the accuracy of the measurements was essentially limited by this dimension. However, the reproducibility of the results pointed to the reliability of the measurements.

Absolute field determinations were made by using a fluxmeter with search coils provided by the manufacturer. The fluxmeter was of the torsionless-suspension type, which was supposed to be used with an external circuit resistance not greater than 1.0 ohm. Because of the range of field, which would affect the fluxmeter, this external circuit contained very long leads which probably exceeded 1.0 ohm resistance. The measurements were made by turning the coil over in the magnetic field so that the flux $\phi$ threading the coil varied from $\phi_0$ to $-\phi_0$ in a short time, of the order of 1 sec. The data supplied by the manufacturer of the instrument gave the formula

$$\text{Field in gauss} = \frac{10{,}000 \times \text{divisions deflected}}{\text{no. of turns} \times \text{mean area}}$$

Because $\phi$ varied from $\phi_0$ to $-\phi_0$, the area must be doubled to give the proper value of the field, so that the formula becomes

$$H = \frac{10{,}000d}{2na}$$

where n is the number of turns, a is the mean area, d is the deflection of the meter, and H is the field in gauss. The coil used was of mean area 5 sq cm and consisted of four turns. This coil gave deflections of the order of 5 divisions.

The results obtained are summarized in Fig. 4.3. The principal errors arise from the finite size of the compass needle, too high an external resistance, and limitations in the fluxmeter itself. The plot was made in the rear of tank 1 of the XA magnet, 39 in. below the top of the magnet. The results are somewhat incomplete because of limited accessibility to certain regions around the magnet. Absolute field determinations were taken on the central line and 30 deg and 60 deg east of the central line from a point 2.75 in. from the tank wall in the center of the gap width.

2.3 Flux Plots in the Source Region of the G Insulators for the XA-2 Tank. Flux plots of the field configuration in the XA-2 tank in the XA magnet were made in the source region and near the insulators supporting the accelerating electrodes. The method used was that involving a compass (⅝ in. in diameter) and drawing board as described in the preceding section, using ¼ in. cross-section paper. It was determined that the error in making the plots did not exceed ⅛ in. at any point along the line of force.

In the case of the source-region measurements,[3] plots were made in five defining planes—two horizontal, two vertical, and one diagonal (Fig. 4.4). This was done with the auxiliary shims in place in the tank. The measurements were made with no tank faceplate. Since the faceplate normally used with the tank was made of magnetic iron, the field when the tank is in use will probably be slightly different than that determined by these flux plots. An example of the type of results obtained is shown in Fig. 4.4. This plot was made in a horizontal plane 14 in. above the bottom tank wall.

In the case of the flux plots around the insulators,[4] the same general techniques as described above were used. Plots were made in four planes, as shown in Fig. 4.5, so as to approximately intersect one corner of each insulator. Just one line intersecting each side of each insulator was determined. The absolute magnitude of the error in the measurements was ⅛ in. or less at any position along the line of force, as in the case of the source-region measurements. An example of a plot is shown in Fig. 4.5. This plot was made in the A plane. The insulator positions have been indicated in phantom. The double lines in the center of the plot indicate that the top and bottom plots were not taken without moving the drawing board.

2.4 Effect of 0.5-in. Magnetic Steel Tank Side Wall on the Field in the XA-2 Tank.[5] It was felt desirable to know the effect of the magnetic side walls on the magnetic field inside the tank. Many magnetic measurements are made in the region of the mouths of the tanks, and it would be useful to be able to apply a transformation factor to these measurements so that they would closely approximate the field in some other region of the same tank, namely, in the back of the tank or near the side walls. An occasion for making the measurements arose in connection with designing auxiliary shims for XA, XAX, and the Alpha plant (see Sec. 2.6). Measurements had been made on these magnets in the region of the mouth of the tank, and it was desired to transform these measurements to indicate what the uniformity of the field would be like near the tank side walls where the auxiliary shims were to be installed.

The absolute field strength was determined at the position labeled "F" in Fig. 4.6 by rotating a 584 turn-sq cm flip coil through 180 deg. The changes in field strength toward the mouth of the tank were determined by moving an 18,824 turn-sq cm search coil from the beginning of the run through the location of the flip coil and out of the mouth of the tank in 2-in. jumps. (See Sec. 10.2, Boxcar Technique, in Chap. 2.) The coil was mounted on a bakelite rod screwed into a car that moved on a track. The measurements were first made without any magnetic material covering the mouth of the tank. A 0.5-in. mild-steel plate 28 by 64 in. was then clamped over the central portion of the mouth of the tank. The measurements were repeated with one measuring track placed on the inside of the tank and another outside the tank extending out beyond the magnetic plate. All measurements were made using a type P ballistic galvanometer.

The results obtained are shown in the form of curves in Fig. 4.7. It was felt that the magnetic field distributions, with and without steel plate, were sufficiently close together to make it possible to design auxiliary shims on the basis of the field measurements with no steel side wall present. Furthermore, the field distributions obtained for XA and XAX were very nearly alike. Consequently, auxiliary shims were designed on the basis of the measurements made on XAX.

2.5 Measurements with Shim-region Device in the XA Magnet. The equipment for studying the maghetic field in the region between the linear shims has been described briefly in Chap. 2 of this volume. Prior to shipping this equipment to Oak Ridge for tests in the plant, it was used for some magnetic field measurements in the XA magnets in tank XA-1. These measurements were made in the period Aug. 17 to 31, 1943.[6]

These tests were carried out to test the performance of the shim-region device and at the same time to check the theoretical criteria

for the magnetic field configuration in the shim region. In view of the fact that the experimental units being tested in the XA magnet performed satisfactorily, the results obtained in the magnetic tests could possibly be used to modify the acceptance criteria for the plant tests. The methods of taking the data and analyzing them were essentially the same as already described in Chap. 2. The location of the linear magnetic shims ($D_1 - \alpha$) in the tanks is shown in Fig. 4.8.

Measurements were made with the linear magnetic shims in position as originally installed in the tank and then again after they had been moved to make tilt measurements (see below) and supposedly returned to their initial positions. Rather surprisingly the results for the latter case were more satisfactory than for the first case. However, in all runs the experimental and theoretical curves differed at all points by less than the acceptance criterion of 3 cm. The maximum difference was about 2 cm and the curves for the median plane fitted extremely well (less than 1 cm). The results indicated that the magnetic field in the region of the linear shims was quite satisfactory as far as the accepted theoretical criteria would indicate. However, the tests pointed to the necessity for exercising a good deal of judgment in making a decision on any given tank.

During the period that the above tests were being made, a number of measurements of the effect on the magnetic field produced by tilting the linear shims was carried out.[7] In view of the fact that the results obtained showed the method to be generally unsatisfactory, only a brief description of the tests will be given here. These tests were undertaken with a view to tilting the shims in tanks in the plant where the acceptance criteria were not met so as to make the necessary corrections.

Experimental curves of $\int h_z \, dx$ were obtained for the shims in their original positions and then again with the shims, or portions of them, tilted in various ways, using the shim-region device (arc of coils). A tilt of about 2 deg was normally used. In finding the effect of a tilt on the magnetic field, comparison was made between the difference curve for the theoretical $\int h_z \, dx$ curves, no tilt and tilt, and the difference curve for the corresponding experimental curves. The agreement between the difference curves was found to be unsatisfactory in all cases for the plane of measurement nearest the tilted shim. No effect of the tilt appeared to be felt in the median and farther plane of measurement ($\pm$ 7.75-in. planes were used, measured from the median plane).

The reasons for the lack of agreement are not too clear, although the difficulty in making a unique comparison of the curves undoubtedly plays a large part. In addition, the theoretical curves were calculated on the basis that the space between the tilted shims and the tank walls

would be stuffed with iron. This was not done in practice. In any case the results indicated that the tilt method, as developed to that time, would be of little value in correcting magnetic fields falling outside the acceptance criteria. Fortunately, as will be seen later in this chapter, none of the tanks tested at the plant required such correction. It would appear that the only feasible method of making corrections when the necessity arises is by trial and error. During the period that the above tests were made, several measurements of the magnetic field in the source region were made, using the source-region device. The results showed that the field satisfied the acceptance criteria.

During the electric-shim program (see Division I, Volume 4, the National Nuclear Energy Series), it became necessary to ascertain the magnetic field configuration in the XA-2 tank of the XA magnet so as to determine the best possible isotope separation. For this purpose a shim-region device, similar to the wooden arc of coils used in the $D_1$ and $R_1$ tanks, was constructed (see Secs. 2.7 and 2.8). It was possible to use this arc of coils with the tank evacuated, using flexible cables passing through Wilson seals to control the unit. The measurements were recorded by photographing the run traces on a 9-in. electronic oscilloscope fluxmeter. A standard flip coil was rotated through 180 deg to determine the absolute magnitude of the field. Measurements were made in the median plane and the +8- and −8-in. planes (measured from the median plane). The tank was evacuated to approximately 0.1 atm for the measurements.

The results obtained gave data regarding the expected effect of the electric shim on the beam trajectories. Figure 4.9 shows the expected spread in the beam pattern when an electric shim with a theoretically ideal voltage is used (the ideal electric shim is supposed to reduce the geometrical defocusing to zero). This figure is for the median plane and a ±12-deg beam divergence at the source. It will be observed that the beam spread is at least 0.7 mass unit. There is a general overall tilt in the field, indicating that the receiver should be rotated so that the right side is nearer the source than the left side by an amount approximately 0.8 mass unit or about 0.15 in.

2.6 Auxiliary Shim Measurements.[1] The magnetic measurements made in the source region in tanks on race track 1 at Oak Ridge (see Sec. 3 of this chapter) showed that the field drops off toward the side of the tank at such a rapid rate that it is not possible to use sources closer than about 15 in. to the tank side wall. To compensate for this weakening of the field and thus obtain more usable tank volume, a program was undertaken to design magnetic shims (auxiliary shims) to be placed above and below the source region.[8] The method of calculating such shims[9] is discussed in Chap. 4 of Volume 4 of Division I of this series.

It was decided to test auxiliary shims in one of the XA tanks before considering their use in the plant. Consequently, shims of the dimensions shown in Fig. 4.10 were installed in the XA-2 tank and magnetic measurements made to find their effect on the field. The absolute field was determined in the "flip" regions of Fig. 4.11, and the change in field toward the tank side wall was measured by moving an 18,824 turn-sq cm search coil in 2-in. jumps along the run. All measurements were made using a type P ballistic galvanometer.

The results obtained are shown in the curves of Fig. 4.11. These curves show that a source can be placed within 10.5 in. of the side wall of the tank, where the magnetic field satisfies the acceptance criterion of 0.3 per cent per inch change in intensity. Previous measurements showed that the source must be placed 16.5 in. from the side wall when auxiliary shims are not used. This represents a gain of 6 in. of usable tank space in the X direction. Furthermore, the fact that the fields in both the +8- and the −8-in. planes are the same is a strong indication that there is little if any tilt in the field.

Although the improvement in the magnetic field in the source region due to the use of auxiliary shims is quite pronounced, they were not installed at the plant. This was due to developments at the plant which began to lessen the importance of the Alpha units.

2.7 Magnetic Measurements in Tank $D_1$. A good deal of the experimental work on the electromagnetic separation of the uranium isotopes was at first carried out in tanks placed between the poles of the 184-in. magnet in the Radiation Laboratory. For the most part two tanks were used simultaneously with this magnet. Consequently each tank was necessarily placed fairly near the edges of the poles. The rapidity with which the program was pursued precluded the possibility of investigating the nature of the fields in these tanks in any detail. However, a few rather general studies of the fields were made in order to tie this factor in with the process requirements.

Stray-field measurements[2] around the tank $D_1$ were carried out using essentially the same equipment and techniques as in the case of the XA magnet (see above). However, in this case the coil used consisted of only two turns (same area) because of the stronger field. The results obtained are shown in Fig. 4.12. This plot was made 8 in. west of the eastern extremity of the $D_1$ tank (see Fig. 4.12). The closest approach to the faceplate was 0.75 in. because of the presence of copper cooling pipes. The plot was made with the source, which had an iron faceplate, in place. When absolute measurements were made the source was in place and stainless-steel holders were used for the source and receiver units. The plots show lines of somewhat smaller

curvature than in the case of the XA magnet. Also, distortion appears near the tank because of the iron top and bottom tank walls. A tilt of the lines of force is observed, which is undoubtedly due to the placement of the tank in the gap (near the bottom pole piece).

Prior to the testing of the shim-region device (see Chap. 2) in the XA magnet (above), another such device had been constructed and used in the shim region of the $D_1$ tank.[10] This particular device had none of the finer mechanical features of the unit built for the plant tests, being to a large extent of wooden construction and consisting of only one arc of coils. The device will not be described in detail, in view of the fact that it was used very little. Runs were made in the $D_1$ tank, in the median plane, in the plane 8 in. below the median plane, and in that 8 in. above the median plane.

The curves obtained are not included here. However, a brief description of the results will be given. In the median plane, the theoretical and experimental curves coincided almost perfectly (everywhere to within 1 per cent or less of the change in field, or about 0.1 per cent of the homogeneous part of the field). Away from the median plane the theoretical curve was calculated for a height of 7.22 in. from the median plane, while the measurements were made at 8 in. The two curves could not then be directly compared. An extrapolation of the theoretical curve to 8 in. was therefore made. The small deviation observed between this curve and the experimental curve was, in all likelihood, due to the error introduced by the extrapolation, which could not be exact.

At the time the above measurements were being made in the shim region of the $D_1$ tank, contour maps of the field in the neighborhood of the source were also obtained.[10] An example of the contour maps is given in Fig. 4.13. It will be noticed that the field falls off at the rate of 0.22 per cent per inch at $J_1$ along the line G to GK. This means, of course, that the lines curve outward toward the west side of the tank 8 in. below the median plane. On the other hand, the corresponding plot for the median plane shows a drop in the field of only 0.05 per cent per inch, indicating that the lines are almost perfectly straight in the median plane. In general the contour maps showed the field to be too strong at the top of the tank, roughly satisfactory in the median plane, and too weak at the bottom. Superimposed on this general trend was a rise in the field strength in the top plane as the edge of the tank is approached, a very small drop in the median plane, and a larger drop in the lower plane. On the basis of the results, uniformity shims for the source region were designed. Such shims would be expected to nearly straighten out the field between the lower and median planes. To help in the region of the top plane, a dig-in rather than a shim would have been necessary. However,

an inhomogeneous field in the top plane would be expected to have less of a detrimental effect on the beam than the corresponding situation for the lower plane (see Division I, Volume 4). Uniformity (or auxiliary) shims were installed in the tank, but no detailed magnetic measurements were made.

2.8 Magnetic Measurements in Tank $R_1$. Tank $R_1$ was used for experimental purposes, being placed in the gap of the 184-in. magnet resting on top of the $D_1$ tank. As in the case of this latter tank, few detailed measurements of the magnetic field in and around tank $R_1$ were carried out. The few tests which were made will be discussed briefly here.

Stray-field measurements[2] were carried out using the same equipment and techniques as for the XA and $D_1$ tanks. The coil was the same as in the case of the $D_1$ tank. A plot of the field is shown in Fig. 4.14. This plot was made at the position of the central receiver faceplate, 70 in. east of the western extremity of the tank, with the mapping board placed with its edge against the faceplate. This faceplate was made of copper reinforced by stainless steel. Similar plates were used to hold the receiver unit. The plots approached the bottom pole face within 1 to 2 in.

An examination of Fig. 4.14 shows that the flux lines are slightly curved, with a very large radius of curvature. A considerable distortion is evident near the top wall of the tank (which is steel), this distortion extending outward less than 3 in. A similar distortion effect shows up near the pole face of the 184-in. magnet. The plot also shows a tilt in the magnetic field at a distance of approximately 14 in. from the faceplate. This tilt disappears as the tank is approached and reappears very near the tank. This could be considered as an indication of the usual edge effects showing as a tilt because the tank is not centered in the gap.

The arc of coils in the wooden device discussed briefly in the preceding section was used to study the field in the $R_1$ tank[11] for some sump tests (see Division I, Volume 4). Figure 4.15 shows the positions of the arcs in the source being used. The arc of coils was set with one end fixed at the arc for the beam path being tested. The other end was moved through an angle from + 10 to −10 deg in 2-deg jumps. The arc of coils was used in the median plane of the tank and at 5.25-in. planes above and below the median plane. The measurements for the different planes were coordinated by dropping the whole arc from one plane to the other at the 0-deg angle. A flip-coil (582 turn-sq cm) measurement was made in the median plane at the 90-deg position of the arc of coils when it was in the 0-deg position.

It was decided that the arc of coils would not give sufficient information to make the necessary adjustments of the sump components.

The last coil of the arc of coils (near the receiver position) was 18 in. from the 180-deg position. Because of the inhomogeneity of the field in the $R_1$ tank near the receiver, insufficient information regarding the field in this region was obtained. The measurements were made with the tank at atmospheric pressure, since it was assumed that deflections produced in the tank wall when under vacuum would be negligibly small. Subsequent measurements did not bear out this assumption.

2.9 Magnetic Field Measurements on the 37-in. Magnet.[12] Measurements of the magnetic field in the gap of the 37-in. magnet were made in order to find the highest field obtainable with the existing generating equipment. In the process a magnetization curve was obtained.

The measurements were made using a 584 turn-sq cm flip coil which was placed in the center of the tank (19.5 in. in from the front and 22 in. from the sides) and in the median plane (8.25-in. gap). The coil was flipped through 90 deg and the impulse measured by means of a ballistic galvanometer. This was done twice for each of a series of magnet currents ranging from 100 to 435 amp. This latter current was the maximum obtainable after allowing the generator to run for some time. The galvanometer was calibrated for line-turn sensitivity using a Hibbert magnetic standard, and the galvanometer deflections were changed to oersteds. The sensitivity of the galvanometer was found to be 346 oersteds per centimeter.

The magnetization curve which was obtained is shown in Fig. 4.16. The accuracy of the results was limited to 2 per cent by the accuracy of the ammeter expressing magnet current. The highest current obtainable, 435 amp, produced a magnetic field of 11,800 oersteds.

2.10 Magnetic Field Measurements on the 60-in. Magnet.[13] These measurements were made in March 1944. A 149.1 turn-sq cm flip coil was placed as nearly as possible in the center of the tank (31.75 in. in from the inside of the tank wall and between the two cyclotron dees) and approximately in the median plane. The magnet current was adjusted to a series of values ranging from 50 to 400 amp (the lowest and highest obtainable). At each different current value the coil was flipped through 180 deg and the resultant impulse measured by means of a ballistic galvanometer. Two or more flips were taken until the deflections checked. At the higher fields (12,000 oersteds and above) it was necessary to use an Ayrton shunt to prevent off-scale deflections. The galvanometer was calibrated for sensitivity using a Hibbert magnetic standard, and the galvanometer deflections were converted to oersteds.

The magnetization curve obtained is shown in Fig. 4.17. The accuracy of the results was limited to 2 per cent by the accuracy of the

ammeter measuring magnet current. The highest current obtainable produced a field of 15,000 oersteds, and the lowest current a field of 2706 oersteds.

## 3. MAGNETIC TESTS IN THE PLANT

3.1 Tests with the Shim-region and Source-region Devices in Race Track 1 (Bldg. 9201-1).[14,15] The first race track of the Alpha I plant was ready for magnetic tests in the fall of 1943. To make these tests, a group of Radiation Laboratory employees went to Oak Ridge in September 1943. The necessary test equipment, including the shim-region device and the source-region device, had been shipped to Oak Ridge previously. The Berkeley group was assisted in carrying out the tests by personnel from Tennessee Eastman Corporation and Stone & Webster Engineering Corporation.

The general procedure adopted in making measurements with the shim-region device has already been described in Chap. 2 of this volume, and it will not be reported here. Examples of the type of data obtained, together with a discussion of the method used to compare theoretical and experimental curves, have also been given in the above chapter. The device was used to study the shim region in 71 tanks of the first track,[14] which are denoted by the letter M in Fig. 4.18. It was found that the magnetic fields in all these tanks met the theoretical specifications. The closest approach of any of the measurements to the limit of 3-cm galvanometer deflection was 2.8 cm. This was the case for tanks 41 and 71, where right plane refers to the plane 8 in. to the right of the median plane as one faces the tank (from outside or inside the track). Nearly all of the curves for the median plane showed a flattening of the peak. The only tanks in which this did not occur are 1, 30, 40, 45, and 65. In the case of tank 65, bulging of the peak occurred. An example of the flattening effect is shown in Fig. 4.19, for tank 52.

Of the 71 tanks measured, 51 showed an indentation in both left and right planes. Of the remaining tanks, two (1 and 30) showed no indentation in either plane. The rest of the tanks showed an indentation in either the left or the right planes. The presence of this indentation was almost certainly associated with the shim shape rather than with the positioning of the shims in the tanks. This same explanation probably applies to the flattening of the peaks noted above. It must be recalled in this regard that the shims consisted of plane surfaces while the theoretical criteria were derived on the basis of smoothly curved surfaces. The average maximum differences for the left, median, and right planes for tanks on the outside of the track were 1.2 cm, 0.91 cm, and 1.7 cm, respectively. The corresponding figures for tanks on

the inside of the track were 1.63 cm, 1.09 cm, and 1.5 cm, respectively. Therefore, there appeared to be better agreement for the left plane than for the right plane on the outside of the track. The reverse was true for tanks on the inside of the track. Figure 4.20 shows the indentation occurring in the right plane of tank 55.

An examination of the measurements of the shim positions indicated some correspondence between these measurements and the magnetic measurements. In those cases where the shim surfaces were asymmetrically located with respect to the median plane of the tank, the fits of the curves differed for the left and right planes. It was not possible to obtain any quantitative agreement between the shim positions and the maximum discrepancies of the curves. The fit of the experimental and theoretical curves was, in general, as good for tanks on the curved sections of the track as for tanks on the straight portion.

Measurements with the source-region device were carried out during the same period in which the above tests were made.[14, 15] The tanks in which the measurements were made are denoted by the letter C in Fig. 4.18. The results obtained indicated that the field remained quite uniform until the point $M_0$ is reached (see Fig. 2.56). The field at $M_0$ was on the average 1.34 per cent below that at Z over the 20 tanks in which the measurements were made. The average fields at A and B were respectively 3.61 and 2.87 per cent below the field at Z. Since A and B were only 7 in. from $M_0$, it is seen that the field changes rapidly in this neighborhood. Every deflection measured fell well within the theoretical criteria. As a matter of fact, $dh_z/dx$ satisfied the most stringent criterion, namely, 0.2 per cent of the homogeneous field per inch up to a distance of 4 or 5 in. from the source toward the side walls. The only Z runs which satisfied the most stringent criterion of 0.1 per cent of the homogeneous field per inch (or 3 oersteds per inch) were those through the point $U_0$, where the effect of the shim and the edge of the tank was not felt. The largest deflections were obtained in the outside tanks. Indications were that there might be a tilt of the field in practically all of the tanks measured. Measurements for the +8- and −8-in. planes differ by amounts greater than possible errors in measurements. Furthermore, the rates of change of $h_z$ along the Z axis for the +7- and −7-in. planes differ appreciably in some cases. There was apparently no connection between the fields in the +8- and −8-in. planes and the position of the tank in the track. It may be possible that the asymmetry observed was due to the placement of the tank pads.

It should be noted that throughout the period of the shim-region and source-region measurements, the magnet current was not regulated. However, the current did not change sufficiently, while data were being

obtained in any one tank, to introduce any appreciable error in the results. In conclusion it may be said that the measurements on the first magnet at the process plant indicated that the magnetic field was in every respect satisfactory for use with calutron units, and that the measurements of the positions of the shims in the tank were sufficient to guarantee a satisfactory magnetic field in the region between the shims. The measurements in the region of the source justified the conclusions which were drawn from the model tests made in Berkeley. Magnetic measurements of this type were not carried out on any of the other magnets at the plant.

3.2 Other Magnetic Measurements Made on Track 1 (Bldg. 9201-1). In addition to the measurements described above some measurements were made on the stray fields and on the magnetic forces between the tank walls and the cores. A magnetization curve for one of the tanks in the track was made and the efficiency computed.

The stray-field measurements[16] were carried out with a large coil of 4200 turn-sq cm and a fluxmeter. Readings were taken in a horizontal plane 3 ft from the floor. The components of the stray field at this height and at 6-in. intervals were found by flipping the coil through 180 deg by hand. Measurements were made both on the inside and the outside of the track. From the values of the components it was possible to find the absolute value of the stray field. The results obtained, which are probably accurate to within 5 or 10 per cent, are compared with those secured on the model of the track in Figs. 4.21 and 4.22. The model measurements were made at a homogeneous field strength of 3400 gauss, whereas those on the track were made at about 2900 gauss. This accounts in part for the fact that the stray field around the track is weaker than that around the model. However, the difference in field strength is not believed to be sufficient to account for the differences exhibited in these figures and may possibly be accounted for by the fact that the types of iron in the track and the model are different magnetically and that the structures of the coil tanks are somewhat dissimilar. The measurements on the track showed that the stray field is appreciably weaker inside the track than outside. Furthermore, the stray field is weaker on the straight than on the curved portion of the track and more pronouncedly so on the outside than on the inside.

The force between the tank wall and core was obtained on the Alpha I model by measuring the average magnetic field strength. No information concerning variations of the field strength was obtained. The construction of the race track is such that relatively large variations in magnetic intensity may occur, which could result in an appreciably different force than that determined from the average magnetic field intensity. Measurements of the field variation between tank 45 and

coil tank 24a were made. The variations were determined by moving a coil in 2-in. jumps along a vertical line between the tank and the core. A galvanometer was used and the deflections were recorded photographically. A number of vertical runs were made at distances ranging from 10 to 40 in. from the front of the tank. The absolute field strength on each vertical run at a distance of 31 in. from the top of the tank was determined by means of the flip coil.

A calculation of the force between the tank wall and the core was made on the basis of the average magnetic field strength over the run as well as on the basis of the average of the squares of the field strength. Using the average field strength over the run, the force is proportional to the average value of $H^2$. The average of the squares of the magnetic field is given by

$$\overline{H}^2 = \sum_{1}^{n} H_i^2/n$$

where $H_i$ stands for the average field strength over each 2-in. jump made. The magnetic force is then proportional to $\overline{H}^2$. The force calculated from the average of the squares of the field strength is about 1 per cent greater than the force calculated from the average of the field strengths. From the model tests it was estimated that the force might be about 20 per cent higher than the measured value, owing to irregularities in the gap between the core and tank wall. Actually the effect of the irregularities is almost negligible.

The average difference between the force for four runs was about 1 per cent, the greater force in each case being that calculated from the average of the squares in the magnetic field strength. The average field strength in the tank wall–core gap for all runs was about 3550 oersteds, as compared to a field strength of very nearly 3000 oersteds in the tanks. The first value is therefore about 18 per cent greater than the second. The corresponding figure for the model tests was about 22 per cent. The average force between one tank and the core, using the average of the field strength for all runs, is about 45 tons.

In connection with this discussion of the magnetic forces on the tanks, a phenomenon which was observed on the race track is of some interest. After the race track had been energized for several days, during which time one quadrant had been used for vacuum testing, a check on the positions of the tanks in this quadrant showed that some of them had moved as much as 2.5 in. out of the gaps.[17] Those on the outside of the track moved toward the outside and those on the inside moved toward the inside of the track. The evidence available at the time together with later tests pointed to magnetic forces producing this effect.

The explanation of this force on the tanks is based on the fact that the tanks in the magnet will take up the position which reduces the reluctance of the magnet to a minimum. The force in dynes on the tank will be equal to the energy contained in the volume of the new field which appears when the tank moves 1 cm. Suppose A is the flux in a tank for one position and B is the flux in the rest of the gap. Then the total flux is A + B. If the tank is moved 1 cm out of the gap to a new position A′, then the flux in the tank is still A but that behind the gap is B + C (see Fig. 4.23). The total flux through the magnet is A + B + C. The volume of the flux in C is 1 cm × 139 in. × 28 in. or 25,103 cc. The flux density inside the tank is 3400 oersteds but in the gap behind the tank there is 4 in. less iron and the flux is approximately 3400 × 25.5/29.5 = 2939 oersteds. The energy in 1 cc of flux is $2939^2/8\pi + 3.427 \times 10^5$ ergs. The total energy in C is $3.427 \times 10^5 \times$ 25,103 ergs + $8.628 \times 10^9$ ergs. The force on the tank is $8.628 \times 10^9$ dynes or 9.71 tons.

This argument depends on the fact that there is very little field in existence at position D near the mouth of the tank. If there is a large stray field going from the cores around the mouth of the tank, then when the tank moves out, there is a smaller change in the flux in the region D. The tank occupies space where there was flux; if D is the amount of flux which was at D before the tank moved, then the total flux is A + B + C − D and the change in flux is C − D rather than C alone. Since the strength of the stray field decreases rapidly away from the normal position of the tank, the force on the tank will increase as it moves out of the gap. The maximum possible force will be 9.71 tons, with the presence of a field at D reducing this. As the tank moves farther out of the gap, eventually a point will be reached where the 2-in. walls will saturate and the tank will tend to pull back into the gap.

Experiments were carried out in the XBX magnet to test the above explanation. It was concluded from these tests that the force on the Alpha tanks tending to push them out of the gaps lies somewhere between 9.71 and 4.53 tons. On the basis of the results, it was recommended that all Alpha tanks should be fastened to the other tank in the gap or to the core.

A magnetization curve[14] was taken in tank 89 with the flip coil on the source-region exploring device. The results are exhibited in Fig. 4.24. The magnet current values listed along the abscissa were taken from potentiometer readings. Readings were taken only to a magnet current of about 6200 amp. The resulting curve is quite linear over the range covered.

The efficiencies of tanks 89 and 95 are shown in the following table:

| Tank | Total current, amp | Field | Efficiency, % |
|---|---|---|---|
| 89 | 6500 | 2675 | 93.6 |
| 95 | 6500 | 2725 | 95.3 |

The over-all efficiency of the magnet was calculated to be about 94 per cent. The measurements made were not very complete because of the pressure of time. However, enough data were obtained to give some comparison of the performance of the track with that of the model. The magnetic performance of the track is better than predicted from the model experiment. An indication of this is given by the stray-field measurements already mentioned. The field in the source region of each tank is more uniform than that expected from model results and from measurements in the XA unit in Berkeley. It was concluded that it should be possible to use an arc as close as 14 in. to the tank wall and still keep within the 0.5 mass unit criterion for broadening of the beam focus.

3.3 Magnetic Measurements on Race Track 6.[18] No measurements were made in the shim region, as the excellent results obtained in testing track 1 showed that a dimensional check of the shim positions was entirely adequate. Measurements of the field in tank 96, which is adjacent to the end yoke across the north end of the magnet, were made in the median plane and in planes which were 8 in. on either side of the median plane. The purpose of the measurements was to study asymmetry produced by the location of this tank next to the yoke. Some of the results obtained are shown in Fig. 4.25, which shows the variations in magnetic field strength in a horizontal plane 72 in. above the bottom of tank 96 and 8 in. to the left of the median plane. The results showed that at 48 in. from the mouth of the tank, the field was 0.6 per cent higher on the left-hand plane than on the right-hand plane. This could be due to two things: first, an actual asymmetry in the field, and second, to a slight asymmetry in the placing of the search coil. In any case the asymmetry was not sufficient to cause a noticeable effect on the ion beams, especially as the asymmetry was in the opposite direction at other points in the tank.

Contour maps of the field in tank 84 were obtained and some of the results are shown in Fig. 4.26. Referring to this figure, the point A, 28 in. in from the mouth of the tank and 72 in. from the bottom in the median plane, was chosen arbitrarily as the reference field. The numbers on the contour lines indicate the percentage change in the field from that point in the tank. The field at A was approximately 3050 oersteds, though this was varied over a small range during the

week while measurements were being made. All measurements were corrected for this change in field on the assumption that the shape of the field remained the same for small changes in the absolute value of the field. There was some indication that the field in tank 96 was higher than that in tank 84. Measurements in tank 84 gave 3000 oersteds at 4800 amp of exciting current, while in tank 96 the field was 3128 oersteds at 4800 amp. Both measurements were made 28 in. in from the mouths of the tanks and 72 in. up from the bottoms in the median planes. However, in neither tank were there sufficient data to determine accurately the relative operating voltages of the tanks.

3.4 Magnetic Measurements on Magnet XBX.[19,20] A magnetization curve was obtained for this magnet, using the standard flip-coil procedure. A flip coil of 480.2 turn-sq cm was used at a distance of 18 in. from the bottom and the same distance from the mouth of tank 1. Hibbert standard A (tap 10) was used to determine the absolute magnetic field strength. Since the switchboard ammeter was not correct, it was necessary to calibrate this meter by means of a potentiometer. The potentiometer was connected across the 100-mv 1500-amp shunt in the circuit. The magnetization curve obtained with the end coils on 66⅔ per cent taps is given in Fig. 4.27.

With all coils of the magnet on the 100 per cent taps, a current of 438 amp gave a field strength of 7700 oersteds, and 99 per cent of the magnetomotive force was effective in producing flux in the gap. With the end coils on 66⅔ per cent taps, a current of 475 amp produced a field strength of 6400 oersteds, and 96 per cent of the magnetomotive force was effective in producing flux in the gap. The experimental error in these measurements was at least 5 per cent. The shape of the field in the gap was obtained by taking flux plots, using compass and drawing board. A check of the accuracy of this method was made by determining the same line twice, and this check indicated that the error was not greater than 1/16 in. The field was found to be extremely uniform, having a radius of curvature of 56.5 cm 1¾ in. in from the mouth of the gap, corresponding to a variation of field strength of 4.47 per cent per inch. There was no tilt in the lines of force within the limit of experimental error. This indicated that the 66⅔ per cent taps on the end coils were the correct ones to use.

Stray-field measurements were made using a commercial fluxmeter, with prepared test coils of areas 300 and 20 sq cm, respectively. The shape of the field agreed generally with the stray field determined from the model of XBX. Referring to Fig. 4.28, it is interesting to note that, at a point 1 ft away from the center coil on line C, the stray field dropped to zero. The field inside the room housing the magnet dropped below 16 oersteds along the lines b, c, d, and e. Along line a, the field did not drop below 16 oersteds inside the room.

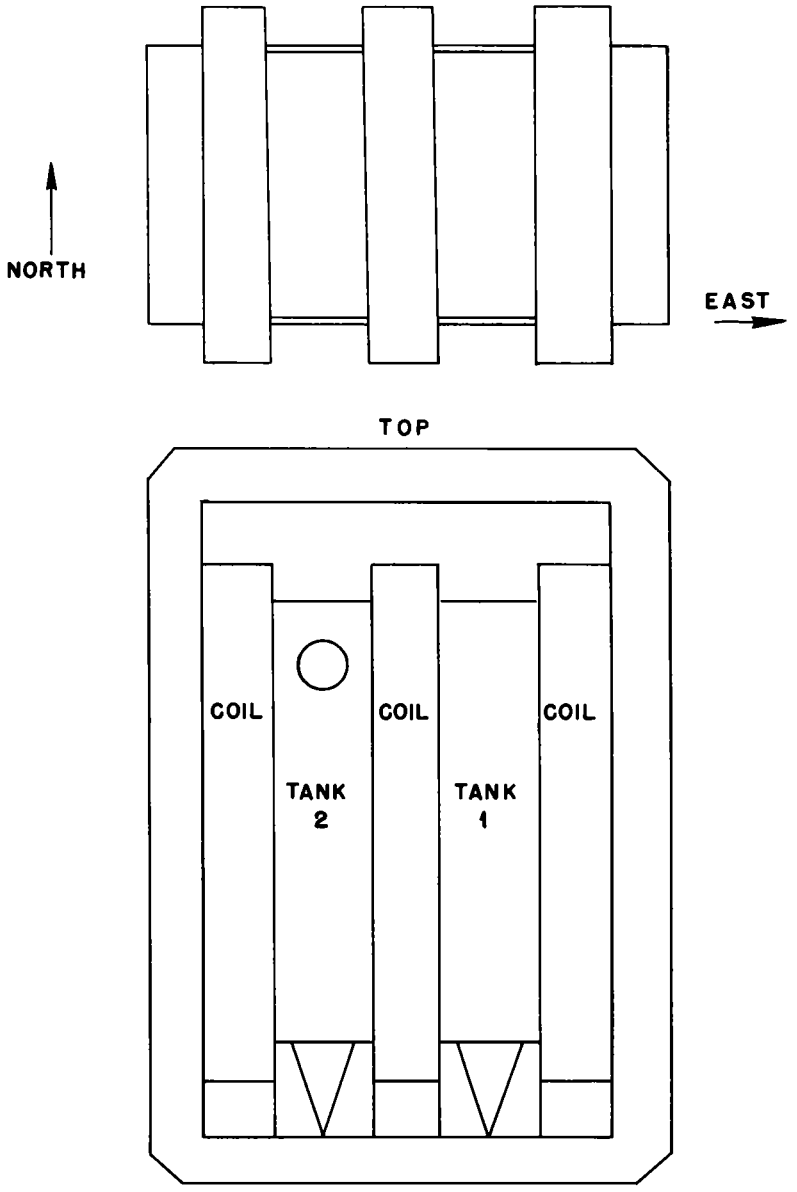


Fig. 4.1—View of the XA magnet.

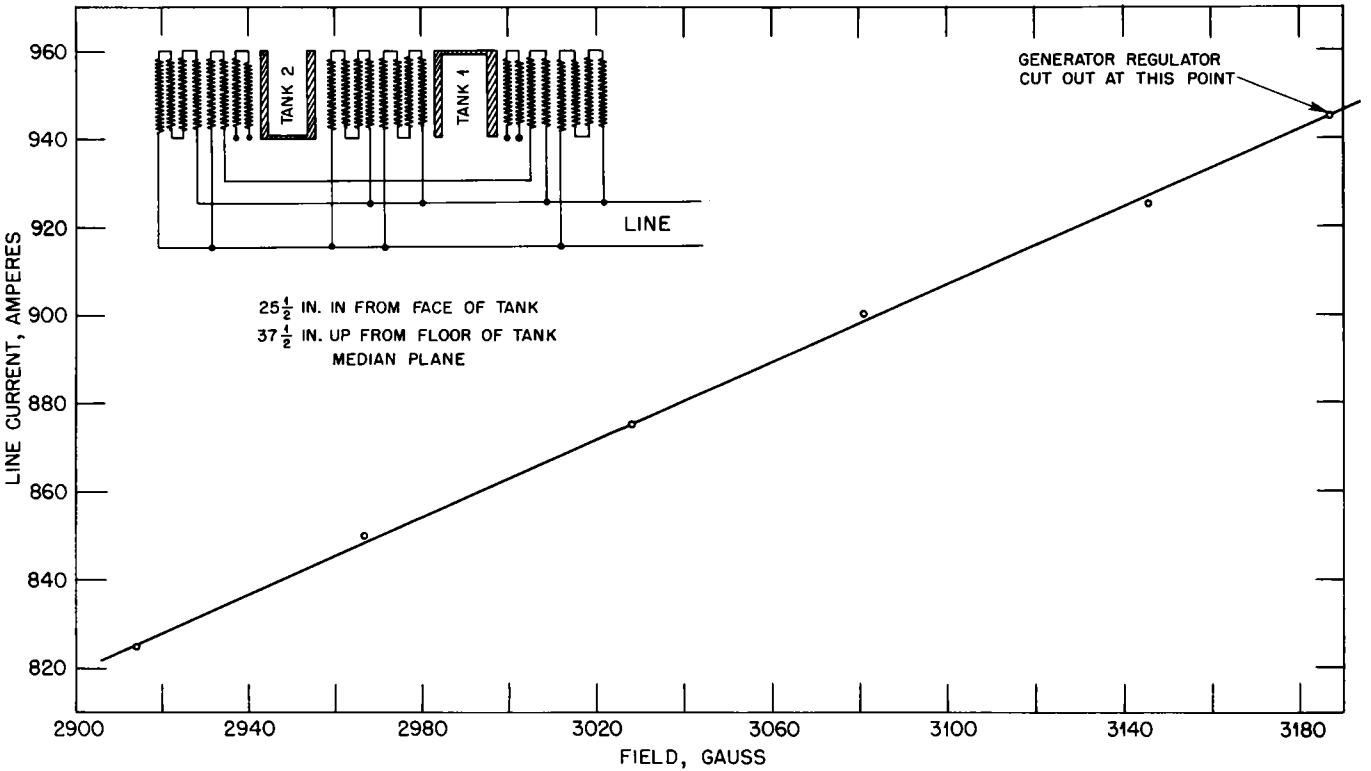


**Fig. 4.2 — Magnetization curve for the XA magnet.**

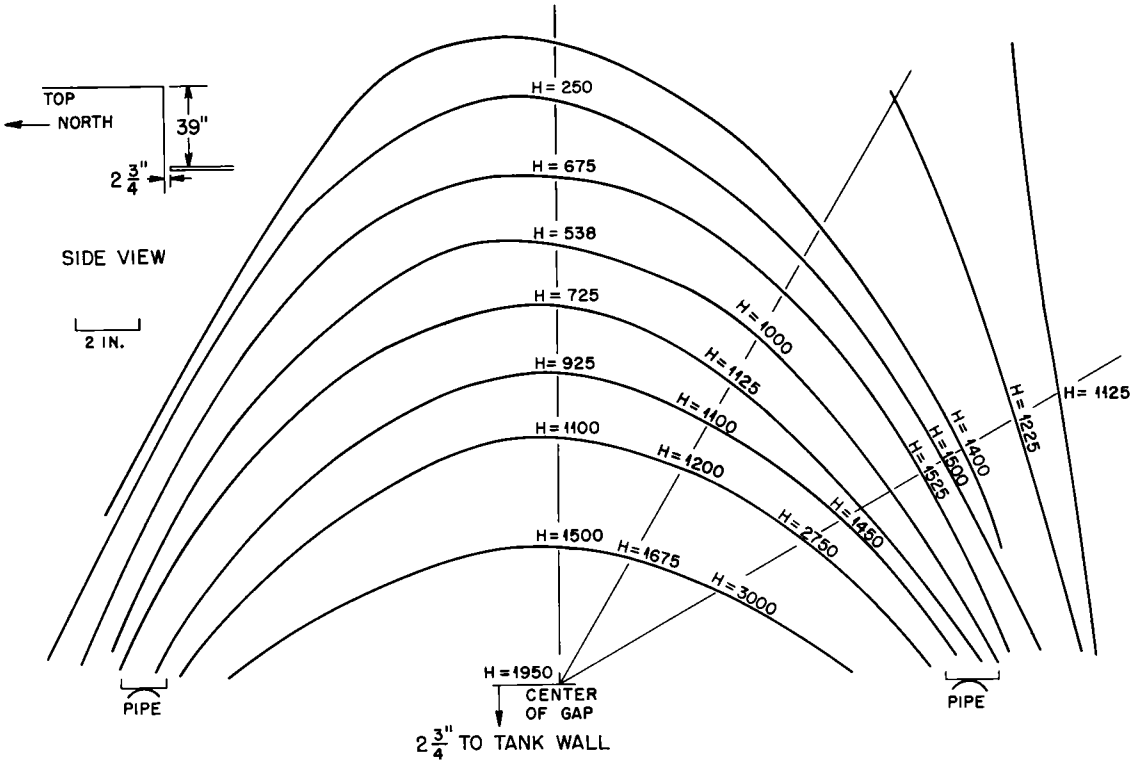


Fig. 4.3—Stray-flux plot around the XA magnet.

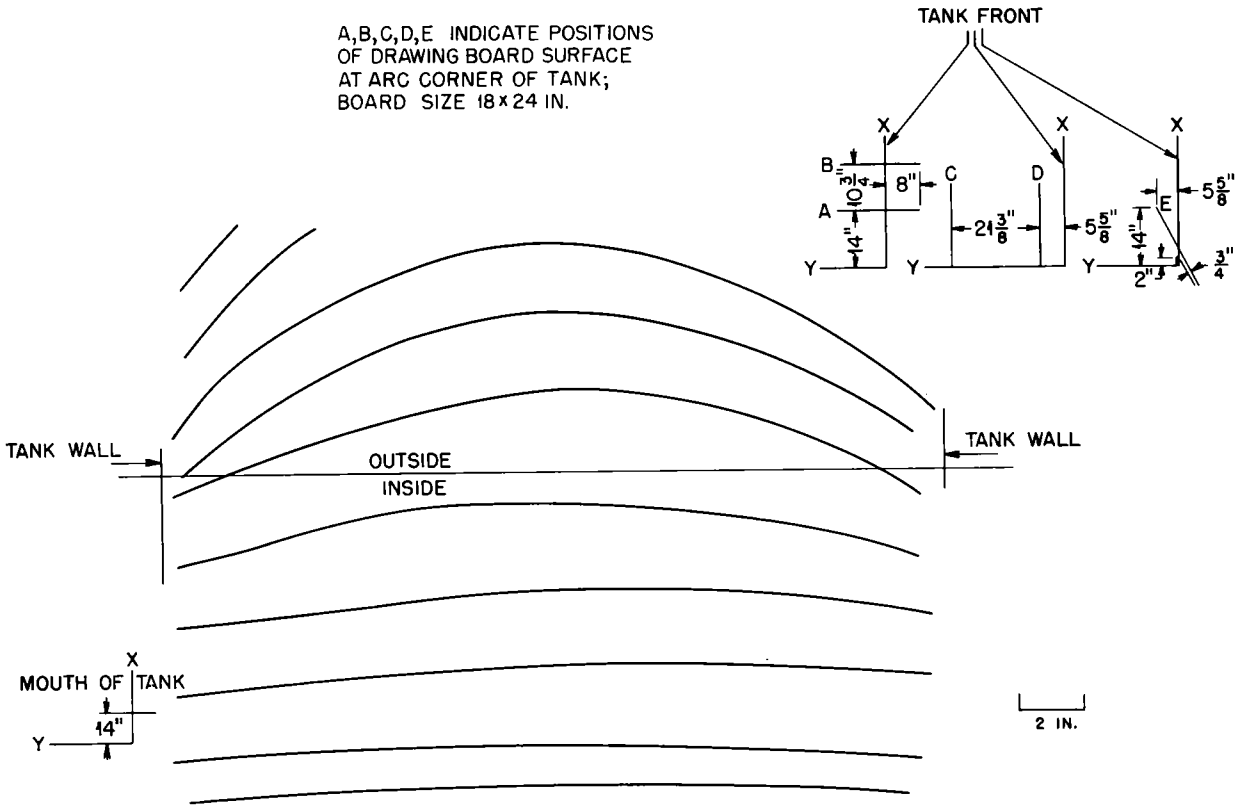


Fig. 4.4 — Flux plot in the source region of the XA-2 tank.

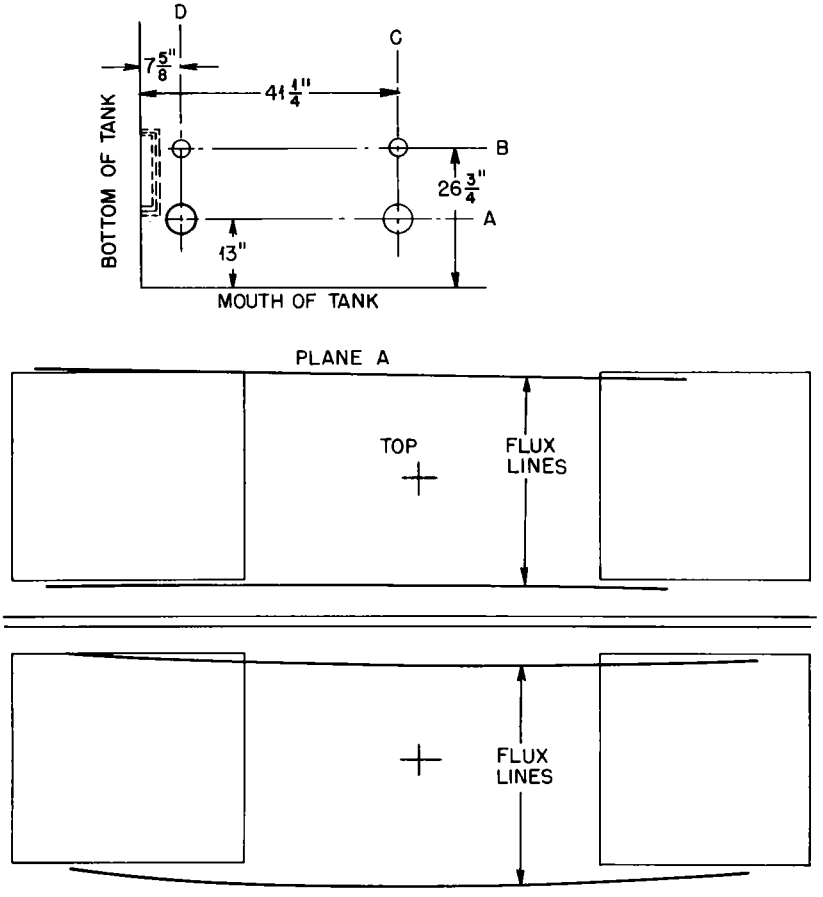


**Fig. 4.5 — Flux plot in the region of the G insulators for the XA-2 tank. Plots were made in planes A,B,C, and D.**

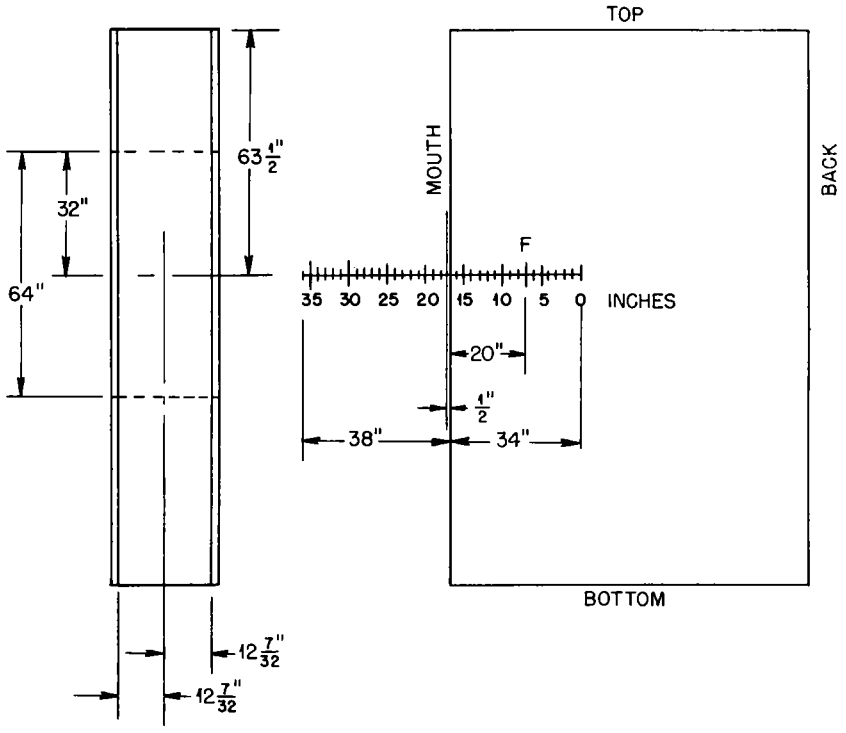


**Fig. 4.6—Locations of measurements in finding effect of ½-in. magnetic-steel side wall.**

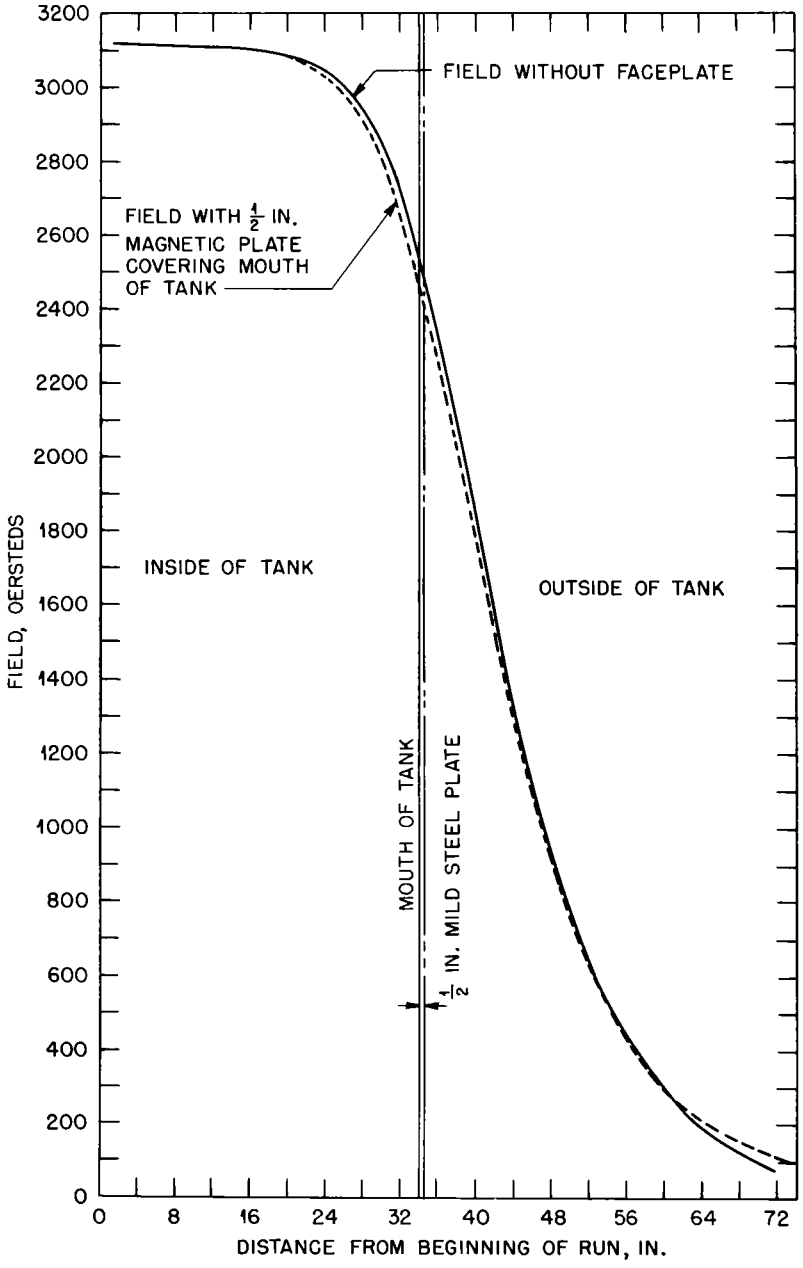


**Fig. 4.7 — Effect of magnetic steel side wall on field, tank XA-2.**

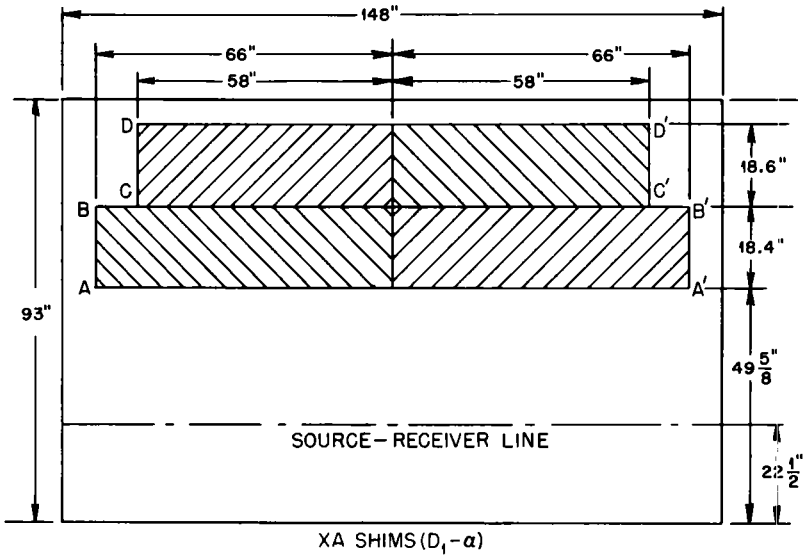


**Fig. 4.8—Location of linear magnetic shims in XA-1 tank.**

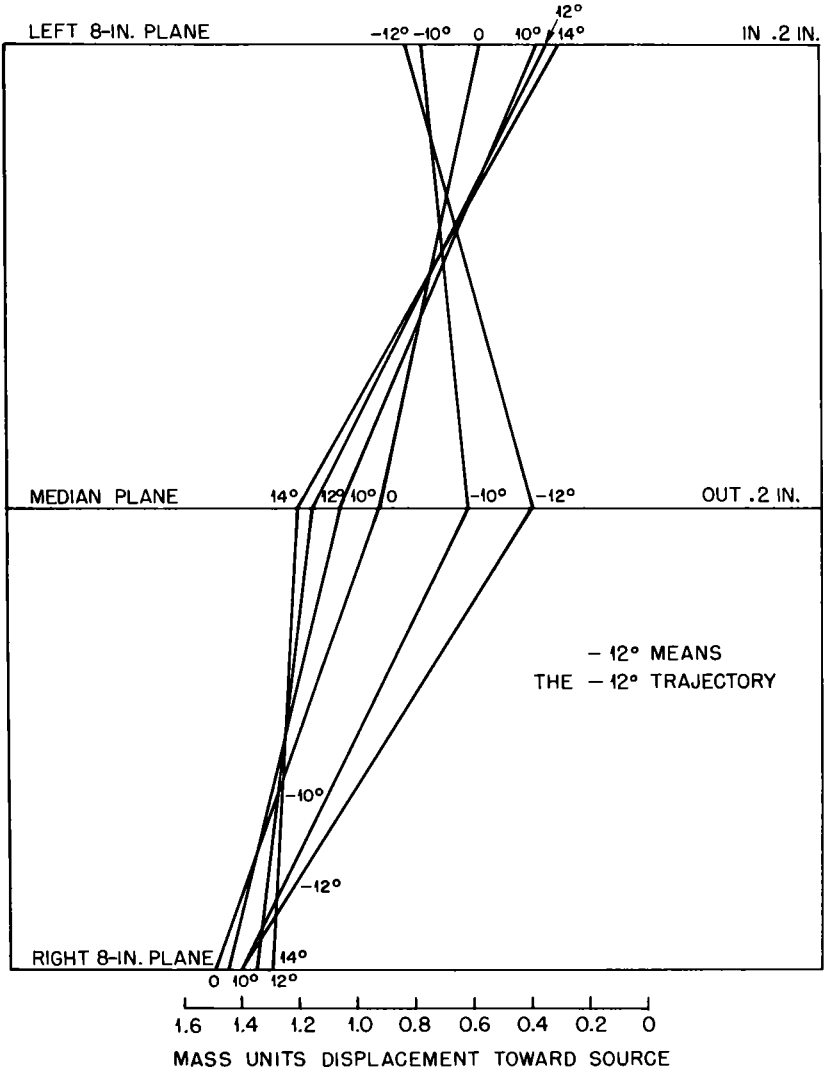


**Fig. 4.9 — Expected beam pattern with ideal electric shims, tank XA-2.**

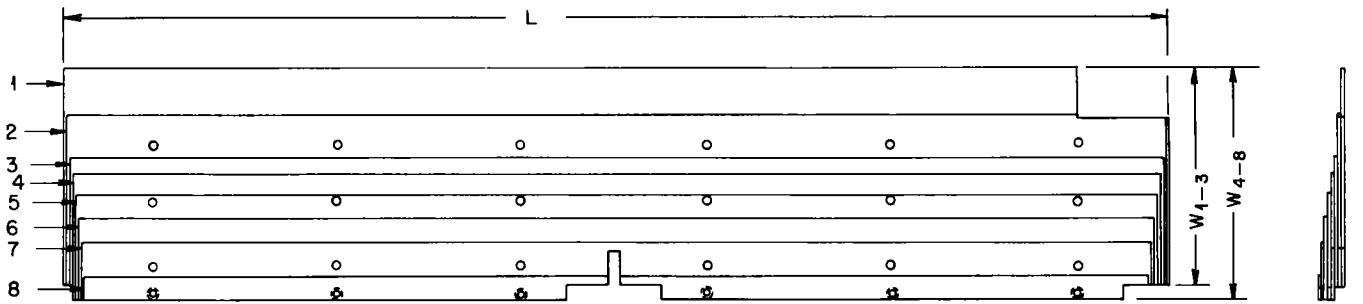


| SEGMENT NO. | L(LENGTH, IN.) | W (WIDTH, IN.) | NO. HOLES |
|---|---|---|---|
| 1 | 48 | $9\frac{3}{8}$ | 18 |
| 2 | $47\frac{3}{4}$ | $7\frac{5}{16}$ | 18 |
| 3 | $47\frac{1}{2}$ | $5\frac{9}{16}$ | 12 |
| 4 | $47\frac{1}{4}$ | $5\frac{3}{8}$ | 18 |

| SEGMENT NO. | L (LENGTH, IN.) | W (WIDTH, IN.) | NO. HOLES |
|---|---|---|---|
| 5 | 47 | $4\frac{9}{16}$ | 18 |
| 6 | $46\frac{3}{4}$ | $3\frac{1}{2}$ | 12 |
| 7 | $46\frac{1}{2}$ | $2\frac{17}{32}$ | 12 |
| 8 | $46\frac{1}{4}$ | 1 | 6 |

Fig. 4.10—Location of auxiliary shims in tank XA-2.

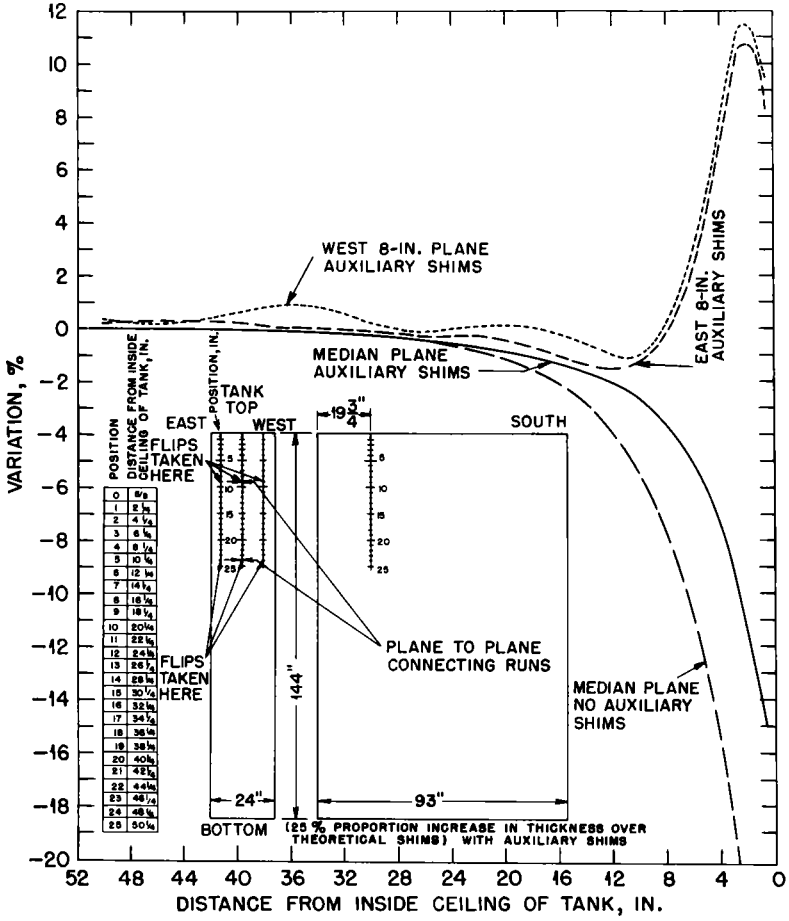


Fig. 4.11 — Effect of auxiliary shims on magnetic field, tank XA-2.

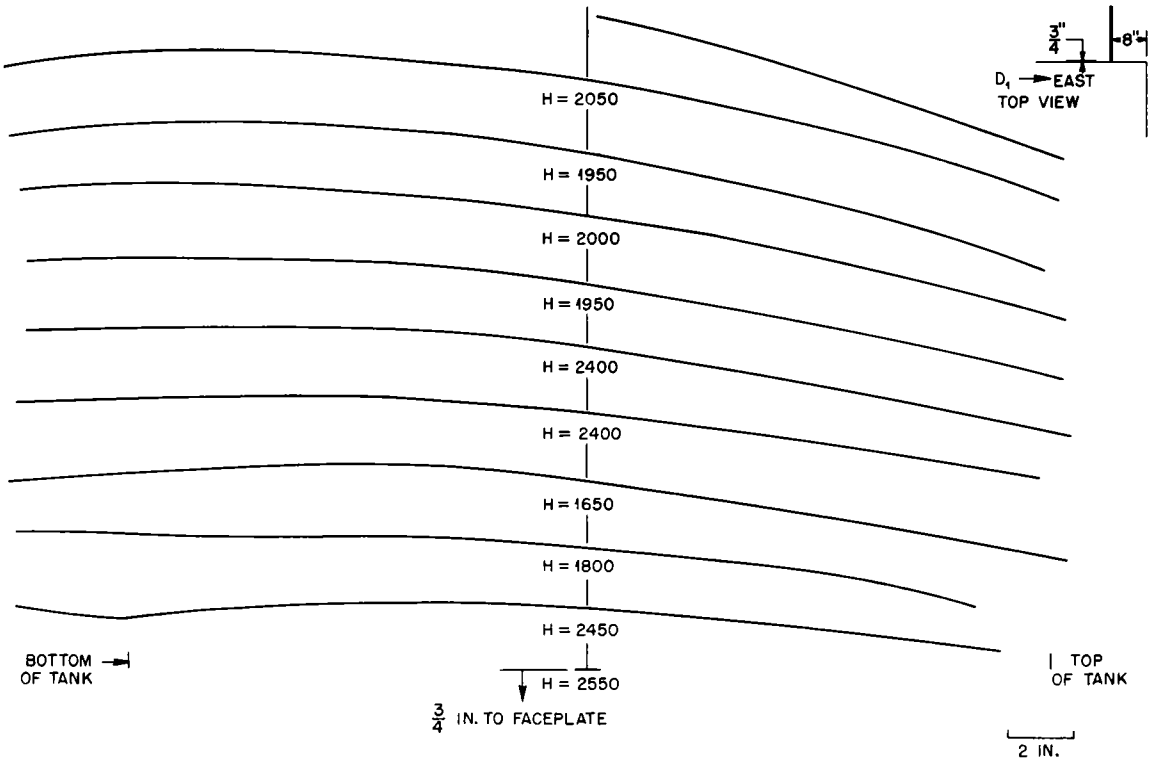


Fig. 4.12 — Flux plot for the $D_1$ tank.

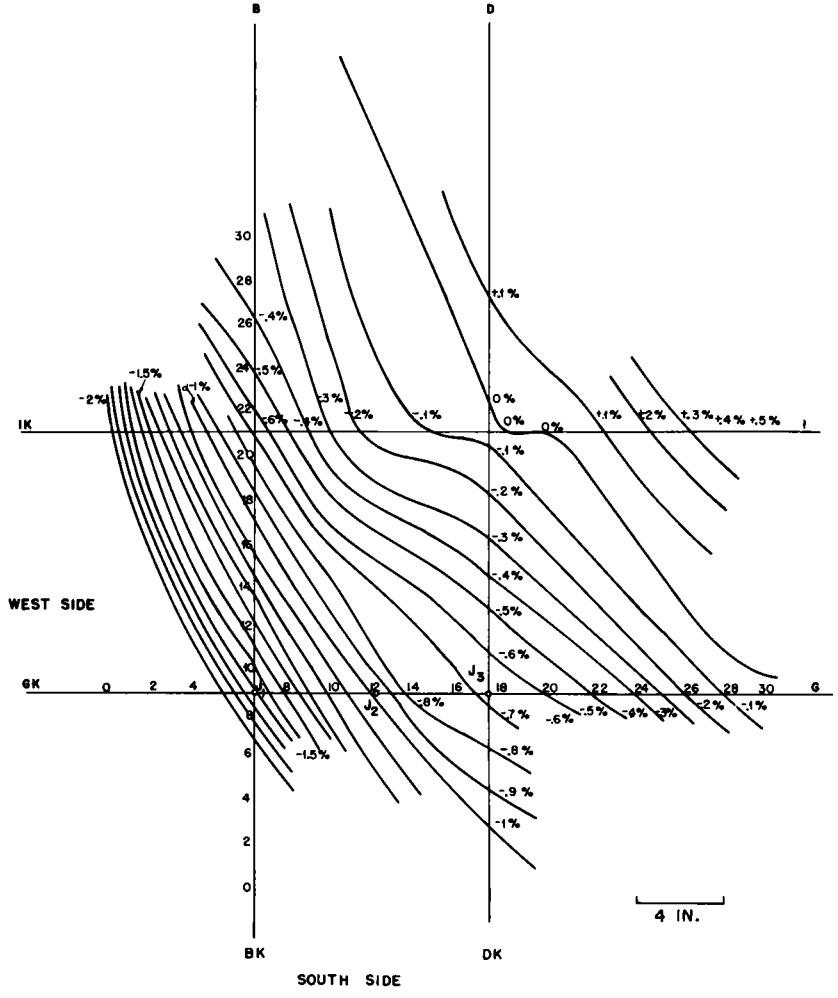


Fig. 4.13—Contour map in the source region of tank $D_1$.

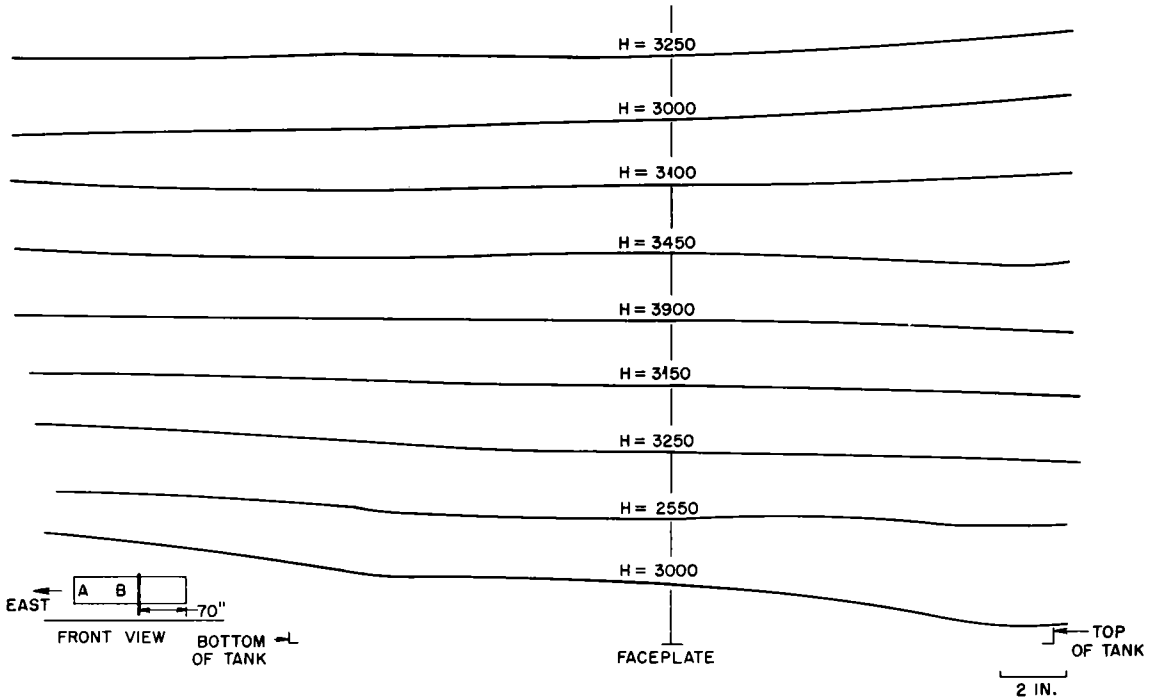


Fig. 4.14 — Flux plot for the $R_1$ tank.

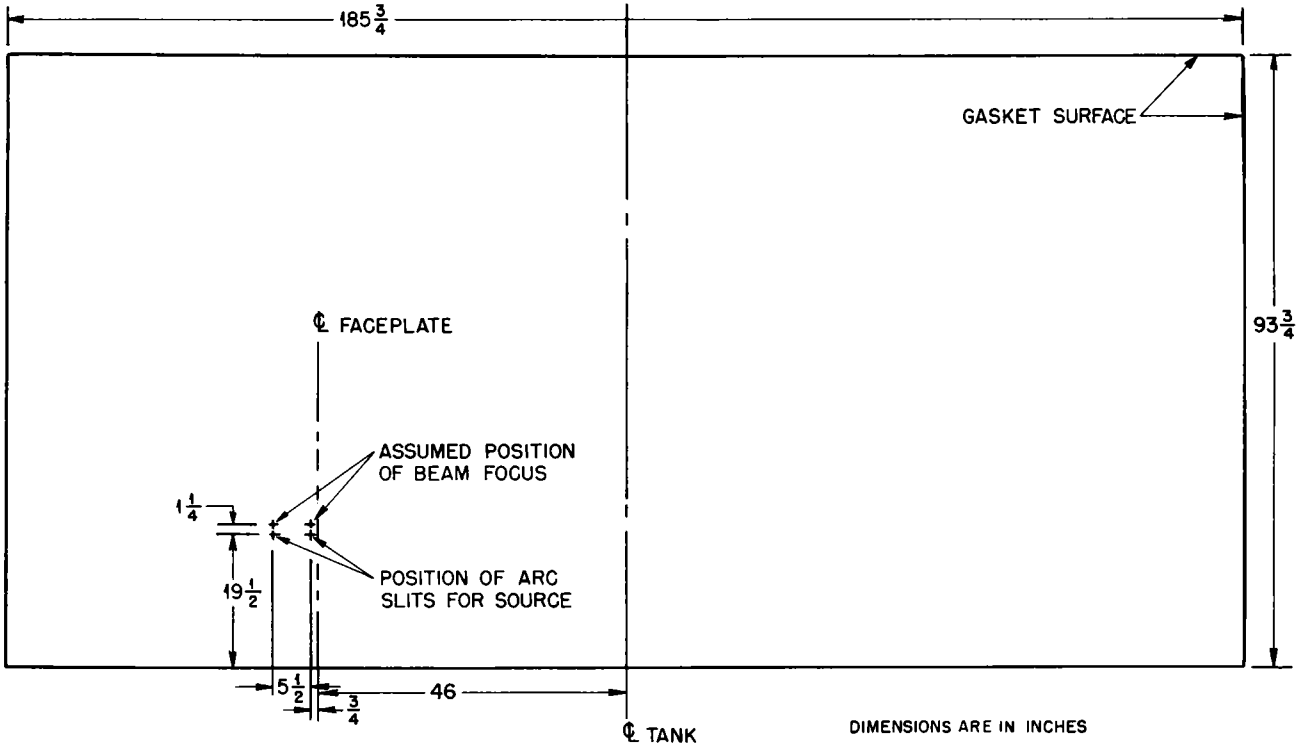


**Fig. 4.15 — Positions of arc of coils for $R_1$ measurements.**

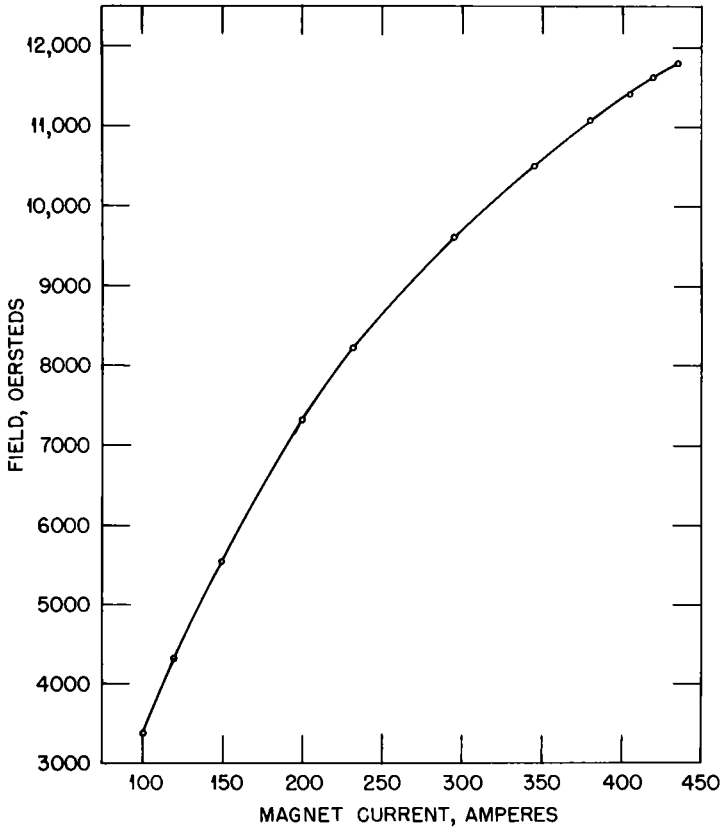


**Fig. 4.16—Magnetization curve for the 37-in. cyclotron magnet.**

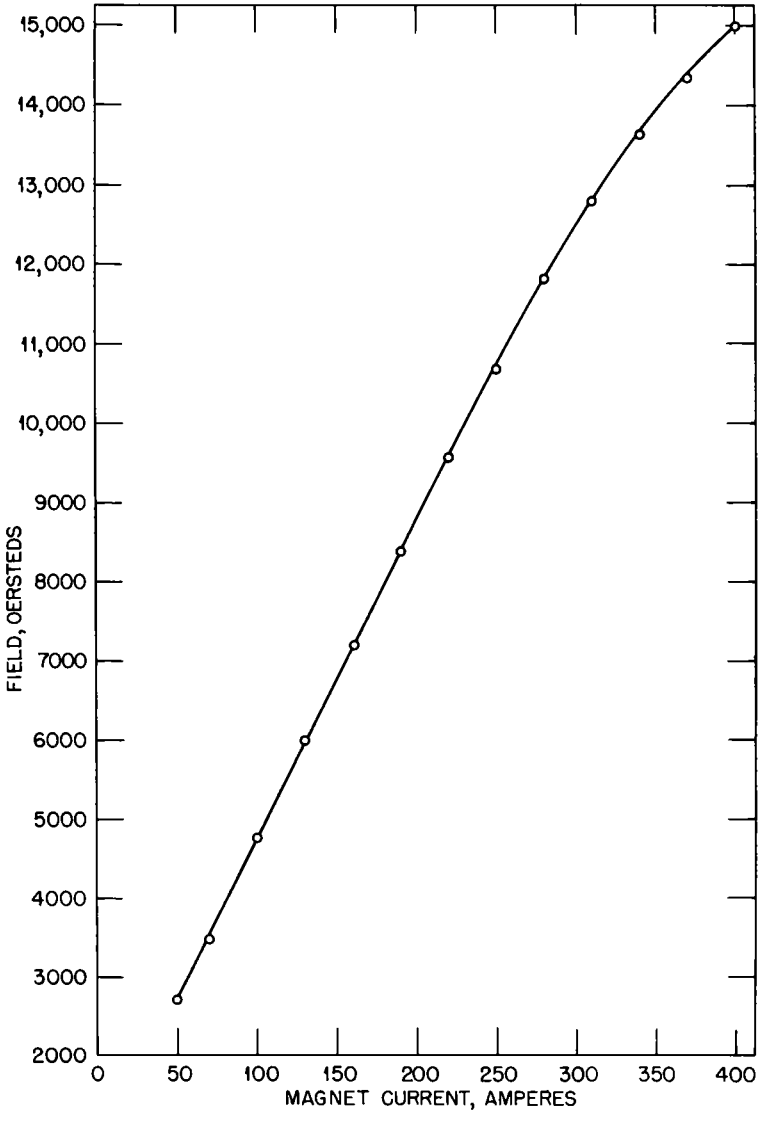


**Fig. 4.17—Magnetization curve for the 60-in. cyclotron magnet.**

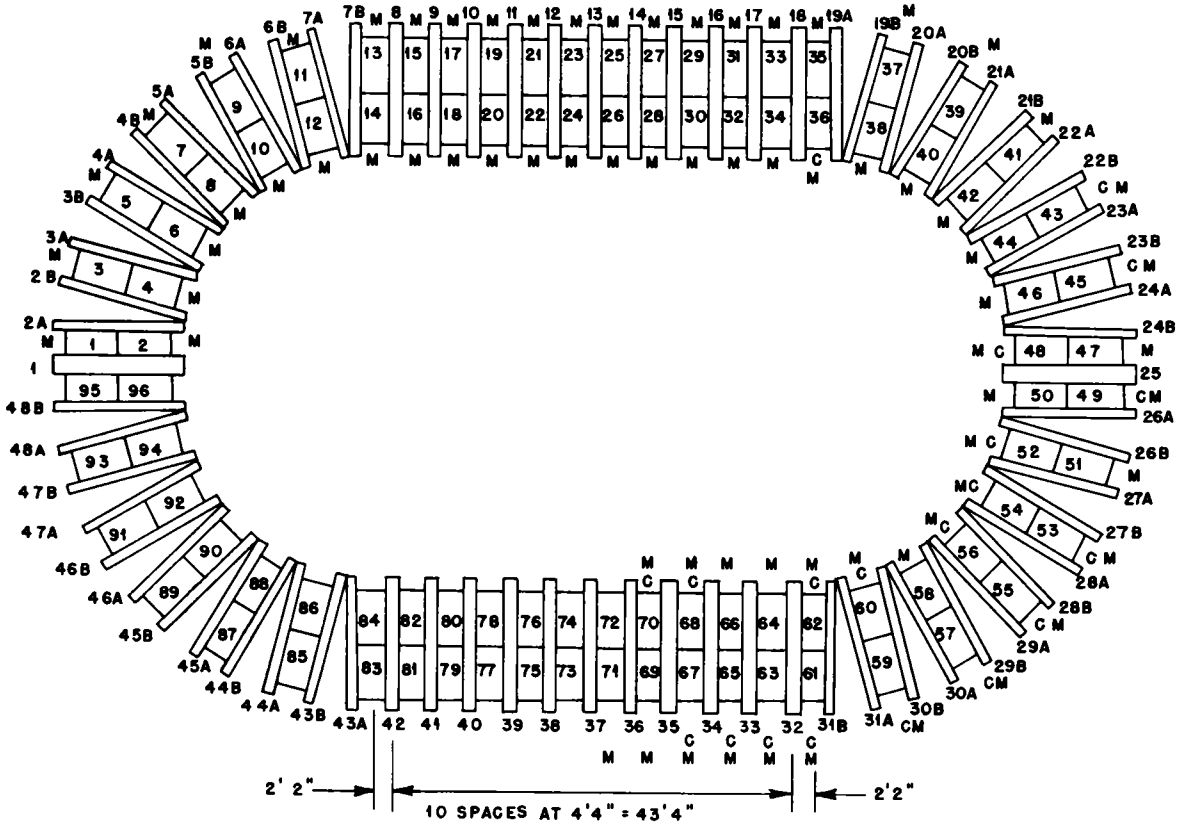


Fig. 4.18—Plan view of race track 1 (Alpha I plant).

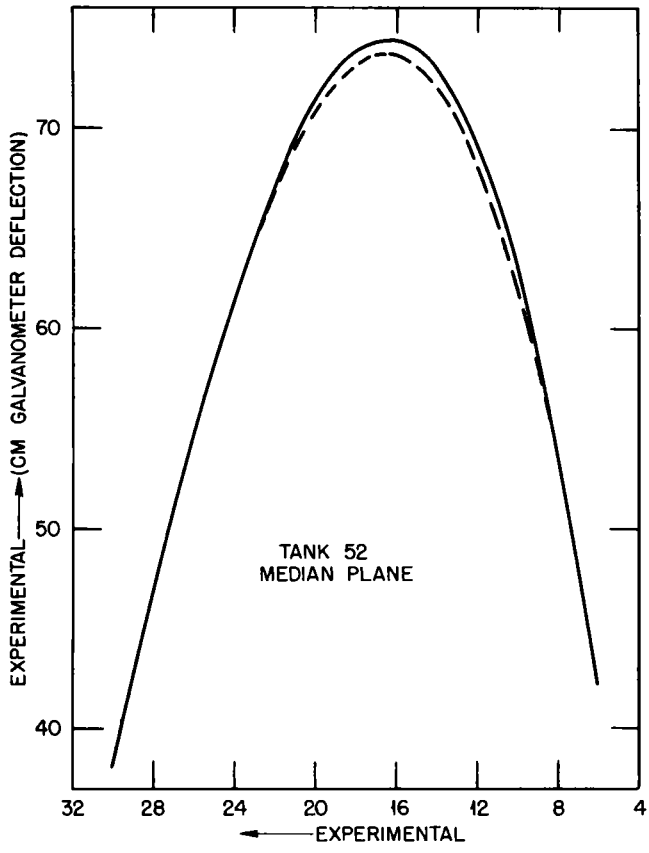


**Fig. 4.19—Flattening of peak for curve in median plane, tank 52.**

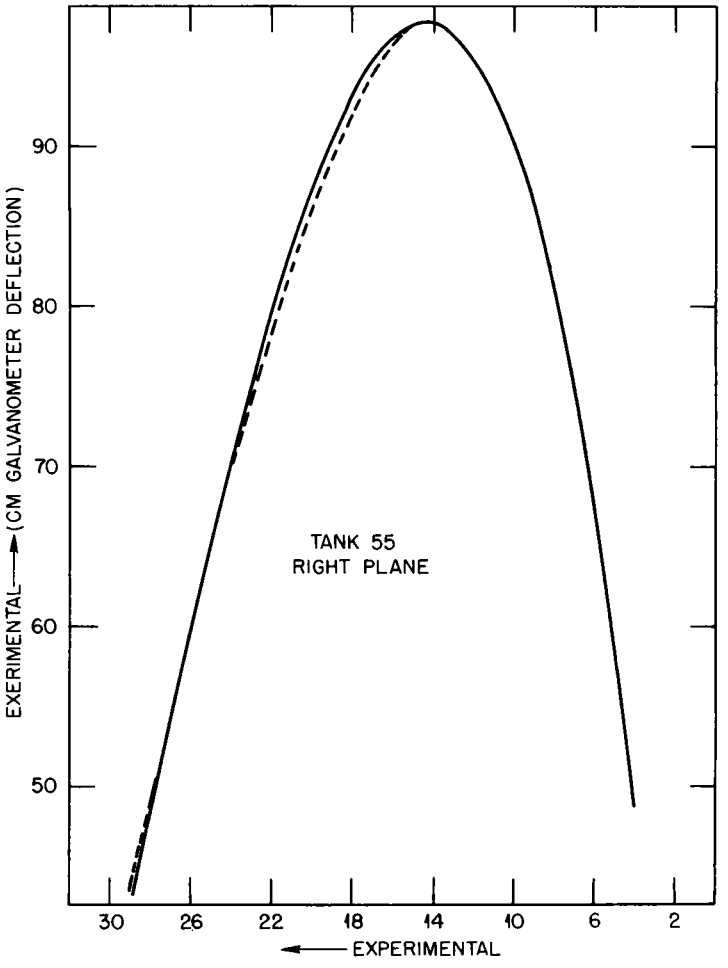


**Fig. 4.20—Indentation in right plane of tank 55.**

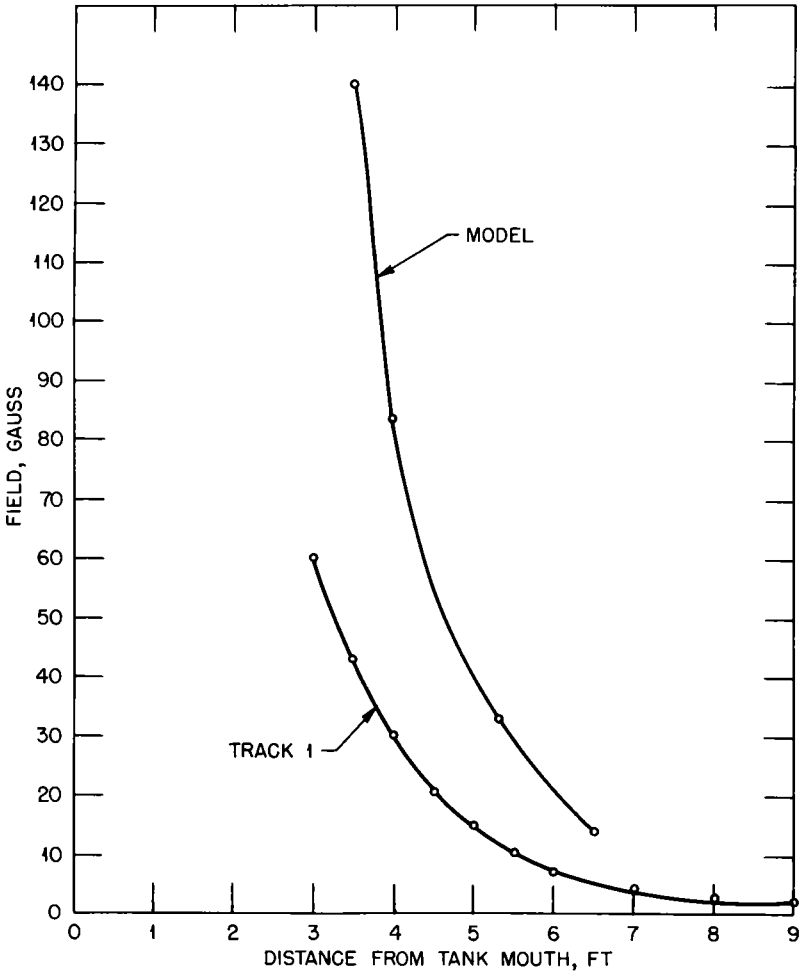


**Fig. 4.21—Stray magnetic field outside tank 43 (race track 1).**

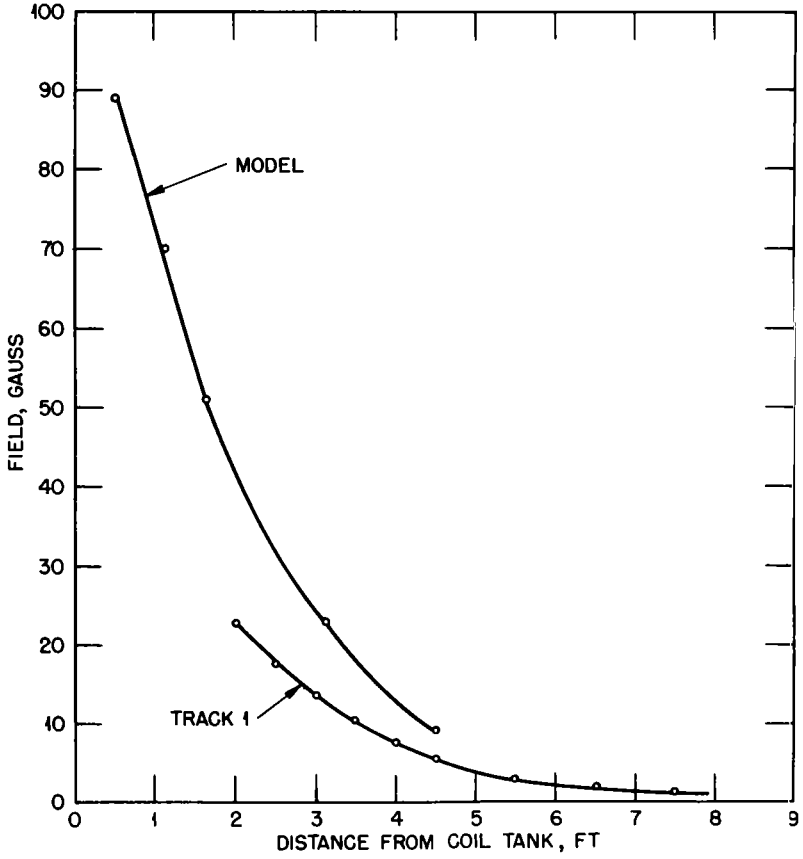


**Fig. 4.22—Stray magnetic field between tanks 41 and 43 (race track 1).**

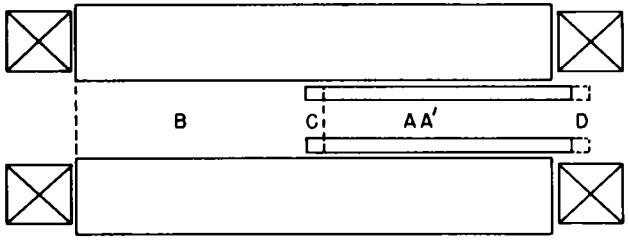


Fig. 4.23—Sketch for explanation of Alpha tank motion.

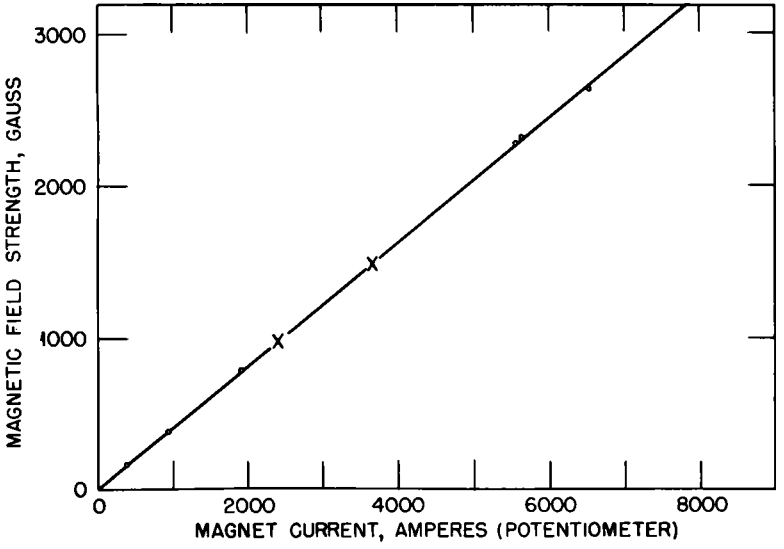


Fig. 4.24—Magnetization curve for tank 89 in race track 1.

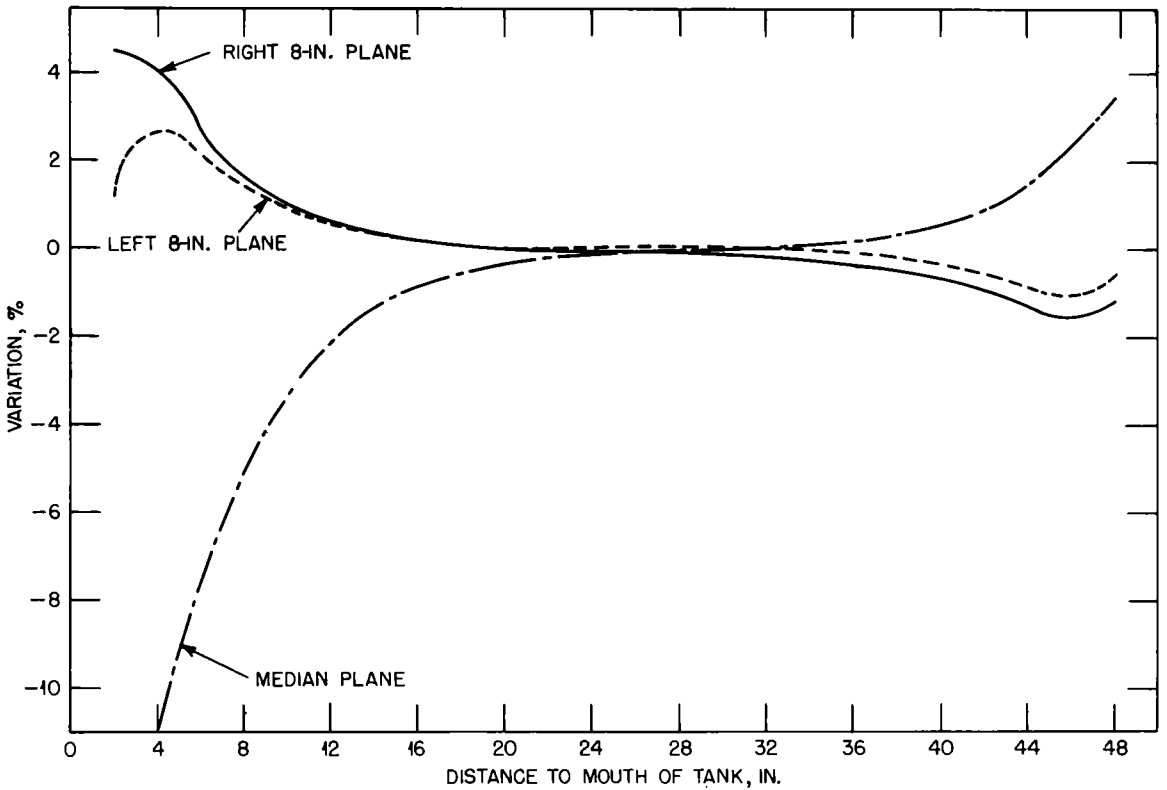


**Fig. 4.25—Field distribution in tank 96, race track 6.**

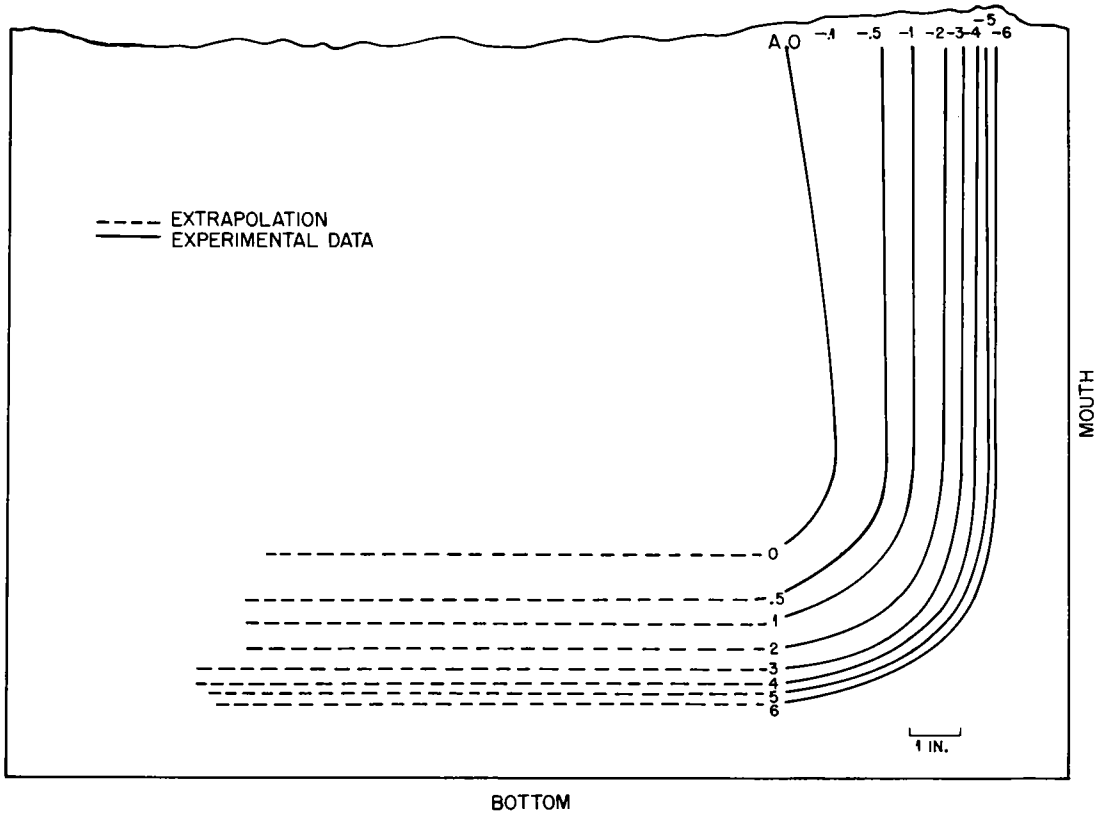


**Fig. 4.26—Contour map for tank 84, race track 6.**

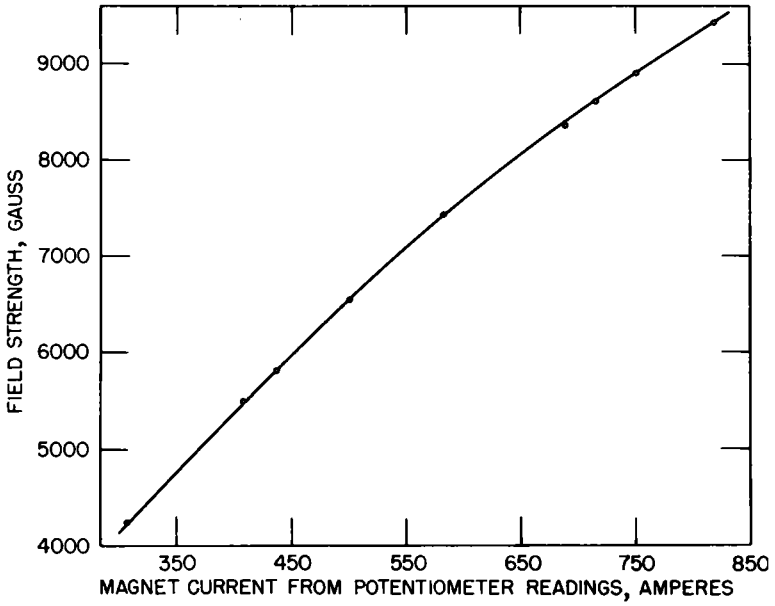


**Fig. 4.27—Magnetization curve for magnet XBX.**

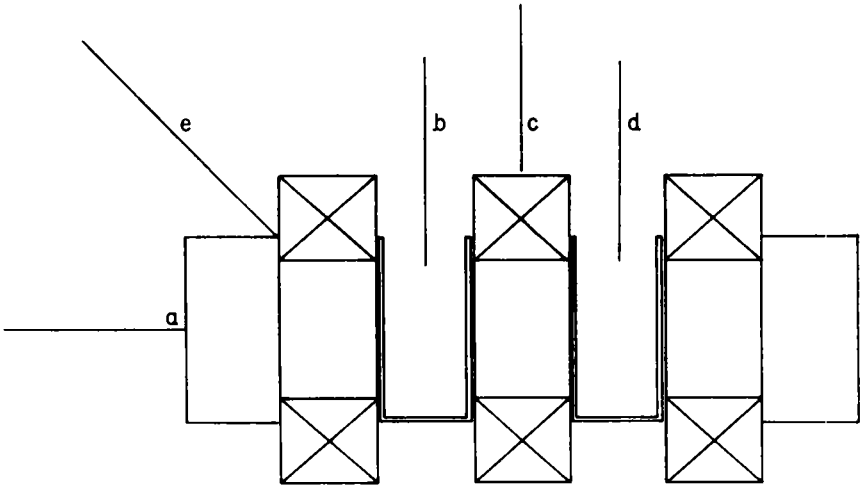


**Fig. 4.28—Positions of stray-field measurements on magnet XBX.**

## REFERENCES


1. W. P. Ball, R. W. Henderson, J. R. Akers, A. J. Hulse, and W. M. Powell, Magnetization Curve for the XA Magnet, Report RL 27.6.29, Nov. 28, 1943.
2. E. Stearns, M. Hammond, and M. Seegmiller, Plots of External Fields for XA, $R_1$, and $D_1$, Report RL 27.6.12, June 9, 1943.
3. E. Stearns and N. Huston, Plotting of the Magnetic Field Configuration Near the Arc, for XA-2, without Faceplate, Report RL 27.6.14, July 29, 1943.
4. E. Stearns and W. M. Powell, Flux Plots in the Region of the Insulators Supporting the G in XA-2, Report RL 27.6.15, Aug. 8, 1943.
5. W. P. Ball, The Effect of a One-Half-Inch Magnetic Steel Tank Side Wall on the Field inside the Process Tank in XA, Report RL 27.6.39, Apr. 6, 1944.
6. A. Guthrie, Measurements on XA, Report RL 27.6.7a, Sept. 27, 1943.
7. A. Guthrie, Tilt Measurements on XA, Report RL 27.6.7, Aug. 19, 1943.
8. W. M. Powell, Construction, Installation and Performance of the XA-2 Auxiliary Shims, Report RL 27.6.41, May 20, 1944.
9. R. K. Wakerling, A. Latter, and A. Guthrie, Design of Auxiliary Shims, Report RL 27.6.31, Feb. 20, 1944.
10. W. M. Powell and R. Lomanitz, Examination of the Field in the $D_1$ Tank, Report RL 27.6.13, July 22, 1943.
11. W. M. Powell, W. P. Ball, T. Finkelstein, and W. Parkins, Measurements of $R_1$ Tank with Wooden Arc of Coils After Removal of Vacuum Lock, Report RL 27.6.30, Dec. 14, 1943.
12. A. J. Hulse, J. R. Akers, W. M. Powell, and W. P. Ball, 37-Inch Z Field Measurement, Report RL 27.6.36, Mar. 15, 1944.
13. A. J. Hulse, J. R. Akers, W. P. Ball, and W. M. Powell, 60-Inch Magnetic Field Measurements, Report RL 27.6.38, Mar. 20, 1944.
14. A. Guthrie, R. K. Wakerling, N. Dalkey, and A. Latter, Magnetic Measurements on Race Track 1, Report RL 27.6.27, Jan. 17, 1944.
15. A. Latter, A. Guthrie, and N. Dalkey, Tolerances on Alpha-1 Shims and Process Tanks, Report RL 27.6.33, Jan. 10, 1944.
16. A. Guthrie, Stray Field Measurements on Race Track 1, Report RL 27.6.26, Nov. 19, 1943.
17. W. M. Powell, E. V. Stearns, and R. R. Wisner, Tank Motion in the Alpha Race Track, Report RL 27.6.23, Nov. 29, 1943.
18. W. M. Powell, E. Hudson, and F. A. Smith, Magnetic Measurements on Race Track 6, Report RL 27.6.44, Aug. 28, 1944.
19. W. M. Powell and E. V. Stearns, Performance Tests on Magnet XBX, Report RL 27.6.20, Oct. 16, 1943.
20. A. Guthrie, Magnetization Curve on XBX, Report RL 27.6.25, Nov. 27, 1943.

# INDEX

G



M



N



P

AEC, Oak Ridge, Tenn.